Dissertation

submitted to the

Combined Faculties for the Natural Sciences and for Mathematics

of the Ruperto-Carola University of Heidelberg, Germany

for the degree of

Doctor of Natural Sciences

presented by

Diplom-Biologist Anna-Lena Scherr

born in: Bad Dürkheim

Oral-examination: .....

The Role of anti-apoptotic Bcl-2 Proteins for colorectal Cancer Development and Progression

Referees: Prof. Dr. Michael Boutros

Prof. Dr. med. Henning Schulze-Bergkamen

„Because the world exists, the limits of probability have already been exceeded. “

-J. Gaarder-

For my parents, with gratitude

TABLE OF CONTENTS

SUMMARY **7**

ZUSAMMENFASSUNG **9**

INTRODUCTION **11**

1.1 The Intestine **11**

1.2 Colorectal Cancer **13**
1.2.1 Epidemiology, Classification and Treatment 13
1.2.2 Molecular Pathogenesis 15

1.3 Programmed Cell Death **17**
1.3.1 Apoptosis 18
1.3.1.1 Intrinsic Apoptosis 20
1.3.1.2 Extrinsic Apoptosis 22
1.3.2 Autophagy 24
1.3.3 Necroptosis 26

1.4 Knockout Mouse Models **28**
1.4.1 Knockout Mice of Bcl-2 Family Members 28
1.4.2 Intestine-specific Knockout of Cell Death- and Inflammation-related Proteins 30

1.5 Aim of this Work **31**

MATERIAL AND METHODS **33**

2.1 Cell Culture Methods **33**
2.1.1 Cultivation, Thawing and Freezing of eukaryotic Cells 33
2.1.2 Transfection of Cells with siRNA and Plasmid-DNA 34
2.1.2.1 siRNA Transfection 34
2.1.2.2 Plasmid-DNA Transfection 35
2.1.3 Cell Death Assays 35
2.1.3.1 MTT-Assay 35
2.1.3.2 LDH-Assay 36
2.1.4 FACS Analysis of Cell Death and Proliferation 36
2.1.5 Migration Assays 37
2.1.5.1 Scratch Assay 37
2.1.5.2 3D Cell Culture 38
2.1.6 Invasion Assay 39
2.1.7 Tissue Culture 39

2.2 Protein Analyses **40**
2.2.1 Protein Isolation 40
2.2.1.1 Protein Isolation from cultured Cells 40
2.2.1.2 Protein Isolation from Tissues 41
2.2.2 Bradford Assay 42

2.2.3 SDS-PAGE 43
2.2.4 Western Blot 45

2.3 DNA and RNA Analyses 47
2.3.1 RNA Isolation 47
2.3.1.1 RNA Isolation from cultured Cells 47
2.3.1.2 RNA Isolation from Tissues 47
2.3.2 Reverse Transcription and qRT-PCR 48
2.3.3 Mouse Genotyping 50
2.3.4 Agarose Gel Electrophoresis 52
2.3.5 Sanger Sequencing 53

2.4 Histological Analyses 54
2.4.1 Hematoxylin and Eosin Staining 54
2.4.2 Immunohistochemistry 55
2.4.3 TUNEL Assay 57

2.5 Mouse Models 58
2.5.1 Breeding and Organ Removal 58
2.5.2 AOM/DSS Model and Mouse Endoscopy 59

2.6 Statistical Analysis 60

RESULTS 61

3.1 Expression Levels of anti-apoptotic Bcl-2 Proteins in human colorectal Cancer 61

3.2 The Role of anti-apoptotic Bcl-2 Proteins for human colorectal Cancer Cells in vitro 62
3.2.1 Knockdown of anti-apoptotic Bcl-2 Proteins does not lead to spontaneous Cell Death Induction ... 63
3.2.2 Knockdown of anti-apoptotic Bcl-2 Proteins does not exert anti-proliferative Effects on CRC Cells 64
3.2.3 Anti-apoptotic Bcl-2 Proteins influence the migratory Ability of CRC Cells 65
3.2.4 Knockdown of anti-apoptotic Bcl-2 Proteins inhibits the Invasiveness of CRC Cells 71
3.2.5 The pan-Bcl-2 Inhibitor Obatoclax delays Cell Cycle Progression and inhibits Migration of CRC Cells 72
3.2.6 Expression of Migration Markers after Downregulation or Inhibition of anti-apoptotic Bcl-2 Proteins 76
3.2.7 Downregulation or Inhibition of anti-apoptotic Bcl-2 Proteins sensitizes CRC cells towards Oxaliplatin 77

3.3 The Role of anti-apoptotic Bcl-2 Proteins for Physiology and Carcinogenesis in the murine Intestine in vivo 78
3.3.1 The intestine-specific Bcl-x_L knockout Mouse 79
3.3.1.1 The Knockout of Bcl-x_L in intestinal epithelial Cells causes no spontaneous Phenotype 80
3.3.1.2 Loss of Bcl-x_L inhibits Carcinogenesis in an inflammation-driven Tumor Model 82
3.3.1.3 Tumors of Bcl-$x_L^{\Delta IEC}$ Mice show increased Cell Death without compensatory Proliferation 83
3.3.2 The intestine-specific Mcl-1 knockout Mouse 86
3.3.2.1 The Knockout of Mcl-1 in intestinal epithelial Cells induces Cell Death 89
3.3.2.2 The Death of intestinal epithelial Cells in Mcl-$1^{\Delta IEC}$ mice is accompanied by increased Proliferation 93
3.3.2.3 Mcl-$1^{\Delta IEC}$ mice display severe Inflammation in the entire Intestine 94
3.3.2.4 Mcl-$1^{\Delta IEC}$ mice show spontaneous Tumor Development in the Intestine 97

3.4 Inhibition of anti-apoptotic Bcl-2 Proteins in a 3D Cell Culture Approach 99

3.5 Inhibition of anti-apoptotic Bcl-2 Proteins in an ex vivo Tissue Culture System 101

DISCUSSION 103

4.1 Expression Levels of anti-apoptotic Bcl-2 Proteins in human colorectal Cancer Cells and their Impact on Proliferation 104

4.2 The Role of anti-apoptotic Bcl-2 Proteins for colorectal Cancer Cell Migration and Invasiveness 105

4.3 The Role of anti-apoptotic Bcl-2 Proteins for intestinal Tissue Homeostasis and colorectal Cancer Onset and Progression in Mice 110

4.3.1 The intestine-specific Bcl-x_L knockout Mouse 111

4.3.2 The intestine-specific Mcl-1 knockout Mouse 114

4.4 Clinical Relevance of the chemical Inhibition of anti-apoptotic Bcl-2 Proteins 118

4.5 Conclusion 120

4.6 Outlook 120

REFERENCES 122

LIST OF FIGURES 143

LIST OF TABLES 144

LIST OF ABBREVIATIONS 145

CONTRIBUTIONS 151

ACKNOWLEDGEMENTS 152

Anti-apoptotic Bcl-2 (B-cell lymphoma 2) proteins such as Bcl-2 itself, Bcl-x_L and Mcl-1, prevent mitochondrial activation and thereby the induction of the intrinsic apoptotic signaling pathway. Since the avoidance of cell death is a prerequisite for malignant transformation, anti-apoptotic proteins are frequently overexpressed in tumor cells. Additionally, there is growing evidence that Bcl-2, Bcl-x_L and Mcl-1 also play a role in other cellular processes, such as cell cycle regulation, DNA repair and autophagy induction, which can also be important for the onset and progression of cancer.

One of the most frequently diagnosed malignancies worldwide is colorectal cancer. Even though improvements in treatment and population screenings have led to a decreased mortality in many countries, especially patients with metastasized colorectal cancer still face a poor prognosis. Until now, it has been an open question whether and to which extend anti-apoptotic Bcl-2 proteins influence colorectal cancer initiation, progression and metastasation, with a few studies showing contradictory results. Hence, the purpose of this work was to shed more light on the role Bcl-2, Bcl-x_L and Mcl-1 play for the maintenance of intestinal tissue homeostasis and for colorectal cancer development and outgrowth.

First, their expression levels in the human intestinal mucosa as well as in adenoma and adenocarcinoma tissue were determined. This revealed a significant increase of Bcl-x_L in the malignant state and an unaltered expression of Bcl-2. By contrast, Mcl-1 has been found to be significantly downregulated in colorectal cancer specimens. Results obtained in subsequent *in vitro* experiments clearly showed that Mcl-1 has an anti-proliferative effect which cancer cells preclude by downregulation of the protein. Neither in intestinal epithelial cells nor in colorectal cancer cells has a cell cycle inhibiting mode of action been described so far for Mcl-1. Additionally, further *in vitro* experiments have shown for the first time that the siRNA mediated silencing of anti-apoptotic Bcl-2 proteins significantly decreased the migratory capacity and invasiveness of human colorectal cancer cells.

In a second step, protein functions were studied in further detail *in vivo*. Since previous publications showed that the constitutive deletion of both Bcl-x_L and Mcl-1 induces embryonic lethality, two intestine-specific knockout mouse models were generated during this work. For the first time, they allowed to study functioning of Bcl-x_L and Mcl-1 in the murine intestine. The mouse models revealed a strong discrepancy between Bcl-x_L and Mcl-1, regarding their influence on tissue maintenance and tumorigenesis. While Bcl-x_L turned out to be dispensable for normal tissue homeostasis, it has been found to be a crucial factor for colorectal cancer cell survival in a chemically induced tumor model. This confers Bcl-x_L tumor-promoting properties and explains its

overexpression in human adenomas and adenocarcinomas. The loss of Mcl-1, by contrast, caused a severe intestinal phenotype, comprising high levels of cell death, an accompanying increase of proliferation and chronic inflammation. From an age of about six months, spontaneous tumorigenesis was observed in intestine-specific Mcl-1 knockout mice which was promoted by the loss of the anti-proliferative effect Mcl-1 exerts on intestinal epithelial cells and the inflammatory environment. Therefore, it has been proven that Mcl-1 possesses tumor-suppressing properties in the intestine, what explains its downregulation in human colorectal cancer specimens.

The presented results highly recommend the utilization of Mcl-1 sparing inhibitors in the context of colorectal cancer treatment. A first step towards clinical application was done in this work by treating viable human colorectal cancer tissue *ex vivo* with the Bcl-x_L/Bcl-2-specific inhibitor ABT-737. Subsequent analyses revealed a significantly decreased viability of human colorectal cells in presence of the inhibitor. Since proliferation turned out to be unaltered under ABT-737 treatment, inhibition of Bcl-x_L in combination with classical chemotherapy could be an interesting approach for further studies with a focus on clinical applicability.

Anti-apoptotische Bcl-2 (B-cell lymphoma 2) Proteine wie Bcl-2 selbst, Bcl-x_L und Mcl-1 verhindern die Aktivierung von Mitochondrien und damit die Induktion des intrinsischen Apoptose-Signalweges. Da die Zelltodvermeidung eine zentrale Voraussetzung für die maligne Transformation von Zellen ist, sind anti-apoptotische Proteine in Krebszellen häufig überexprimiert. Zudem gibt es vermehrt Hinweise darauf, dass Bcl-2, Bcl-x_L und Mcl-1 auch in anderen zellulären Prozessen wie der Zellzyklusregulation, der DNA-Reparatur und der Autophagie-Induktion eine Rolle spielen, welche die Entstehung und Progression von Tumoren ebenfalls entscheidend beeinflussen können.

Eine der weltweit am häufigsten diagnostizierten Krebserkrankungen ist das kolorektale Karzinom. Obwohl die Mortalitätsrate durch gezielte Vorsorgeuntersuchungen und verbesserte Therapiemöglichkeiten in vielen Ländern sinkt, haben vor allem Patienten mit metastasiertem kolorektalem Karzinom weiterhin eine schlechte Prognose. Bisher konnte die Frage, ob und in welchem Maße anti-apoptotische Bcl-2 Proteine die Entstehung, Progression und Metastasierung von Darmkrebs beeinflussen, nicht abschließend geklärt werden. Daher war es Ziel dieser Arbeit die Funktion von Bcl-2, Bcl-x_L und Mcl-1 für die Aufrechterhaltung der intestinalen Gewebehomöostase sowie für die Entstehung und das Fortschreiten des kolorektalen Karzinoms zu untersuchen.

Im ersten Schritt wurde die Expression der entsprechenden Proteine sowohl in humaner Darmschleimhaut als auch in Adenom- und Adenokarzinomgewebe festgestellt. In der Auswertung zeigte sich in Tumorzellen eine signifikant erhöhte Bcl-x_L Expression und ein unverändertes Level an Bcl-2. Im Gegensatz dazu war die Expression von Mcl-1 im humanen kolorektalen Karzinom signifikant verringert. Anschließend durchgeführte *in vitro* Experimente konnten eindeutig belegen, dass Mcl-1 eine anti-proliferative Wirkung besitzt, welche Krebszellen durch Herunterregulierung des Proteins umgehen. Diese Zellzyklus-regulierende Funktion von Mcl-1 wurde bisher weder in intestinalen Epithelzellen noch in kolorektalen Karzinomzellen beschrieben. Durch die Arbeit mit humanen Darmkrebszelllinien konnte des Weiteren erstmals gezeigt werden, dass die siRNA-vermittelte Abnahme anti-apoptotischer Bcl-2 Proteine die Migration und Invasivität von kolorektalen Karzinomzellen signifikant verringert.

Für eine tiefergehende Analyse der Proteinfunktionen wurden diese in einem zweiten Schritt *in vivo* untersucht. Da sich in früheren Studien herausgestellt hat, dass die konstitutive Deletion von sowohl Bcl-x_L als auch Mcl-1 im Mausmodell pränatal letal ist, wurden zwei darm-spezifische *Knockout*-Mausmodelle für diese Arbeit generiert. Diese Modelle ermöglichten zum ersten Mal eine detaillierte Analyse der Funktion von Bcl-x_L und Mcl-1 im murinen Darm *in vivo*. In den

generierten *Knockout*-Mäusen zeigte sich eine erhebliche Diskrepanz zwischen Bcl-x_L und Mcl-1 hinsichtlich ihrer Rolle für die Aufrechterhaltung der intestinalen Gewebehomöostase und die Entstehung und Progression von Darmkrebs. Während Bcl-x_L für die Gewebehomöostase verzichtbar erscheint, hat es sich in einem chemisch induzierten Karzinogenesemodell als entscheidender Faktor für das Überleben von kolorektalen Karzinomzellen herausgestellt. Diese Funktion, welche Bcl-x_L tumorförderndernde Eigenschaften verleiht, erklärt seine Überexpression in humanen Adenomen und Adenokarzinomen. Im Gegensatz dazu führte der Verlust von Mcl-1 in intestinalen Epithelzellen zur Ausbildung eines starken Phänotyps, welcher hohe Zelltodraten mit einhergehender Erhöhung der Proliferation und chronischer Inflammation umfasste. Ab einem Alter von etwa sechs Monaten kam es zudem zu spontaner Karzinogenese in darm-spezifischen Mcl-1 *Knockout*-Mäusen, welche durch das Wegfallen der anti-proliferativen Wirkung von Mcl-1 und durch das inflammatorische Milieu begünstigt wurde. Damit konnte gezeigt werden, dass Mcl-1 im Darm eine tumorsupprimierende Funktion innehat, was seine signifikant verringerte Expression in humanen kolorektalen Karzinomen erklärt.

Im Hinblick auf mögliche Therapiestrategien für Patienten mit kolorektalem Karzinom, sprechen die vorgelegten Daten daher für die Verwendung von Bcl-x_L/Bcl-2-spezifischen Inhibitoren. Ein erster Schritt in Richtung klinischer Anwendung wurde in dieser Arbeit durch die *ex vivo* Behandlung von vitalem, humanem Darmkrebsgewebe mit dem Bcl-x_L/Bcl-2-spezifischen Inhibitor ABT-737 gemacht. Nachfolgende Analysen zeigten, dass der Inhibitor in der Lage war die Viabilität von kolorektalen Karzinomzellen signifikant zu verringern. Da zudem gezeigt werden konnte, dass sich die Proliferation in Anwesenheit des Inhibitors nicht verändert, könnte sich die Inhibition von Bcl-x_L auch in Kombination mit klassischer Chemotherapie als interessanter Ansatz für weitere Studien mit der Ausrichtung auf klinischer Anwendbarkeit erweisen.

1.1 The Intestine

Anatomically, the mammalian intestine can be divided into the small intestine and the colon. Starting with its proximal end, the small intestine is further subdivided into duodenum, jejunum and ileum, whereas to colon comprises caecum, colon, rectum and anal canal. Over its entire length, the gut is lined with a single-layer epithelium, accomplishing the primary intestinal tasks of digestion and resorption of nutrients and water. In order to promote nutrient uptake in the small intestine, its surface area is dramatically enlarged by the formation of epithelial protrusions, termed villi. Each villus is surrounded by several tubular invaginations, the so called crypts of Lieberkühn. The colon, that is responsible for stool condensation, displays a flat luminal surface possessing only crypts. In addition to digestion and nutrient uptake, the epithelial cells consolidate to an effective barrier against pathobionts. With approximately four days in the small intestine and six days in the colon, the intestinal epithelium displays an extremely high turnover rate and shows thereby the highest self-renewing capacity among mature mammalian tissues[1,2]. This vigorous tissue renewal might be partly due to persistent assaults from microorganisms and the luminal content, leading to high rates of cell death[3]. The loss of up to 10^{11} epithelial cells per day in humans is compensated by a small population of adult stem cells, which are located at the base of all crypts of Lieberkühn. The progeny of dividing stem cells are transit-amplifying cells, which divide 3-5 times until they finally differentiate into specialized epithelial cell types while migrating upwards along the crypt axis. If the cells reach the tip of the villus, they get detached from the extracellular matrix (ECM) and are shed into the gut lumen, where they die via anoikis[4]. The four major cell types originating by differentiation are absorptive enterocytes, which secrete hydrolytic enzymes in order to promote digestion and which are responsible for the absorption of nutrients, mucous-secreting goblet cells, hormone-producing enteroendocrine cells and Paneth cells, which secrete bactericidal substances like lysozyme and defensins. In addition, the intestinal epithelium contains a few other cell types, such as tuft cells, cup cells and M cells, but their precise functions are not very well understood until now[5]. Depending on their primary function, the different intestinal segments display varying cellular composition. Accordingly, the epithelium in the duodenum, where nutriments are decomposed, contains predominantly enterocytes, whereas goblet cells have a higher density in the ileum. Paneth cells are located in the entire small intestine but not in the colon. They are the only subset of differentiated cells which do not migrate upwards, but instead settle down to be closely associated with stem cells at the crypt base. Another difference between Paneth cells and other differentiated intestinal cells is their relative longevity with a turnover rate of 3-6 weeks (Figure 1)[6].

Besides their function in innate immunity and antibacterial defense, Paneth cells are important for maintaining the stem cell niche. They express various niche factors, including EGF (epidermal growth factor), Wnt-3a and Notch ligands Dll1 and Dll4[7]. The balance of stemness and cellular differentiation is tightly regulated and gets controlled by four signaling pathways.

The most important one in this context is the Wnt signaling pathway. In the absence of Wnt-protein ligands, the amount of β-catenin in the cells is low because it gets constitutively degraded. This process is mediated by a multiprotein destruction complex, comprising CK1α (serine/threonine kinases casein kinase 1 alpha) and GSK3 (glycogen synthase kinase 3) as well as the scaffold proteins APC (adenomatous polyposis) and axin. Subsequent to the complex-mediated phosphorylation of β-catenin, it is targeted for polyubiquitination and proteosomal destruction. In the canonical pathway, continuous phosphorylation of ß-catenin is terminated by binding of Wnt-protein ligands to their receptor complex, which is composed of a member of the Frizzled receptor family and co-receptors LRP5 or LRP6 (low density lipoprotein receptor-related protein)[8]. Hence, β-catenin accumulates in the cytoplasm and translocates into the nucleus, where it activates members of the DNA-binding protein family TCF/LEF (lymphoid enhancer-binding factor/T-cell factor) by displacing the co-repressor Groucho. The activated transcription factor enhances the expression of various target genes important for proliferation and the maintenance of stemness. Canonical Wnt signaling is amplified by Lgr5 (Leucine-rich repeat-containing G-protein coupled receptor 5) and its close homologue Lgr4, which are a facultative part

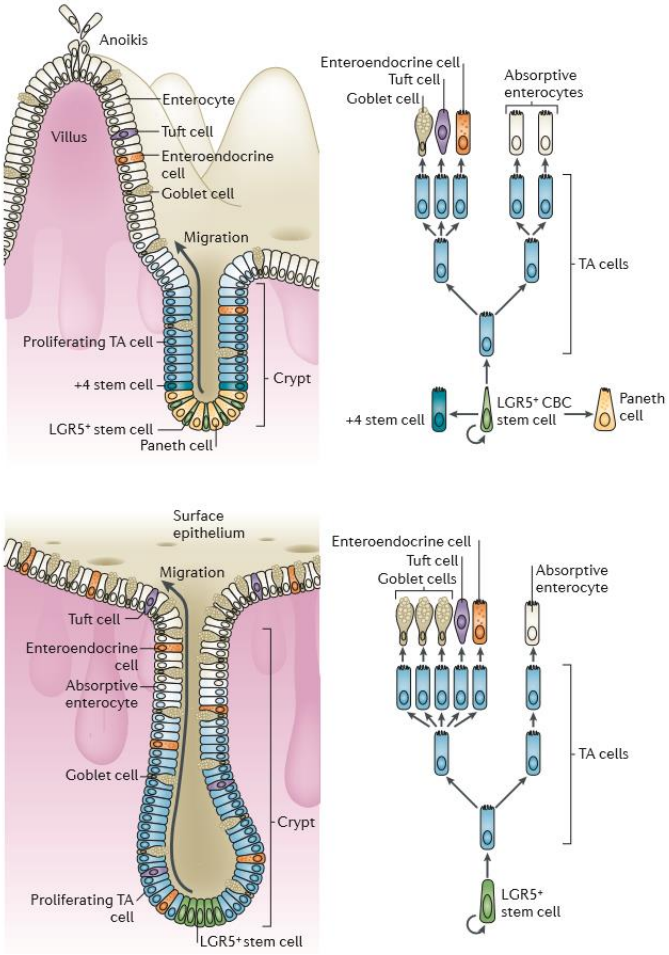

Figure 1: Structure and cellular composition of the intestinal epithelium. In the small intestine (upper panel), the surface area is enlarged by the formation of villi and crypts. At the crypt base, Lgr5+ stem cells are located, which are interspersed with Paneth cells. The 4+ stem cells can restore the stem cell compartment, subsequent to injury. The progeny of dividing stem cells are transit-amplifying (TA) cells, which differentiate into the various epithelial cell types (enterocytes, enteroendocrine cells, Tuft cells, Goblet cells and Paneth cells). If the cells reach the tip of the villus, they get detached from the extracellular matrix (ECM) and are shed into the gut lumen, where they die via anoikis. The colon (lower panel) displays a flat luminal surface, possessing only crypts. Here, TA cells differentiate into enterocytes, enteroendocrine cells, Tuft cells, and Goblet cells, whereas Paneth cells are absent in the colon. Image was taken with permission from Barker, Nat Rev, 2014.

of the receptor complex. The structure of Lgr5 with its seven transmembrane domains resembles the one of Frizzled receptors. Lgr5 binds the Wnt agonists R-spondin 1–4 (roof plate-specific spondin), resulting in full Wnt activation in intestinal stem cells[9,10]. The exclusive expression of Lgr5 enables its application as marker for intestinal stem cells[11]. The second pathway being active in the stem cell niche is the Notch signaling pathway. The Notch receptor displays an extracellular ligand binding-, a transmembrane- and an intracellular domain. Binding of the ligands Dll1 and DII4, which are expressed on neighboring Paneth cells, induces proteolytic cleavage and release of the intracellular domain, which translocates into the nucleus where it modifies gene expression. If Notch signaling is interrupted, stem cells and TA cells preferentially differentiate into secretory cells at the expense of the absorptive cell population[12]. In order to keep the different cellular subsets balanced, some secretory precursor cells up-regulate DII1 on their own surface. In this way, surrounding TA cells experience active Notch signaling during differentiation, what finally leads to enterocyte development[13]. Stem cell proliferation is promoted by the mitogenic effect of EGF signaling. Upon ligand binding, the EGF receptor transmits the signal via the Mek/Erk (mitogen-activated protein kinase kinase /extracellular signal-regulated kinases) signaling axis. Activated Erk subsequently phosphorylates transcription factors like c-myc and c-Fos, leading to the activation of a genetic program that supports proliferation[14]. Unlike the mentioned pathways, BMP (bone morphogenetic protein) signaling is active in the villus compartment. Binding of BMP to its receptor, induces mobilization and complex formation of members of the SMAD (mothers against decapentaplegic) protein family. Subsequent to their translocation into the nucleus, they repress stemness genes. The aberrant expression of the BMP inhibitor Noggin in villi, results in ectopic crypt formation, underlining the importance BMP signaling has for intestinal epithelial cell (IEC) differentiation[15].

Since the ablation of Paneth cells is not sufficient to terminate stem cell-driven tissue homeostasis in the intestine, there seem redundant sources for the production of niche factors. In the colon, where Paneth cells are generally absent, stem cell associated goblet cells might be the crucial niche components[16].

1.2 Colorectal Cancer

1.2.1 Epidemiology, Classification and Treatment

Colorectal cancer (CRC) is one of the most frequently diagnosed cancers throughout the world, with an estimated incidence of 1.4 million cases per year. In addition, it is a main cause for cancer related death in humans[17]. Due to a higher prevalence of risk factors like obesity and smoking in developed countries, incidences are especially high in Australia/New Zeeland, Europe and Northern America

and lowest in countries of South-Central Asia and Western Africa[17]. The noted increase in previously low-risk countries like Japan or Slovakia is most likely correlated with the adoption of western dietary and lifestyle[18]. Another reason for higher incidences in developed countries is the higher average age of western societies. 70 % of patients with CRC are diagnosed in an age of 50-80 years[19]. Besides sociodemographic and lifestyle factors, also disease-related factors like diabetes[20] and inflammatory bowel disease[21] increase the risk of intestinal tumor formation. Inherited forms of CRC, with known mutational patterns, such as Lynch syndrome (non-polyposis colon cancer) and FAP (familial adenomatous polyposis), account for only 3-5 % of all cases. The contribution of other genetic factors like single nucleotide polymorphisms (SNPs) and their interaction with environmental modalities is still not very well understood[22]. Despite high incidence rates, estimated mortality is decreasing in a large number of countries. This is most probably due to improvements in population screening and treatment[23,24]. Patient prognosis mainly depends on the tumor stage at the time of diagnosis. Compared to patients diagnosed with CRC in a localized stage, the presence of distant metastasis declines five-year survival rates from over 90 % to 12 %[25]. Due to the venous drainage, colon cancer metastasizes most often into the liver, whereas deep rectal cancer most commonly spreads into the lung. In rare cases, distant metastases can also affect bones and brain[26]. The general classification is done according to invasion depth at the primary tumor side (T stage), lymph node involvement (N stage) and the appearance of distant metastasis (M stage). In order to include not only the spreading of tumor cells, but also their malignancy, the UICC (Union Internationale contre le Cancer) society defined disease stages, which are all based on the TNM staging but slightly differ between tumor entities. For CRC, the UICC defined the following stages: *UICC stage 0*: Tumor *in situ,* which has no contact to vasculature or the lymphatic system. *UICC stage 1*: Tumor entered the connective tissue (T1) or even the musculature (T2), but lymph node and distant metastases are absent (N0, M0). *UICC stage 2*: Tumor reached the outer intestinal wall (T3) or already entered neighboring tissue (T4), whereas lymph node and distant metastases are still absent (N0, M0). *UICC stage 3*: Lymph nodes, but not distant organs are affected (N1, M0). *UICC stage 4*: Occurrence of distant metastasis (M1)[27].

Dependent on the staging, therapeutic approaches are determined and range from surgical resection of tumors in early stages to chemotherapeutical treatment as (neo)adjuvant therapy of late stage tumors. Chemotherapeutic regimens often contain a combination of the pyrimidine analog 5-fluorouracil (5-FU)[28] and the platinum-based agent oxaliplatin[29], or a combination of 5-FU and the Topoisomerase-inhibitor Irinotecan[30]. Furthermore, classical chemotherapy can be accompanied by the administration of antibodies against EGFR (epidermal growth factor receptor) or against VEGF (vascular endothelial growth factor). Antibody-mediated blockage of EGFR leads to an inhibition of its downstream signaling, which normally induces cellular survival and

proliferation[31]. Capturing of VEGF prevents neo-angiogenesis, that is crucial for the survival of growing tumors. Patients with deep rectal carcinomas sometimes benefit from a neoadjuvant radiotherapy, that increases the chance of preserving the anal sphincter.

1.2.2 Molecular Pathogenesis

Most colorectal tumors occur in a sporadic manner and develop from premalignant lesions in the "adenoma-carcinoma sequence" (Figure 2). This model, first postulated by Vogelstein and co-workers, describes the multistep process of malignant transformation and its characteristic driver-mutations.

An early event in CRC development is a mutation of the APC gene, occurring in more than 70 % of colorectal adenomas[32]. Via destabilization of ß-catenin, APC acts as a negative regulator of the Wnt-signaling pathway[33]. Wnt target genes allow cell cycle progression and are normally activated in replicating stem cells and progenitor cells located at the crypt base. Their constitutive activation leads to continuous proliferation with subsequent cellular outgrowth.

Other factors relevant for cellular growth and differentiation are the monomeric GTPase KRAS (Kirsten rat sarcoma viral oncogene homolog) and its downstream effector BRAF (v-Raf murine sarcoma viral oncogene homolog B).

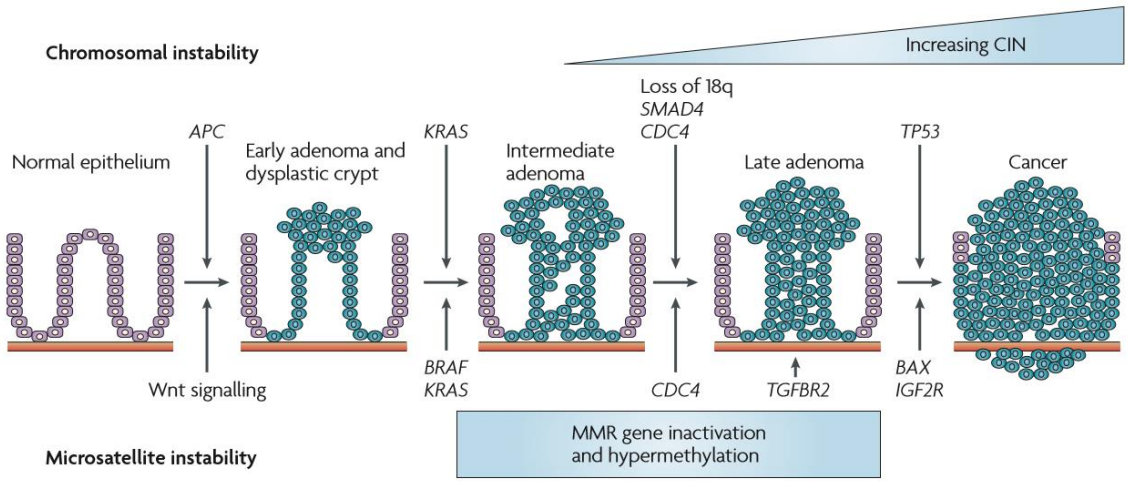

Figure 2: The adenoma-carcinoma sequence. During the course of malignant transformation, intestinal epithelial cells accumulate characteristic driver-mutations like the initial loss of APC (adenomatous polyposis coli) and gain-of-function mutations in KRAS or BRAF, leading to a continuous conveyance of pro-survival and proliferation signals. Later on, loss-of-function mutations occur in the TP53 gene and chromosome 18q is frequently lost due to chromosomal instability (CIN). Microsatellite instable (MSI) CRCs are characterized by a deficient DNA mismatch repair (MMR) system. They often carry a slightly different set of mutations than CIN CRCs, with first alterations in the Wnt-signaling and a higher frequency of BRAF instead of KRAS mutations. Subsequently, altered microsatellites often occur in the genes coding for the TGFß receptor 2 (TGFBR2), the insulin-like growth factor 2 receptor (IGF2R) and Bax. Image was taken with permission from Walther et al., Nat Rev, 2009.

Approximately 30-40 % of colorectal tumors show mutated KRAS, leading to a permanent activation of the Mek/Erk signaling pathway[34].

The accumulation of driver mutations is often accompanied by chromosomal instability (CIN), depicted by aberrant chromosome numbers or structural changes. This process can lead to the loss of alleles (loss of heterozygosity), with the remaining ones often being hit by a mutation. Frequently, genes on the long arm of chromosome 18 (18q21) are affected. In this region the gene encoding for the transmembrane protein DCC (deleted in colorectal cancer) is located. Since it inhibits proliferation in the absence of its ligand Netrin-1, it has a conditional tumor suppressor function[35]. Another gene located on 18q encodes for SMAD4, which is a downstream target of the Mek/Erk pathway[36]. As described for KRAS mutations, activation of this signaling pathway promotes survival and proliferation. When it finally comes to the transition from the adenoma to the carcinoma stage, loss-of-function mutations in the TP53 (tumor protein p53) gene are common[37]. In case of DNA damage, the p53 protein induces cell cycle arrest in order to facilitate DNA repair or initiates cell death if the correction is not successful. Besides the adenoma-carcinoma sequence, two other pathways of genomic instability, namely microsatellite and epigenetic instability, have been reported in CRC.

Microsatellite instability (MSI) is frequently caused by a deficient DNA mismatch repair (MMR)[38]. This mechanism senses and repairs errors in the nucleotide assembling, which can occur during DNA replication. Especially repetitive DNA segments, also known as microsatellites, are error prone due to slippage of the DNA polymerase. The frequency of instable microsatellites is therefore used as an indicator for defects in the MMR system and for further classification into microsatellite high (MSI-H: ≥ 30% of markers instable) and microsatellite low (MSI-L: < 30% of markers instable) tumors. Tumors with a proficient MMR are defined as being microsatellite stable (MSS). MMR deficiencies can occur sporadic or as a result of germline mutations in MMR genes like MLH1 (mutL homolog 1) or MSH2 (mutS homolog 2) [39]. The latter one leads to Lynch syndrome development, as an inherited form of CRC[40]. Patients with MSI-H (MSI high) colorectal cancer have a better prognosis than patients with microsatellite stable tumors. This correlation is partly attributed to a higher immunogenicity of MSI tumors, resulting from a MMR-deficiency induced generation of frameshift antigens[41]. Therefore, MSI-H tumors often display a high density of tumor-infiltrating lymphocytes[42]. Currently a scoring system, taking type, distribution and density of tumor-infiltrating lymphocytes in account, is developed as refinement of the conventional TNM classification[43]. In a recent approach, T-cell function in MSI-H tumors is boosted by the application of immune checkpoint inhibitors. Especially the utilization of an inhibitor targeting the PD-1 (programmed death) pathway in T_{h1} cells, which normally decreases T-cell mediated cytotoxicity, seems promising[44].

Epigenetic instability can cause changes in protein expression without altering the nucleotide sequence. Therefore, it has been proposed as an alternative mechanism of gene silencing in the course of malignant transformation. Promotor regions commonly contain repetitive CpG islands (Cytosine-Guanosin dinucleotide), to which methyl groups can be attached. Methylation of the promotor region typically represses gene transcription. Thus, tumor suppressor genes can be transcriptionally inactivated by promotor hypermethylation, defining the CpG island methylator phenotype (CIMP)[45]. CIMP in addition to an activating BRAF mutation characterizes a subclass of colorectal tumors typically found in the proximal colon[46] and evolved from sessile serrated adenomas. These tumors frequently display high levels of microsatellite instability, provoked by exceeding MLH1 gene promotor methylation[47].

1.3 Programmed Cell Death

First descriptions of the concept of naturally occurring cell death date back to the nineteenth century. In a monograph, published in 1842, Carl Vogt described cell death occurring in the notochord of metamorphic midwife toads[48]. Emanating from this observation it took more than a hundred years to perceive cell death as genetically determined and actively controlled cellular decay, termed programmed cell death (PCD) [49]. In the 1970s the newly developed electron microscopy allowed Kerr, Wyllie and Currie to distinguish different cell death forms for the first time by means of their ultrastructural hallmarks[50]. They coined the word “apoptosis” to describe morphological changes displayed by cells which undergo programmed cell death. These cells display characteristics like cytoplasmic shrinkage, nuclear condensation (karyopyknosis) and membrane blebbing. “Necrosis”, by contrast, describes a mode of uncontrolled cell death, induced by acute cellular injury that leads to cellular swelling and rupture[50].

Closer investigation of signaling pathways contributing to PCD, revealed autophagy and necroptosis as additional modes of controlled cell death, apart from apoptosis. The remarkable complexity and fine control of cellular death, points to the importance PCD has for maintaining tissue homeostasis. Therefore, unbalanced cell death is a key factor in the development of divers pathologies. In addition, altruistic cell death is important during development of all multicellular organisms. In the course of vertebrate embryogenesis, for example, interdigital cells are removed by programmed cell death[51]. In the mature stage, exceeding cell death can cause neurodegenerative disorders like Parkinson´s or Alzheimer´s disease[52]. Insufficient cell death, on the other hand, can be responsible for autoimmune diseases or cancer development[53]. A better dissection and understanding of the molecular pathways responsible for cell death prevention in malignant tissues is hence a prerequisite for therapy improvement.

1.3.1 Apoptosis

Among all modes of PCD, apoptosis is the most prominent and best studied one. It is a highly conserved process which can be triggered by a plenty of stimuli. These stimuli can be subdivided into external ones like binding of death ligands, such as TNFα (tumor necrosis factor alpha), and internal ones like exceeding DNA damage or protein aggregation in the cytoplasm. Depending on the kind of initiating trigger, apoptosis can therefore be executed via the extrinsic or the intrinsic signaling pathway. Both pathways depend on the activation of caspases which are the main players, responsible for amplifying the apoptotic signal and executing cellular destruction. The release of granzyme B-containing granules by cytotoxic T-lymphocytes (CTLs) or natural killer (NK) cells, represents a third mode of caspase activation. In humans, the caspase family contains 13 members which are expressed as inactive zymogens in almost all cells[54,55]. They belong to the class of cysteine proteases and cleave their substrate after aspartic acid residues, to what the name "c-aspase" refers to. With regard to their function, caspases are broadly divided into apoptotic initiator (caspase 2, -8, -9, -10), apoptotic effector (caspase 3, -6, -7) and inflammatory caspases (caspase 1, -4, -5, -11, -12S/L). Caspase 14 expression is mainly confined to epithelial cells and seems important for keratinocyte terminal differentiation[56]. By contrast to inflammatory caspases, initiator and effector caspases induce and execute apoptosis as an immunologically silent mode of cell death. All caspases have a similar structure, comprising a pro-peptide followed by a C-terminal protease effector domain, containing a large and a small subunit. The pro-domain of the inflammatory caspases and of caspase 9 as initiator of the intrinsic apoptotic pathway, is known as "caspase activation and recruitment domain" (CARD)[57]. The pro-domain of caspase 8 and 10, as initiators of the extrinsic apoptotic pathway, contains "death effector domains" (DEDs)[58]. The zymogens get activated by proteolytic separation and subsequent close reassembly of the large and small subunit. In case of effector caspases, this cleavage is carried out by initiator caspases, whereas initiator caspases get auto-activated. Activated effector caspases orchestrate the demolition of the cell and thereby induce its characteristic phenotypical changes. Cleavage of actin microfilaments and microtubular proteins as major components of the cytoskeleton, contributes to membrane blebbing and retraction of the cell. Especially proteolytic activation of the Roh effector ROCK1 (Rho associated coiled-coil containing protein kinase 1), a regulator of actin cytoskeleton dynamics, seems important for this process[59]. Since the actin cytoskeleton has an additional role in maintaining the nuclear envelope, ROCK1 activation also initiates nuclear fragmentation[60]. This gets supported by the caspase-mediated disintegration of the nuclear lamina[61]. Cellular rounding and retraction is further promoted by the proteolytic degradation of adhesion molecules including β and γ-catenin as well as cadherins[62,63]. In addition, caspase activity leads to the loss of cytoplasmic membrane symmetry with subsequent exposure of phosphatidylserine (PS) on the membrane

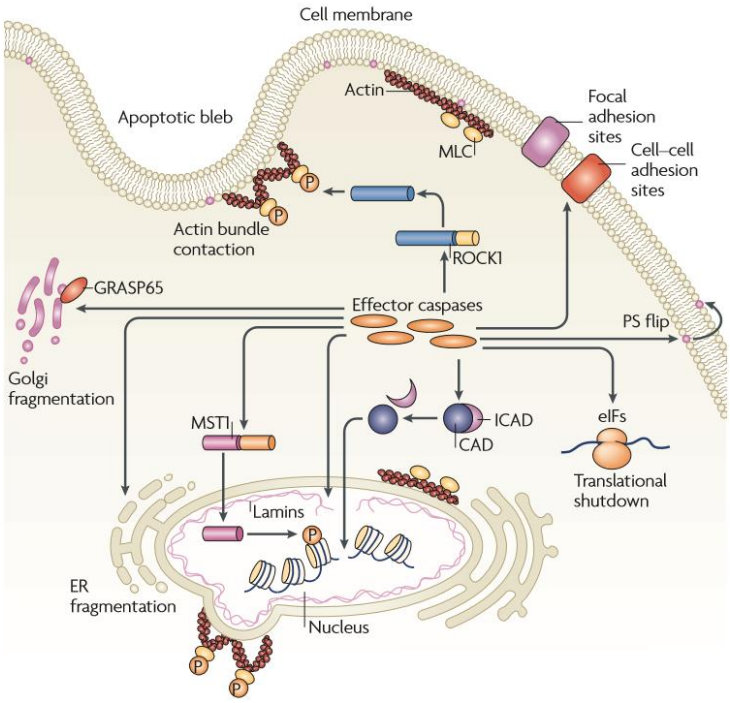

Figure 3: Caspase-mediated cellular decomposition. During apoptosis, effector Caspases get activated, which then mediate the proteolytic shutdown of the cell. Nuclear fragmentation gets executed by cleavage of the nuclear lamina and the inactivation of ICAD (inhibitor of caspase activated DNase), which in turn releases the DNase CAD (caspase-activated DNase). Furthermore, active Caspases are required for the exposure of phosphatidylserine (PS) on the membrane surface and the proteolysis of adhesion proteins, both facilitating the removal of apoptotic corpses by phagocytes. Organelles like Golgi and ER get fragmented by cleavage of stacking proteins and by proteolysis of factors important for transcription and translation, protein synthesis gets terminated. Cleavage of cytoskeletal components and the Rho effector ROCK1 leads to membrane blebbing and the formation of apoptotic bodies. Together, the Caspase-mediated proteolytic events cause morphological changes which are characteristic for apoptotic cells. Image was taken with permission from Taylor et al., Nat Rev, 2008.

surface. The newly exposed phospholipid serves as an uptake signal, facilitating the removal of apoptotic corpses by phagocytes[64]. Besides the induction of all these structural changes, activated caspases also shut-off essential housekeeping mechanisms and life-supporting systems in the cell. In this context, one of the main processes is DNA condensation and fragmentation. It facilitates clearance and prevents the release of DNA into the extracellular space, what could provoke autoimmune responses[65]. Initial chromatin condensation is preluded by histone 2B (H2B) phosphory-lation[66]. Since the responsible kinase MST1 (mammalian sterile20) needs proteolytic activation, this event is also caspase-dependent[67]. The final DNA disintegration is executed by the endonuclease CAD (caspase-activated DNase). Caspase -mediated cleavage of ICAD (inhibitor of caspase activated DNase) liberates CAD, which subsequently catalyzes the inter-nucleosomal DNA fragmentation[68]. Other levels of cellular closedown are caspase-mediated degradation of factors important for transcription and translation[69], as well as the fragmentation of cellular organelles, such as the Golgi apparatus and the endoplasmatic reticulum (ER). Destabilization of the Golgi seems to involve proteolysis of the stacking protein GRASP65 (Golgi reassembling and stacking protein)[70]. In late apoptotic stages, redistribution of the ER supports apoptotic bleb formation, which is important for chromatin enclosure[71]. Even though the mitochondrial network gets also dismantled during apoptosis, caspases seem to play a minor role in this process. Instead, conformational changes of two pro-apoptotic members of the Bcl-2 (B-cell lymphoma 2) protein family and their assembly into mitochondrial pores, appear to be responsible for mitochondrial fragmentation[72]. The formation of pores in the outer mitochondrial membrane

(OMM) and the following release of soluble proteins from the mitochondrial intermembrane space is called mitochondrial outer membrane permeabilization (MOMP) and it is the central step in the initiation of the intrinsic apoptotic signaling pathway.

1.3.1.1 Intrinsic Apoptosis

This mode of apoptotic cell death can be induced by a plethora of intracellular stressors, such as high amounts of reactive oxygen species (ROS), DNA damage, cytosolic Ca^{2+} overload or accumulation of misfolded proteins. Despite the heterogeneity of initiating stimuli, they all converge at the outer mitochondria membrane. There, all further events are orchestrated by members of the Bcl-2 protein family. The Bcl-2 gene was first discovered at the breakpoint region of a frequent chromosomal translocation in human B-cell follicular lymphomas, where its transcription becomes enhanced[73,74]. In comparison to other oncogenes, Bcl-2 does not increase cellular proliferation but inhibit apoptotic cell death[75]. Later on, other family members sharing homologous domains with Bcl-2 (BH domains) have been discovered. With regard to their structure and function, three distinct subgroups can be defined.

Members of the first subgroup, such as Mcl-1 (myeloid cell leukemia sequence 1), Bcl-x_L (B-cell lymphoma extra-large) and Bcl-2 itself, display anti-apoptotic function. They share four homology domains (BH1-4) and are mainly integrated into the outer mitochondrial membrane where they maintain membrane integrity by directly inhibiting their pro-apoptotic relatives from the second subgroup. Pro-apoptotic proteins were originally described to contain three BH (BH1-3) domains but structure-based alignment with other Bcl-2 family members redefined the BH4 domain as a structural motif present in both pro- and anti-apoptotic members[76]. The group of anti-apoptotic effectors comprises the pore-forming factors Bax (Bcl-2-associated X protein) and Bak (Bcl-2 antagonist/ killer) as well as Bok (Bcl-2-related ovarian killer protein). Even though, the latter one displays similar domain architecture to Bax and Bak, there is only little evidence that it is also an effector showing resembling function. Under physiological conditions, Bax and Bak are sequestered and thereby inhibited by their anti-apoptotic kin. BH3-

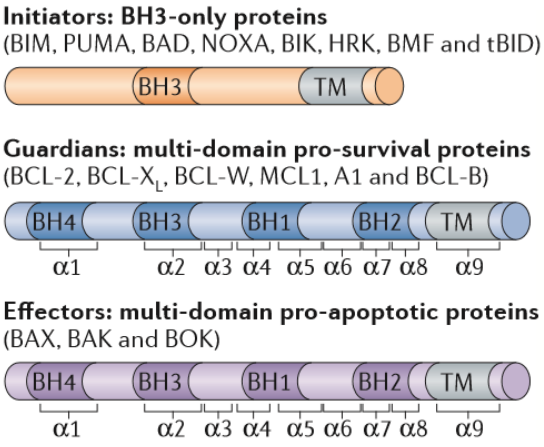

Figure 4: Subgroups of the Bcl-2 protein family. With regard to their structure and function, three subgroups have been defined. The pro- and anti-apoptotic groups share four Bcl-2 homology (BH) domains, whereas the BH3-only proteins only possess the third out of four homology domains. Most family members additionally contain a transmembrane (TM) domain, which allows their attachment to mitochondria. Image was taken with permission from Czabotar et al., Nat Rev, 2014.

only proteins, such as BID (Bcl-2-interacting domain death agonist), BIM (Bcl-2-interacting mediator of cell death) and BAD (Bcl-2 antagonist of cell death), build the third subgroup. They only possess the third out of four homology domains, as their name indicates. Since BH3-only proteins are transcriptionally or posttranscriptionally induced by cytotoxic signals, they work like a molecular switch, sensing and integrating the cellular stress level. If a critical threshold is reached, BH3-only proteins induce mitochondrial activation by two mechanisms[77]. They either can bind to and thereby neutralize anti-apoptotic proteins[78] or directly activate the pro-apoptotic ones[79]. For neutralization, BH3-only proteins bind with an amphipathic helix, located in their BH3 domain, to the hydrophobic groove of anti-apoptotic proteins[80]. Due to slight differences in their BH3 domains and in the binding grooves of their anti-apoptotic partners, some BH3-only proteins like BAD and NOXA are selective for specific anti-apoptotic proteins, whereas others like BIM, PUMA and tBid exhibit a broader range of action[81]. Besides the indirect activation of Bax and Bak via inhibition of anti-apoptotic proteins, some BH3-only proteins (e.g. BIM and BID) are capable to directly induce Bax and Bak oligomerization and thereby mitochondrial activation[82]. Generally, Bak is located at the outer mitochondrial membrane, positioned by its transmembrane domain[83], whereas Bax shows a primarily cytosolic distribution with a smaller subset being also associated with mitochondria. Apoptotic stimuli shift the ratio of soluble and membrane bound Bax, leading to its accumulation at the outer mitochondrial membrane[84]. Here, the formerly inert monomers Bax and Bak exhibit conformational changes and build membrane perforating homo-oligomers. Despite crystallographic studies, the exact molecular structure of the emerging pores is unknown so far[85]. Since the loss of one pro-apoptotic effector induces no phenotype, the roles of Bax and Bak for MOMP induction seem largely redundant. By contrast, a combined loss of Bax and Bak leads to apoptosis inhibition in many cell types and impairs proper tissue development[86,87].

In most cases, permeabilization of the outer mitochondrial membrane is a point of no return, since it has multiple lethal consequences. Because the membrane potential ($\Delta\psi_m$) cannot longer be maintained, the depending process of mitochondrial ATP synthesis gets aborted. In addition, apoptosis-promoting factors, such as cytochrome c, AIF (apoptosis-inducing factor), endonuclease G, SMAC (second mitochondria-derived activator of caspases)[88] and HtrA2 (high temperature requirement protein A2), get released from the intra-membrane space (IMS). Both dissipation of $\Delta\psi_m$ and loss of cytochrome c, leads to the inhibition of the respiratory chain and subsequently to overproduction of ROS. In the cytosol, cytochrome c fosters conformational changes of the soluble factor APAF1 (Apoptotic protease activating factor 1), leading to its assembly and the formation of a heptameric structure, called apoptosome. The apoptosome recruits pro-caspase 9 and induces its activation through conformational changes or autocatalytic cleavage[89,90] and thereby initiates the proteolytic cascade that ends in cellular decomposition[91]. But even in the absence of caspase

activity, MOMP induces cell death, albeit with slower kinetics than in the caspase-driven mode. In this context, AIF and endonuclease G play an important role, since they are capable to translocate into the nucleus and mediate DNA fragmentation in a caspase-independent manner[92,93]. SMAC and HtrA2 promote apoptosis via inhibiting the anti-apoptotic function of members of the IAP (inhibitors of apoptosis) protein family, such as XIAP (X-linked IAP), which normally bind and thereby neutralize certain caspases[94,95]. The pro-apoptotic mechanisms induced by MOMP display a notable redundancy and their necessity and relative contribution in the execution of intrinsic apoptosis seem to vary in different organismal and cellular scenarios.

1.3.1.2 Extrinsic Apoptosis

This apoptotic modality can be provoked by the binding of lethal ligands, such as FAS ligand (FASL also known as CD95L), TNFα and TRAIL (TNF-related apoptosis inducing ligand also known as TNFSF10) to their respective death receptors. The six death receptors described until now are FAS (APO-1/CD95)[96], TNF-R1 (CD120a)[97], TRAIL-R1 (DR4)[98], TRAIL-R2 (APO-2/DR5/KILLER/TRICK2)[99], DR3 (APO-3/LARD/TRAMP/WSL1)[100] and DR6[101]. Together they build a subclass of the tumor necrosis factor receptor superfamily, whose members mediate diverse processes like proliferation, differentiation and cell death[102]. Characteristically, death receptors display an extracellular ligand-binding domain, a transmembrane domain and an intracellular protein-protein interaction domain, called death domain (DD). The DD comprises a conserved sequence of 80-100 residues which form a bundle of six α-helices[103,104]. In comparison to death receptors, dependence receptors dispatch pro-apoptotic signals in the absence of their ligand. An example for this class is the netrin-1 receptor DCC, which is frequently lost during malignant transformation of intestinal cells, as the name indicates[105,106].

The probably best characterized death receptor-mediated signaling cascade is the prototypic pathway elicited by FASL binding. With the discovery of FAS (TNF receptor superfamily member 6) in 1989, the first surface receptor, capable of inducing cell death, was found[107,108]. In the absence of its ligand, FAS assembles to generate loose trimeric complexes which get stabilized upon ligand binding. FASL gets primarily expressed as a surface protein on cytotoxic T-cells and NK-cells, but a soluble version can be produced by its MMP7 (matrix metalloproteinase 7) -mediated truncation[109]. Subsequently to ligand binding, a conformational change of the receptor subunits gets initiated, allowing the assembly of a multiprotein complex called DISC (death inducing signaling complex) at the cytosolic tail of the receptor. Via its own DD, the adaptor molecule FADD (FAS-associated protein with a DD) gets recruited and bound to the activated receptor[110]. In addition to its DD, FADD contains a death effector domain (DED) which in turn is important for the recruitment and sequestering of pro-caspase 8 or -10 to the resulting supramolecular complex where they get

autoproteolytically activated[111,112]. The following cascade exhibit varieties in different cell types. In "type I cells", such as lymphocytes, the activated initiator caspases directly mediate the proteolytic maturation of effector caspase 3 and -7 without mitochondrial commitment. In "type II cells" like hepatocytes and pancreatic β cells, activated caspase 8 cleaves and thereby activates the BH3-only protein BID [113]. tBID (truncated BID), as the emerging cleavage product, bridges the extrinsic and the intrinsic apoptotic pathway by fostering mitochondrial membrane permeabilization[114]. In contrast to type II cells, which depend on mitochondrial activation, type I cells can also show MOMP but they do not rely on it for proper cell death execution.

c-FLIP (cellular FLICE/caspase-8-inhibitory protein) can inhibit death receptor stimulated apoptosis by binding to the DISC via its own DED whereby pro-caspase 8 binding is competitively inhibited. c-FLIP is expressed as long (c-FLIP$_L$), short (c-FLIP$_S$), and c-FLIP$_R$ splice variants, which have been shown to even upregulate cytoprotective and pro-survival signaling proteins including Akt (also known as protein kinase B), Erk and NF-κB (nuclear factor kappa-light-chain-enhancer of activated B cells)[115]. Subsequent to strong receptor stimulation or in presence of high c-FLIP$_S$ and c-FLIP$_R$ levels, c-FLIP$_L$ can also act in a pro-apoptotic manner by promoting pro-caspase 8 activation[116]. Previous to auto-proteolytic activation, pro-caspase 8 shows a very restricted substrate range, including only itself and c-FLIP. Two pro-caspase 8-mediated cleavage products of c-FLIP, namely p43-FLIP and p22-FLIP, have been reported. They both induce NF-κB signaling by activating the enzyme IKK (IκB kinase)[117]. IKK-mediated phosphorylation of IκB (inhibitor of NF-κB) leads to its degradation and the release of NF-κB, which subsequently translocates to the nucleus. In its role as transcription factor, NF-κB upregulates the expression of anti-apoptotic proteins, such as Bcl-2[118], c-FLIP[119] and IAPs[120].

Whereas ligand binding to TRAIL-R1 and TRAIL-R2 induces events similar to those following FAS activation, stimulation of TNF-R1 (TNF receptor 1) leads to the recruitment of a slightly different set of proteins. First of all, the adaptor molecule TRADD (TNF-R associated death domain) and the kinase RIP1 (receptor interacting serine/threonine kinase 1) get recruited to the DD of the receptor. TRADD then binds TRAF2 (TNF-R associated factor 2), which in turn recruits cIAP1 and cIAP2 (cellular inhibitor of apoptosis). In the emerging supramolecular complex, called "complex I" (or TNF-R1 signaling complex), RIP1 gets polyubiquitinated by these two. Subsequently, IKK and its activator TAK1 (TGF-beta activated kinase 1) get recruited to the newly synthesized, Lys63-linked polyubiquitin chain, what finally leads to the induction of the NF-κB signaling pathway[121]. In a process, which is not yet fully understood, a second complex assembles in the cytoplasm, temporally following complex I formation. This so called "complex II" contains TRADD and TRAF2 but not the receptor itself anymore. Via the DD of TRADD, FADD gets recruited, what is followed by binding of other DISC components, such as pro-caspase 8 and -10 as well as c-FLIP[122]. Since the signaling transmitted by complex I increases the expression of pro-survival factors like c-FLIP via

NF-κB activation, complex II-induced cell death is normally prevented. Only if complex I is prematurely decomposed, TNF-R1 signaling culminates in apoptosis execution[123].

1.3.2 Autophagy

Macroautophagy (hereafter referred to as autophagy) is an evolutionary highly conserved catabolic process, which allows cells to recycle excess or dysfunctional content and refuel energy reservoirs. The concept relies on the sequestration and engulfment of cellular content by double-membrane vesicles, called autophagosomes. In a second step, autophagosomes fuse with lysosomes and in the acidic milieu the emerging autolysosomes provide, their cargo gets degraded by hydrolases. Autophagy gets classically induced by starvation or nutrient deprivation and plays thereby a cytoprotective role under unfavorable conditions. On the other hand, dysregulated or excessive induction of autophagy may lead to cell death. Due to the high relevance autophagy genes have for cell death and other fundamental processes, such as proliferation and immune response, it has been associated with various pathologies, including cancer, neurodegenerative disorders and autoimmune conditions[124].

Even though the term "autophagy", what literally means self-eating, was coined already in the sixties by the Nobel Prize-winner de Duve, understanding of the exact molecular processes has begun only a decade ago. Since then, more than 30 autophagy-related genes (Atg) have been discovered in yeast (mainly Saccharomyces cerevisiae), followed by the identification of respective homologues in higher eukaryotes[125]. A subset of these Atg proteins, called core molecular machinery, is essential for autophagosome formation and comprises distinct groups: The ULK complex (unc51-like kinase), which is responsible for autophagy induction, the PI3KC3 complex (class III phosphatidylinositol 3-kinase), which is important for membrane nucleation, Atg9 and VMP1 (vacuole membrane protein 1), which probably recruit lipids to the isolation membrane and two ubiquitin-like conjugation systems, which are necessary for autophagosomal membrane expansion and vesicle closure[126]. All these different complexes get recruited to the side of autophagosome formation, termed phagophore assembly side (PAS), where pro-autophagic signals converge at the level of mTORC1 (mammalien target of Rapamycin complex 1). If amino acids and growth factors are available, the PI3KC1 complex (class I phosphatidylinositol 3-kinase) activates mTORC1, which then represses the ULK complex by direct interaction[127]. In the opposite scenario, declining ATP/AMP ratios get sensed by AMPK (AMP-activated protein kinase) which then activates the ULK complex directly by phosphorylation and indirectly by suppressing mTORC1 activity. The ULK complex consists of Ulk1/2, Atg101, FIP200 (focal adhesion kinase family interacting protein of 200 kD) and Atg13, with the latter ones being required for Ulk1 localization to the emerging phagophore[128]. Phagophores develop most frequently at the contact sites between the

endoplasmatic reticulum and mitochondria[129]. But other membranes and organelles like the nuclear and the cytoplasmic membrane as well as the Golgi apparatus may also be a source of lipids for autophagosome formation[130]. If the ULK complex is active under nutrient-deficient conditions, it recruits the PI3KC3 complex to the isolation membrane[131]. This complex consists of Beclin-1, Vps34 (vacuolar protein sorting 34) and Vps15. Upon stimulation, Vps34 produces phosphatidyl inositol 3-phosphate, which is necessary for the nucleation of the phagophore[131]. Via binding to the BH3-domain of Beclin1, the anti-apoptotic proteins Bcl-2, Bcl-x_L and Mcl-1 are capable of inhibiting autophagy induction, while their anti-apoptotic function stays unaffected[132]. Thus, BH3-only proteins not only induce apoptosis, but also enhance the autophagic flux by disrupting the binding between Beclin-1 and their anti-apoptotic relatives (Figure 5). Two factors also important for autophagosome formation are the transmembrane proteins Atg9 and VMP1. Atg9 is normally located in the Golgi network and late endosomes and VMP1 in the plasma membrane but upon autophagy induction, both factors colocalize with the autophagosomal marker proteins Beclin-1 and LC3 (microtubule-associated protein light chain 3). VMP1 most likely supports the recruitment of Beclin-1 and other components of the PI3KC3 complex to the phagophore. Its overexpression is sufficient to induce autophagy even under nutrient-rich conditions[133]. Atg9 cycles between the Golgi, endosomes and autophagosomes, potentially contributing to the delivery of lipids for autophagosomal membrane formation[134]. For the subsequent step of membrane elongation, two ubiquitin-like conjugation systems, both of which contain Atg7, are required. In the first conjugation system, sequential reactions by the E1-like enzyme Atg7 and the E2-like enzyme Atg10 lead to the conjugation of Atg12 and Atg5, which subsequently form a complex with Atg16L1 by non-covalent binding[135]. In the second complex, the conjugation partner LC3 needs first to be cleaved at its C terminus by Atg4. Cleavage leads to the exposure of a glycine residue, which is conjugated to phosphatidylethanolamine (PE) in a successive reaction, mediated by Atg7 and the E2-like enzyme Atg3[136]. The lipidated form of LC3, termed LC3 II, stably associates with

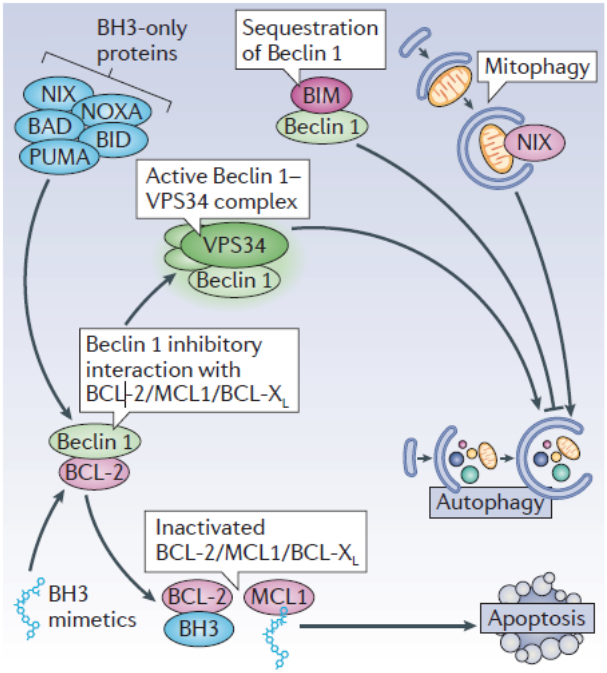

Figure 5: Anti-apoptotic Bcl-2 proteins inhibit autophagy. Via binding to the BH3-domain of Beclin-1, Bcl-2, Bcl-x_L and, to a lower extend, Mcl-1 inhibit autophagy induction. Thus, BH3-only proteins as well as BH3 mimetics are able to enhance the autophagic flux by disrupting the binding between Beclin-1 and their anti-apoptotic relatives. The BH3-only protein BIM seems an exception, because it sequesters and thereby mislocalizes Beclin-1. Image was taken with permission from Marino et al. Nat Rev, 2014.

the autophagosomal membrane. Since LC3 lipidation is considered to be a hallmark of autophagosome formation, the ratio of cytosolic LC3 (LC3 I) and membrane bound LC3 II provides information about autophagic flux intensity[137]. In mammals, the LC3 orthologs GATE-16 (Golgi-associated ATPase enhancer of 16 kDa) and GABARAP (gamma-aminobutyric-acid-type-A-receptor-associated protein), are also conjugated to PE and localize on the expanding phagophore[138]. The Atg12-Atg5 conjugate acts as an E3-like enzyme in the LC3 conjugation system, promoting Atg3 substrate specificity[139]. Consequently, defects in the first conjugation system simultaneously lead to insufficient LC3 lipidation[140]. The molecular function of the LC3–PE conjugate seems associated with hemifusion of autophagosomal membranes. Since LC3-deficient cells exhibit smaller autophagosomes than wild-type cells, this process seems to be required for determining autophagosomal size[141].

Autophagic cargo is often labeled by Lys63-linked polyubiquitin chains, which can be bound by a variety of adaptors, such as sequestosome 1 (SQSTM1 also known as p62). These adaptor molecules contain a LC3-interacting region (LIR), which specifically interacts with LC3 and its orthologs. Thus, organelles and proteins destined for degradation, get directed to nascent autophagosomes. Since p62 and other adaptors are decomposed together with the normal cargo, their abundance enables an indirect measurement of the autophagic flux[137]. In the final stage, the autophagosomal maturation, autophagosomes fuse with lysosomes to form autolysosomes where the cargo gets degraded in order to regenerate nutrients. If subsequently the ATP/AMP ratio increases, mTOR (mechanistic target of rapamycin) gets reactivated and start to attenuate autophagy. In addition, mTOR activity generates proto-lysosomal vesicles that seclude from autolysosomes to restore lysosomal homeostasis in the cell[142].

The autophagic process gets induced by stimuli, such as misfolded proteins, exceeding intracellular Ca2+ concentrations and hypoxia, which would also be capable of initiating apoptosis. Hence, autophagy is often the last attempt to rescue a cell, but cell death is induced if the level of stress exceeds a critical duration or reaches a certain intensity threshold. Due to this, the mere occurrence of autophagosomes in dying cells is not conclusive for an autophagic cell death (ACD). Real ACD can be prevented by autophagy inhibition and final cell death events are mediated by an increased autophagic flux instead of the apoptotic or necroptotic machinery[143]. Studies in mice suggest, that ACD has no essential role in mammalian development and tissue homeostasis but it seems to contribute to pathological or drug-induced cell loss[144–146].

1.3.3 Necroptosis

Originally, necrosis was regarded as an uncontrolled mode of cell death, accidentally induced by physiochemical disruptions and mechanical traumata. However, recent studies identified several

genetically controlled and tightly orchestrated modes of regulated necrosis[147,148], from which necroptosis is the best studied one. Necroptosis can be induced by several triggers, including genotoxic stress like alkylating DNA damage[149] and cytotoxic agents. The ligation of death receptors, such as FAS and TNF-R1, is also capable of inducing necroptosis, if caspase 8 activity is inhibited at the same time[150]. Ligation of the TNF-R1 elicits prototypic necroptotic signaling, which depends on the two key factors RIP1 and RIP3.

Upon ligand binding, complex I assembles at the cytosolic receptor tail and the present cIAPs mediate Lys63-linked polyubiquitination of RIP1. The subsequent activation of NF-κB, upregulates the transcription of anti-apoptotic genes such as TNFAIP3 (TNFα-induced protein 3, also A20) and c-FLIP$_L$. In a negative feedback loop, TNFAIP3 mediates polyubiquitination of RIP1 with Lys48-linked chains, what assigns it for proteasomal degradation. By contrast, CYLD (cylindromatosis) removes the Lys63-linked polyubiquitin chains from RIP1, leading to the dissociation of RIP1 from the receptor and the formation of a cytosolic DISC (complex II), comprising RIP1, RIP3, TRADD, FADD, pro-caspase 8 and c-FLIP[151]. Since the deubiqitination of RIP1 changes its signaling function from pro-survival to pro-death, CYLD acts as a molecular switch, determining cells fate upon TNF-R1 stimulation. If pro-caspase 8 is present in complex II, it gets autoproteolytically activated and this finally leads to cell death execution via the extrinsic apoptotic signaling pathway.

In the absence of pro-caspase 8 or when it is inactivated, RIP1 associates with RIP3, resulting in their auto- and transphosphorylation and formation of a microfilament-like complex, termed necrosome[152]. Accordingly, necroptosis implementation can be abrogated by targeting the kinase domain of RIP1 with the inhibitor necrostatin 1. This compound selectively prevents the interaction between RIP1 and RIP3, but spares the pro-survival role of RIP1 in the NF-κB signaling pathway[153]. Phosphorylation of human RIP3 on Ser227 (or Ser232 in mice) leads to the recruitment of MLKL (mixed-lineage kinase domain-like protein) and its RIPK3-mediated phosphorylation (pMLKL). pMLKL assembles to oligomers, which subsequently translocate to the plasma membrane in order to form membrane disrupting pores by binding to PIP (phosphatidylinositol phosphates). The following influx of Na^+ and Ca^{2+} leads to an osmose-based increase of intracellular pressure, that finally culminates in membrane rupture[154,155].

Since neither RIP3$^{-/-}$ nor MLKL$^{-/-}$ mice display developmental or homeostatic defects, necroptosis seems to play only a minor role in this context, probably as a back-up system if caspases are inhibited. By contrast, the response to various virus infections relies on proper necroptotic signaling. Compared to apoptosis, necroptosis is an immunologically conspicuous process, which mobilizes the immune system. Hence, vaccinia virus infected mice succumb to infection more rapidly if they lack RIP3[152].

1.4 Knockout Mouse Models

The generation of knockout mice by either transgenic or gene-targeted approaches allows detailed analyses of protein functions *in vivo*. Since the constitutive deletion of a gene can cause prenatal lethality or induce various phenotypes in multiple tissues, spatial or temporal control of gene deletion is useful under some circumstances. For this purpose, the Cre/loxP system is applied, allowing conditional deletion of the target gene[156]. A loxP (locus of crossover in P1) site is a nucleotide sequence that comprises a core sequence of 8 base pairs, which determines the orientation, and two flanking palindromic repeats of 13 base pairs each. The Cre (creates recombination) recombinase is an enzyme that belongs to the protein family of integrases and is derived from the bacteriophage P1. It recognizes the specific sequence of loxP sites and is able to catalyze DNA recombination between two loxP sites[157]. Depending on their directionality, the intermediate DNA segment gets either excised or inverted. The Cre recombinase is naturally not existent in mammals and needs transgenic expression in mice. Via choosing a tissue-specific promotor for the respective gene, expression of the Cre recombinase can be spatially restricted. If such a Cre expressing mouse line, is crossbread with a strain harboring the gene of interest flanked by two loxP sites with equal orientation (floxed gene), some of the resulting offspring will carry both the floxed gene and the Cre-expressing transgene. Further crossbreeding of this progeny finally leads to the generation of mice with a tissue-specific knockout, in case the gene of interest was homozygously floxed[158]. Via fusing the Cre recombinase with a mutated ligand-binding domain of the estrogen receptor (CreER), Cre activity can be temporally controlled. In the absence of its ligand tamoxifen, CreER is trapped in the cytosol and thus inactive. The treatment of mice with tamoxifen induces translocation of CreER into the nucleus and the subsequent excision of floxed genes[159].
Intestine specificity of a knockout can be reached by choosing the regulatory region of the murine Villin gene as promotor in charge, being responsible for expression of the Cre recombinase (VilCre). Studies with a VilCre reporter mouse strain revealed that genetic recombination of target genes, and thus Cre expression, gets initiated at day 12.5 of embryogenesis and that it is maintained during entire adulthood. Moreover, the application of a tamoxifen-dependent VilCre reporter mouse line (VilCreER) showed a high persistence of the recombined locus, subsequent to tamoxifen treatment of the mice. Since intestinal epithelial cells have particular high turnover rates, this indicates that intestinal stem cells get targeted as well[160].

1.4.1 Knockout Mice of Bcl-2 Family Members

Genetically engineered mouse models have been a key biological tool for the definition and understanding of different cell death subroutines, going far beyond the morphology-based

differentiation of cell death modalities, used in the beginning. Furthermore, the possibility of spatiotemporally controlled gene deletion enabled researchers to accurately dissect the role of specific cell death-related proteins for development, tissue homeostasis and pathologic processes. *Anti-apoptotic Bcl-2 proteins:* The constitutive deletion of both Mcl-1 and Bcl-x_L results in embryonic lethality. Mcl1$^{-/-}$ embryos die at a very early time point because they fail to implant *in utero*. Interestingly, this is not due to an increased apoptosis rate, but rather to a delayed maturation of the blastocyst, indicating additional roles of Mcl-1 beyond cell death regulation[161]. By contrast, Bcl-$x_L^{-/-}$ embryos survive until day 13.5 of embryogenesis and die from cell death-related defects in hematopoiesis and neuronal development[162]. Although Bcl-2$^{-/-}$ mice are viable, they display growth retardation and a short overall survival of only 1-2 month[163]. They show immune deficiencies due to apoptotic involution of thymus and spleen and get gray fur because of an inefficient melanin synthesis. Finally, Bcl-2$^{-/-}$ mice succumb to polycystic kidney disease, caused by defective renal epithelial cells[164]. Even though there is remarkable endogenous expression of Bcl-2 in the colonic stem cell region, its loss seems to have only limited effects on intestinal tissue homeostasis. One study showed an increased amount of cell death events at the base of colonic crypts, whereas cell death levels in the small intestine were unaffected[165]. The remaining two anti-apoptotic proteins A1 and Bcl-w, seem to play only subsidiary roles for development and tissue homeostasis. In contrast to humans, mice carry four genes encoding A1. A1A$^{-/-}$ mice are essentially normal, except of increased apoptosis rates of their granulocytes and mast cells cultured *ex vivo*[166]. Bcl-w-deficient males display insufficient spermatogenesis and are therefore sterile, but apart from this Bcl-w $^{-/-}$ mice are developmentally normal[167].

Pro-apoptotic Bcl-2 proteins: Neither Bax$^{-/-}$ nor Bak$^{-/-}$ mice display severe developmental or homeostatic deficiencies. Bax-deficient male mice are sterile due to a defect in sperm cell differentiation and both gender show a slight increase in the number of neurons and a mild lymphoid hyperplasia, but otherwise they are normally developed and viable[168]. The only phenotype shown by Bak$^{-/-}$ mice, is a mild platelet hypertrophy[169]. By contrast, the combined loss of Bax and Bak causes aberrant survival of cells which are normally eliminated during embryogenesis and thereby defects like interdigital webs, an imperforate vaginal canal and exceeding numbers of lymphoid and myeloid cells. A remarkable subset of Bax/ Bak double knockout mice die prenatally or directly after birth, indicating a high redundancy in the activity profile of Bax and Bak[87,170].

BH3-only proteins: BH3-only proteins can induce apoptosis by either neutralizing anti-apoptotic proteins[78] or by activating pro-apoptotic ones. The knockout of BIM, PUMA or BID, which are important for the neutralization of anti-apoptotic proteins, results in the development of stronger phenotypes than the loss of BAD, BIK, HrK (activator of apoptosis harakiri), BMF or NOXA, which

promote the activity of pro-apoptotic proteins. Mice displaying a deficiency of one of the activating BH3-only proteins are essentially normal with regard to development, survival and fertility. By contrast, PUMA is crucial for cell death induction subsequent to a variety of apoptotic stimuli, including p53-dependent and -independent ones[171,172]. Furthermore, the loss of PUMA renders mice more resistant to DSS (dextran sodium sulfate)-induced colitis and reduced apoptosis of intestinal epithelial cells[173]. $BIM^{-/-}$ mice display a hyperplasia of lymphoid and myeloid cells, what normally results in the development of a severe autoimmune disease, to which the mice finally succumb[174]. Bid seems most important for the extrinsic apoptosis in "type II cells" like hepatocytes, in which proper cell death execution requires mitochondrial activation. Consistently, $Bid^{-/-}$ mice are resistant to Fas-induced hepatocellular death and fatal hepatitis[175].

1.4.2 Intestine-specific Knockout of Cell Death- and Inflammation-related Proteins

Apoptosis: Intestine-specific deletion of caspase-3 as the most important effector caspase, has no effect with regard to development, cell death rates or morphology of the intestine. This might be due to non-apoptotic cell death pathways, which get activated when caspase-dependent pathways fail[176]. In addition, the relative irrelevance of caspase-3 for intestinal tissue homeostasis could be also explained by the hypothesis that shedding of intestinal epithelial cells is a rather passive process induced by spatial density. By contrast, mice deficient for caspase-8 or FADD, as two central factors in the extrinsic apoptotic signaling pathway, display spontaneous development of terminal ileitis and colitis, accompanied by loss of Paneth cells, reduction of goblet cells, lymphocyte infiltration and enhanced cytokine levels[177,178]. The fact that the loss of an apoptosis-initiating caspase leads to increased epithelial cell death, can be explained by the necroptosis inhibiting function of caspase-8. It has been demonstrated that partial caspase-8 activity, which is too weak for apoptosis induction, is sufficient for necroptosis prevention, mediated by RIP1 cleavage[179,180]. Concordantly, dying cells in intestine-specific caspase-$8^{-/-}$or $FADD^{-/-}$ mice display morphological characteristic, such as organelle swelling and absent chromatin condensation, being typical for a necrotic cell death. This shows that caspase-8 activity needs to be tightly controlled in both directions, in order to maintain intestinal tissue homeostasis. The intestine-specific deletion of c-FLIP, as key regulator of caspase-8 activity, results in cell death induction, lymphocyte infiltration and severe weight loss[181]. The initial cellular response to TNF-R1 stimulation is survival-promoting NF-κB signaling. The disturbance of this signaling pathway by deletion of components of the IKK complex (IKK1, IKK2, NEMO/NF-κB essential modulator) or the IKK complex activating kinase TAK 1 (TGF-β-activated kinase 1) in intestinal epithelial cells, results in cell death induction as default cellular response to TNF and the development of spontaneous colitis[182,183]. Intestinal TAK 1 deletion even leads to direct postnatal lethality, caused by intestinal bleeding[184]. The intestine-specific loss

of Stat3, as a possible target of NF-κB, renders mice more susceptible towards chemically induced colitis and the respective animals show due to increased apoptosis rates, defects in epithelial restitution[185,186].

Necroptosis: A recent study reported elevated levels of RIP3 and MLKL in children with inflammatory bowel disease (IBD)[187]. Until today, no intestine-specific RIP3 or MLKL knockout mouse lines have been generated. However, mice with a constitutive deletion of RIP3 or MLKL are essentially normal with regard to development, survival and fertility[188,189]. Only if challenged by vaccinia virus infection, $RIP3^{-/-}$ mice display an insufficient inflammatory response[152]. By contrast, deletion of RIP1 in intestinal epithelial cells, leads to caspase-8 mediated apoptosis and spontaneous development of severe intestinal inflammation, resulting in a short overall survival[190]. Since RIP1 and caspase-8 negatively regulate each other, the phenotype can be rescued by additional knockout of caspase-8 in IECs.

1.5 Aim of this Work

Colorectal cancer is one of the most frequently diagnosed cancers throughout the world, with especially high incidences in developed countries[17]. In addition, it is a main cause for cancer related death in humans. Despite substantial progress in the development of targeted therapies, patients with metastasized CRC still face a poor prognosis[191]. Since cell death avoidance is a classical hallmark of cancer, the frequently shown overexpression of anti-apoptotic Bcl-2 proteins in diverse tumor entities is comprehensible[192,193]. In CRC, high Bcl-x_L expression has been shown to correlate with lower tumor differentiation and poorer overall patient survival[194]. In contrast, high Bcl-2 levels seem to correlate with a favorable clinical outcome[195]. Since anti-apoptotic proteins have always been described as being redundant, with regard to mitochondria activation, the mentioned findings are contradicting and underline the necessity of a better understanding of their relevance and commitment in CRC. There is growing evidence that anti-apoptotic proteins play also a role in other cellular processes important for cancer initiation and progression, which might provoke the reported differences. For instance, Mcl-1 has been shown to inhibit cell cycle progression via binding of PCNA (proliferating cell nuclear antigen)[196] and CDK1 (Cyclin depending kinase 1)[197]. In addition, it has been implicated in DNA damage repair[198], what further enhances the probability of Mcl-1 having a tumor suppressor role besides its cell death-preventing function.

In a first step, this study aimed at evaluating the expression of anti-apoptotic proteins in human intestinal mucosa, in primary colorectal tumors and in corresponding liver metastases. Furthermore, the influence of Bcl-2, Bcl-x_L and Mcl-1 on malignancy-relevant processes like proliferation, migration and invasiveness should be analyzed *in vitro*. Since the constitutive deletion of both Mcl-1 and Bcl-x_L results in embryonic lethality, the generation of intestine-specific knockout

mice was intended, in order to study protein function in further detail *in vivo*. In a last step it was planned to transfer gained information into a translational approach, testing the clinical value of Bcl-2 inhibitors in a tissue culture system.

Taken together, the objective of this work was to evaluate the role of anti-apoptotic Bcl-2 proteins for intestinal tissue homeostasis and for colorectal tumor initiation and progression in mice and men.

2.1 Cell Culture Methods

All cell culture work was done under laminar flow. The consumables and work materials were autoclaved or disinfected with 70% ethanol (v/v) before use. In the cell culture room gloves and a lab coat were worn routinely.

2.1.1 Cultivation, Thawing and Freezing of eukaryotic Cells

RPMI Medium (Gibco)	*# 61870-010, Thermo Fisher, Schwerte, Germany*
Fetal Calf Serum (FCS)	*# 16000044, Thermo Fisher, Schwerte, Germany*
Penicillin/Streptomycin (10 000 U/ml)	*# P4333, Sigma-Aldrich, Munich, Germany*
Trypsin-EDTA Solution	*# T3924, Sigma-Aldrich, Munich, Germany*
Dimethyl sulfoxid (DMSO)	*# 20385.01, Serva, Heidelberg, Germany*
Phosphate Buffered Saline (PBS) (Gibco)	*# 14190-094, Thermo Fisher, Schwerte, Germany*

Human CRC cell lines HT29 and SW480 were purchased from ATCC (Manassas Virginia, USA). Cells were grown in cell culture flasks as an adherent layer and were maintained in a humidified atmosphere (37°C, 5% CO_2) in RPMI cell culture medium supplemented with 10% FCS and 1% Penicillin/Streptomycin.

Prior to use, all components as well as PBS and trypsin were preheated to 37°C in a water bath to prevent temperature stress. In order to split the cells, culture medium was aspirated and the cells were washed once with PBS and subsequently detached by trypsinization (1 ml trypsin per 75 cm^2) for 5 minutes at 37°C. Afterwards, the trypsin-mediated digestion of cells was terminated by the addition of 9 ml fresh medium and cells were resuspended by gently pipetting up and down with a serological pipet. Cell suspension was transferred into a 15 ml Falcon and centrifuged for 3 min at 200 x g. The trypsin-containing supernatant was discarded and the pellet was again resuspended in 10 ml of fresh culture medium. 1 ml of cell suspension was transferred into a new 75 cm^2 cell culture flask and the total volume was adjusted with fresh and preheated medium to 22 ml. The cells were routinely tested for contaminations and subcultured twice a week.

To prevent high passage numbers (> 20), new vials from the stock were regularly thawed. Therefore, vials were taken out of the liquid nitrogen and kept on dry ice until further processing. Since the high amount of DMSO (dimethyl sulfoxide) in the freezing medium gets cytotoxic at room

temperature, cells were resuspended in 14 ml of cold cell culture medium (4°C). Subsequently cell suspension was transferred into a 15 ml Falcon and centrifuged for 3 min at 200 x g. Supernatant was aspirated and cells were resuspended in 8 ml of fresh and preheated cell culture medium, transferred into a cell culture flask (25 cm^2) and incubated at 37°C.

For the purpose of freezing, cells were grown in a 150 cm^2 cell culture flask until they reached confluency. Afterwards they were detached, centrifuged and resuspended as described already. Total cell number was determined by using a cell counter (BioRad, Munich, Germany). Cells were pelleted again by centrifugation, supernatant was discarded and FCS was added according to the cell number (900 µl FCS per 1×10^6 cells). 900 µl of cell suspension were transferred to each cryovial and supplemented with 100 µl DMSO. Subsequently vials were placed in a cryobox at -80◦C overnight before being transferred to liquid nitrogen for long-term storage. The cryobox contains isopropanol and causes in this way a slow (-1°C/min) freezing of cells in order to prevent cell damage.

2.1.2 Transfection of Cells with siRNA and Plasmid-DNA

Lipofectamine RNAiMAX	*# 13778150, Thermo Fisher, Schwerte, Germany*
Lipofectamine LTX with PLUS Reagent	*#15338100, Thermo Fisher, Schwerte, Germany*
OptiMEM (Gibco)	*# 31985070, Thermo Fisher, Schwerte, Germany*
Phosphate Buffered Saline (PBS) (Gibco)	*# 14190-094, Thermo Fisher, Schwerte, Germany*

One day before transfection $2{,}5\times10^6$ (HT29 and SW480) or $0{,}75\times10^6$ (MEFs) cells were seeded onto a 12-well plate in order to reach a confluency of 70-80 % at the time of transfection.

2.1.2.1 siRNA Transfection

For each well, two reaction tubes containing 125 µl of OptiMEM were prepared. To the first one, 160 nM siRNA were added, whereas the other one was supplemented with 2 µl of Lipofectamin RNAi Max. All applied siRNAs were purchased by MWG Biotech (Ebersberg, Germany), with sequences as indicated in Table 1. After gently inverting the tubes, reaction mixtures were incubated for 5 min at room temperature (RT). Subsequently, both mixtures were combined, gently mixed and incubated for another 20 min at RT in order to allow complex formation. In the meantime, cells were washed once with PBS and afterwards the well was filled up with 750 µl of OptiMEM. The reaction mixture was added dropwise to the well while the plate was gently rocked back and forth. In this way, a final volume of 1 ml and a final siRNA concentration of 40 nM per well

were reached. After 6 h of incubation (37°C, 5% CO_2), transfection medium was aspirated and replaced by fully supplemented cell culture medium.

Target	siRNA Sequence
Bcl-2	5′-uaauaacgugccucaugaaTT-3′ (sense) 5′-uucaugaggcacguuauuaTT-3′ (antisense)
Bcl-x_L	5′-gcuuggauaaagaugcaaTT-3′ (sense) 5′-uugcaucuuaucccaagcAG-3′ (antisense)
Mcl-1	5′-aaguaucacagacguucucTT-3′ (sense) 5′-gagaacgucugugauacuuTT-3′ (antisense)
Scrambled	5′-ggcuscguccaggagcgcaccTT-3′ (sense) 5′-ggugcgcuccuggacgguagccTT-3′ (antisense)

Table 1: siRNAs used for the transfection of eukaryotic cells.

2.1.2.2 Plasmid-DNA Transfection

For each well, one reaction tube containing 250 µl of OptiMEM was prepared. After adding 1,25 µl of PLUS Reagent and 0,5 µg of plasmid-DNA, components were mixed by gently inverting the tube and incubated for 5 min at RT. Afterwards, the reaction mixture was supplemented with 3,125 µl of Lipofectamine LTX, gently mixed and incubated for another 20 min at RT. In the meantime, cells were washed once with PBS and afterwards the well was filled up with 750 µl of OptiMEM. The reaction mixture was added dropwise to the well while the plate was gently rocked back and forth. In this way, a final volume of 1 ml and a final plasmid-DNA concentration of 0,5 µg per well were reached. After 6 h of incubation (37°C, 5% CO_2), transfection medium was aspirated and replaced by fully supplemented cell culture medium.

Mcl-1 was cloned in a pEF4 vector, whereas Bcl-2 (kind gift of W. Roth, Institute of Pathology, Mainz) and Bcl-x_L (kindly provided by M. Li-Weber and P.H. Krammer, German Cancer Research Center, Heidelberg, Germany) were cloned in a pcDNA3 vector. Corresponding empty vectors were used as controls and transfection efficiency was validated by GFP transfection and subsequent FACS (fluorescence-activated cell sorting) analysis.

2.1.3 Cell Death Assays

2.1.3.1 MTT-Assay

3-(4,5-dimethylthiazol-2-yl)-2,5-diphenyltetrazolium bromide (MTT)	*# M5655, Sigma-Aldrich, Munich, Germany*
2-propanol	*# I9516, Sigma-Aldrich, Munich, Germany*
Phosphate Buffered Saline (PBS) (Gibco)	*# 14190-094, Thermo Fisher, Schwerte, Germany*

In this colorimetric assay, MTT serves as an indicator for the metabolic activity of cells. Since this often correlates with cellular viability, the MTT-assay is frequently used to assess cell death. By reduction, the yellowish tetrazolium dye MTT gets converted into the purple and insoluble Formazan.

The MTT-assay was used in order to determine the effects of different inhibitors and chemotherapeutics on cellular viability. Therefore, $1x10^6$ cells were seeded onto a 12-well plate, grown to a confluency of 70-80 % and treated as required. 5 mg of MTT powder were dissolved in 1ml PBS and kept in the dark until further use (light sensitive). 100 µl of MTT solution (per 1 ml cell culture medium) were directly added into the well without aspirating the cell culture medium in advance, resulting in a 1:10 dilution. After gently rocking the plate back and forth, it was incubated for 3 h at 37°C (5% CO_2). Subsequently, the MTT-containing medium was aspirated and accrued Formazan in viable cells was solubilized by the addition of 500 µl 2-propanol per well. After an incubation time of 15 min at RT on a rocker plate, absorbance was quantified by spectrometric measurement at 550nm.

2.1.3.2 LDH-Assay

Cytotoxicity Detection Kit (LDH) *# 11644793001, Roche, Mannheim, Germany*

In this assay, the enzyme lactate dehydrogenase (LDH) reduces NAD to NADH, which then converts a tetrazolium salt into a colored Formazan product (λmax = 450 nm). Since LDH is a soluble cytoplasmatic enzyme, its presence in the supernatant of cell or tissue cultures is indicative for damaged plasma membranes. Due to the linearity of the assay, measured color intensity allows the relative quantification of cytolysis[199].

The LDH assay was used to determine the effect of the BH3 mimetic ABT-737 on the viability of cultured colorectal cancer tissue. Therefor, 100 µl supernatant were transferred into a 96-well plate and mixed with 100 µl freshly prepared reagent solution as indicated in the manufacturer´s protocol. Subsequently, the plate was incubated for 15 min at RT under light exclusion and absorbance was quantified by spectrometric measurement at 490nm.

2.1.4 FACS Analysis of Cell Death and Proliferation

Apoptosis, DNA Damage, Cell Proliferation Kit *#562253, BD Biosciences, Heidelberg, Germany*

For the analyses the "Apoptosis, DNA Damage and Cell Proliferation Kit" from BD Biosciences was used. For the determination of the proliferative capacity it contains the synthetic nucleoside bromodeoxyuridine (BrdU), which gets incorporated into the DNA of replicating cells. By using a BrdU-specific antibody, proliferating cells can thus be identified. For the analysis of DNA damage, the kit comprises an antibody against gH2AX. If DNA damage occurs, histone H2AX gets phosphorylated at serine 139 (gH2AX) what recruits DNA damage repair proteins. For the measurement of apoptosis, the kit provides an antibody against cleaved PARP.

$2{,}5\times10^6$ HT29 or SW480 cells were seeded onto a 12-well plate, grown to a confluency of 70–80% and transfected or treated as indicated. Prior to harvest, cells were incubated with 20 µM BrdU for 1 h. Hereafter, the culture medium was transferred into FACS tubes and living cells were detached by using Accutase as described under 2.1.5.2 and pooled with the former cell culture medium. After centrifugation at 300 x g for 5 min, the supernatant was discarded and the cell pellets were resuspended in 100 µl of Perm Solution per tube and incubated on ice for ~20 min. After that, tubes were filled up with 1 ml Wash Buffer and cells were pelleted by another centrifugation at 300 x g for 5 min. Supernatant was discarded and cells were resuspended in 100 µl of Plus Perm Buffer, incubated on ice for 10 min, diluted with 1ml Wash Buffer and centrifuged at 300 x g for 5 min. The same procedure was repeated once again with 100 µl Perm Solution and an incubation time of 5 min. Meanwhile, 30 µl DNase working solution per FACS tube were prepared by diluting the DNase stock solution with PBS in a 3:10 ratio. Cells were resuspended in 100 µl DNase working solution, incubated at 37°C for 1 h and centrifuged at 300 x g for 5 min. The DNase solution, which helps to expose the BrdU epitopes, was discarded and cells were incubated with the antibodies under light exclusion for 20 min at RT. The solution contained 5 µl of each antibody, diluted in 30 µl Wash Buffer per tube. After a final centrifugation at 300 x g for 5 min, cells were resuspended in 400 µl Wash Buffer and analyzed by FACS analysis.

2.1.5 Migration Assays

2.1.5.1 Scratch Assay

The scratch assay was used to compare the migratory ability of colorectal cancer cells after siRNA- or inhibitor-mediated manipulation.

$2{,}5\times10^6$ HT29 cells were seeded onto a 12-well plate, grown to a confluency of 70–80% and transfected or treated as indicated. On the following day, the cell monolayer was scratched by using a sterile pipette tip. Wells were washed with medium to remove detached cells and images were immediately captured using an inverted microscope (CKX41, Olympus Inc., Hamburg, Germany) equipped with a digital color camera (XC30, Olympus Inc.). The exact image position within the well

was marked to allow surveillance of gap closure in the very same sector. The gap closure was measured over 72 h, in which a picture was taken every 24 h, using CellSense® imaging software (Olympus Inc.). Thereby, gap sizes were determined by multiple measurements (every 200 µm) of the distance between the edges of the monolayer and mean values were calculated.

2.1.5.2 3D Cell Culture

Accutase	*# A6964, Sigma-Aldrich, Munich, Germany*
Dimethyl sulfoxide (DMSO)	*# 85190, Thermo Fisher, Schwerte, Germany*
OCT mounting medium	*# SA62550, Science Services, Munich, Germany*
37 % Formaldehyde Solution	*# F1635, Sigma-Aldrich, Munich, Germany*
Phosphate Buffered Saline (PBS) (Gibco)	*# 14190-094, Thermo Fisher, Schwerte, Germany*

A three-dimensional cell culture fosters cell-cell interactions and allows long-term treatment. Compared to the conventional flat cell culture, this resembles much better the conditions found in a normal tissue. In this assay, cells are grown in Alvetex inserts (Reinnervate, Sedgefield, UK), holding a 200 µm thick polystyrene scaffold with a defined pore size of about 40 µm.
For the comparison of the migratory ability after manipulation of anti-apoptotic proteins, cells were either transfected or treated with inhibitors. For transfection, $2{,}5\times10^6$ HT29 cells were seeded onto a 12-well plate, grown to a confluency of 70–80% and transfected as indicated. On the following day, scaffolds were rendered hydrophilic by flooding them with 80% sterile filtered ethanol followed by two washing steps with cell culture medium. Transfected cells were washed once with PBS and detached by incubating them for 5 min at 37°C in a humidified atmosphere and with 250 µl of Accutase per well. Compared with trypsin, detachment with Accutase is more gentle and therefore appropriate for the transfer of transfected cells. In 200 µl of cell culture medium, $1x10^6$ cells were carefully seeded drop by drop onto the scaffold. 3 hours after seeding, wells were gently flooded from below with fully supplemented RPMI until scaffolds were fully covered. The medium was aspirated and renewed every second day. In case of inhibitor treatment, cells were seeded onto the scaffold without previous transfection. 24 h after seeding, medium was changed and additionally supplemented with the respective inhibitor or DMSO as control. Each time the medium was renewed, it got supplemented with the respective compounds. After 5 days, in which the transfected or inhibitor treated cells had time to migrate into the scaffold, inserts were washed twice in PBS. Scaffolds were detached from the inserts, transferred into vinyl specimen molds (Sakura Finetek, Torrance, USA) covered with OCT mounting medium and gradually frozen in the

gas phase of liquid nitrogen. Deeply frozen scaffolds were cryosectioned (Cryostat, Thermo), fixed in 4% PFA (paraformaldehyde) and immunohistochemically stained as indicated.

2.1.6 Invasion Assay

Accutase	*# A6964, Sigma-Aldrich, Munich, Germany*
Hoechst 33342	*# 62249, Thermo Fisher, Schwerte, Germany*
Phosphate Buffered Saline (PBS) (Gibco)	*# 14190-094, Thermo Fisher, Schwerte, Germany*

Matrigel invasion chambers (BD) with a pore size of 8 µm were used to study the invasive capacity of SW480 cells. Matrigel consists of proteins, such as collagen and laminin, which are secreted by mouse sarcoma cells (Engelbreth-Holm-Swarm cells)[200]. The gelatinous secret resembles the extracellular matrix which cannot be overcome by non-invasive cells.

$2{,}5\times10^6$ SW480 cells were seeded onto a 12-well plate, grown to a confluency of 70–80% and transfected as indicated. On the following day, invasion chambers were hydrated in supplement-free RPMI cell culture medium in a humidified atmosphere for 2 h. Subsequently, invasion chambers were transferred as inserts into a 12-well cell culture plate, containing 750 µl RPMI supplemented with 10% FCS in each well. Transfected cells were washed once with PBS and detached by using Accutase as described. After harvesting, 3×10^5 cells were resuspended in 500 µl FCS-free RPMI and seeded on top of the Matrigel. Since only the cell culture medium beneath the invasion chamber contained FCS and because FCS serves as a chemoattractant, cells started to invade the Matrigel. After 48 h, non-invasive cells on the upper surface of the invasion chamber were removed by scrubbing with a cotton tipped swab. Cells that overcame the Matrigel were fixed on the lower surface of the insert with 80% EtOH for 30 min. Subsequently, nuclei were stained by using Hoechst 33342 for 15 min and washed in PBS. In order to quantify the amount of invaded cells, five pictures of every insert were taken using a fluorescence microscope (Keyence, Neu-Isenburg, Germany) and the number of Hoechst-positive nuclei was determined by counting.

2.1.7 Tissue Culture

ABT-737	*# S1002, Selleckchem, Munich, Germany*
Dimethylsulfoxid (DMSO)	*# 20385.01, Serva, Heidelberg, Germany*
10 % Formalin	*# HT501128, Sigma-Aldrich, Munich, Germany*
Paraffin wax	*# 327204, Sigma-Aldrich, Munich, Germany*

Tumor tissue from 9 patients with CRC was collected upon surgical resection of the primary tumor. Written informed consent from all donors was obtained and analyses were done anonymously. The usage of patient tissue for research purposes was approved by the local ethics committee of the University Hospital of Heidelberg (S-649/2012). Tumor tissue was cut into 300 µm thick slices by a Leica VT1200 S vibrating blade microtome (Leica, Wetzlar, Germany), transferred onto porous filter membrane inserts and placed in culture medium (DMEM supplemented with penicillin: 100U/ml and streptomycin: 100mg/ml) containing six-well plates. Tissue specimens were kept in a humidified atmosphere (37°C, 5% CO2) at the air-liquid interface for up to 94 hours. After 24 hours of incubation in medium, cancer specimens were treated with the small molecule inhibitor ABT-737 (10µM) or the respective vector substance (DMSO) for 72 hours, by supplementing the culture medium with the mentioned compounds. Finally, tissue slices were fixed in 10 % formalin and paraffin-embedded. 4 µm sections were stained with Hematoxylin and Eosin (H&E) as described under 2.4.1 and tissue viability was determined by a trained pathologist.

2.2 Protein Analyses

2.2.1 Protein Isolation

2.2.1.1 Protein Isolation from cultured Cells

Sodium Chloride (NaCl)	*# 9265.1, Roth, Karlsruhe, Germany*
Trizma Base/Hydrochloric acid (Tris/HCl)	*# 9090.1, Roth, Karlsruhe, Germany*
Nonylphenylpolyethylenglycol (NP-40)	*# 28324, Thermo Fisher, Schwerte, Germany*
Sodium Dodecyl Sulfate (SDS)	*# CN30.3, Roth, Karlsruhe, Germany*
Protease Inhibitor Cocktail (PI)	*# 04693116001, Roche, Mannheim, Germany*
1,4 Dithiothreitol (DTT)	*# 6908.2, Roth, Karlsruhe, Germany*
Phenylmethyl sulphonyl fluoride (PMSF)	*# 6367.2, Roth, Karlsruhe, Germany*
Sodium fluoride (NaF)	*# 2618.1, Roth, Karlsruhe, Germany*
Sodium orthovanadate	*# 450243, Sigma-Aldrich, Munich, Germany*
Phosphate Buffered Saline (PBS) (Gibco)	*# 14190-094, Thermo Fisher, Schwerte, Germany*

Cells were grown in 12-well plates and transfected or treated as indicated. Prior to the experiment, 2 x RIPA buffer (Radioimmunoprecipitation Assay buffer) without supplements was generated and kept at 4°C until further use.

2 x RIPA buffer:	Example for a final volume of 50ml:
240 mM NaCl	2,4ml 5M NaCl stock solution
100 mM Tris/HCl (pH 8.0)	10ml 0,5M Tris/HCl (pH 8,0) stock solution
2% (v/v) NP-40	1ml
0,2% (w/v) SDS	100mg
-	Fill up to 50ml with MilliQ H_2O

Table 2: Components for the preparation of 2 x RIPA lysis buffer.

For protein isolation, cells were washed twice with precooled PBS (4°C) and harvested by addition of 60 µl fully supplemented 1x RIPA lysis buffer per well.

	1ml	1,5ml	2ml	5ml
RIPA (2x) [µl]	500	750	1000	2500
PI [µl]	20	30	40	100
DTT [µl]	1	1,5	2	5
PMSF [µl]	10	15	20	50
NaF [µl]	40	60	80	200
Vanadate [µl]	1	1,5	2	5
MilliQ H_2O [µl]	428	642	856	2140

Table 3: Components for the preparation of supplemented 1 x RIPA lysis buffer.

The 12-well plates were incubated on ice for 20 min and subsequently cells were detached and mechanically destroyed with a cell scraper. The suspension was transferred into a 1,5 ml tube and centrifuged for 20 min at 13.000 x g and 4°C to get rid of cellular debris. The supernatant was transferred into a new reaction tube and samples were stored at -80°C.

2.2.1.2 Protein Isolation from Tissues

AllPrep DNA/RNA/Protein Mini Kit	*# 80004, Qiagen, Hilden, Germany*
ß-Mercaptoethanol	*# 444203, Merck, Darmstadt, Germany*
Urea	*# U4883-6X, Sigma-Aldrich, Munich, Germany*
Ethanol absolute	*# 32205, Sigma-Aldrich, Munich, Germany*

Tissue specimens were weighted and pieces of 20-30 mg were transferred into Precellys tubes, prefilled with beads (Bertin Technologies, Montigny-le-Bretonneux, France), snap frozen in liquid nitrogen and kept on dry ice until 600µl of lysis buffer (RLT buffer, AllPrep kit) were added. Prior to use, the RLT buffer was supplemented with 14,3 M β-mercaptoethanol (10µl ß-MeEtOH per 1 ml RLT buffer). Subsequent to this, tissue lysis was fostered by using the Precellys Homogenizer 24. Grinded specimens were centrifuged (16.000 x g, 4°C, 3 min) in order to get rid of the beads and remaining cell debris. For all further steps the AllPrep kit has been used. In order to remove the DNA, the supernatant was transferred onto a AllPrep DNA spin column, placed in a 2 ml collection tube. The column was centrifuged at 8000 x g for 30 sec and to the flow-through 350 µl of 100% ethanol were added. The mixture was homogenized by pipetting up and down and in order to remove the RNA, 700 µl were transferred onto a RNeasy spin column, placed in a 2 ml collection tube. The column was centrifuged at 8000 x g for 15 sec and the flow-through was collected for further processing. If the total volume of the ethanol mixture exceeded 700 µl, this last step was repeated and the second flow-through was pooled with the first one in a 2 ml reaction tube. Subsequent to the addition of 1 ml APP buffer to the flow-through, samples were mixed by vortexing and incubated for 10 min at RT. Afterwards, proteins were pelleted by centrifugation at 15.000 x g for 10 min at RT. The supernatant was discarded and the pellet was washed with 500 µl of 70 % ethanol. Subsequently, the protein pellet was dried at RT until it became matt white. Depending on the pellet size, 50-500 µl of 8M urea were added in order to resolve the proteins. For long-time storage, samples were kept at -80°C.

2.2.2 Bradford Assay

Bradford reagent	*# 5000205, BioRad, Munich, Germany*
Bovine Serum Albumine (BSA)-Standard	*# 23209, Thermo Fisher, Schwerte, Germany*

The Bradford assay is a colorimetric analysis, used for the determination of protein concentrations. It relies on the dye Coomassie Brilliant Blue G-250, which shifts its absorbance spectrum maximum after protein binding from the red (470 nm) to the blue (595 nm) wavelength range.
Depending on the expected protein concentrations, the samples were prediluted 1:2 to 1:10 with MilliQ water. 5 µl of each sample were transferred into a 96-well plate, filled up with 250 µl Bradford reagent and incubated for 5 min in the dark at RT. Afterwards, absorbance was quantified by spectrometric measurement at 595 nm. For better results, all measurements were done in duplicates. The simultaneous utilization of a BSA protein standard (0; 0,25; 0,5; 0,75; 1; 1,25; 1,5 µg/µl) allowed an absolute quantification of proteins in the sample via linear regression.

2.2.3 SDS-PAGE

30% acrylamide	*# A124.1, Roth, Karlsruhe, Germany*
Trizma Base (Tris)	*# A1086, AppliChem, Darmstadt, Germany*
Sodium Dodecyl Sulfate (SDS)	*# CN30.3, Roth, Karlsruhe, Germany*
Ammonium persulfate (APS)	*# 9592.5, Roth, Karlsruhe, Germany*
Tetra-methylethylenediamine (TEMED)	*# 2367.1, Roth, Karlsruhe, Germany*
Glycerol	*# 6962.1, Roth, Karlsruhe, Germany*
ß-Mercaptoethanol	*# 444203, Merck, Darmstadt, Germany*
Bromphenol blue	*# B0126, Sigma-Aldrich, Munich, Germany*
Glycine	*# A1067, AppliChem, Darmstadt, Germany*

The method of sodium dodecyl sulfate (SDS) polyacrylamide gel electrophoresis (PAGE) is used to separate proteins by size. The anionic detergent SDS is used to mask the initial protein charge. By binding proportional to the protein mass, complexes with a constant charge to mass ratio are formed. Moreover, SDS leads to a denaturation of the present proteins. Together with β-mercaptoethanol, which reduces sulfhydryl-groups, this ensures a linear shape of all proteins, with the result that mainly protein mass influences the distance covered in the gel. The fractionation of proteins takes place in a polyacrylamide gel, which is, depending on the size of the protein of interest, prepared with different acrylamide concentrations. For most protein sizes, gels containing 12% acrylamide were used. Addition of the radical initiator APS (ammonium persulfate) starts the polymerization reaction, which is then catalyzed by TEMED (tetramethylethylenediamine).
Before use, the gel chamber was cleaned with 80% ethanol (v/v) and put together as described in the manufacturer´s manual (BioRad). Afterwards, the separating gel solution was prepared and gently poured between the glass plates. To remove eventually occurred bubbles, isopropanol was immediately added on top. After polymerization, the isopropanol was removed and replaced by the stacking gel. Comb-insertion allowed slot formation.

	Separating Gel				Stacking Gel
acrylamide concentration	7%	10%	12%	15%	4%
H_2O [ml]	5,0	4,0	3,3	2,3	2,7
30% acrylamide [ml]	2,3	3,3	4,0	5,0	0,67
1,5M Tris [ml]	2,5	2,5	2,5	2,5	-
1M Tris [ml]	-	-	-	-	0,5

10% SDS [µl]	100	100	100	100	40
10% APS [µl]	100	100	100	100	40
TEMED [µl]	4	4	4	4	4

Table 4: Components for the preparation of two acrylamid-gels.

Protein samples were mixed with 5x sample buffer in a 1:5 ratio and heated up for 5 min at 95°C. The 5x protein sample buffer was prepared in advance and kept at -20°C for long-time storage. Currently used aliquots were stored at RT.

5 x sample buffer:	Example for a final volume of 100ml:
50% (v/v) Glycerol	50ml
10% (w/v) SDS	10g
50mM Tris	6,056g
25% (v/v) β-Mercaptoethanol	25ml
0,25mg/ml Bromphenol blue	25mg
-	Fill up to 100ml with MilliQ H_2O

Table 5: Components for the preparation of 5 x protein sample buffer.

After transferring the gel into an electrophoresis chamber (BioRad system) filled with 1x running buffer, the comb was removed and slots were rinsed with buffer before samples and marker were loaded. Prior to each run, the running buffer was freshly prepared by diluting 100 ml of 10 x running buffer with 900 ml MilliQ H_2O. First, an electric tension of 80 V was applied. After the dye front reached the separating gel, the tension was increased to 120 V and kept constant till the end of the electrophoresis run.

10 x running buffer:	Example for a final volume of 1l:
1% (w/v) SDS	10g
25mM Tris-Base	30,28g
190mM Glycine	142,63g
-	Fill up to 1l with MilliQ H2O

Table 6: Components for the preparation of 10 x running buffer.

2.2.4 Western Blot

Methanol	*# 32213, Sigma-Aldrich, Munich, Germany*
Trizma Base (Tris)	*# A1086, AppliChem, Darmstadt, Germany*
Glycine	*# A1067, AppliChem, Darmstadt, Germany*
skim milk powder	*# T145.2, Roth, Karlsruhe, Germany*
Bovine Serum Albumine (BSA)	*# T844.4, Roth, Karlsruhe, Germany*
Tween 20	*# P2287, Sigma-Aldrich, Munich, Germany*
Sodium azide	*# 08591, Sigma-Aldrich, Munich, Germany*
Enhanced Chemiluminescence Substrate(ECL)	*# NEL103001EA, PerkinElmer, Rodgau, Germany*

In order to enable immuno-detection of specific proteins, a wet blot was performed. Subsequent to the size-dependent protein separation via SDS-PAGE, the gel was taken out of the cassette and the stacking gel was removed. The gel, a nitrocellulose membrane, six sheets of Whatman paper and two sponges were assembled as described in the manufacturer's protocol (BioRad). Air bubbles were removed by carefully rolling a glass rod over the sandwich. Afterwards the blot sandwich was inserted into the wet blot chamber, which was filled up with 1 x transfer buffer. Prior to blotting, the transfer buffer was freshly prepared by diluting 100 ml of 10 x transefer buffer with 700 ml MilliQ H_2O and 200 ml methanol. The buffer was reused 3-4 times until it was discarded and freshly prepared for the next blotting procedures. For the protein transfer, the chamber was kept at 4°C and a constant tension of 90 V for 2 h was applied.

10 x transfer buffer:	Example for a final volume of 1l:
25 mM Tris-Base	30,28g
190 mM Glycine	142,63g
-	Fill up to 1l with MilliQ H_2O

Table 7: Components for the preparation of 10 x transfer buffer.

Subsequently, the gel was discarded and unspecific binding sites on the membrane were blocked with 5% skim milk powder or 5% BSA (both w/v) in PBS-T (0,1% Tween 20 in PBS) for 1h at RT on a shaking device or at 4°C over night. Afterwards, the membrane was incubated with the primary antibody, diluted in skim milk or BSA containing PBS-T and supplemented with 1% sodium azide as indicated. Dependent on the antibody affinity, the incubation was done for 1 h at RT or alternatively over night at 4°C. After washing the membrane three times for 5 min in PBS-T, it was incubated with an appropriate, horseradish peroxidase-coupled secondary antibody. The secondary antibody

was diluted 1:10000 in PBS-T containing 0,5% of skim milk (w/v). Again the membrane was incubated for 1h on a slow shaking device at RT. Once again the membrane was washed thrice for 5 min in PBS-T and another time in PBS (Phosphat-Buffered Saline) to diminish foam formation. Proteins of interest were now detected by enhanced chemiluminescence reaction. Therefor, ECL reaction agents were mixed in a 1:1 ratio and immediately poured onto the membrane. An incubation time of approximately 5 min in the dark allowed the HRP-mediated (horseradish peroxidase) oxidation of luminol with hydrogen peroxide as the oxidizing agent. The resulting chemiluminescence was detected with a radiographic film, developed with the CP1000 developing machine from AGFA (Mortsel, Belgien).

Antibody	Species	Order number, Company	Dilution
Primary Antibodies			
Bcl-2	mouse	# ab692, abcam	1:500 in 0,5% Milk
Bcl-xL	rabbit	# 2764, Cell Signaling	1:1000 in 5% BSA
Caspase 8	rabbit	# 4927, Cell Signalng	1:1000 in 5% Milk
clCaspase 3	rabbit	# 9664, Cell Signaling	1:1000 in 5% Milk
clCaspase 8	rabbit	# 9429, Cell Signaling	1:1000 in 5% BSA
(cl)Caspase 9	rabbit	# 9504, Cell Signaling	1:1000 in 5% Milk
clPARP	rabbit	# 5625, Cell Signaling	1:1000 in 5% BSA
E-Cadherin	rabbit	# 4065, Cell Signaling	1:1000 in 5% BSA
Lgr5	rabbit	# ab75850, abcam	1:1000 in 5% BSA
Mcl-1 (for mouse)	rabbit	# 600-401-394, Rockland	1:2000 in 5% Milk
Mcl-1 (for human)	rabbit	# sc-819, Santa Cruz	1:200 in 0,5% Milk
MLKL	goat	# sc-165025, Santa Cruz	1:200 in 5% Milk
N-Cadherin	rabbit	# 4061, Cell Signaling	1:1000 in 5% BSA
p-MLKL	rabbit	# ab196436, abcam	1:1000 in 5% BSA
tBid	rabbit	# PC645-10T, Merck Millipore	1:1000 in 5% BSA
Tubulin	mouse	# T8203-25UL, Sigma	1:5000 in PBS-T
Secondary Antibodies			
Anti-goat	donkey		1:10000 in 0,5% Milk
Anti-mouse	goat	#sc-2031, Santa Cruz	1:10000 in 0,5% Milk
Anti-mouse (for Tubulin)	goat	#1070-05, SouthernBiotech	1:10000 in 0,5% Milk
Anti-rabbit	goat	#sc-2030, Santa Cruz	1:10000 in 0,5% Milk

Table 8: Antibodies used for Western blot analyses.

2.3 DNA and RNA Analyses

2.3.1 RNA Isolation

2.3.1.1 RNA Isolation from cultured Cells

TRI reagent	*# T9424, Sigma-Aldrich, Munich, Germany*
Chloroform	*# C2432, Sigma-Aldrich, Munich, Germany*
2-propanol	*# I9516, Sigma-Aldrich, Munich, Germany*
Ethanol absolute	*# 32205, Sigma-Aldrich, Munich, Germany*
Phosphate Buffered Saline (PBS) (Gibco)	*# 14190-094, Thermo Fisher, Schwerte, Germany*

Cells were grown in 12-well plates and transfected or treated as indicated. For RNA isolation, cells were washed twice with precooled PBS (4°C), before the wells were filled with 250 µl of chilled PBS in which cells were detached and mechanically destroyed with a cell scraper. The suspension was transferred into a 1,5 ml tube and centrifuged for 5 min at 200 x g and 4°C. The supernatant was discarded and the pellet was resolved in 500 µl of TRI reagent. Since the contained phenol and chloroform can be hazardous to health, this step and all following ones were performed under a hood. The suspension was incubated for 5 min at RT and occasionally vortexed in the meantime. 100 µl of chloroform were added and the mixture was vortexed until it became milky, before it was incubated for 10 min at RT. Hereafter, the solution was centrifuged for 15 min at 19.000 x g and 4°C, resulting in phase separation. The upper, aqueous phase was transferred into a new reaction tube and supplemented with 500 µl 2-propanol. After inverting the tube for several times, the mixture was incubated for 10 min at RT and subsequently centrifuged for 40 min at 14.000 x g and 4°C to pellet the RNA. The supernatant was discarded and the pellet was washed twice with 75% ethanol. Hereafter, the pellet was air-dried until it became transparent and finally it was solved in 30-50µl of RNase-free water. Isolated RNA was quantified by using an Epoch Microplate Spectrophotometer (BioTek, Winooski, VT, USA) and kept at -80°C for long-time storage.

2.3.1.2 RNA Isolation from Tissues

AllPrep DNA/RNA/Protein Mini Kit	*# 80004, Qiagen, Hilden, Germany*
ß-Mercaptoethanol	*# 444203, Merck, Darmstadt, Germany*
Ethanol absolute	*# 32205, Sigma-Aldrich, Munich, Germany*

For RNA isolation from tissues, again the "AllPrep DNA/RNA/Protein Mini Kit" was used. Tissue specimens were homogenized and lysates were further processed as described under 2.2.1.2. To the flow-through from the AllPrep DNA spin column, 350 µl of 100% ethanol were added. The mixture was homogenized by pipetting up and down and subsequently 700 µl were transferred onto a RNeasy spin column, placed in a 2 ml collection tube. The column was centrifuged at 8000 x g for 15 sec, allowing the RNA to bind to the solid phase. If the total volume of the ethanol mixture exceeded 700 µl, this last step was repeated in order to increase RNA yield. The RNeasy spin column was washed with 700 µl of RW1 buffer, followed by centrifugation at 8000 x g for 15 sec. The flow-through was discarded and the column was washed with 500 µl of RPE buffer, followed by another centrifugation at 8000 x g for 15 sec. The washing step with 500 µl of RPE buffer was repeated, but this time the column was centrifuged at 8000 x g for 2 min. The flow-through was discarded and an additional centrifugation for 1 min at full speed was done to get rid of remaining buffer. Hereafter, the RNeasy spin column was placed into a new 1,5 ml reaction tube and 30-50µl of RNase-free water were poured directly on top of the column membrane. By a final centrifugation for 1 min at 8000 x g, the RNA was eluted. If high RNA yields were expected, the elution step was repeated. Isolated RNA was quantified by using using an Epoch Microplate Spectrophotometer (BioTek, Winooski, VT, USA) and kept at -80°C for long-time storage.

2.3.2 Reverse Transcription and qRT-PCR

Omniscript Reverse Transcription Kit	*# 205111, Qiagen, Hilden, Germany*
QuantiTect SYBR-Green PCR Kit	*# 204143, Qiagen, Hilden, Germany*
Deoxynucleotide Set (dNTPs)	*#DNTP100, Sigma-Aldrich, Munich, Germany*

In order to study gene expression, the abundance of a particular mRNA can be relatively quantified by performing a quantitative real-time polymerase chain reaction (qRT-PCR). Therefor, isolated RNA needs to be transcribed into complementary DNA (cDNA) by a RNA-dependent DNA polymerase. This so called reverse transcriptase is normally found in retroviruses which convert their genomic RNA into cDNA in order to integrate into the host genome.

For reverse transcription the "Omniscript Reverse Transcription Kit" was used. 1 µg of total RNA was filled up with RNase-free water to a final volume of 14,5 µl. In order to denature the secondary RNA structure, the samples were incubated for 5 min at 65°C and subsequently chilled on ice. Finally, 5,5 µl of the reverse transcription master mix, containing the enzyme, oligo-dT primer and deoxynucleotide triphosphates (dNTPs), were added and the mixture was incubated for 1 h at 37°C to allow reverse transcription.

Reverse Transcription Master Mix	1 x
10 x Reverse Transcription Buffer	2 µl
dNTPs (5mM)	2 µl
Reverse Transcriptase	1 µl
oligo-dT primer (10 µM)	0,5 µl

Table 9: Components for the preparation of the reverse transcription master mix.

Afterwards, the samples were filled up with 20 µl $H_2O_{PCR\text{-}Grade}$ and stored at 4°C for up to one week, or at -80°C for long-time storage.

Like in the conventional PCR, the qRT-PCR leads to the amplification of specific DNA segments across several orders of magnitude. Which segment gets amplified is thereby defined by the primers which bind to the 3´ends of the DNA target region and serve as starting point for the DNA polymerase. The peculiarity of the qRT-PCR is the presence of a DNA-intercalating dye, which is only after DNA-binding able to emit a fluorescence signal if it gets excited. In which PCR cycle the fluorescence signal exceeds the background signal for the first time, depends on the initial amount of target DNA and thereby on the level of gene expression. This cycle is called “crossing point” from which the Cp-value can be calculated. Since the qRT-PCR allows only relative quantification, the expression of each target gene is normalized to the expression of a so called “house-keeping gene”, which shows stable expression under various conditions.

In our experiments, SYBR-Green was applied as DNA-intercalating dye and the expression of GAPDH (Glycerinaldehyde-3-Phosphate-Dehydrogenase) was determined and used for normalization. Furthermore, “QuantiTect Primer Assays” and the “QuantiTect SYBR-Green PCR Kit” by Qiagen have been used. Prior to the run, a separate master mix for each target was prepared, containing the fluorescent dye and the specific primers.

Quantitative Real-Time PCR Master Mix	1 x
SYBR-Green	5 µl
$H_2O_{PCR\text{-}Grade}$	3 µl
Primer	1 µl

Table 10: Components for the preparation of the quantitative real-time PCR master mix.

9 µl of master mix were transferred into a 96-well plate and supplemented with 1,5 µl of cDNA. For better results, all measurements were done in duplicates and one negative control per subset was generated by replacing the cDNA with H_2O. After sealing the plate, measurements were done with

the LightCycler 480 from Roche (Risch, Switzerland). The qRT-PCR program contained an initial 15 min denaturation step at 95°C, followed by 35 PCR cycles. Each cycle comprised a 15 sec denaturation step at 95°C, followed by a 30 sec annealing step at 55°C and a final 30 sec elongation step at 72°C. Data analysis was done by using the Light Cycler 480 SW 1.5 software.

2.3.3 Mouse Genotyping

Proteinase K	*# EO0491, Thermo Fisher, Schwerte, Germany*
Trizma Base/Hydrochloric acid (Tris/HCl)	*# 9090.1, Roth, Karlsruhe, Germany*
Ethylene Diamine Tetra Acetate (EDTA)	*# 8040.3, Roth, Karlsruhe, Germany*
Sodium Dodecyl Sulfate (SDS)	*# CN30.3, Roth, Karlsruhe, Germany*
RedTaq Ready PCR Reaction Mix	*# R2523, Sigma-Aldrich, Munich, Germany*
Magnesium chloride ($MgCl_2$)	*# M8266, Sigma-Aldrich, Munich, Germany*

In order to determine the genotype of our mice, biopsies were taken by trimming the tail tip three weeks after birth. For digesting the tissue, each biopsy was transferred into a reaction tube filled with 50 µl of proteinase K solution and was incubated over night at 56°C. The proteinase K solution was freshly prepared prior to each genotyping experiment by mixing proteinase K and the respective buffer in a 1:10 ratio.

Proteinase K Buffer:	Example for a final volume of 500 ml:
100 mM Tris-HCl (pH 7,6)	7,9 g
20 mM EDTA (pH 8,0)	2,9 g
0,5 % (w/v) SDS	0,25 g
-	Fill up to 500 ml with MilliQ H_2O

Table 11: Components for the preparation of the proteinase K buffer.

On the following day, 1 ml MilliQ H_2O was added to each sample and samples were stored at 4°C until further use. Prior to the polymerase chain reaction (PCR), 10 µl of each sample were further diluted in 90 µl MilliQ H_2O. For each target gene, a master mix was prepared using the "RedTaq Ready PCR Reaction Mix", which contains the thermostable DNA polymerase Taq and dNTPs. Since an organ-specific deletion of a target gene requires both the presence of the gene encoding for the Cre recombinase and in addition the floxed target gene, two distinct master mixes with the respective primers were prepared for each sample.

Target Gene	Primer Sequence
Bcl-xL	*for.* 5´- CCG ATT GTT CAG GAG ACC TTC CTG GCT TC -3´ *rev.* 5´- GAA CTT GCT GCT CTC ATA GGT TTT AAG CCA AG -3´
Cre recombinase	*for.* 5´- GCA CTG ATT TCG ACC AGG TT -3´ *rev.* 5´- CCC GGC AAA ACA GGT AGT TA -3´
Mcl-1	*for.* 5´- GCA GTA CAG GTT CAA GCC ATG -3´ *rev.* 5´- CTG AGA GTT GTA CCG GAC AA -3´
Δ Mcl-1	*for.* 5´- ACG CTC TTT AAG TGT TTG GCC -3´ *rev.* 5´- CTG AGA GTT GTA CCG GAC AA -3´

Table 12: Primers used for mouse genotyping.

For determination of the flox status, no internal control was needed because the amplification of the DNA segment is independent from the existence of a loxP side. If the loxP side is present, the amplified fragment gets merely enlarged and is thereby distinguishable from the wild-type allele. The master mix for the Cre PCR was supplemented with an additional primer pair for the Actin encoding gene. This internal control helped to differentiate between Cre negative samples and failures in the PCR procedure. The annealing temperature in the PCR program was adjusted to the GC content (guanine-cytosine content) of the primers as indicated in Table 13.

Cre	1 x [µl]
Cre: 310 bp; Actin: 510 bp	
RedTaq	7,5
$MgCl_2$	0,6
Primer Cre for.	0,25
Primer Cre rev.	0,25
Primer Actin for.	0,5
Primer Actin rev.	0,5
H2O	4,65
14,25 µl per tube + 0,75 µl DNA	
1x: 95°C for 5 min;	
40x: 95°C for 30sec; 59°C for 30sec; 72°C for 30sec;	
1x: 72°C for 7min	

Mcl-1 (flox)	1 x [µl]
wt: 360 bp; flox: 400 bp	
RedTaq	13,5
$MgCl_2$	1,0
Primer Mcl-1 for.	0,5
Primer Mcl-1 rev.	0,5
H2O	8,5
-	
-	
24 µl per tube + 1 µl DNA	
1x: 95°C for 5 min;	
40x: 95°C for 30sec; 59°C for 30sec; 72°C for 30sec;	
1x: 72°C for 7min	

Bcl-x_L (flox)	1 x [µl]
wt: 205 bp, flox: ~ 400bp	
RedTaq	13,5
$MgCl_2$	1,0
Primer Bcl-x_L for.	0,5
Primer Bcl-x_L rev.	0,5
H2O	8,5
-	
-	
24 µl per tube + 1 µl DNA	
1x: 95°C for 5 min;	
35x: 95°C for 30sec; 63°C for 30sec; 72°C for 30sec;	
1x: 72°C for 7min	

Table 13: Components for the preparation of the indicated PCR master mixes and the corresponding PCR programs.

2.3.4 Agarose Gel Electrophoresis

Agarose	*# 2267.4, Roth, Karlsruhe, Germany*
DNA ladder (GeneRuler® 100 BP Plus)	*# SM0321, Fermentas, St. Leon Rot, Germany*
Ethidium Bromide 1%	*# A1152, AppliChem, Darmstadt, Germany*
Trizma Base (Tris)	*# A1086, AppliChem, Darmstadt, Germany*
Boric Acid	*# B7901, Sigma-Aldrich, Munich, Germany*
Ethylene Diamine Tetra Acetate (EDTA)	*# 8040.3, Roth, Karlsruhe, Germany*

DNA amplificates, produced in the PCR process, can be separated by agarose gel electrophoresis in a size-dependent manner. Therefor, a gel was prepared by diluting 2 % (w/v) of agarose in 1 x TAE (Tris-acetate-EDTA) buffer. The mixture was heated up in the microwave until it became completely transparent.

50 x TAE Buffer:	Example for a final volume of 1 l:
	600 ml of MilliQ H_2O
2 M Tris-Base (pH 7,6)	242 g
1 M acetic acid	57,1 ml
50 mM EDTA	100 ml 0,5 M EDTA (pH 8.0)
-	Fill up to 1 l with MilliQ H_2O

Table 14: Components for the preparation of 50 x TAE buffer.

Afterwards, the agarose solution was cooled down to approximately 60°C and subsequently it was supplemented with 0,00005 % of the DNA-intercalating substance ethidium bromide (EtBr). Since EtBr is mutagenic and teratogenic, this step and all further ones were done under a hood. After the agarose solution was poured into the intended chamber, a comb was inserted to allow slot formation before the gel became firm by reaching RT. The electrophoresis chamber was filled with 1 x TBE and the comb was removed before samples and marker were loaded and an electric tension of 120 V was applied. Dependent on their size, DNA fragments move to the anode with a different velocity, leading to their separation. After the run, the bands were made visible by illuminating the gel with UV-light (λ= 254nm). This leads to an excitation of intercalated EtBr, which in turn emits detectable fluorescence (λ = 605nm).

2.3.5 Sanger Sequencing

10 x PCR reaction buffer	*# 18067017, Thermo Fisher, Schwerte, Germany*
Magnesium chloride ($MgCl_2$)	*# M8266, Sigma-Aldrich, Munich, Germany*
Deoxynucleotide Set (dNTPs)	*#DNTP100, Sigma-Aldrich, Munich, Germany*
Taq DNA Polymerase	*# 12346086, Thermo Fisher, Schwerte, Germany,*

In order to examine the presence of microsatellite instability in tumor regions, DNA from tumor and normal, Mcl-1 containing tissue was isolated following manual microdissection. Subsequently, a set of non-coding long mononucleotide markers were analyzed as indicators for microsatellite instability (Table 15).

Marker	Repeat	Gene	CHR	Prod. Size [bp]	Primer Sequence
AA003063	*A23*	uPAR Plasminogen Activ. Scgb1a1 Secretoglobin	*16*	*87*	*for.* 5´- ACGTCAAAAATCAATGTTAGG -3´ *rev.* 5´- CAGCAAGGGTCCCTGTCTTA -3´
U12235	*A24*		*7*	*86*	*for.* 5´- GCTCATCTTCGTTCCCTGTC -3´ *rev.* 5´- CATTCGGTGGAAAGCTCTGA -3´
L24372	*A27*		*19*	*90*	*for.* 5´- GGG AAG ACT GCT TAG GGA AGA-3´ *rev.* 5´- ATTTGGCTTTCAAGCATCCATA -3´
AC096777	*T27*		*17*	*138*	*for.* 5´- TCCCTGTATAACCCTGGCTGACT -3´ *rev.* 5´- GCAACCAGTTGTCCTGGCGTGGA -3´
AC096777	A33		17	153	*for.* 5´- TACAGAGGATTGTCCTCTTGGAG-3´ *rev.* 5´- GCTGCTTCACTTGGACATTGGCT-3´

Table 15: Mononucleotide markers and primers used for MSI analyses of murine intestinal tumors.

In addition, coding mononucleotide markers located in the genes Sdccag1, Elavl3, Glis2, and Tmem107 were evaluated for the presence of length alterations between Mcl-1-negative tumor regions and normal tissue.

All amplifications were performed using fluorescently labeled (FITC) oligonucleotide primers, which were designed with the software primer3. The PCR reaction mix had a total volume of 5 µl and contained the ingredients listed in Table 16.

Obtained PCR products were separated on an ABI3130xl genetic analyzer (Applied Biosystems, Darmstadt, Germany) and raw data were further analyzed with the Genescan analysis software (Applied Biosystems). A sample was defined as microsatellite instable, if novel peaks occurred in tumor compared to normal tissue, or if the ratio of peak areas of corresponding peaks in tumor and normal tissue revealed values ≤ 0.5 or ≥ 2[201].

PCR reaction mix	1 x
10 x reaction buffer	0,5 µl
$MgCl_2$	1,5 mM
dNTPs	200 mM
Primer for.	0,3 mM
Primer rev.	0,3 mM
Taq DNA polymerase	0,1 U
H2O	respectively
Final volume: 5 ml	
1x:	94°C for 4 min;
35x:	94°C for 30sec; 58°C for 45sec; 72°C for 30sec;
1x:	72°C for 6min

Table 16: Components for the preparation of the indicated PCR master mixes and the corresponding PCR programs.

2.4 Histological Analyses

2.4.1 Hematoxylin and Eosin Staining

37 % Formaldehyde Solution	*# F1635, Sigma-Aldrich, Munich, Germany*
Phosphate Buffered Saline (PBS) (Gibco)	*# 14190-094, Thermo Fisher, Schwerte, Germany*
Hematoxylin	*# GHS380, Sigma-Aldrich, Munich, Germany*
Eosin	*# HT110380, Sigma-Aldrich, Munich, Germany*
Xylene	*# 247642, Sigma-Aldrich, Munich, Germany*
Roti Histokitt II mounting medium	*# T160.1, Roth, Karlsruhe, Germany*

A hematoxylin and eosin (H&E) staining is frequently done for morphological tissue evaluation since it allows the discrimination of different cellular structures. Hematoxylin is basic and binds therefore acidic cellular components like DNA and RNA, which get stained in violet or dark blue. By contrast, eosin is an acidic dye that binds to the majority of proteins, which are due to the positively charged amino acid side chains of arginine and lysine acidophilic in most cases. Eosin colors bound structures in bright pink.

After isolating murine tissues as described under 2.5.1, 8 µm cryosections were cut (Cryostat, Thermo) and kept at -80°C for long-time storage. Prior to the staining, sections were defrosted at RT until they were completely dry. Thereafter, tissue sections were fixed in 4% PFA for 15 min under light exclusion and washed three times for 10 min in PBS. After rinsing object slides with ddH_2O for 1 min, specimens were incubated in hematoxylin for 5 min at RT and subsequently blued for 5 min in tap water. Hereafter, object slides were again rinsed with ddH_2O for 1 min and stained with eosin for 1 min at RT. Tissue specimens were dehydrated by rinsing in a series of graded alcohols (70 %, 96 %, 99%), followed by an additional incubation step in 99 % ethanol for 1 min. Finally, sections were incubated in xylene for 5 min, covered with anhydrous Roti Histokitt II mounting medium and covered with cover slips.

2.4.2 Immunohistochemistry

NovoLink Polymer Detection System	*# RE7290-CE, Leica Biosys., Wetzlar, Germany*
Xylene	*# 247642, Sigma-Aldrich, Munich, Germany*
Phosphate Buffered Saline (PBS) (Gibco)	*# 14190-094, Thermo Fisher, Schwerte, Germany*
Ethanol absolute	*# 32205, Sigma-Aldrich, Munich, Germany*
OCT mounting medium	*# SA62550, Science Services, Munich, Germany*
37 % Formaldehyde Solution	*# F1635, Sigma-Aldrich, Munich, Germany*

Immunohistochemical analyses allow a direct evaluation of protein expression levels and protein expression patterns within single cells and whole tissue specimens. Staining on cryosections as well as paraffin-embedded ones was performed by using the “NovoLink Polymer Detection System”. This kit contains a peroxidase-blocking reagent, a protein-blocking reagent, a polymer solution, a diaminobenzidine (DAB) solution and hematoxylin.

All human tissues were paraffin-embedded and were therefor dewaxed and rehydrated by incubating tissue specimens twice in xylene for 10 min, followed by a serial incubation in graded alcohols (99%, 96%, 70%) for 5 min each. Finally, tissue slides were rinsed in ddH_2O for 5 min.

All murine tissues were isolated as described under 2.5.1, transferred into vinyl specimen molds (Sakura Finetek, Torrance, USA), covered with OCT mounting medium (Science Services, Munich, Germany) and gradually frozen in the gas phase of liquid nitrogen. Subsequently, 8 µm cryosections were cut (Cryostat, Thermo) and kept at -80°C for long-time storage. Prior to the staining, sections were defrosted at RT until they were completely dry. Thereafter, tissue sections were fixed in 4% PFA for 15 min under light exclusion, washed five times for 10 min in PBS, one time for 5 min in TBS-TTX to allow membrane permeabilization and one last time for 5 min in ddH_2O. All washing

steps were performed on a shaking device. At this point, the protocols for paraffin-embedded and cryosections converge and all following steps were done uniformly. In order to unmask the antibody-binding sites, object slides were transferred into cuvettes filled with citrate buffer (pH6) and cooked five times for 3 min in the microwave. Subsequent to the antigen-retrieval, object slides were kept in the citrate buffer until they cooled down to RT. After washing again for 5 min in ddH_2O, tissue sections were circuited with a DAKO-Pen which is water repelling and allows in this way to reduce the amount of all following reagents, such as antibody solutions. In order to reduce the background staining, endogenous peroxidase in the tissue was inhibited by incubating the specimens for 15 min with the peroxidase-blocking reagent (~ 50µl per object slide, depending on the tissue size) in a wet chamber. Blocking reagent was removed by constantly flushing the specimens with ddH_2O for 1 min, followed by two washing steps in TBS-TTX for 5 min each. Unspecific binding sites were blocked by incubating the tissue sections for 10 min with 50µl of the protein-blocking reagent in a wet chamber, whereupon the specimens were again washed twice in TBS-TTX for 5 min. The applied primary antibody was diluted in PBT as indicated (Table 17) and poured onto the tissue specimen, which were then incubated in a wet chamber at RT or, if necessary, at 4°C over night. After washing the specimens thrice for 5 min in TBS-TTX, tissue sections were incubated with the polymer solution for 30 min in a wet chamber at RT. The polymer solution contains HRP-coupled anti-mouse and anti-rabbit secondary antibodies. During the following three washing steps for 5 min in TBS-TTX, the DAB working solution was prepared by diluting the DAB solution with the DAB-substrate buffer in a 1:20 ratio. Under light exclusion, the DAB working solution was poured onto the tissues and incubated in a wet chamber as indicated. During the incubation time, the horse radish peroxidase converts the hydrogen peroxide, leading to an oxidation-induced color change of the DAB-chromogen. This reaction was terminated by washing the specimens three times for 5 min with ddH_2O. Subsequently, nuclei were counterstained for 3-5 min with hematoxylin, which needs to be blued by an incubation in tap water for 5 min. After washing the specimens one last time for 5 min in ddH_2O, tissues were coated with aqueous Aquatex mounting medium and covered with cover slips.

Primary Antibody	Order number, Company	Incubation	Dilution
Reactivity: mouse			
Bcl-xL	# 2764, Cell Signaling	30min, RT	1:350 in PBT
CD3	# ab16669, abcam	30min, RT	1:100 in PBT
CD20	# PA5-16701, Thermo Scientific	20 h, 4°C	1:150 in PBT
CD68	# ab125212, abcam	20 h, 4°C	1:3000 in PBT
clPARP	# ab32064, abcam	15 h, 4°C	1:500 in PBT

Ki67	# ab16667, abcam	30 min, RT	1:500 in PBT
LC3	# 3868, Cell Signaling	15 h, 4°C	1:1000 in PBT
Lysozyme	# ab108508, abcam	15 h, 4°C	1:2000 in PBT
Mcl-1	# 600-401-394, Rockland	20 h, 4°C	1:1000 in PBT
RIPK1	# AP00087PU-N	15 h, 4°C	1:500 in PBT
Reactivity: human			
Bcl-2	# LS-B6772, LSBio	20 h, 4°C	1:50 in PBT
Bcl-xL	# 2764, Cell Signaling	1 h, RT	1:200 in PBT
clPARP	# 5625, Cell Signaling	20 h, RT	1:50 in PBT
Ki67	# ab16667, abcam	30 min, RT	1:200 in PBT
Mcl-1 (h)	# HPA031125, Sigma-Aldrich	20 h, 4°C	1:150 in PBT

Table 17: Antibodies used for immunohistochemical staining.

2.4.3 TUNEL Assay

RNase-Free DNase Set	*# 79254, Qiagen*
37 % Formaldehyde Solution	*# F1635, Sigma-Aldrich, Munich, Germany*
In Situ Cell Death Detection Kit, Fluorescein	*# 11684795910, Roche, Risch, Switzerland*
DAPI-containing mounting medium	*# AKS-38448, Dianova, Hamburg, Germany*
Phosphate Buffered Saline (PBS) (Gibco)	*# 14190-094, Thermo Fisher, Schwerte, Germany*

During apoptosis the DNA gets fragmented and displays single- and double-strand breaks afterwards. This can be used for the identification of apoptotic cells by labeling the emerging free 3´-OH ends with modified nucleotides in an enzymatic reaction. The polymerization is catalyzed by the terminal-deoxynucleotidyl-transferase (TdT), with fluorescein-labeled dUTP as substrate. In this way, labeled cells in a tissue section can be identified under a fluorescence microscope (Keyence, Neu-Isenburg, Germany) as being apoptotic. Terminal deoxynucleotidyl transferase dUTP nick end labeling (TUNEL) staining was performed by using the “In Situ Cell Death Detection Kit, Fluorescein”. In order to detect apoptotic enterocytes in the murine gut mucosa, the intestinal tissue was isolated, covered with OCT mounting medium and gradually frozen in the gas phase of liquid nitrogen as described in 2.5.1. 8 µm cryosections were cut (Cryostat, Thermo) and kept at -80°C for long-time storage. Prior to the staining, sections were defrosted at RT until they were completely dry. Thereafter, tissue sections were fixed in 4% PFA for 20 min under light exclusion and washed three times for 10 min in PBS. Cell membranes were permeabilized by incubating tissue specimens

with chilled (4°C) permeabilization buffer for 2 min on ice. This process was terminated by washing the sections twice for 5 min in PBS. In order to generate a positive control, one specimen was incubated for 10 min at RT with 50 µl DNase I solution (~ 1500 U/ml in 50 mM Tris-HCl, pH 7.5, 1mg/ml BSA) and washed twice for 5 min in PBS, afterwards. Meanwhile, the TUNEL reaction mix was freshly prepared by mixing Enzyme Solution (vial 1) and Label Solution (vial 2) in a 1:10 ratio. All components of the TUNEL reaction mix were permanently kept on ice and since some ingredients are potentially carcinogenic, the work was done under a hood. 50-100µl of the reaction mixture were poured onto each tissue section and specimens were incubated for 1h at RT in a wet chamber. To generate a negative control, one tissue specimen was incubated with Label Solution only. Finally, sections were washed twice for 5 min in PBS, coated with DAPI-containing mounting medium and covered with cover slips. TUNEL-stained specimens were imaged with a fluorescence microscope (Keyence, Neu-Isenburg, Germany), using a 488 nm excitation laser with emission at 530 nm.

2.5 Mouse Models

2.5.1 Breeding and Organ Removal

Phosphate Buffered Saline (PBS) (Gibco)	*# 14190-094, Thermo Fisher, Schwerte, Germany*
OCT mounting medium	*# SA62550, Science Services, Munich, Germany*

Mice expressing the Cre-recombinase under control of the Villin-promoter (Villin-Cre) were kindly provided by Dr. W. Chamulitrat (University Hospital Heidelberg, Germany). Mice carrying loxP-flanked alleles of Bcl-x_L (Bcl-x_L^{FLOX}) were obtained from Prof. Y.-W. He (Duke University School of Medicin, Durham, NC, USA) and Mcl-1^{FLOX} mice from Dr. WG Kaelin (Dana-Farber Cancer Institute, Boston, USA). All these mouse strains have a C57BL/6-background. In order to generate mice with a conditional loss of Mcl-1 (Mcl-$1^{\Delta IEC}$) or Bcl-x_L (Bcl-$x_L^{\Delta IEC}$) in intestinal epithelial cells, Villin-Cre mice were crossbred with the respective flox-strain. Later on, Bcl-$x_L^{\Delta IEC}$ mice were bred in a homozygous manner, whereas males showing a homozygous loss of Mcl-1 are infertile. For this reason, only males with a heterozygous flox-status were used for further breeding in the Mcl-$1^{\Delta IEC}$ strain. Since the expression of the Cre-recombinase have been shown to induce gastric inflammation[202], Villin-Cre mice were chosen as control group for all experiments performed. Mice were housed in individually ventilated cages at the SPF animal facility of the University Hospital in Heidelberg, Germany and kept under a 12 h light cycle with *ad libitum* feeding. All experiments on mice were

conducted according to institutional, national and European animal regulations and protocols were approved by local government authorities.

In order to isolate the intestine, mice were sacrificed by cervical dislocation and the bowel cavity was opened. The colon was removed, rinsed with PBS and it´s length was measured. If the tissue was subsequently analyzed by immunohistochemistry, the colon was transferred covered with OCT mounting medium and gradually frozen in the gas phase of liquid nitrogen. By contrast, later protein or RNA analyses required isolation of the mucosal layer. After longitudinal opening of the colon, the mucosa was separated from the subjacent layers by wiping it off with the edge of an object slide. The isolated tissue was transferred into a 1,5 ml reaction tube and snap frozen in liquid nitrogen.

2.5.2 AOM/DSS Model and Mouse Endoscopy

Azoxymethane (AOM)	*# A5486, Sigma-Aldrich, Munich, Germany*
Dextran Sodium Sulfate (DSS)	*# 0216011025, MP Biomedicals, Santa Ana, CA, USA*

Ten-week old Bcl-$x_L^{\Delta IEC}$ and Villin-Cre mice (n=10 per group) with a body weight > 20 g were injected intraperitoneally with AOM (10 mg per kg body weight). Experimental groups were similar with regard to age and sex ratio.

The mutagenic agent AOM initiates intestinal tumor formation, which is promoted by three cycles of the pro-inflammatory reagent DSS in the drinking water (2% w/v). Each cycle lasted 7 days with 14 days of recovery in between. During DSS treatment, the health status was determined each day by using body weight and diarrhea severity as main parameters. For evaluation of diarrhea severity, the following score was used:

0. No diarrhea: solid stool with no sign of soiling around the anus.
1. Mild diarrhea: formed stool that appears moist on the outside. Some signs of soiling around the anus.
2. Diarrhea: unformed stool with a mucous-like appearance. Considerable soiling around the anus.
3. Severe diarrhea: mostly clear or mucous-like liquid stool with very minimal solid present and considerable soiling around anus.
4. Bloody diarrhea: severe diarrhea with bloody contingent and considerable soiling around anus.

High-resolution mouse endoscopy was performed[203] with a Mainz COLOVIEW endoscopic system (Karl Storz, Tuttlingen, Germany). Prior to endoscopy, mice were anesthetized with 5% isoflurane

in oxygen. For anesthesia maintenance, the concentration of the anesthetic was reduced to 2% isoflurane in oxygen. Mice were taped onto a warming plate (37°C) in order to preserve body temperature and the endoscope was carefully introduced via the anus. The endoscopic camera allowed capturing of high quality pictures, which were suitable for tumor monitoring. Eighty days after AOM injection, mice were sacrificed by cervical dislocation and bowel cavity was opened. The colon was removed, rinsed with PBS and opened longitudinally. Colorectal tumors were counted and tumor diameters were measured with a sliding caliper. Some tumors were taken for immunohistochemical analyses, whereas others were used for protein isolation as described.

2.6 Statistical Analysis

Collected data were descriptively shown and mean values were taken as measures of location, depicted as means + SD (standard deviation). In case of a gaussian data distribution and independent groups, an unpaired, two-sided Student´s T-test was applied for statistical analysis. If groups were dependent, as it was the case in the tissue culture experiments, for instance, a paired, two-sided Student´s T-test was performed. Non-parametric data, like the grading of an immunohistochemical staining, were statistically evaluated by using the Mann-Whitney U test. The coefficient of determination (R^2) was calculated with Excel to analyze how close the depicted data fit to the linear regression line. R^2 lies always between 0 and 1 and the higher the value for R^2, the better the linear regression fits the obtained data. R 3.1.3 statistic software was used for all other statistical analyses (www.R-project.org). *p*-values < 0,05 were considered significant and are indicated as following: $*p < 0{,}05$, $**p < 0{,}01$, $***p < 0{,}001$.

3.1 Expression Levels of anti-apoptotic Bcl-2 Proteins in human colorectal Cancer

Avoidance of cell death is a prerequisite for cancer development and chemotherapy resistance. One possible mechanism for the longevity of malignant cells is the overexpression of cell death preventing proteins, such as anti-apoptotic Bcl-2 proteins.

In order to evaluate whether the expression of Bcl-2, Bcl-x_L and Mcl-1 is also altered in human CRC, intestinal mucosa and colorectal tumor specimens were immunohistochemically analyzed. Therefor, a tissue microarray (TMA), containing spots of healthy colon mucosa, adenoma tissue and adenocarcinoma tissue, was obtained from the Tissue Bank of the National Center for Tumor Diseases (NCT, Heidelberg, Germany).

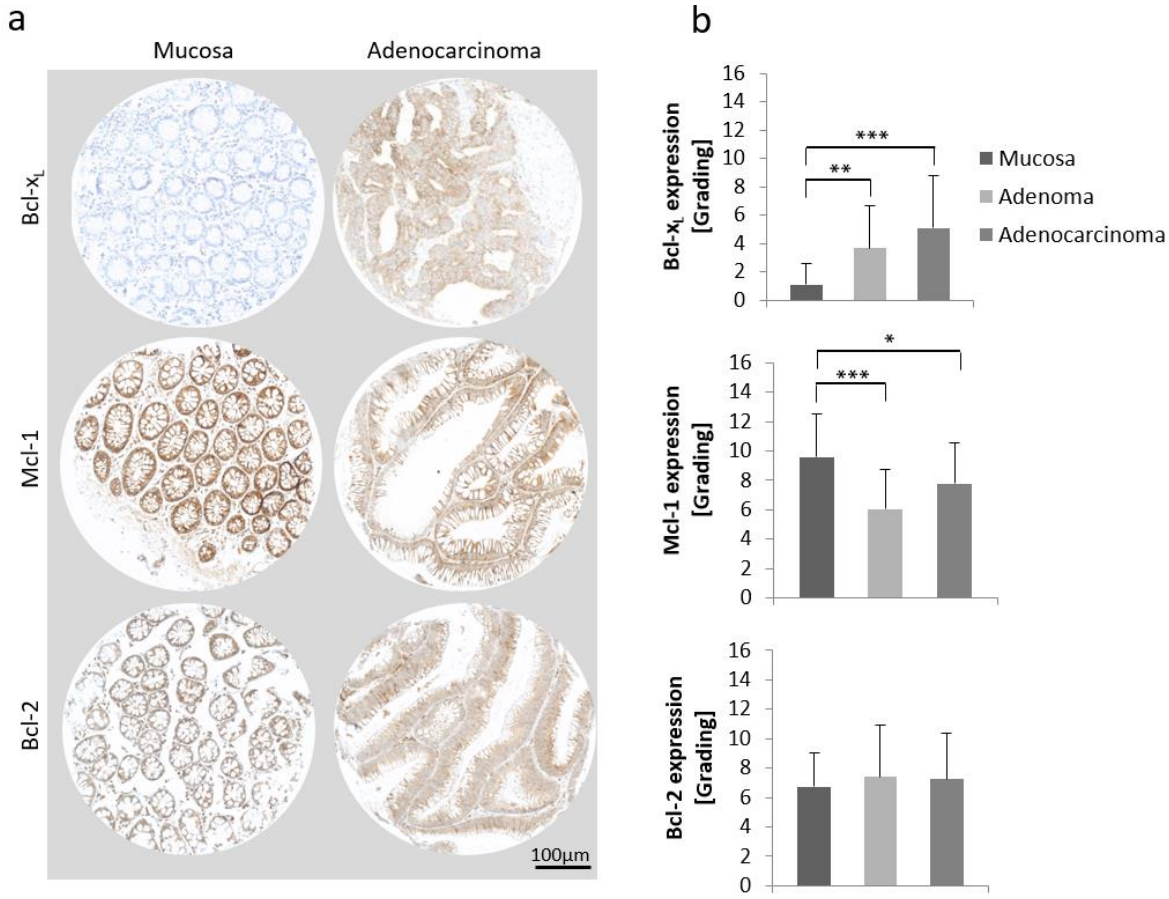

Figure 6: Expression levels of anti-apoptotic Bcl-2 proteins in human CRC. **a)** IHC staining against Bcl-x_L, Mcl-1 and Bcl-2 on a TMA, containing normal mucosa (n=13), adenoma (n=22) and adenocarcinoma tissue (n=61). Exemplary spots of mucosal and adenocarcinomal tissue are shown. **b)** Evaluation of staining intensities by multiplying values for staining quantity and quality. All p-values are calculated using mucosa as control group. Bcl-x_L is significantly overexpressed in adenomas and adenocarcinomas and Mcl-1 shows a decreased expression whereas Bcl-2 shows no deregulated expression. Values are expressed as means + SD. *p < 0,05; **p < 0,01; ***p < 0,001.

In adenomas, Bcl-x_L was found to be significantly overexpressed ($p<0,01$), if compared to normal mucosa, with a further increase in adenocarcinomal tissue ($p<0,001$). For Bcl-2, no significant differences in the expression levels were found. Mcl-1 was found to be significantly downregulated in adenomas ($p<0,001$) with a slight rebound in the malignant stage ($p<0,05$).

Furthermore, the expression levels of Bcl-x_L and Mcl-1 were compared between primary colorectal tumors and corresponding liver metastases, derived from 10 patients. The respective tissue specimens were taken upon surgical resection in the department of general and transplantation surgery of the Heidelberg University Hospital. Analysis of the immunohistochemical staining revealed neither for Bcl-x_L, nor for Mcl-1 significantly altered expression levels in primary tumors and metastases.

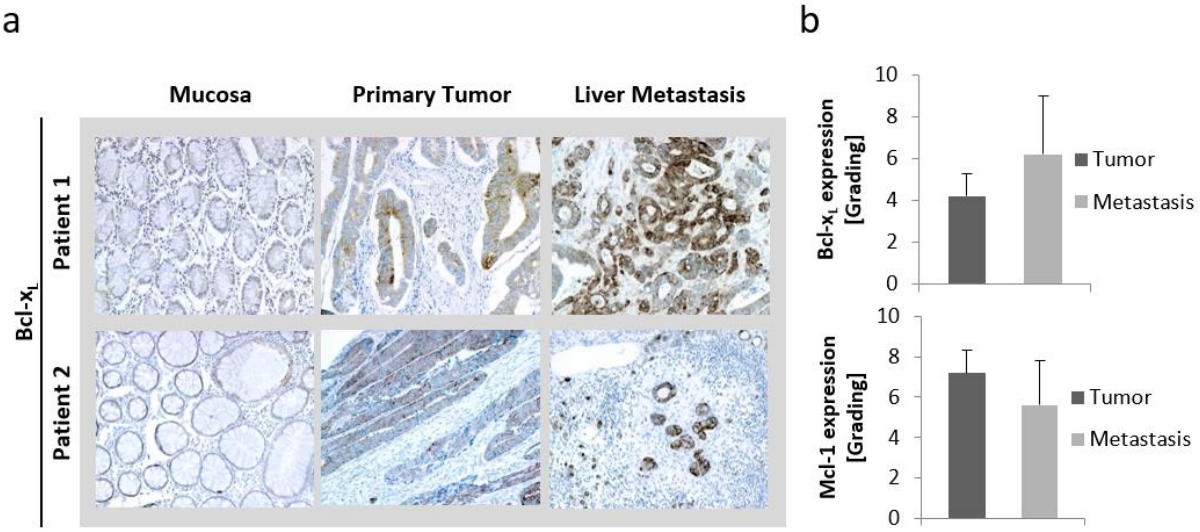

Figure 7: Expression levels of Bcl-x_L and Mcl-1 in primary tumors and liver metastases. **a)** IHC staining against Bcl-x_L on normal mucosa, primary colorectal tumors and corresponding liver metastases (n=10 patients). Pictures of 2 exemplary patients are shown. **b)** Evaluation of staining intensities by multiplying values for staining quantity and quality, showing neither for Bcl-x_L nor for Mcl-1 significantly altered expression levels in primary tumor and metastases. Values are expressed as means + SD.

3.2 The Role of anti-apoptotic Bcl-2 Proteins for human colorectal Cancer Cells in vitro

For all experiments assessing the function of Bcl-2 proteins *in vitro*, human colorectal cancer cell lines HT29 and SW480 were chosen. In these cells, the expression levels of our proteins of interest were downregulated to evaluate their function for viability and proliferation as well as for migration and invasiveness of CRC cells.

For downregulation of gene expression, small interfering RNAs (siRNA) were used. siRNA sequences, complementary to the respective target mRNA, were calculated by means of the Eurofins blasting program.

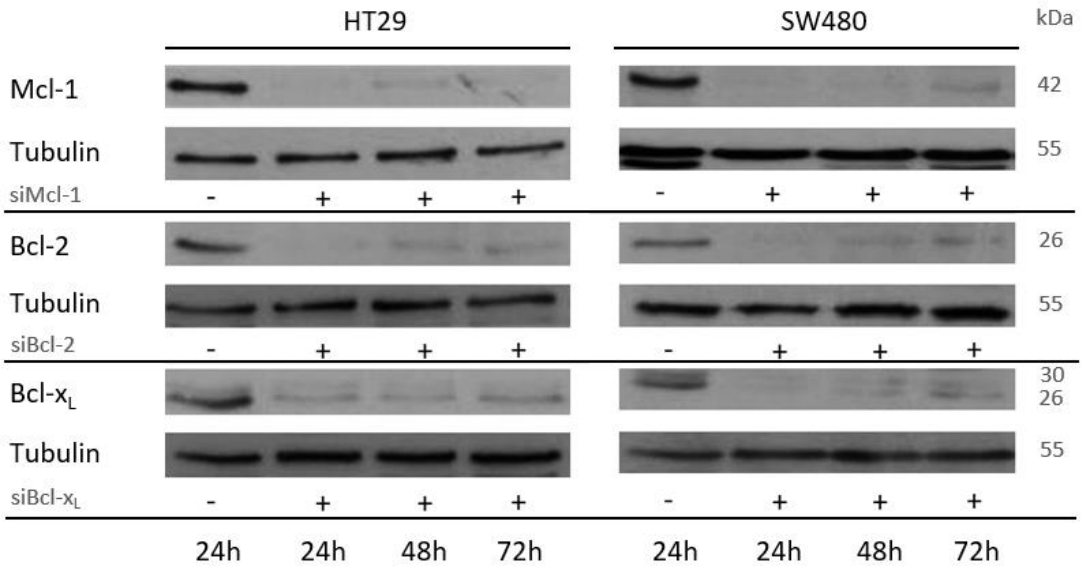

Figure 8: siRNA mediated knockdown of anti-apoptotic Bcl-2 proteins in human CRC cells. Western blot analyses of HT29 (left) and SW480 (right) cells after siRNA mediated knockdown of Mcl-1, Bcl-2 or Bcl-x_L 24, 48 and 72 h post transfection. Tubulin served as loading control. The Western blots presented are representative of three independent experiments.

Post transfection, the expression of Mcl-1, Bcl-2 and Bcl-x_L was determined on the protein level by Western blot analysis. This showed, that all utilized siRNAs could efficiently downregulate the respective protein expression in both cell lines. As a control, cells were transfected with an unspecific siRNA (scrambled siRNA/siSc), which is not complementary to any mRNA in the cell. Since some of the planned experiments required incubation times of more than 24 h, knockdown stability was additionally tested for up to three days. This revealed that the achieved knockdowns are stable for at least 72 h.

3.2.1 Knockdown of anti-apoptotic Bcl-2 Proteins does not lead to spontaneous Cell Death Induction

In a first approach, the siRNA mediated knockdown of anti-apoptotic Bcl-2 proteins was used to examine their importance for the viability of colorectal cancer cells. Therefore, cells were transfected with the respective siRNAs before viability was determined by a MTT assay. The results show that the knockdown of none of the anti-apoptotic Bcl-2 proteins lead to spontaneous cell death induction in HT29 or SW480 cells. Since a MTT assay always displays combined information about cell death and proliferation, this finding was further validated by FACS analysis of cleaved PARP (Poly(ADP-ribose)-Polymerase)-positive cells. In this case, staurosporine (STS) treated cells were used as a positive control. Neither in HT29 nor in SW480 cells, the silencing of anti-apoptotic Bcl-2 proteins lead to a significant increase of cleaved PARP-positive cells if compared to siSc transfected controls. Western blot analysis revealed no counter-regulatory upregulation of kin proteins if one anti-apoptotic Bcl-2 protein was silenced (data not shown).

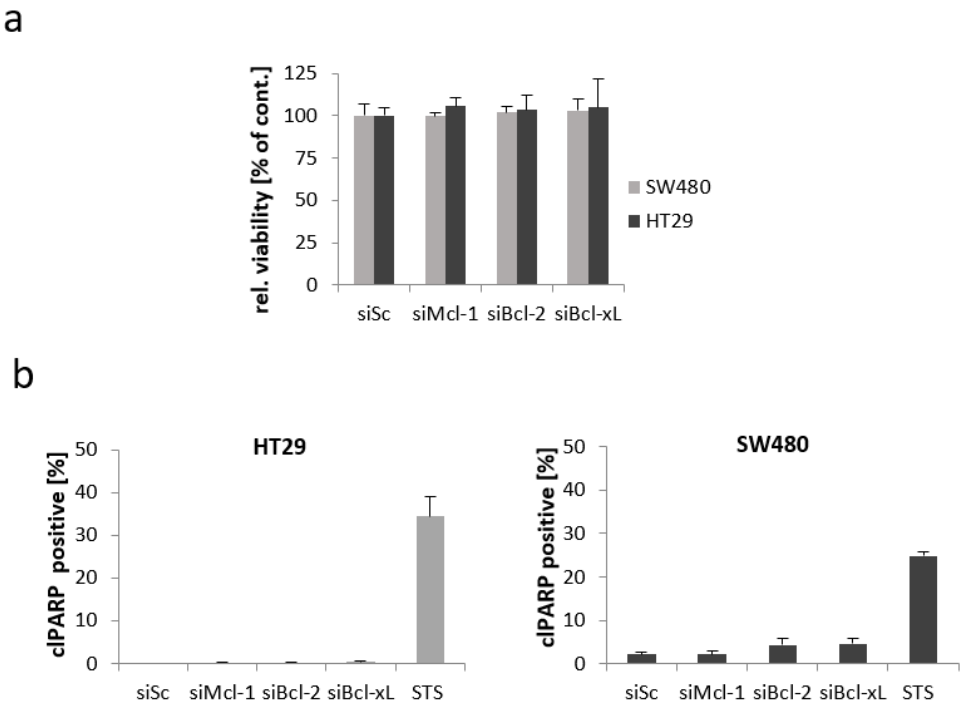

Figure 9: Viability of human CRC cells after siRNA mediated knockdown of anti-apoptotic Bcl-2 proteins. **a)** MTT-Assay of SW480 and HT29 cells after knockdown of Mcl-1, Bcl-2 and Bcl-x_L. **b)** Flow cytometric analyses of cleaved PARP-positive HT29 (left) and SW480 (right) cells, 48 h after knockdown of Mcl-1, Bcl-2 and Bcl-x_L. 24 h Staurosporine treatment (1 µM) served as a positive control for cell death induction. Flow cytometry analysis was performed in triplicates. All values are expressed as means + SD. Assays are representative of at least three independent experiments.

3.2.2 Knockdown of anti-apoptotic Bcl-2 Proteins does not exert anti-proliferative Effects on CRC Cells

Next, the role of anti-apoptotic Bcl-2 proteins for the proliferative capacity of CRC cells was evaluated by BrdU FACS analysis. Therefor, HT29 and SW480 cells were transfected with siRNA and incubated with the thymidine analogon bromodeoxyuridine (BrdU), which gets incorporated into the DNA of replicating cells. Subsequent FACS analysis of BrdU-positive cells revealed a higher basal proliferation level in HT29 (38,6% BrdU-positive) than in SW480 (21,1% BrdU-positive) cells.

The knockdown of Bcl-2 or Bcl-x_L lead neither in HT29 (siBcl-2: 37,3%; siBcl-x_L: 37,4%) nor in SW480 cells to a significant alteration of proliferation rates. By contrast, the diminution of Mcl-1 increased the amount of BrdU-positive HT29 cells significantly from 38,6% to 47,5% ($p<0,05$). In SW480 cells, a comparable pro-proliferative effect was detected after Mcl-1 knockdown. Here the percentage of BrdU-positive cells increased from 21,1% to 25,6% ($p<0,05$). This means that the knockdown of Mcl-1 increases the amount of proliferating cells, compared to the respective initial values, by approximately one fifth in both cell lines (Figure 10 a and b). To validate these findings, a proliferation kinetic for SW480 cells was compiled by cell counting at different time points after transfection. In line with the results obtained from the BrdU FACS analysis, solely the knockdown of Mcl-1 significantly changed proliferation rates over time (Figure 10 c).

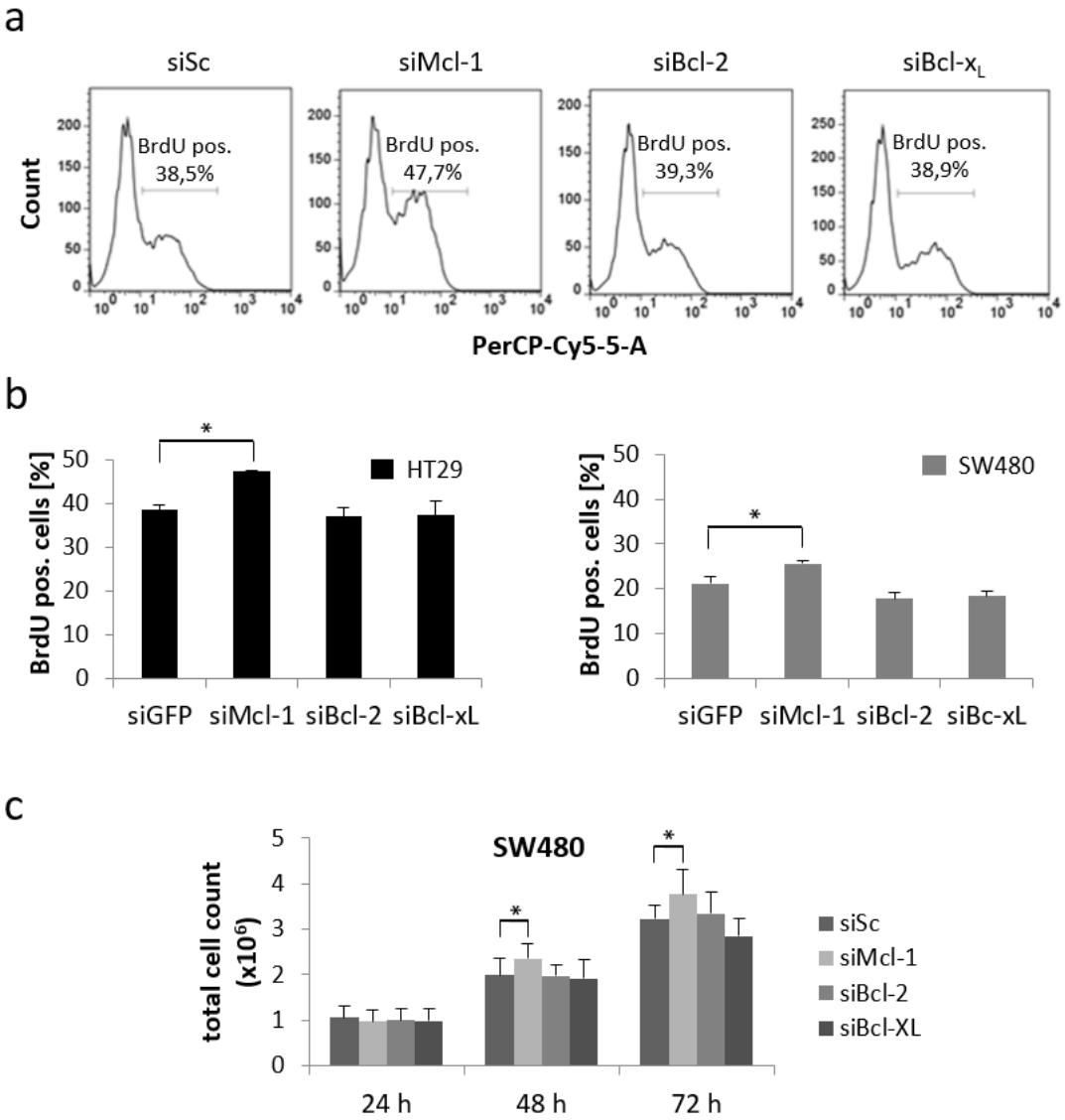

Figure 10: Proliferation of human CRC cells after siRNA mediated knockdown of anti-apoptotic Bcl-2 proteins. SW480 and HT29 cells were transfected with siRNA against Mcl-1, Bcl-2 and Bcl-x_L. 24 h post transfection, cells were pulsed with 20 µM BrdU and prepared for flow cytometry. **a)** Representative original flow cytometry data with HT29 cells, stained with an anti-BrdU antibody coupled to PerCP-CY5.5 fluorophore. **b)** Flow cytometric analyses for BrdU incorporation in HT29 (left) and SW480 (right) cells. **c)** Total cell count of SW480 cells after knockdown of Mcl-1, Bcl-2 and Bcl-x_L. Cells were seeded on 6 well plates, harvested and counted 24, 48 and 72 h post transfection. Values are expressed as means + SD. Assays were run in triplicates (flow cytometry) and sextuplicates (cell counting). Assays are representative of three independent experiments. *$p < 0,05$.

3.2.3 Anti-apoptotic Bcl-2 Proteins influence the migratory Ability of CRC Cells

The experiments regarding viability and proliferation showed, that siRNA mediated knockdown of anti-apoptotic Bcl-2 proteins does not negatively influence the number of CRC cells. This is an important prerequisite to study the role, anti-apoptotic Bcl-2 proteins play for the migratory capacity of CRC cells. For visualization of cellular migration, scratch assays on monolayers of transfected HT29 and SW480 cells were performed.

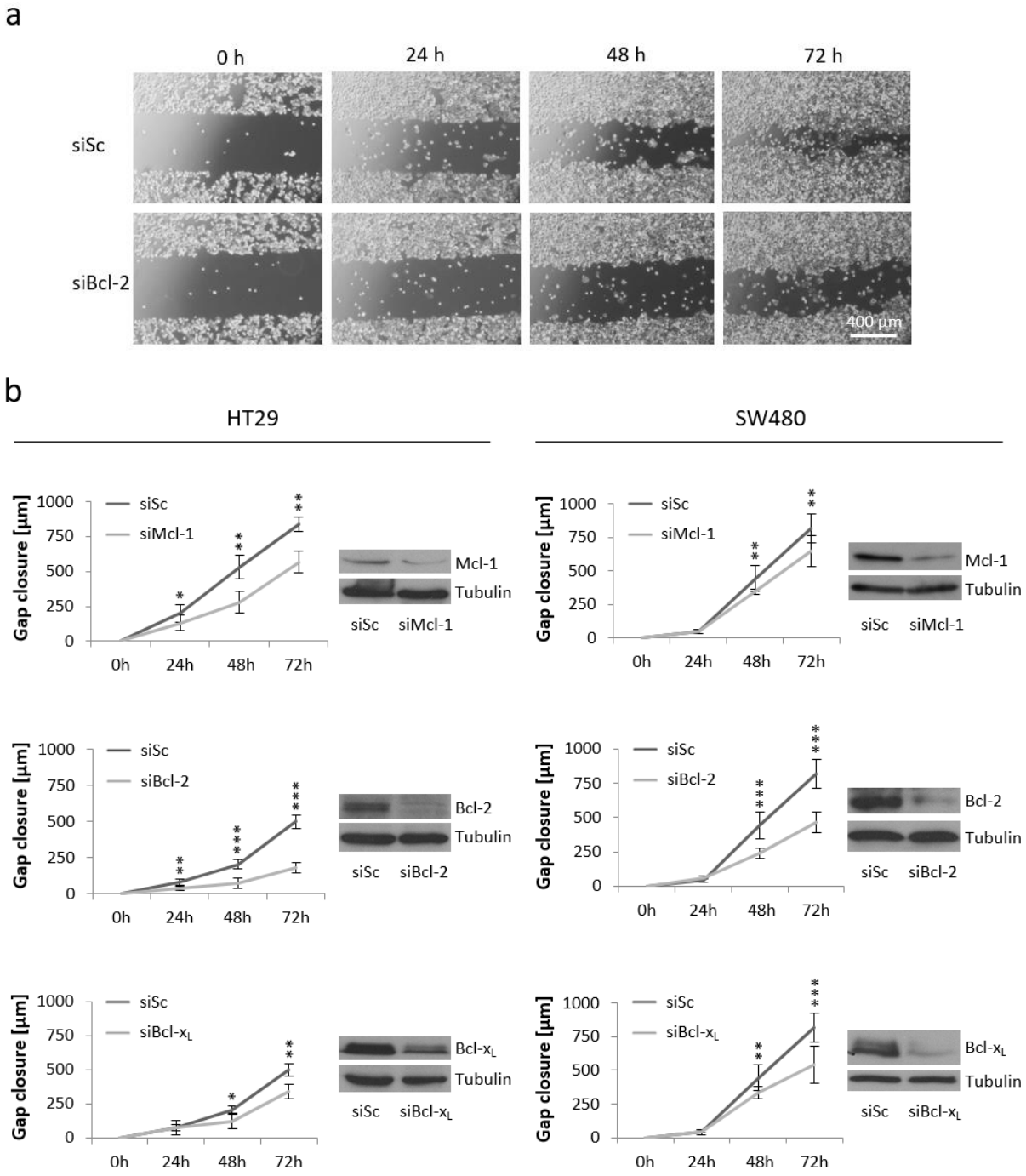

Figure 11: Migratory capacity of human CRC cells after siRNA mediated knockdown of anti-apoptotic Bcl-2 proteins. SW480 and HT29 cells were transfected with siRNA against Mcl-1, Bcl-2 and Bcl-x_L. Subsequently, the cell monolayer was scratched by using a sterile pipette tip and gap closure was measured 24, 48 and 72 h afterwards. Finally, cells were lysed and proteins were harvested in order to proof knockdown stability. **a**) Representative pictures of a scratch assay, showing gap closure capacity of HT29 cells after knockdown of Bcl-2. Scale bar indicates magnification for all panels. **b**) Gap closure kinetics of HT29 cells (left) and SW480 cells (right) after knockdown of Mcl-1, Bcl-2 and Bcl-x_L and corresponding Western blots. Values are expressed as means ± SD. Assays are representative of at least three independent experiments. *p < 0,05; **p < 0,01; ***p < 0,001.

Gap distances were measured every day over a time period of 72 h in total. Therefor, the exact image position within the well was marked to allow surveillance of gap closure and calculation of average migration distances in the very same sector. After 72 h, clear differences in transfected and mock transfected control cells were apparent. The knockdown of all three anti-apoptotic Bcl-2 proteins significantly slowed down gap closure in both HT29 (siMcl-1: $p<0,01$; siBcl-2: $p<0,001$; siBcl-x_L: $p=<0,01$) and SW480 cells (siMcl-1: $p< 0,01$; siBcl-2: $p < 0,001$; siBcl-x_L: $p < 0,01$). In both cell lines, the most conspicuous effect was observed after knockdown of Bcl-2, which decreased the migration distance to 56% of the siSc transfected control in SW480 and to 36% in HT29 cells (Figure 11 b).

Even though, scratch assays are most commonly used for evaluating the migratory ability of cells, an additional 3D cell culture model was applied to validate the obtained findings. This model is based on a polystyrene scaffold, which facilitates cellular interactions and movement of cells. Compared to conventional 2D cell culture models, it resembles a more physiological environment (Figure 12 a). Since the altered culture conditions might influence cell growth, proliferation was analyzed prior to the migration experiment. Due to their morphology, it is difficult to quantify SW480 by counting if they are grown in 3D cell culture. Therefore, the following experiments were primarily done with HT29 cells.

After transfection, HT29 cells were transferred onto the scaffolds and grown for 72 h. Subsequently, scaffolds were sectioned and cells were stained with Hematoxylin and Eosin to allow determination of cell numbers by counting. In addition, immunohistochemical staining of Ki67, as an additional approach to assess proliferation, was performed. The results obtained with both approaches underlined the previous findings on proliferation, showing no significant changes in total cell counts after knockdown of Bcl-x_L and Bcl-2 and a significant increase in total cell count after knockdown of Mcl-1 ($p<0,05$). This observation was also mirrored by a significant increase from 53% to 61% of Ki67-positive cells after siRNA mediated knockdown of Mcl-1 ($p<0,05$). By contrast, no significant changes in Ki67 positivity were observed after knockdown of either Bcl-2 or Bcl-x_L (Figure 12 b).

Regarding cellular motility, the knockdown of all anti-apoptotic Bcl-2 proteins significantly decreased covered distances. Since cells maintained their morphology and size after knockdown of Mcl-1, Bcl-2 and Bcl-x_L, the reduction of invaded areas is likely caused by impaired migration. Comparable to the findings obtained in the scratch assay, the most striking effect was observed after knockdown of Bcl-2 with a decrease to 54% of the invasion depth of siSc transfected controls (Figure 12 c).

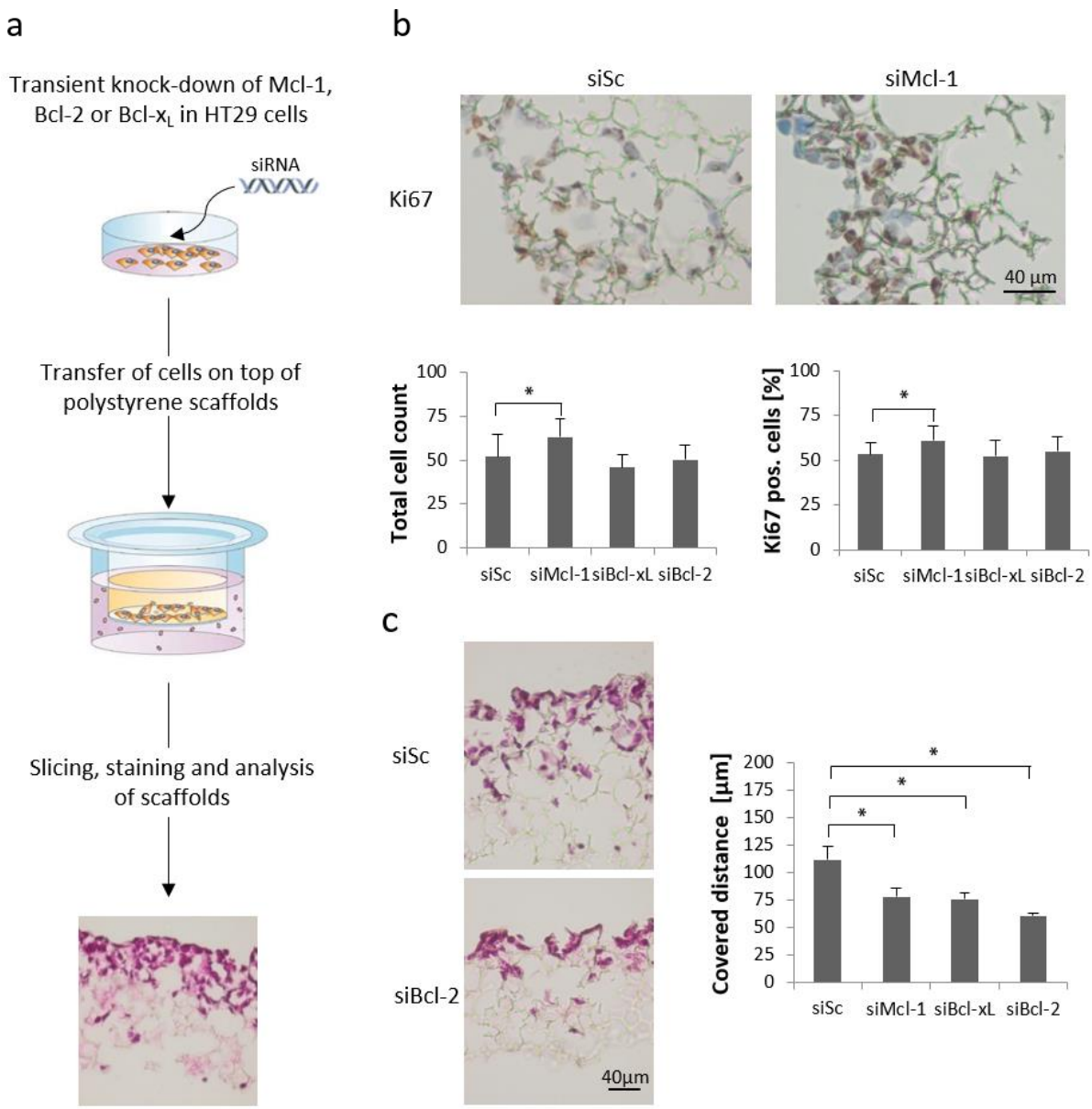

Figure 12: Proliferation and migration of HT29 cells in 3D scaffolds after siRNA mediated knockdown of Mcl-1, Bcl-2 and Bcl-x_L. **a**) Schematic description of the applied three-dimensional cell culture approach. HT29 cells were transfected with specific siRNA against Mcl-1, Bcl-2 or Bcl-x_L. 24 h post transfection, cells were harvested and 1×10^6 cells were seeded onto each scaffold. After 72 h, scaffolds were harvested for further processing. **b**) Representative pictures of HT29 cells in scaffolds after siRNA mediated knockdown of Mcl-1 and immunohistochemical staining of Ki67. Ki67 positive cells were counted for determining proliferation rates (right graph; n = 5 scaffolds per group and 10 visual fields per scaffold). Additionally, total cell numbers in scaffolds were determined by counting (right graph; n = 5 scaffolds per group and 10 visual fields per scaffold). Scale bar indicates magnification for both pictures. **c**) Representative pictures of Hematoxylin and Eosin stained HT29 cells in scaffolds after transfection with scrambled RNA (siSc) or siRNA against Bcl-2 (siBcl-2). Scale bar indicates magnification for both pictures. Invasion depth was measured every 20 µm (n = 5 scaffolds per group and 10 visual fields per scaffold). Values are expressed as mean + SD. Assays are representative of at least three independent experiments. *p < 0,05.

With the overexpression of Mcl-1, Bcl-2 and Bcl-x_L in HT29 and SW480 cells, the influence, anti-apoptotic Bcl-2 proteins have for cell migration, was further validated. Again, a scratch assay as well as a 3D cell culture assay were performed to evaluated whether overexpression potentially reverts the phenotype observed in the knockdown experiments.

For overexpression, cells were transfected with plasmid DNA. Controls were generated by transfecting the cells with the respective empty vectors. Overexpression of anti-apoptotic Bcl-2 proteins did neither alter viability nor proliferation of HT29 or SW480 cells, but the transfection with plasmid DNA *per se* exerted a non-negligible toxicity, especially on HT29 cells.

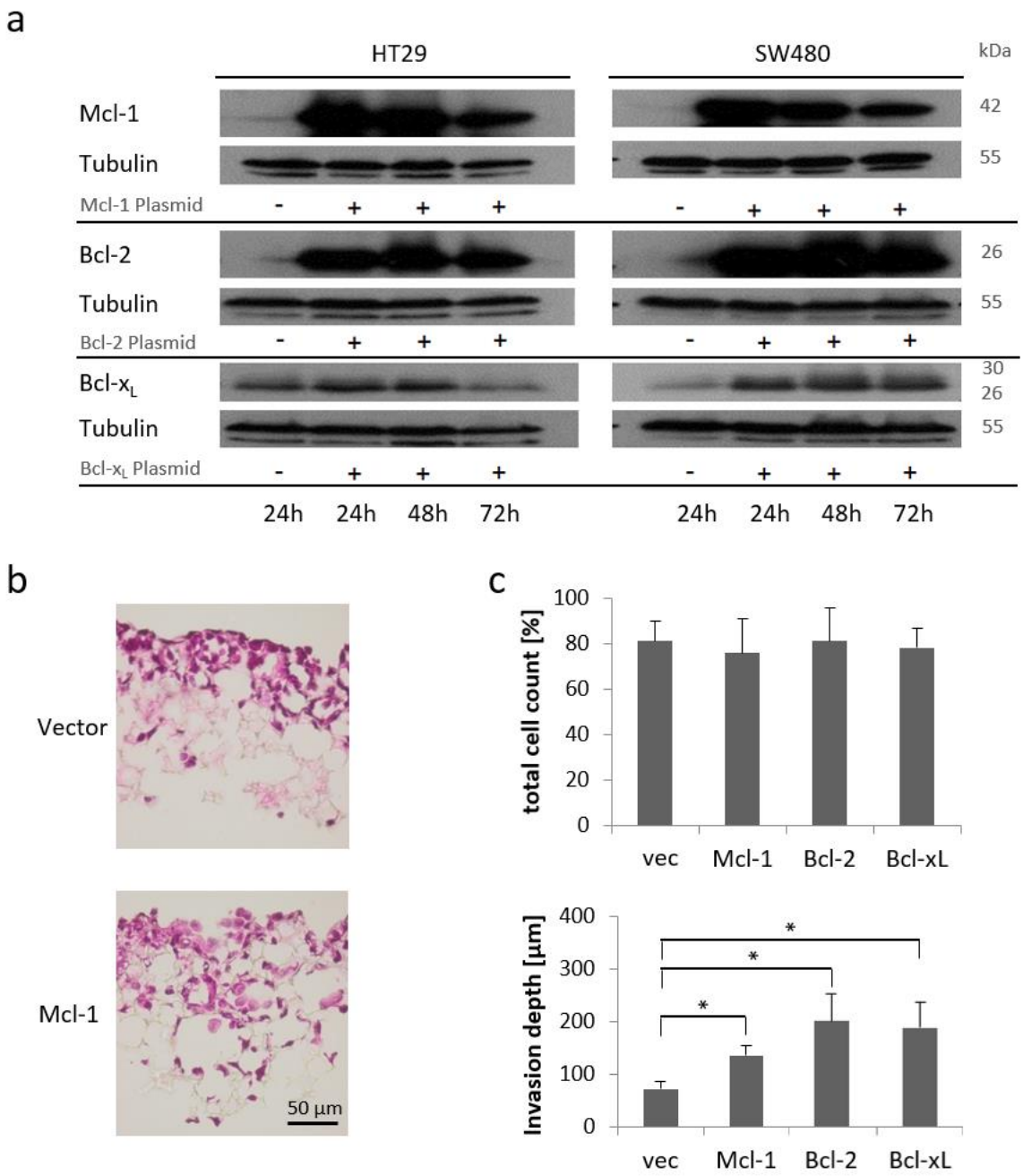

Figure 13: Overexpression of anti-apoptotic Bcl-2 proteins in human CRC cells. **a**) Western blot analyses of HT29 (left) and SW480 (right) overexpressing Mcl-1, Bcl-2 or Bcl-x_L 24, 48 and 72 h post transfection. Tubulin served as loading control. The Western blots presented are representative of three independent experiments. **b**) Representative pictures of Hematoxylin and Eosin stained HT29 cells in scaffolds after transfection with an empty vector or an Mcl-1 expression vector. Scale bar indicates magnification for both pictures. **c)** Total cell numbers in scaffolds were determined by counting (upper graph). Invasion depth was measured every 20 µm (lower graph). n = 5 scaffolds per group and 10 visual fields per scaffold. Values are expressed as mean + SD. Assays are representative of at least three independent experiments. *p < 0,05.

In addition, Western blot analysis showed differences in transfection efficiencies, with the weakest results for overexpression of Bcl-x_L in HT29 cells (Figure 13 a).

Nevertheless, HT29 cells, overexpressing Mcl-1, Bcl-2 or Bcl-x_L, showed a significantly increased motility in polystyrene scaffolds compared to vector transfected controls (Mcl-1: 190%; Bcl-2: 280% and Bcl-x_L: 260%; $p<0,05$; Figure 13 b and c lower graph). Since total cell numbers were not altered after the transfection (Figure 13 c upper graph), the observed increase of invaded areas is likely caused by an enhanced migratory capacity, which seems independent of differences in proliferation or viability. Additionally, a scratch assay was performed with both HT29 and SW480 cells (Figure 14). In SW480 cells, the overexpression of Bcl-2 induced the strongest phenotype, with the covered distance being almost doubled after 72 h (190%; $p<0,001$). Overexpression of Bcl-x_L also lead to a significantly increased motility of SW480 cells (158%, $p<0,001$). Overexpression of Mcl-1 lead only after 48 h to significant differences in covered distances (168%, $p<0,01$). Similar results were obtained after overexpression of Mcl-1, Bcl-2 or Bcl-x_L in HT29 cells. In all cases, significant differences in gap sizes were detected after 48 h (Mcl-1: 288%, $p<0,001$; Bcl-2: 160%, $p<0,001$; Bcl-x_L: 162%, $p<0,001$). After 72 h, by contrast, only HT29 cells overexpressing Mcl-1 showed a significantly increased motility compared with vector transfected control cells (Mcl-1: 248%, $p<0,001$).

In summary, the results conclusively show a correlation between the expression of anti-apoptotic Bcl-2 proteins and the motility of human CRC cells. The knockdown of Mcl-1, Bcl-2 or Bcl-x_L significantly impairs their migratory capacity, whereas overexpression induces a reversed phenotype. In both scenarios, the observed phenotypes seem independent of proliferation and viability.

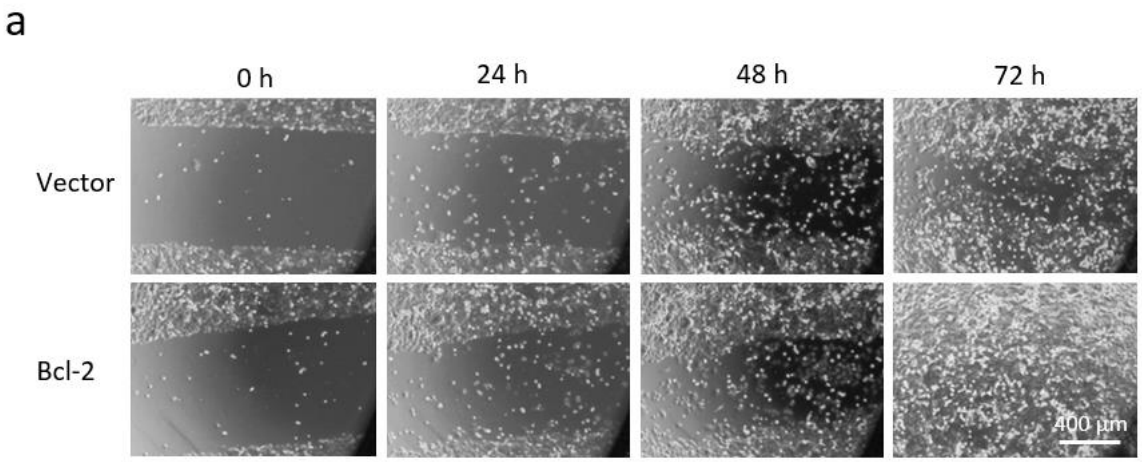

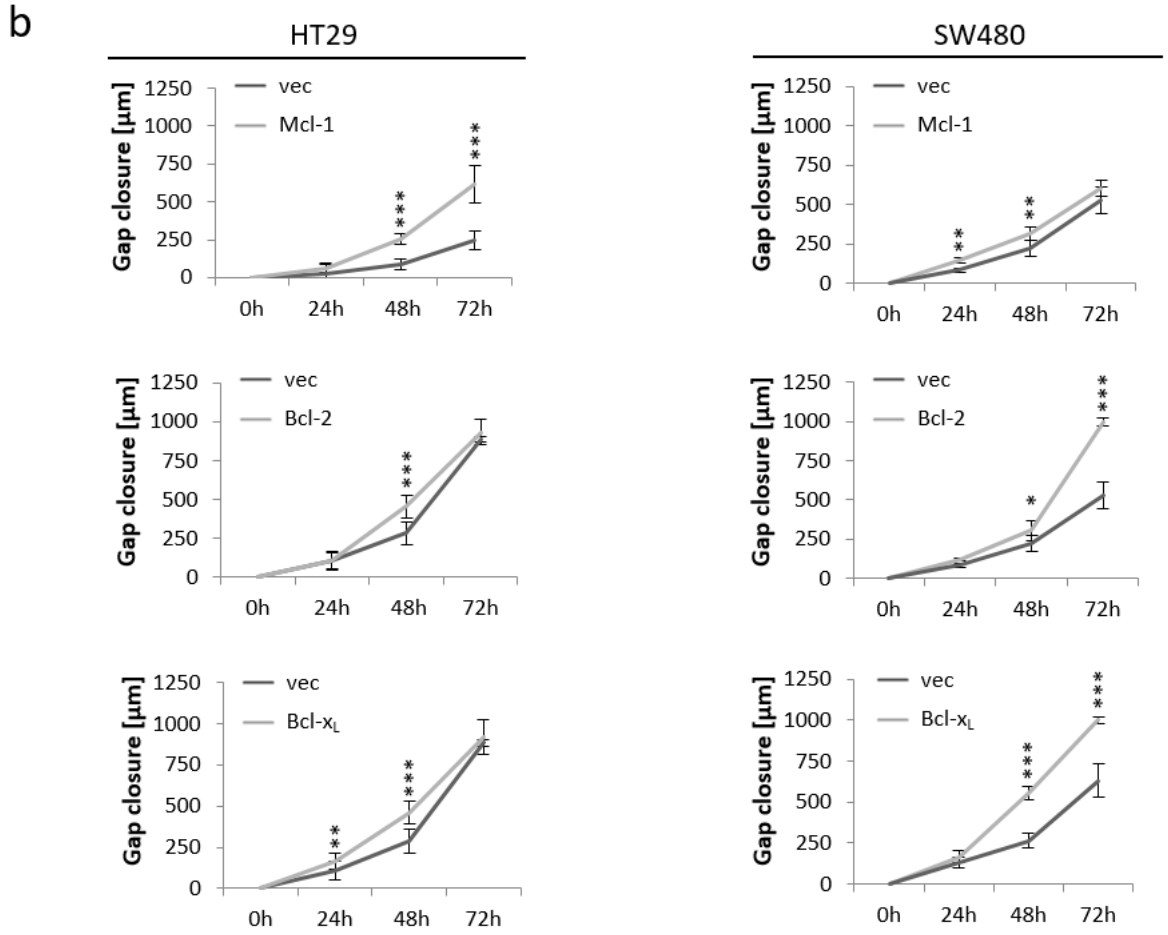

Figure 14: Migratory capacity of human CRC cells after overexpression of anti-apoptotic Bcl-2 proteins. SW480 and HT29 cells were transfected with plasmids expressing human Mcl-1, Bcl-2 or Bcl-x_L. Subsequently, the cell monolayer was scratched by using a sterile pipette tip and gap closure was measured 24, 48 and 72 h afterwards. **a**) Representative pictures of a scratch assay, showing gap closure capacity of SW480 cells overexpressing Bcl-2. Scale bar indicates magnification for all panels. **b**) Gap closure kinetics of HT29 cells (left) and SW480 cells (right) overexpressing Mcl-1, Bcl-2 or Bcl-x_L. Values are expressed as means ± SD. Assays are representative of at least three independent experiments. *p < 0,05; **p < 0,01; ***p < 0,001.

3.2.4 Knockdown of anti-apoptotic Bcl-2 Proteins inhibits the Invasiveness of CRC Cells

For metastasis formation, cancer cells do not only need to migrate but also to actively overcome the extracellular matrix during the invasion process. In order to study the role of anti-apoptotic Bcl-2 proteins in this context, Matrigel-coated Boyden chambers were used. Pre-experiments showed, that only SW480 were capable of getting over this barrier. Hence, the following experiment was performed with this cell line. Subsequent to the siRNA mediated knockdown of Mcl-1, Bcl-2 or Bcl-x_L, cells were transferred onto the Matrigel-coated insert. 48 h after seeding, invaded cells on the lower surface were fixed and nuclei were stained with Hoechst. Counting revealed, that the downregulation of each anti-apoptotic Bcl-2 protein, lead to a significantly decreased invasiveness of SW480 cells. Compared to siSc transfected controls, only 70% Bcl-x_L-deficient cells reached the lower surface ($p < 0,01$). The invasive properties of cells with downregulated Bcl-2 or Mcl-1 were

even more inhibited. Compared to the control, only 38% of Bcl-2-deficient ($p < 0,001$) and 37% of Mcl-1-deficient ($p < 0,001$) SW480 cells could overcome the Matrigel.

Together with the findings on cellular motility, these observations point to a potential role of anti-apoptotic Bcl-2 proteins for metastasis formation.

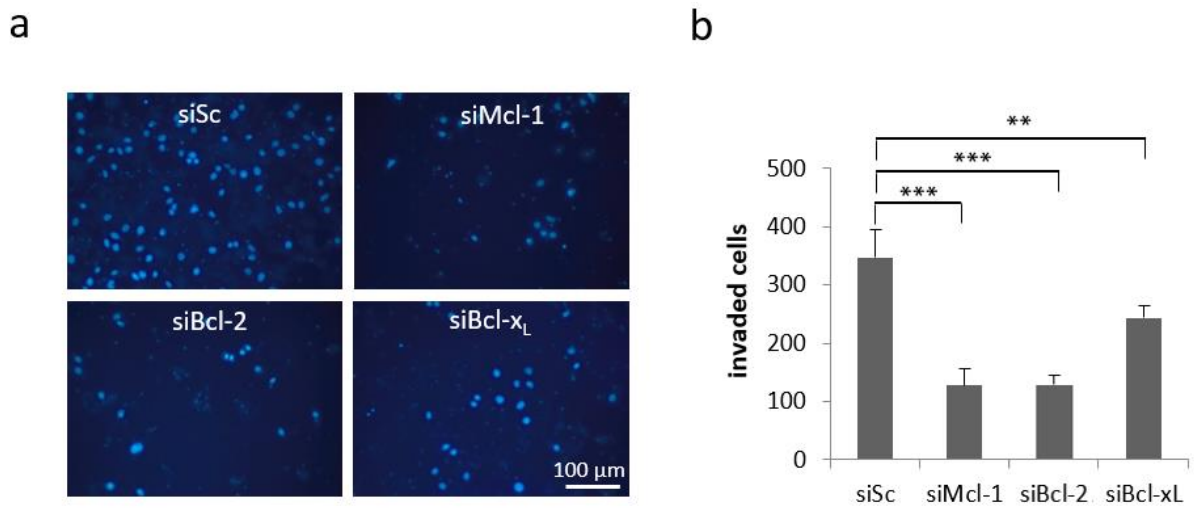

Figure 15: Invasiveness of SW480 cells after siRNA mediated knockdown of anti-apoptotic Bcl-2 proteins. SW480 cells were transfected with siRNA against Mcl-1, Bcl-2 or Bcl-x_L and 3×10^5 cells were transferred onto Matrigel-coated Boyden chambers. 48 h after seeding, nuclei on the lower surface were visualized by Hoechst staining. **a)** Representative pictures of lower insert surface after Hoechst staining (scale bar indicates magnification for all panels). **b)** Five pictures of every insert were taken and the number of Hoechst-positive nuclei was determined by counting. n = 5 inserts per group. Values are expressed as means + SD. Assays are representative of at least three independent experiments. **p < 0,01; ***p < 0,001.

3.2.5 The pan-Bcl-2 Inhibitor Obatoclax delays Cell Cycle Progression and inhibits Migration of CRC Cells

Obatoclax is a small molecule inhibitor, mimicking the function of BH3-only proteins. Via binding to their cleft, Obatoclax inhibits Mcl-1, Bcl-2 and Bcl-x_L as well. The findings on migration and invasiveness of CRC cells after siRNA-mediated knockdown of Mcl-1, Bcl-2 and Bcl-x_L drew a clear picture about the importance of anti-apoptotic Bcl-2 proteins for malignant features of intestinal tumor cells. Hence, the value of Obatoclax as a chemical inhibitor was tested in this context.

First, dose titration was performed in HT29 and SW480 cells, whereupon 0,25 µM and 0,5 µM were chosen for further migration and invasion experiments. These doses are in the sublethal range in both cell lines (Figure 16 a). Because it has been reported that Obatoclax treatment leads to a degradation of anti-apoptotic proteins in cancer cells[204], expression levels of Mcl-1, Bcl-2 and Bcl-x_L were determined under different inhibitor concentrations. Western blot analysis revealed no significant differences in the level of anti-apoptotic Bcl-2 proteins under 0,25 µM, 0,5 µM and 1 µM Obatoclax (Figure 16 b). In order to analyze the effect of Obatoclax treatment on migration, HT29 cells were seeded onto polystyrene scaffolds and subsequently treated with Obatoclax for seven

days. After slicing of the scaffolds, cells were first immunohistochemically stained for cleaved PARP to validate the non-lethality of the chosen doses. Compared to control, no differences in the amount of cleaved PARP-positive cells were found (Figure 16 c, right column). In addition, cells were stained for Ki67 to evaluate the effect of Obatoclax on proliferation. This revealed a negative correlation between Ki67 positivity and Obatoclax concentration (Figure 16 c, left column).

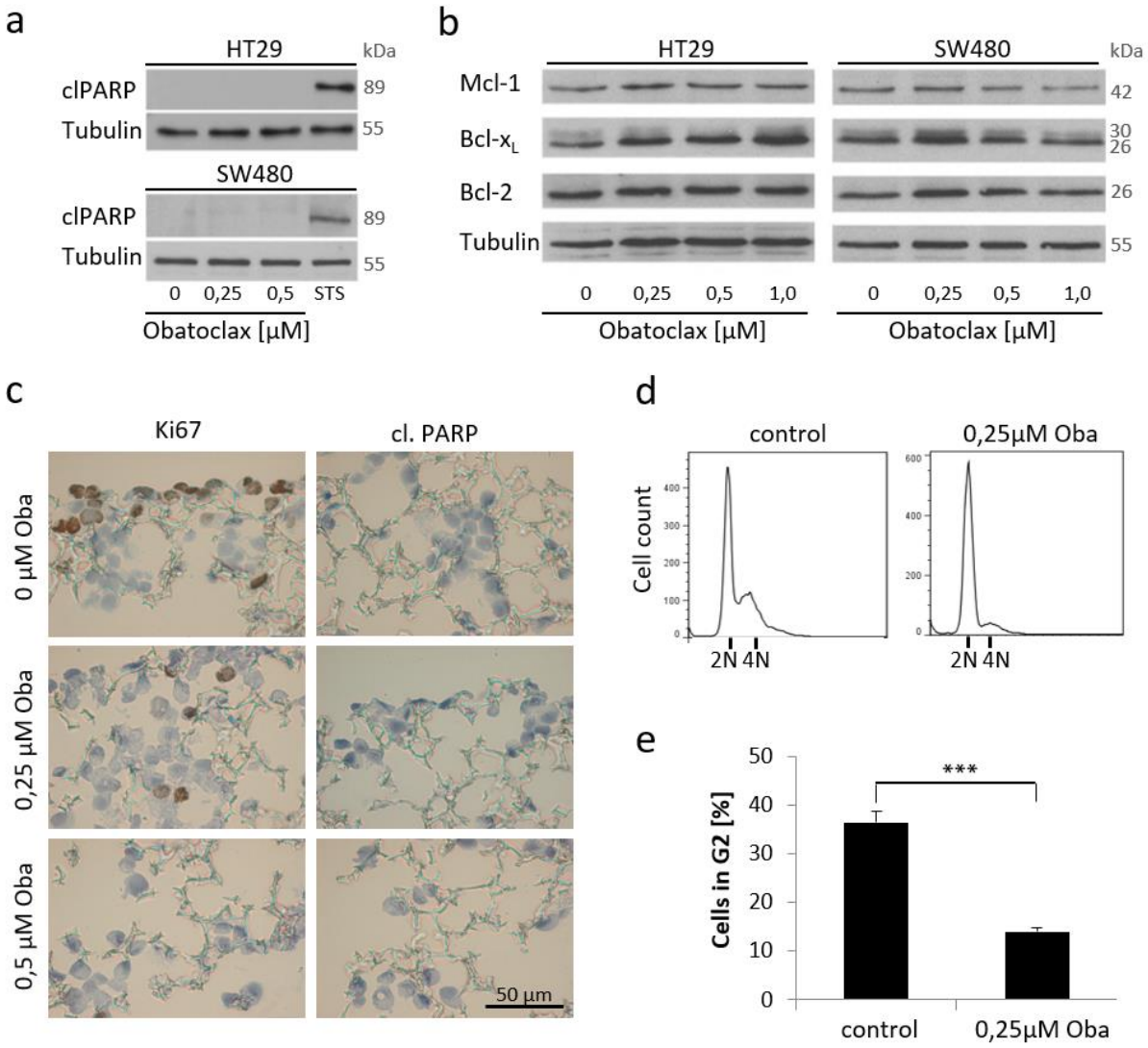

Figure 16: Cell death and proliferation of human CRC cells under treatment with the pan-Bcl-2 inhibitor Obatoclax. **a)** Representative Western blots detecting cleaved PARP in HT29 cells (upper panel) and SW480 cells (lower panel) after 24 h of Obatoclax treatment. Tubulin served as loading control. The positive control was generated by treating cells with 2 µM Staurosporine for 24 h. **b)** Representative Western blots showing expression levels of Mcl-1, Bcl-2 and Bcl-x_L in HT29 cells (left) and SW480 cells (right) after 24 h of Obatoclax treatment. Tubulin served as a loading control. Presented Western blots are representative for at least three blots from independent experiments. **c)** Representative pictures of HT29 cells in scaffolds after 7 days of treatment with Obatoclax. Proliferation and cell death were determined by immunohistochemical staining of Ki67 (left) and cleaved PARP (right). Scale bar indicates magnification for all panels. **d)** Flow cytometric analysis for DNA content in HT29 cells treated with 0,25 µM Obatoclax. 2N = diploid cells in G1-phase, 4N = tetraploid cells in G2-Phase. **e)** Corresponding analysis of cell cycle phase distribution. Values are expressed as means + SD. Assays are representative of at least three independent experiments. ***p < 0,001. Oba = Obatoclax.

For a better quantification of proliferating cells, the DNA content of Obatoclax-treated HT29 cells was determined by FACS analysis. This approach allows to distinguish between diploid (2N) cells in the G1- and tetraploid (4N) cells in the G2-phase. Under 0,25 µM Obatoclax, the percentage of proliferating cells in the G2-phase decreased from 37% to 13% (p<0,001; Figure 16 e). Interestingly, overexpression of anti-apoptotic Bcl-2 proteins did not antagonize this phenotype. Even though the observed differences in proliferation potentially influence migration, the invasion depth of HT29 cells in scaffolds was determined.

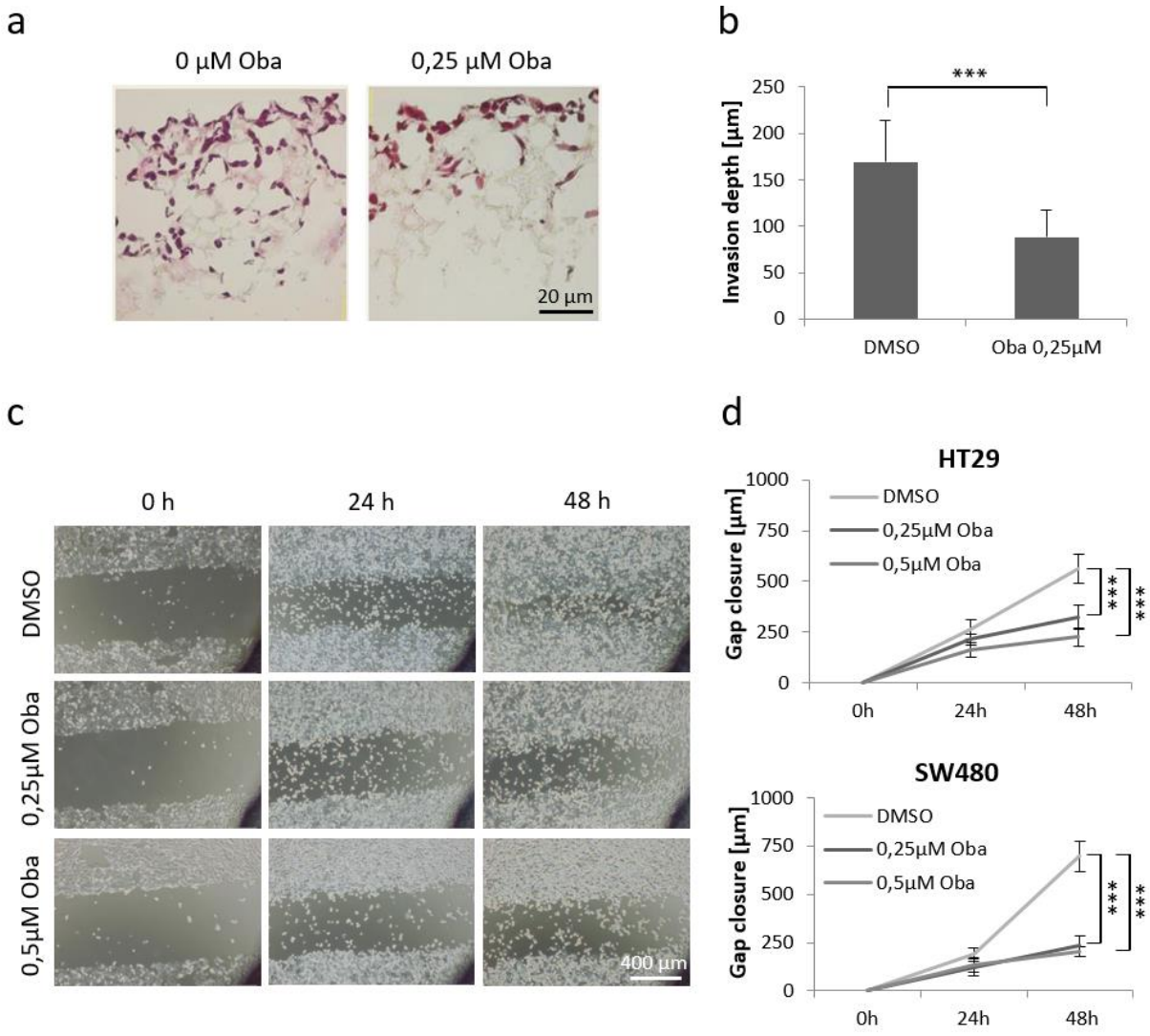

Figure 17: Migratory capacity of human CRC cells under treatment with the pan-Bcl-2 inhibitor Obatoclax. **a)** Representative pictures of Hematoxylin and Eosin stained HT29 cells in scaffolds after 7 days of treatment with Obatoclax. Scale bar indicates magnification for both pictures. **b)** Corresponding analysis of invasion depth in scaffolds. Assays were performed in triplicates and values are expressed as means + SD. **c)** Representative pictures of a scratch assay, showing gap closure capacity of HT29 cells under treatment with Obatoclax. Scale bar indicates magnification for all panels. **d)** Corresponding analysis of covered distances at indicated time points for HT29 (upper graph) and SW480 (lower graph) cells. Bars represent mean ± SD. Assays are representative of at least three independent experiments. ***p < 0,001. Oba = Obatoclax.

0,25 µM Obatoclax induced a striking blockade of migration in 3D long term cell culture. Compared to DMSO-treated controls, the covered distance of Obatoclax-treated cells decreased to 52% ($p < 0,001$; Figure 17 b). To verify the observed migration phenotype, an additional scratch assay was performed. Therefor, again 0,25 µM and 0,5 µM as sublethal doses of Obatoclax were applied and gap closure was measured over a time period of 48 h (Figure 17 c). The results clearly show that Obatoclax massively impairs the migratory capacity of HT29 and SW480 cells in a dose-dependent manner. After 48 h, mean covered distances of HT29 cells were 563 µm in DMSO treated controls, 322 µm in 0,25 µM Obatoclax treated cells and 226 µm in 0,5 µM Obatoclax treated cells ($p < 0,001$ each). SW480 cells overcame in the same time 696 µm under DMSO, 232 µm under 0,25 µM Obatoclax and 204 µm under 0,5 µM Obatoclax treatment ($p < 0,001$ each; Figure 17 d).

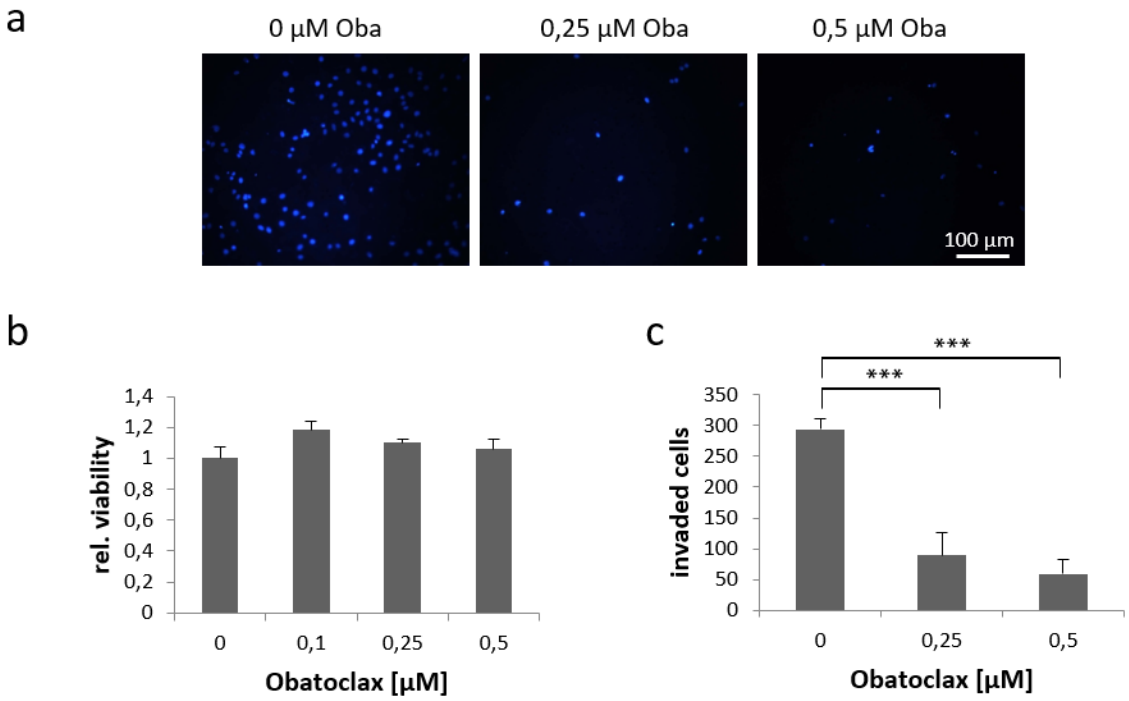

Figure 18: Invasiveness of SW480 cells under treatment with the pan-Bcl-2 inhibitor Obatoclax. SW480 cells were transferred onto Matrigel-coated Boyden chambers and cell culture medium was supplemented with Obatoclax as indicated. 48 h after seeding, nuclei on the lower surface were visualized by Hoechst staining. **a)** Representative pictures of lower insert surface after Hoechst staining. Scale bar indicates magnification for all panels. **b)** Prior to the invasion experiment, proper attachment of SW480 under Obatoclax treatment was tested. Therefor cells were seeded onto cell culture dishes in the presence of the inhibitor. After 24 h a MTT assay was performed, which revealed no impaired attachment under Obatoclax treatment. **c)** In order to quantify invaded cells in the Boyden chamber assay, five pictures of every insert were taken and the number of Hoechst-positive nuclei was determined by counting. n = 5 inserts per group. Values are expressed as means + SD. Assays are representative of at least three independent experiments. ***$p < 0,001$.

Next, the invasiveness of Obatoclax treated SW480 cells was evaluated by a Boyden chamber assay. By contrast to the scratch assay, in which cells are first grown to a confluency of 70-80% before they are treated, the Boyden chamber assay required seeding of cells in Obatoclax containing medium. In order to prove appropriate attachment under these conditions, cells were previously

seeded onto cell culture dishes followed by an MTT assay after 24 h. Since there was no impaired attachment observed in the presence of the inhibitor (Figure 18 b), the invasion assay was performed with the respective concentrations of Obatoclax.

Similar to the result obtained in the migration assay, invasion was strikingly inhibited by Obatoclax, again displaying dose-dependency (Figure 18 c). Compared with the DMSO treated control, the number of invaded cells decreased to 30,3% under 0,25 µM Obatoclax treatment ($p<0,001$) and to 20,2% under 0,5 µM Obatoclax treatment ($p<0,001$).

Taken together the results show, that chemical inhibition of anti-apoptotic Bcl-2 proteins could be a feasible approach to inhibit CRC cell spreading.

3.2.6 Expression of Migration Markers after Downregulation or Inhibition of anti-apoptotic Bcl-2 Proteins

In order to further investigate the molecular mechanisms, being responsible for the observed migration and invasion phenotypes, E-Cadherin expression was determined. E-Cadherin is a transmembrane protein with a key function for the formation of adherents junctions and thus for cellular adhesion.

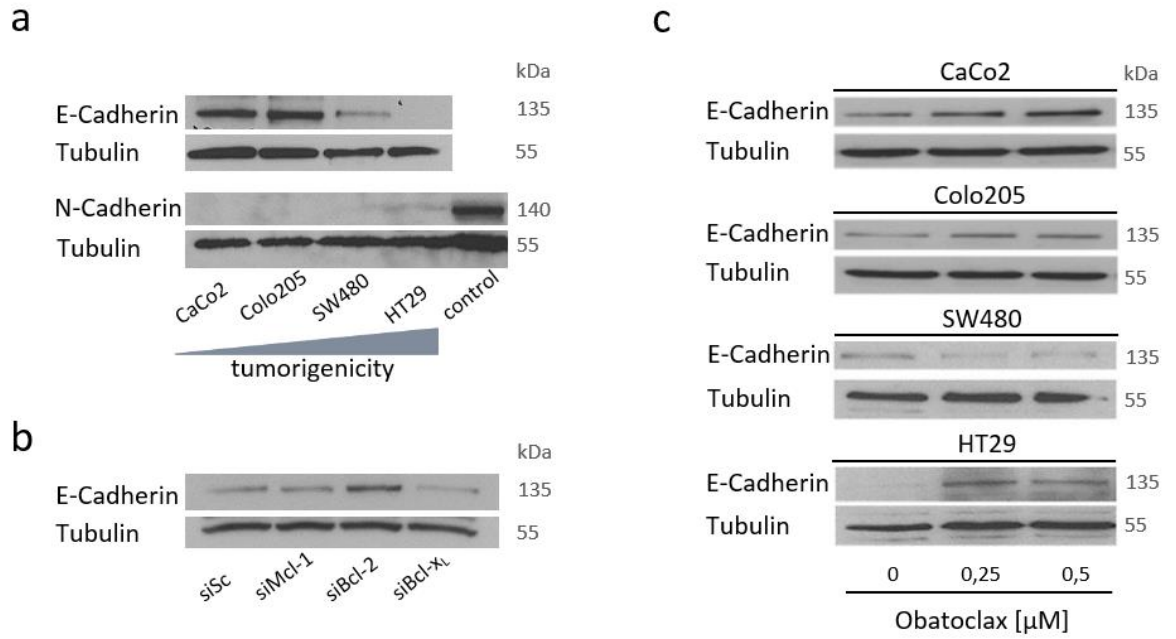

Figure 19: Expression of E- and N-Cadherin in CRC cells before and after downregulation or inhibition of anti-apoptotic Bcl-2 proteins. **a)** Representative Western blots, showing E-Cadherin (upper panel) and N-Cadherin (lower panel) expression in four different human CRC cell lines. Cell lines were ordered according to their tumorigenicity and reveal a negative correlation between tumorigenicity and E-Cadherin expression. **b)** Representative Western blot, detecting E-Cadherin expression in SW480 cells, 72 h after siRNA-mediated downregulation of Mcl-1, Bcl-2 or Bcl-x_L. Analysis revealed an increased expression of E-Cadherin, subsequent to knockdown of Bcl-2. **c)** Representative Western blots, showing E-Cadherin expression in four CRC cell lines after 24 h of Obatoclax treatment. In all cell lines, except of SW480 cells, analysis revealed an increased E-Cadherin expression under 0,25 µM and 0,5 µM Obatoclax. Presented Western blots are representative for at least three blots from independent experiments and Tubulin always served as loading control.

It has been shown that E-Cadherin expression gets decreased during the course of malignant transformation, allowing the cancer cells to leave the primary tumor side[205]. By contrast, the related protein N-Cadherin was found to rather promote cellular migration and invasiveness[206]. In a first approach, the basal expression levels of E- and N-Cadherin in SW480 and HT29 cells were determined by Western blot analysis. SW480 cells are tumorigenic but non-invasive, whereas HT29 cells are tumorigenic, invasive and metastatic. In addition, CaCo2 and Colo205, two other human colorectal cancer cell lines, were used as a comparison. By contrast to SW480 and HT29 cells, these cell lines are non-tumorigenic[207,208]. Impressively, Western blot analysis revealed a negative correlation between E-Cadherin expression and the tumorigenicity of cell lines. As opposed to that, N-Cadherin expression was only detectable in HT29 cells, where it still was very weak compared to the positive control (Figure 19 a). To investigate, whether siRNA mediated knockdown of anti-apoptotic Bcl-2 proteins might recover E-Cadherin expression in SW480 and HT29 cells, transfection and subsequent Western blot analysis were performed. In HT29 cells, the knockdown of Mcl-1, Bcl-2 or Bcl-x_L did not lead to an increase of expression levels above the detection threshold (data not shown). In SW480 cells, E-Cadherin expression was clearly increased after siRNA-mediated knockdown of Bcl-2 (Figure 19 b). Interestingly, in the previous migration and invasion experiments, strongest phenotypes were always observed after knockdown of Bcl-2 (Figure 11). Since chemical inhibition of anti-apoptotic Bcl-2 proteins also reduced the migratory and invasive capacity of CRC cells, E-Cadherin expression levels were additionally measured after Obatoclax treatment. Except of SW480, all cell lines sowed a remarkable recovery of E-Cadherin under 0,25 µM and 0,5 µM Obatoclax (Figure 19 c).

3.2.7 Downregulation or Inhibition of anti-apoptotic Bcl-2 Proteins sensitizes CRC cells towards Oxaliplatin

Even though the siRNA mediated knockdown or chemical inhibition of anti-apoptotic Bcl-2 proteins does not lead to spontaneous cell death induction, a sensitization of CRC cells towards chemotherapeutic agents would be possible. Therefore, HT29 cells were treated with the clinically relevant and commonly used chemotherapeutics Oxaliplatin, 5-Fluorouracil (5-FU) and Irinotecan, subsequently to the downregulation of Bcl-2, Bcl-x_L or Mcl-1. Prior to this, dose-finding was done by titration in order to stay in the sub-lethal range with all substances applied (data not shown). Evaluation of cellular viability by a MTT assay revealed no significant sensitization towards 5-FU or Irinotecan. By contrast, synergistic effects of siRNA mediated silencing in combination with Oxaliplatin treatment were observed, leading to a decrease in viability of about 20%. Similar results were obtained after 3D cultivation of HT29 cells in presence of Obatoclax and Oxaliplatin.

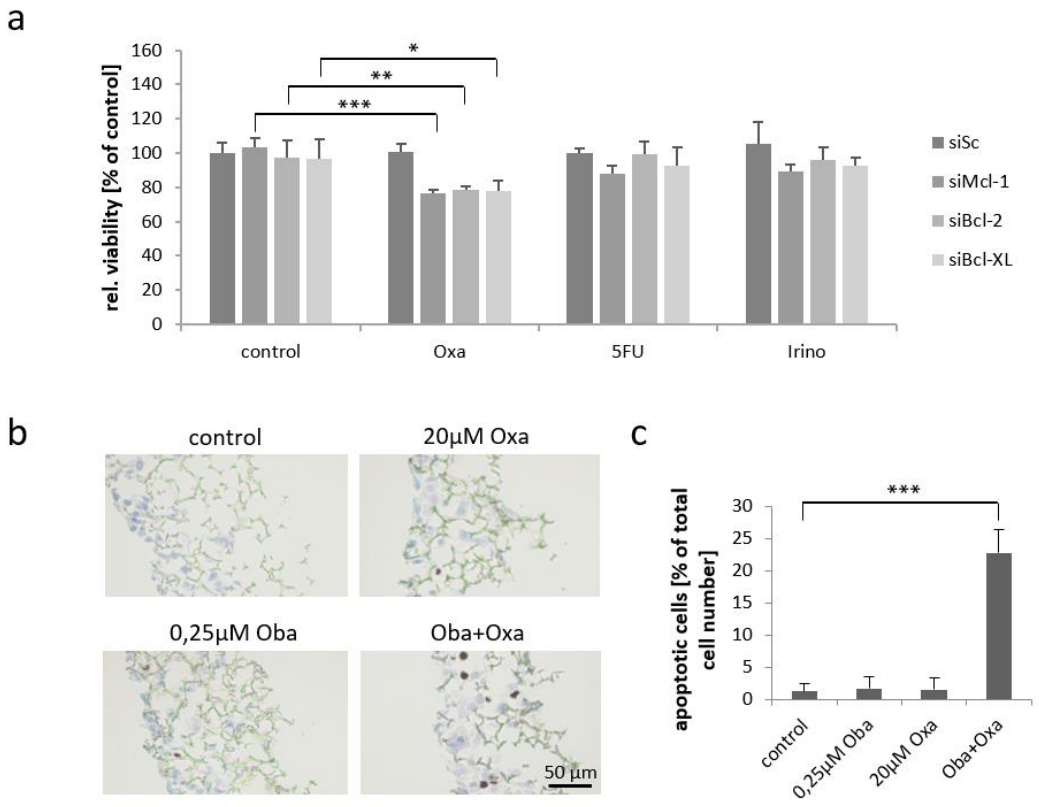

Figure 20: Evaluation of the chemosensitivity of HT29 cells after knockdown or inhibition of anti-apoptotic Bcl-2 proteins. **a)** Viability of HT29 cells, determined by a MTT assay after knockdown of Mcl-1, Bcl-2 or Bcl-x_L, followed by 48h treatment with 20 µM Oxaliplatin (Oxa), 5 µM Irinotecan (Irino) or 38 µM 5-Fluorouracil (5-FU). **b)** Representative pictures of HT29 cells in scaffolds after 5 days of treatment with 0,25 µM Obatoclax (Oba) and 20 µM Oxaliplatin (Oxa). Cell death was determined by immunohistochemical staining of cleaved PARP. Scale bar indicates magnification for all panels. **c)** Corresponding analysis of cell death induction. The number of apoptotic cells was determined by counting. Bars represent mean ± SD. Assays are representative of at least three independent experiments. *p < 0,05; **p < 0,01; ***p < 0,001.

Here, immunohistochemical staining of cleaved PARP and subsequent counting of positive cells revealed an increase of apoptotic cells to 22,8% of the total cell number. This is far above the amount of apoptotic cells in either Obatoclax (1,7%) or Oxaliplatin (1,6%) treated samples and thus the combination of these agents can be considered synergistic.

3.3 The Role of anti-apoptotic Bcl-2 Proteins for Physiology and Carcinogenesis in the murine Intestine in vivo

In order to get more insight into the function of anti-apoptotic Bcl-2 proteins for the maintenance of intestinal tissue homeostasis as well as for colorectal cancer development and progression, two different knockout mouse models were generated. As already mentioned, Bcl-$2^{-/-}$, A1A$^{-/-}$ and Bcl-w $^{-/-}$ mice are viable and have already been described[163–167]. By contrast, the constitutive deletion of both Mcl-1 and Bcl-x_L results in embryonic lethality[161,162]. Hence, the respective genes were deleted in a spatially controlled manner, by utilizing the Cre/loxP system. In this approach, mice

carrying loxP-flanked alleles of Bcl-x_L (Bcl-x_L^{FLOX}) or Mcl-1 (Mcl-1^{FLOX}) were crossbred with mice expressing the Cre-recombinase under control of the Villin-promoter (Villin-Cre). Since Villin is mainly expressed in epithelial cell lineages of the intestinal tract, the progeny displays an intestine-specific deletion of Bcl-x_L or Mcl-1. Because the expression of Cre in the gastrointestinal tract of mice has been shown to induce gastric epithelial atrophy and metaplasia in the absence of floxed alleles[202], Villin-Cre mice were chosen as control group for all experiments. Basal analyses were done with 8 weeks old mice because in this age they reach maturity. In the following, mice were monitored for up to one year.

3.3.1 The intestine-specific Bcl-x_L knockout Mouse

In the genome of the parental Bcl-x_L^{FLOX} strain, exon 1 and exon 2 of the Bcl-x_L gene were flanked by two loxP sites (Figure 21 a). After crossbreeding with Villin-Cre mice, descendants were further bred until littermates displayed homozygosity with regard to their flox status.

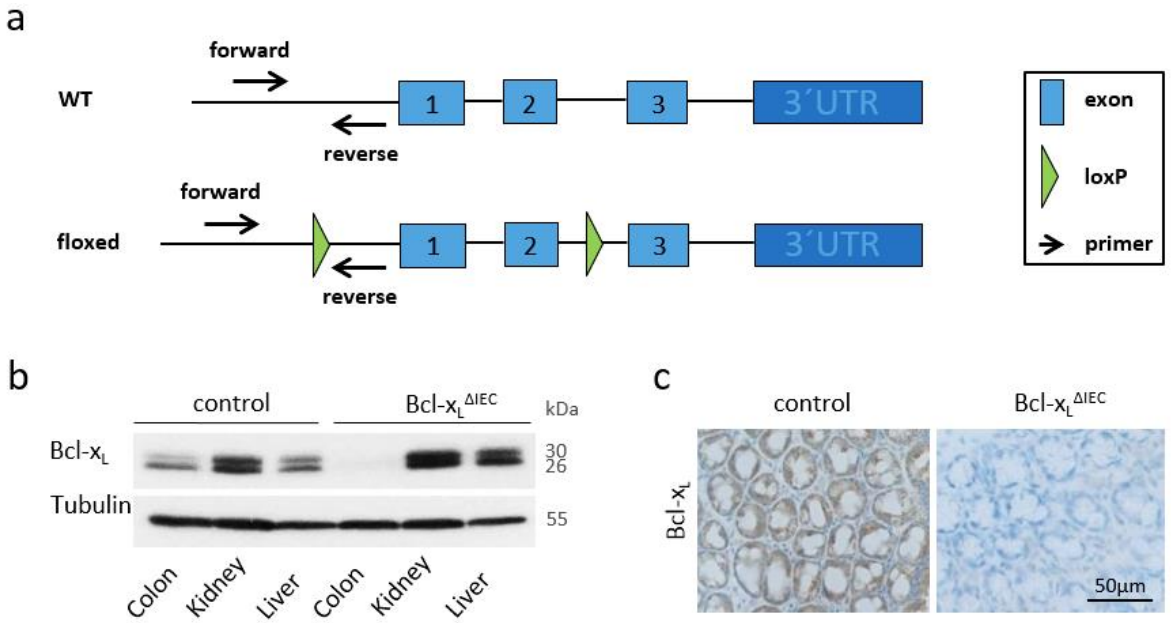

Figure 21: Bcl-x_L expression patterns in Bcl-$x_L^{\Delta IEC}$ and control mice. **a)** Scheme illustrating the targeting strategy for the spatially controlled deletion of Bcl-x_L. Exon 1 and exon 2 of the Bcl-x_L gene were flanked with loxP sites, what leads to their excision, in case the Cre recombinase is expressed. Primer sites were chosen upstream and downstream of a loxP site, allowing determination of the flox status by PCR analysis. Scheme adapted from (Opferman et al., Nature, 2003). **b)** Western blot analysis of proteins extracted from different tissues of Bcl-$x_L^{\Delta IEC}$ and control mice, proving an organ specific deletion. Tubulin served as loading control. **c)** Representative pictures of colonic tissue derived from Bcl-$x_L^{\Delta IEC}$ and control mice. Immunohistochemical staining with an antibody against Bcl-x_L validated the loss of Bcl-x_L in the intestinal epithelial cells of knockout animals. Scale bar indicates magnification for both pictures.

Efficiency and specificity of the deletion were evaluated by Western blot analysis. Since the Villin-promotor has been described to be slightly active also in renal epithelial cells, kidneys from a Bcl-$x_L^{\Delta IEC}$ and a control mouse were harvested and used for protein isolation. In addition, colon and liver

samples were taken and Bcl-x_L expression levels were determined. The blot revealed a complete and organ specific abrogation of Bcl-x_L expression in the intestine of Bcl-$x_L^{\Delta IEC}$ mice (Figure 21 b). The complete loss of Bcl-x_L in intestinal epithelial cells was furthermore validated by immunohistochemical staining (Figure 21 c).

Three weeks after birth, tail biopsies of all littermates were taken in order to determine their genotype by polymerase chain reaction (PCR) and subsequent agarose gel electrophoresis. Since an integrated loxP side only changes the size of the PCR product, no internal control was needed for determining the flox status. By contrast, Actin was detected as an internal positive control in the Cre PCR because samples derived from Cre-negative animals would otherwise show no signal.

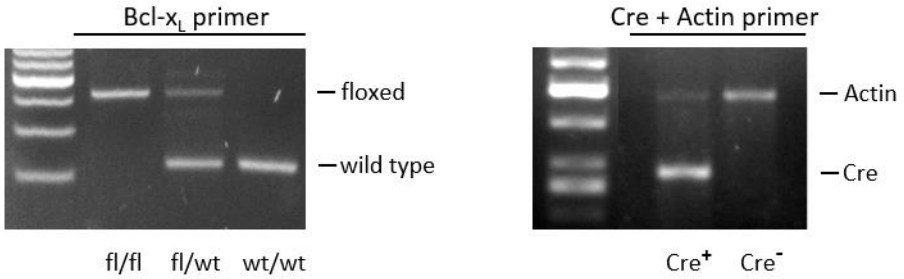

Figure 22: Genotyping of Bcl-$x_L^{\Delta IEC}$ mice. DNA was isolated from tail biopsies of mice with no (wt/wt), one (fl/wt) or two (fl/fl) floxed alleles (left panel) and analyzed by PCR analysis. If loxP sites are included, the PCR product gets larger and thereby distinguishable from the wild type allele. The Cre status was evaluated in a separate PCR (right panel) with primers for Cre and primers for Actin as internal positive control. wt = wild type; fl = floxed.

3.3.1.1 The Knockout of Bcl-x_L in intestinal epithelial Cells causes no spontaneous Phenotype

Bcl-$x_L^{\Delta IEC}$ mice were born healthy and at expected mendelian ratios. Compared to control littermates, they show no phenotype in terms of overall survival and body mass index (BMI) (Figure 23 a). For morphometric analysis, crypt diameter and number in Hematoxylin and Eosin stained colonic crypt sections were determined and revealed a normal crypt architecture and morphology (Figure 23 b). Since the loss of an anti-apoptotic protein might lead to spontaneous cell death induction, a TUNEL assay was performed. Compared to the DNAse treated positive control, neither Cre control nor Bcl-$x_L^{\Delta IEC}$ animals showed a noteworthy amount of TUNEL positive cells in their colon mucosa (Figure 23 c). For quantification of basal cell death, TUNEL-positive cells were counted in five visual fields. With 6,39 TUNEL-positive cells per mm^2 in control mice and 6,18 positive cells per mm^2 in knockout animals, Bcl-$x_L^{\Delta IEC}$ mice showed a perfectly equal amount of dead cells in the colonic epithelium.

Besides its anti-apoptotic function, Bcl-x_L has been shown to inhibit cell cycle progression. Therefore, proliferation levels in the intestinal mucosa of control and Bcl-$x_L^{\Delta IEC}$ mice were evaluated by immunohistochemical staining of Ki67.

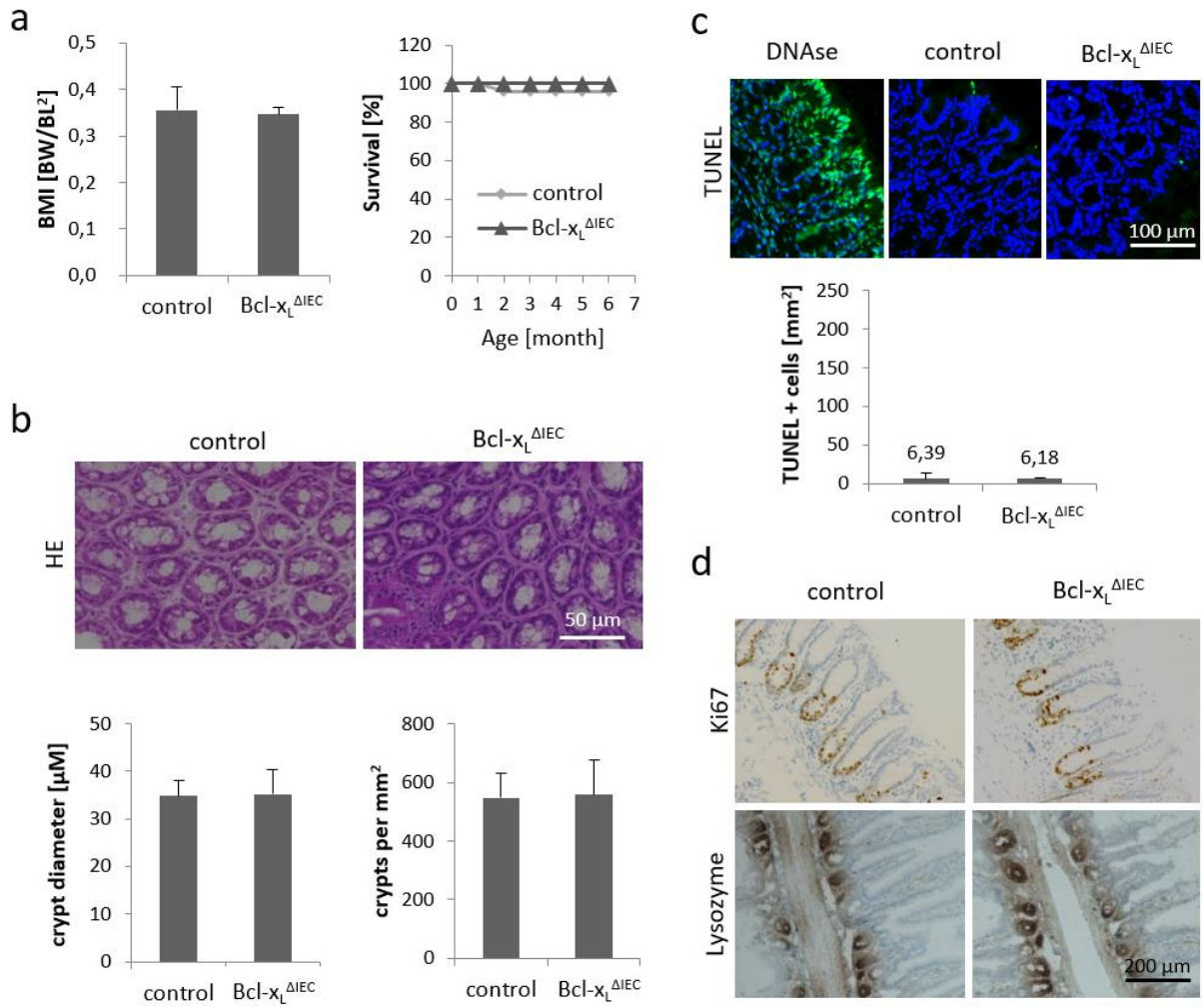

Figure 23: Basal characterization of Bcl-$x_L^{\Delta IEC}$ mice. **a)** Bcl-$x_L^{\Delta IEC}$ mice are born healthy, showing no phenotype in terms of body mass index (BMI) or overall survival (n = 25 per group). The BMI was calculated by division of the body weight (BW; in g) by the squared body length (BL; in cm). **b)** Hematoxylin and Eosin (HE) staining of colonic specimens, revealing the same crypt morphology in Bcl-$x_L^{\Delta IEC}$ and control mice. Scale bar indicates magnification for both pictures. **c)** Evaluation of cell death rates by TdT-mediated dUTP nick end labeling (TUNEL assay) of fragmented DNA. Except the DNAse treated positive control, very few TUNEL positive cells are detectable in colon sections of Bcl-$x_L^{\Delta IEC}$ and control mice. Five pictures of every specimen were taken and the number of TUNEL-positive cells was determined by counting. n = 3 animals per group. Scale bar indicates magnification for all panels. **d)** IHC staining of colonic (for Ki67 staining) and small intestinal (for Lysozyme staining) tissue, showing no differences in proliferation or Paneth cell frequency between Bcl-$x_L^{\Delta IEC}$ and control mice. Scale bar indicates magnification for all panels. Values are expressed as means + SD.

The staining revealed equal amounts of proliferating cells which are located at the crypt base (Figure 23 d, upper panel). Since Paneth cells have been shown to depend on proper accomplishment of autophagy and because Bcl-x_L was found to be an autophagy regulator, Lysozyme as marker protein for Paneth cells, has also been detected. Subsequent analysis disclosed no differences between control and Bcl-$x_L^{\Delta IEC}$ mice in terms of Lysozyme-positive Paneth cell abundance (Figure 23 d, lower panel).

Taken together, these finding indicate that the loss of Bcl-x_L in intestinal epithelial cells does neither influence development or viability of Bcl-$x_L^{\Delta IEC}$ mice, nor the morphology and homeostasis of their intestinal mucosa.

3.3.1.2 Loss of Bcl-x_L inhibits Carcinogenesis in an inflammation-driven Tumor Model

Since the analysis of human CRC specimens showed that Bcl-x_L is significantly upregulated in the malignant state (Figure 6), it was reasonable to conclude that Bcl-x_L has a function for tumor induction or progression and that Bcl-$x_L^{\Delta IEC}$ mice might be more resistant to experimentally induced tumorigenesis.

In order to induce intestinal tumor formation, eight weeks old mice were injected intraperitoneally with the mutagenic agent azoxymethan (AOM). Subsequently, carcinogenesis was promoted by three cycles of the pro-inflammatory reagent dextran sodium sulfate (DSS) in the drinking water (Figure 24 a).

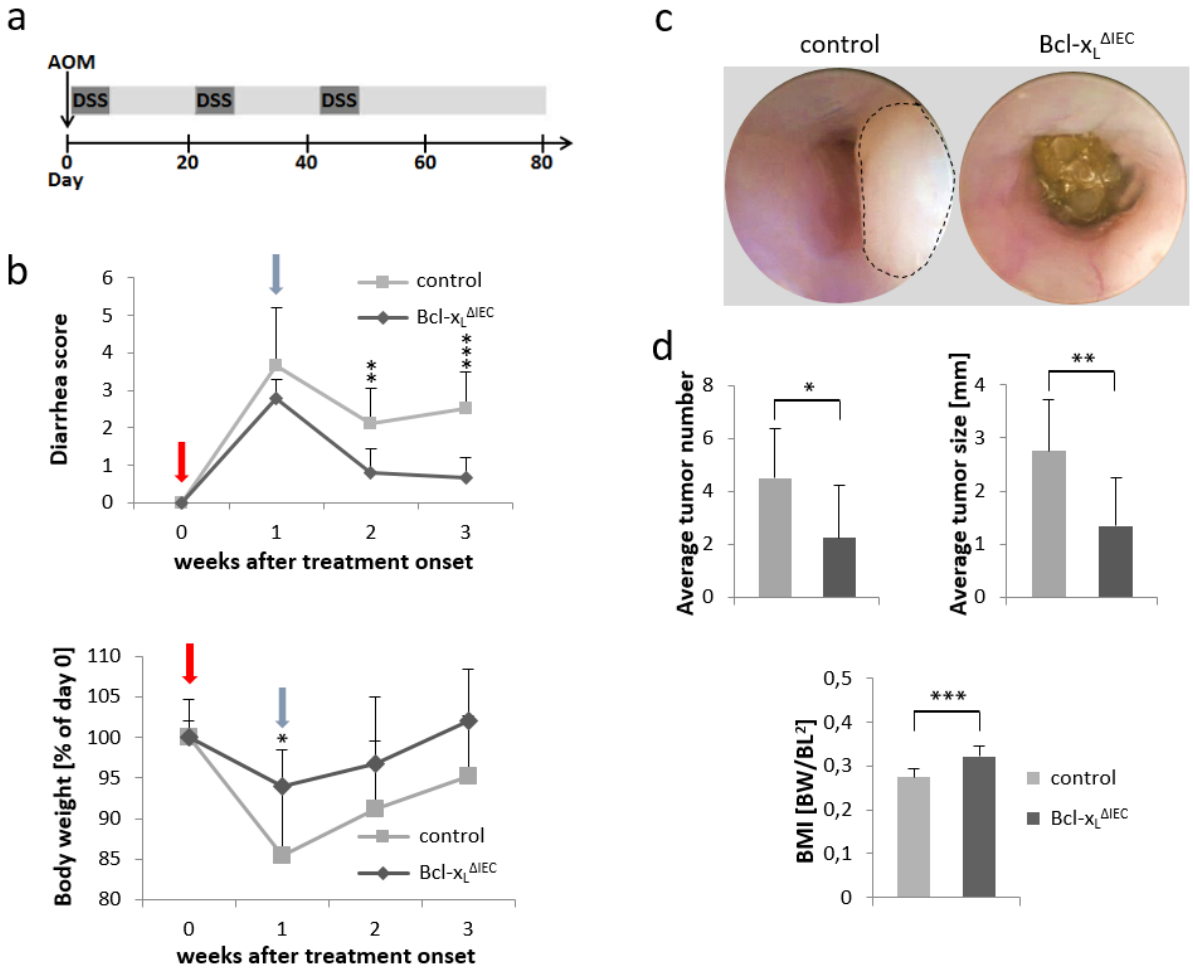

Figure 24: Bcl-$x_L^{\Delta IEC}$ and control mice in an inflammation-driven model for intestinal carcinogenesis. **a**) Schematic treatment course with intraperitoneal injection of azoxymethan (AOM) at the start day and three cycles of dextran sodium sulfate (DSS) in the drinking water (2% w/v). **b**) Diarrhea severity (upper graph) and weight loss (lower graph) after DSS administration (red arrow) and during recovery time (blue arrow). Exemplarily shown for the third DSS cycle. **c**) Endoscopic images of Bcl-$x_L^{\Delta IEC}$ and control mice. The dashed line shows a neoplastic lesion. **d**) The determination of average tumor number ($p < 0,05$) and size ($p < 0,01$) at the end of treatment shows a significantly lower tumor burden in Bcl-$x_L^{\Delta IEC}$ compared to control mice. Furthermore, the body mass index (BMI) is higher in Bcl-$x_L^{\Delta IEC}$ mice ($p < 0,001$). The BMI was calculated by division of the body weight (BW; in g) by the squared body length (BL; in cm). Values are expressed as means + SD. Control mice: n = 8; Bcl-$x_L^{\Delta IEC}$ mice: n = 9. *$p < 0,05$; **$p < 0,01$; ***$p < 0,001$.

Initially, the experiment started with 10 sex (5 males and 5 females per group) and age matched animals per group, but during treatment, two males in the control group as well as one male in the Bcl-x_L knockout group died. During the course of treatment, Bcl-$x_L^{\Delta IEC}$ mice showed a better health status mirrored by less severe diarrhea and less pronounced weight loss during DSS cycles (Figure 24 b). For determining the severity of diarrhea, a scoring system was developed, taking stool liquidity, soiling around the anus and bloody contingents into account. Rigid colonoscopy of mice, 80 days after AOM injection, revealed a higher tumor burden in control animals (Figure 24 c). Finally, mice were sacrificed and intestines were isolated, washed and opened longitudinally. Evaluation of emerged tumors revealed, that both average tumor numbers ($p < 0,05$) as well as mean tumor sizes ($p < 0,01$) were significantly lower in Bcl-$x_L^{\Delta IEC}$ mice compared to controls (Figure 24 d). Furthermore, the BMI was higher in Bcl-$x_L^{\Delta IEC}$ mice at the end of treatment ($p < 0,001$).

To evaluate the inflammatory events occurring during a DSS cycle, 5 additional animals per group were treated with DSS only and sacrificed after the first cycle. Immunohistochemical staining revealed higher amounts of infiltrating CD3+ cells in colon tissue derived from Bcl-$x_L^{\Delta IEC}$ mice (Figure 25).

In summary, the made observations argue for a reduced susceptibility of Bcl-$x_L^{\Delta IEC}$ mice towards chemically induced and inflammation augmented carcinogenesis.

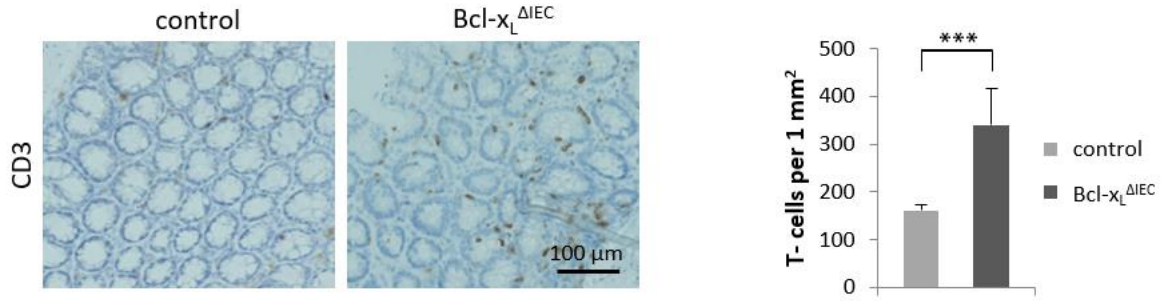

Figure 25: Analysis of immune cell infiltration in the colon of DSS treated Bcl-$x_L^{\Delta IEC}$ and control mice. Immunohistochemical staining with an antibody against CD3, showing an increase of infiltrating T-cells in colon tissue derived from DSS treated (2% w/v; 7 days) Bcl-$x_L^{\Delta IEC}$ mice, compared to DSS treated controls. Scale bar indicates magnification for both pictures. The graph depicts the correlating quantification.

3.3.1.3 Tumors of Bcl-$x_L^{\Delta IEC}$ Mice show increased Cell Death without compensatory Proliferation

After AOM/DSS treatment, Hematoxylin and Eosin staining of tumor-containing colonic sections was done in order to allow morphologic analysis. This identified the gathered neoplastic lesions as being well differentiated adenocarcinomas with similar morphology in Bcl-$x_L^{\Delta IEC}$ and control animals (Figure 26 a, left column).

The lower tumor numbers and decreased tumor sizes in AOM/DSS treated Bcl-$x_L^{\Delta IEC}$ mice could trace back to several causes. I) If the loss of Bcl-x_L is not compensated by other anti-apoptotic Bcl-2 proteins, assaulted intestinal epithelial cells might have a higher tendency to undergo apoptosis. II) Differences in the immunogenicity might attract more immune cells to infiltrate and attack Bcl-x_L negative tumor cells. III) Since Bcl-x_L has been described to play a role in cell cycle control, an altered proliferative capacity of IECs could be responsible for differences in tumor progression.

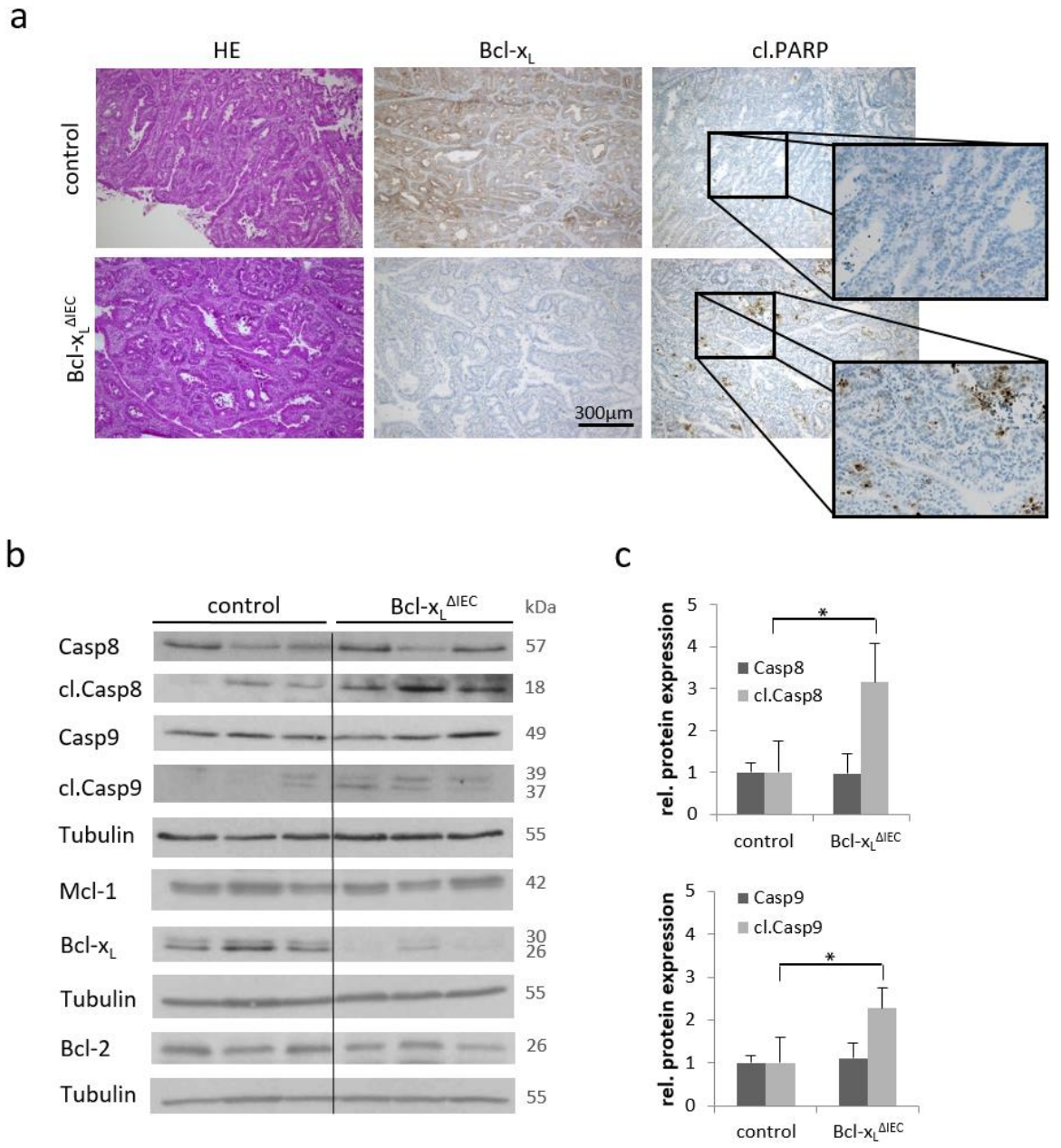

Figure 26: Analysis of cell death events in AOM/DSS induced tumors. **a**) Hematoxylin and Eosin staining (left column), identifying gathered neoplastic lesions as well differentiated adenocarcinomas. Immunohistochemical staining against Bcl-x_L and cleaved PARP (cl.PARP), revealing remarkable amounts of apoptotic cells in tumors derived from Bcl-$x_L^{\Delta IEC}$ mice but not in tumors from control animals. Scale bar indicates magnification for all panels except the enlarged sections. **b**) Representative Western blots, showing no counter-regulatory changes in the expression of Bcl-2 or Mcl-1 but an increase in activated Caspase 8 and 9. Tubulin served as loading control. **c)** Subsequent densitometric analysis, showing a 3,2-fold upregulation of cleaved Caspase 8 (cl.Casp8; $p < 0,05$) and a 2,3-fold upregulation of cleaved Caspase 9 (cl.Casp8; $p < 0,05$) in tumors derived from Bcl-$x_L^{\Delta IEC}$ mice. *$p < 0,05$.

First, expression levels of Bcl-2 and Mcl-1 were determined to investigate, whether the loss of Bcl-x_L induces a compensatory upregulation of its kin proteins. Western blot analysis revealed equal expression of Bcl-2 and Mcl-1 in the mucosa of untreated Bcl-$x_L^{\Delta IEC}$ and control mice as well as in AOM/DSS induced tumors (Figure 26 b). With regard to cell death, tumors derived from Bcl-$x_L^{\Delta IEC}$ mice showed a higher positivity for cleaved PARP after immunohistochemical staining, arguing for an increased rate of apoptosis in Bcl-x_L negative tumors (Figure 26 a). Further immunoblotting was done to characterize the subtype of cell death in tumors of Bcl-$x_L^{\Delta IEC}$ mice. Initiator Caspases 8 and 9 were both found to be activated (Figure 26 b). Subsequent densitometric analysis revealed that the amount of cleaved Caspase 8 was three-fold higher in Bcl-x_L negative tumors than in comparable controls ($p < 0,05$) and the one of cleaved Caspase 9 was more than doubled ($p < 0,05$) (Figure 26 c).

To investigate whether increased lymphocyte infiltration rates might be responsible for the detected cleavage of Caspase 8, immunohistochemical staining was done with antibodies against CD20 to detect B-cells and CD3 to detect T-cells (Figure 27 a, left and middle column).

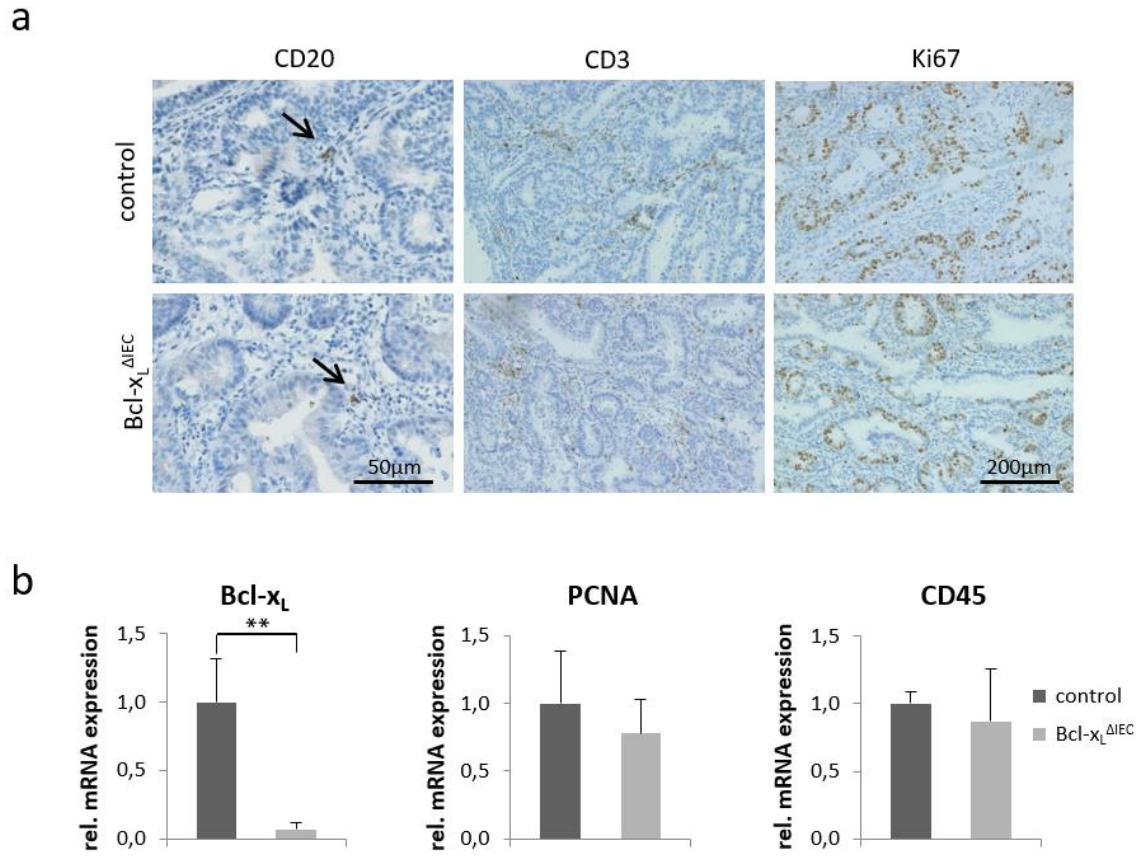

Figure 27: Analysis of proliferation and lymphocyte infiltration in AOM/DSS induced tumors. **a)** Immunohistochemical staining with antibodies against CD20 (B-cells, left column) and CD3 (T-cells, middle column), showing no differences in B-cell (black arrows) or T-cell frequencies in tumors derived from Bcl-$x_L^{\Delta IEC}$ or control mice. Staining against Ki67 (right column), revealing equal proliferation rates in Bcl-x_L negative and control tumors. Left scale bar indicates magnification for the CD20 stained pictures and the right scale bar indicates magnification for the remaining panels. **b)** Determination of Bcl-x_L, PCNA (proliferation, $p = 0,45$) and CD45 (all leukocytes, $p = 0,6$) mRNA levels by qRT-PCR, showing no significant differences in the proliferation rate or leukocyte infiltration in Bcl-x_L negative and control tumors. n=3 per group, measurement done in technical duplicates. $^{**}p < 0,01$.

Staining revealed equal frequencies of T- as well as B-cells in tumors derived from Bcl-$x_L^{\Delta IEC}$ and control mice. Furthermore, RNA was isolated from Bcl-x_L negative and control tumors. The subsequent qRT-PCR analysis displayed unaltered mRNA levels of the pan-leukocyte marker CD45, what further underlines the findings obtained by immunohistochemical analysis (Figure 27 b).

In order to address the last point, tumor tissues were immunohistochemically stained with an antibody against Ki67. Subsequent evaluation showed that the increase in cell death was not accompanied by altered proliferation rates in Bcl-$x_L^{\Delta IEC}$ mice (Figure 27 a, right column). This observation was further validated by qRT-PCR analysis of RNA extracted from tumor tissue. Here the relative mRNA levels of PCNA, as an alternative indicator for proliferating cells, was also not significantly changed (Figure 27 b).

In summary, the obtained data conclusively show that the lower tumor burden found in AOM/DSS treated Bcl-$x_L^{\Delta IEC}$ mice is not due to differences in the immune response or in proliferation, but solely relays on an increased cell death rate.

3.3.2 The intestine-specific Mcl-1 knockout Mouse

In the genome of the parental Mcl-1^{FLOX} strain, exon 1 of the Mcl-1 gene was flanked by two loxP sites (Figure 28 a). After crossbreeding with Villin-Cre mice, descendants were further bred until littermates displayed homozygosity with regard to their flox status. First immunohistochemical analyses showed, that the majority of Mcl-$1^{\Delta IEC}$ mice display a patchy expression pattern (Figure 28 b). By contrast to Bcl-$x_L^{\Delta IEC}$ mice, only about 15% show a complete loss of the targeted protein in the entire intestine. Thus, efficiency and specificity of the deletion were not evaluated by Western blot analysis. Instead, the presence of the recombined gene-product (ΔMcl-1) was detected by PCR analysis. Therefor, primer sites with a high interspace were chosen, making the excision of exon 1 to a prerequisite for proper amplification. In order to proof organ specificity of the recombination event, kidneys and spleens from two Mcl-$1^{\Delta IEC}$ and two control mice were harvested and used for DNA isolation. In both cases, DNA isolated from the colon mucosa of a Mcl-$1^{\Delta IEC}$ mouse, served as positive control. After separation of the PCR product by agarose gel electrophoresis, ΔMcl-1 was solely found in the positive control, indicating an intestine-specific expression of the Cre recombinase (Figure 28 c).

If crossbred in a heterozygous manner, Mcl-$1^{\Delta IEC}$ mice are born in a normal mendelian ratio (Figure 29 a). The minor discrepancy between estimated (18,75%) and effectively born (15,8%) mice that show homozygosity with regard to their flox status in addition to Cre positivity (flox/flox Cre^+), suggests an unaltered prenatal lethality. However, soon after birth, a noteworthy percentage of Mcl-$1^{\Delta IEC}$ pups show a decreased body weight and size, compared to their control littermates.

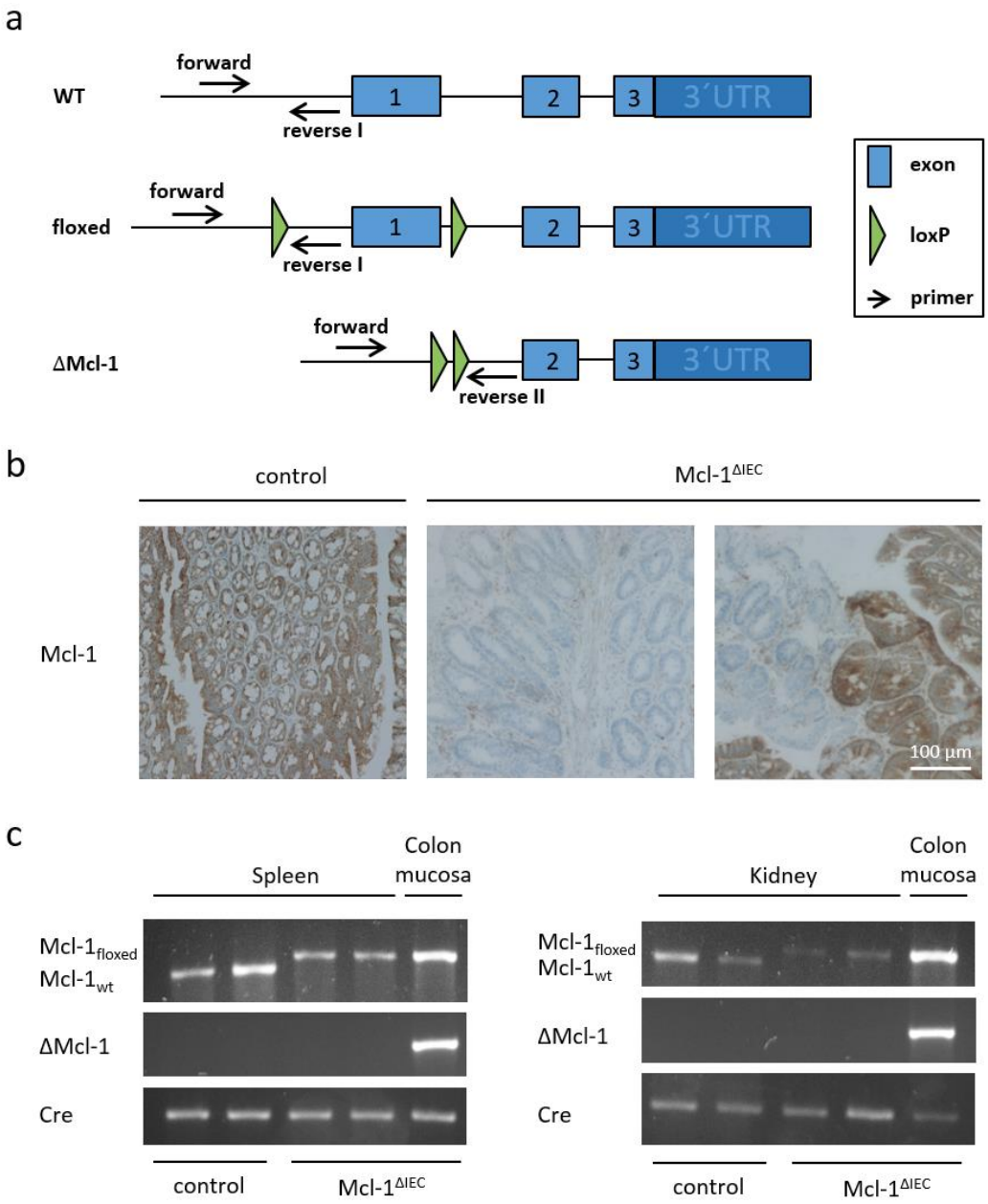

Figure 28: Mcl-1 expression patterns in Mcl-1$^{\Delta IEC}$ and control mice. **a)** Scheme illustrating the targeting strategy for the spatially controlled deletion of Mcl-1. Exon 1 of the Mcl-1 gene was flanked with loxP sites, what leads to its excision, in case the Cre recombinase is expressed. Primer sites were chosen upstream and downstream of a loxP site, allowing determination of the flox status by PCR analysis. Cre expression lead to the occurrence of a recombined Mcl-1 allele, missing exon 1 (ΔMcl-1), which was detected by a different reverse primer. Scheme adapted from (Opferman et al., Nature, 2003). **b)** Representative pictures of colonic tissue derived from Mcl-1$^{\Delta IEC}$ and control mice. Immunohistochemical staining with an antibody against Mcl-1 revealed a patchy expression of the targeted protein in the majority of Mcl-1$^{\Delta IEC}$ mice. Scale bar indicates magnification for all panels. **c)** PCR analysis of DNA extracted from different tissues of Mcl-1$^{\Delta IEC}$ and control mice. The selective occurrence of the recombined gene product in the colon mucosa of Mcl-1$^{\Delta IEC}$ mice, proves an intestine-specific Cre expression in knockout animals.

Immunohistological analyses of their intestines revealed a correlation between these parameters and the abundancy of Mcl-1. The 15% showing a complete loss of Mcl-1 in the entire intestine, are exceptionally small and lightweight (Figure 29 b and c) and normally die within the first six months (Figure 29 d). If Mcl-1$^{\Delta IEC}$ mice display a patchy expression pattern, the overall survival is comparable to the one of their control littermates.

a

Genotype	Estimated [%]	Born [%]
wt/wt Cre$^-$	6,25	5,3
wt/wt Cre$^+$	18,75	21,1
flox/wt Cre$^-$	12,5	7,9
flox/wt Cre$^+$	37,5	47,4
flox/flox Cre$^-$	6,25	2,6
flox/flox Cre$^+$	18,75	15,8

b

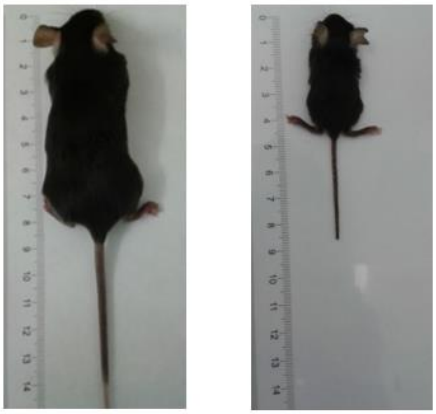

c

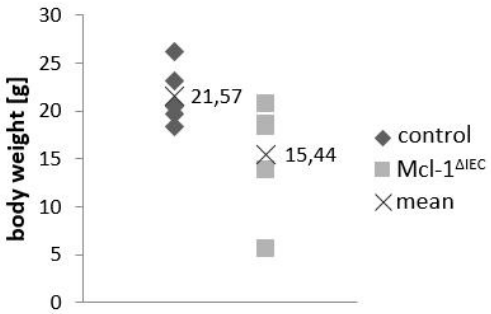

d

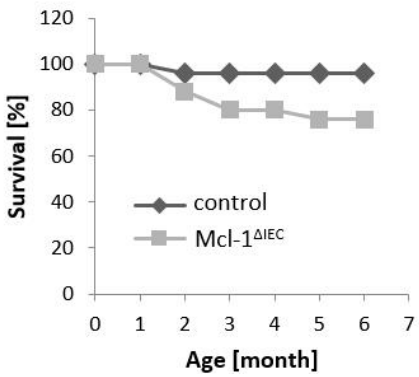

Figure 29: Basal characterization of Mcl-1$^{\Delta IEC}$ mice. **a)** Table recording estimated and effectively occurring genotypes, if mice are crossbred in a heterozygous manner. n=38 animals. **b)** Macroscopic features of an 8-weeks old Mcl-1$^{\Delta IEC}$ and a sex- and age-matched control mouse. **c)** Body weight distribution of 8-weeks old Mcl-1$^{\Delta IEC}$ and control mice (n=5 per group). **d)** Survival rates of Mcl-1$^{\Delta IEC}$ mice compared to control mice (n=25 per group), showing a decreased overall survival for about 15-20% of Mcl-1$^{\Delta IEC}$ mice, what correlates with the percentage of mice displaying a complete loss of Mcl-1. wt = wild type.

Since male mice with two floxed Mcl-1 alleles are unfertile, they were always crossbred in a heterozygous manner what caused the necessity of genotyping all offspring. Three weeks after birth, tail biopsies of all littermates were for genotyping, as it was described for Bcl-x$_L^{\Delta IEC}$ mice. Again no internal control was needed for the Mcl-1 PCR, whereas Actin was detected as positive control in the Cre PCR (Figure 30).

Figure 30: Genotyping of Mcl-1$^{\Delta IEC}$ mice. DNA was isolated from tail biopsies of mice with no (wt/wt), one (fl/wt) or two (fl/fl) floxed alleles (left panel) and analyzed by PCR analysis. If loxP sites are included, the PCR product gets larger and thereby distinguishable from the wild type allele. The Cre status was evaluated in a separate PCR (right panel) with primers for Cre and primers for Actin as internal positive control. wt = wild type; fl = floxed.

3.3.2.1 The Knockout of Mcl-1 in intestinal epithelial Cells induces Cell Death

Morphometric analyses of Hematoxylin and Eosin stained colonic crypt sections, revealed a markedly altered crypt architecture and morphology in Mcl-1 negative areas (Figure 31 a). Both crypt diameter and crypt number per mm^2 were significantly altered ($p < 0,001$) (Figure 31 b). Furthermore, H&E staining showed intestinal epithelial cells undergoing cell death (white arrows) and a remarkable number of infiltrating cells among the crypts. To further investigate the cell death phenotype, a TUNEL assay was performed. For quantification of basal cell death, TUNEL-positive cells were counted in five visual fields. This revealed a 20-fold increase of dying intestinal epithelial cells in Mcl-$1^{\Delta IEC}$ mice ($p < 0,05$) (Figure 31 c).

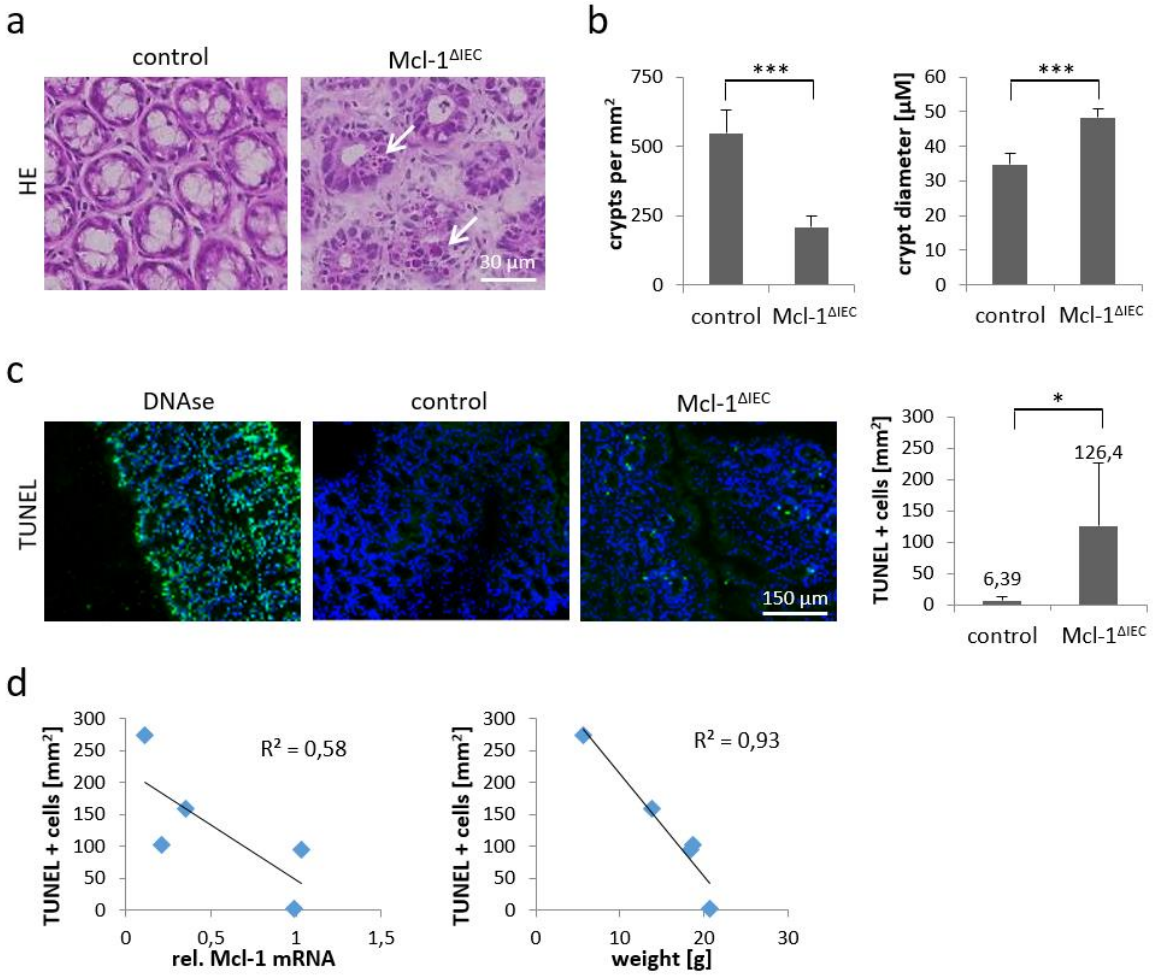

Figure 31: Morphometric analysis of colon specimens derived from Mcl-$1^{\Delta IEC}$ mice. **a)** Hematoxylin and Eosin (H&E) staining of colonic specimens, revealing a markedly altered crypt architecture and morphology in Mcl-1 negative areas, as well as cells undergoing cell death (white arrows) in the colon of Mcl-$1^{\Delta IEC}$ mice. Scale bar indicates magnification for both pictures. **b)** Corresponding quantification of crypt diameter and crypt number per mm^2, showing significant differences in Mcl-$1^{\Delta IEC}$ and control mice ($p < 0,001$). **c)** Evaluation of cell death rates by TdT-mediated dUTP nick end labeling (TUNEL assay) of fragmented DNA, revealing a 20-fold increase of dying cells in the colon of Mcl-$1^{\Delta IEC}$ mice. In order to generate a positive control one specimen was treated with DNAse. Five pictures of every specimen were taken and the number of TUNEL-positive cells was determined by counting. n = 5 animals per group. Scale bar indicates magnification for all panels. **d)** Correlation between TUNEL positive cells and the level of remaining Mcl-1 in the colon, determined by qRT-PCR (left, $R^2 = 0,6$) and between TUNEL positive cells and the body weight (right, $R^2 = 0,9$). Values are expressed as means + SD. *$p < 0,05$; ***$p < 0,001$.

The relatively high standard deviation in the Mcl-1 knockout group is most likely due to the patchy expression of Mcl-1, causing different levels of remaining Mcl-1 in the colon. In order to verify this assumption, RNA was isolated from the sectioned colon and relative Mcl-1 mRNA levels were determined by reverse transcription and subsequent quantitative real-time PCR (qRT-PCR).

If plotted against the number of TUNEL positive cells per mm^2, a negative correlation with a coefficient of determination of $R^2 = 0,58$ appears. Since the amount of remaining Mcl-1 always correlated with the body weight, this parameter was also plotted against the amount of TUNEL positive cells. In this case the negative correlation was even more explicit with a coefficient of determination of $R^2=0,93$ (Figure 31 d).

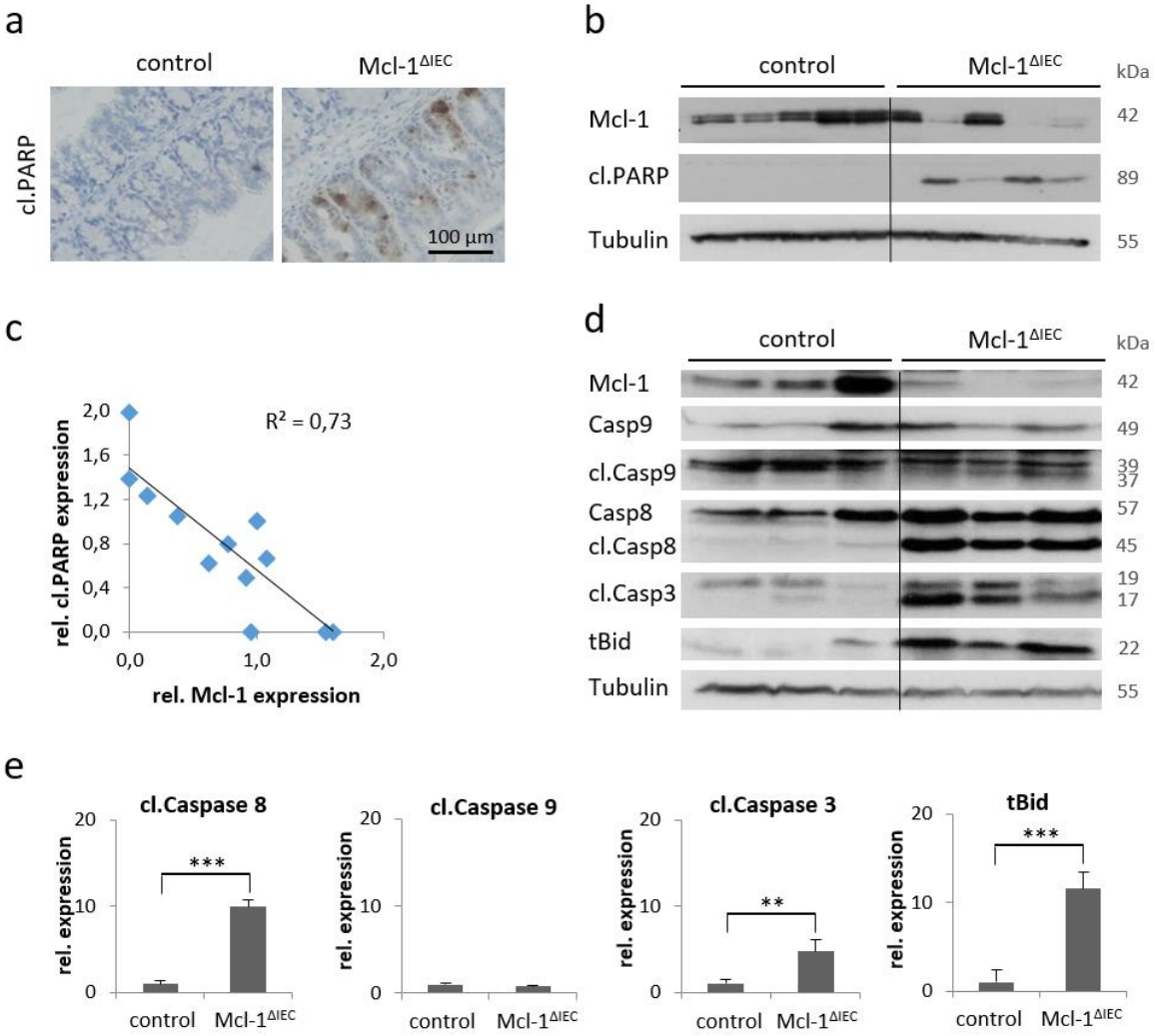

Figure 32: Analysis of apoptosis subroutines in Mcl-1$^{\Delta IEC}$ mice. **a)** IHC staining of colonic specimens, revealing a markedly increase of cleaved PARP positive cells in Mcl-1 negative areas. Scale bar indicates magnification for both pictures. **b)** Representative Western blots, detecting Mcl-1 (upper panel) and cleaved PARP (central panel) in the colon of Mcl-1$^{\Delta IEC}$ and control mice. Tubulin served as loading control. **c)** Correlation between the relative cleaved PARP abundance and the level of remaining Mcl-1 in the colon, determined by Western blot analysis ($R^2 = 0,73$). n = 12 animals. **d)** Representative Western blots, revealing an increase in activated Caspase 8 and 3 as well as an activation of Bid in the colon of Mcl-1$^{\Delta IEC}$ mice. Tubulin served as loading control. **e)** Subsequent densitometric analysis, showing a 9,9-fold upregulation of cleaved Caspase 8 (cl.Casp8; $p < 0,001$), a 4,7-fold upregulation of cleaved Caspase 3 (cl.Casp3; $p < 0,01$), a 11,5-fold upregulation of truncated Bid (tBid; $p < 0,001$) and an unaltered abundance of cleaved Caspase 9 (cl.Casp9) in the colon of Mcl-1$^{\Delta IEC}$ mice. Values are expressed as means + SD. **p < 0,01; ***p < 0,001.

In order to further investigate the molecular subtype of cell death occurring in the intestine of Mcl-$1^{\Delta IEC}$ mice, immunohistochemical staining against cleaved PARP, as a marker for apoptosis, was done (Figure 32 a).

It revealed a clear increase of cleaved PARP positive cells in Mcl-1 negative areas. In addition, proteins were isolated from the intestines of Mcl-$1^{\Delta IEC}$ and control mice and expression levels of Mcl-1 and cleaved PARP were determined by Western blot analysis (Figure 32 b). This Western blot further underlined the previously observed negative correlation between the amount of Mcl-1 and the abundance of dying cells. In total, 12 animals were analyzed with regard to their intestinal Mcl-1 and cleaved PARP levels and the plotting yielded a coefficient of determination of $R^2 = 0,73$ (Figure 32 c).

To determine, whether apoptosis execution is mainly conveyed by the intrinsic or by the extrinsic apoptotic pathway, further Western blot analyses were done. Thereby, levels of activated Caspase 9, as initiator Caspase of the intrinsic pathway, and activated Caspase 8, as initiator Caspase of the extrinsic pathway were detected (Figure 32 d). Western blot analysis revealed a 10-fold increase of cleaved Caspase 8 ($p < 0,001$) but unaltered levels of cleaved Caspase 9, arguing for an involvement of the extrinsic pathway. Levels of truncated Bid (tBid), as an interconnecting element between the extrinsic and the intrinsic pathway, were also notably increased in Mcl-$1^{\Delta IEC}$ mice ($p < 0,001$; Figure 32 e).

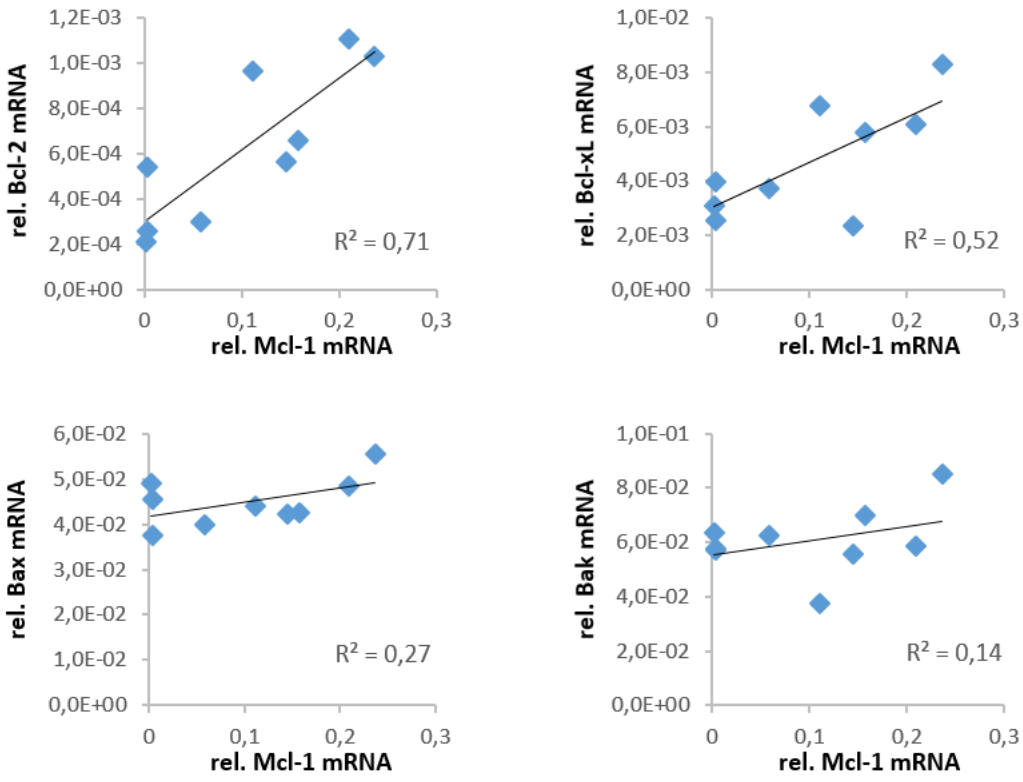

Figure 33: Expression levels of other Bcl-2 proteins in the colon of Mcl-$1^{\Delta IEC}$ mice. Correlation between the level of remaining Mcl-1 and the relative amount of Bcl-2 (upper left, $R^2 = 0,71$), Bcl-x_L (upper right, $R^2 = 0,52$), Bax (lower left, $R^2 = 0,27$) or Bak (lower right, $R^2 = 0,14$), determined by qRT-PCR. n = 9 animals.

For the purpose of determining the expression of kin pro- and anti-apoptotic proteins, RNA was isolated from 9 animals and analyzed by qRT-PCR. The abundance of Bcl-2 and Bcl-x_L, as related anti-apoptotic proteins, showed a positive correlation with the Mcl-1 expression levels (Bcl-2: R^2 = 0,71; Bcl-x_L: R^2 = 0,52). By contrast, no correlation was found between the expression of the pro-apoptotic family members Bax and Bak and the abundance of Mcl-1 (Bax: R^2 = 0,27; Bak: R^2 = 0,14; Figure 33).

Besides its anti-apoptotic function, Mcl-1 also influences autophagy and mitochondrial respiration. Hence, other cell death forms, such as necroptosis, could additionally contribute to the phenotype observed in Mcl-$1^{\Delta IEC}$ mice.

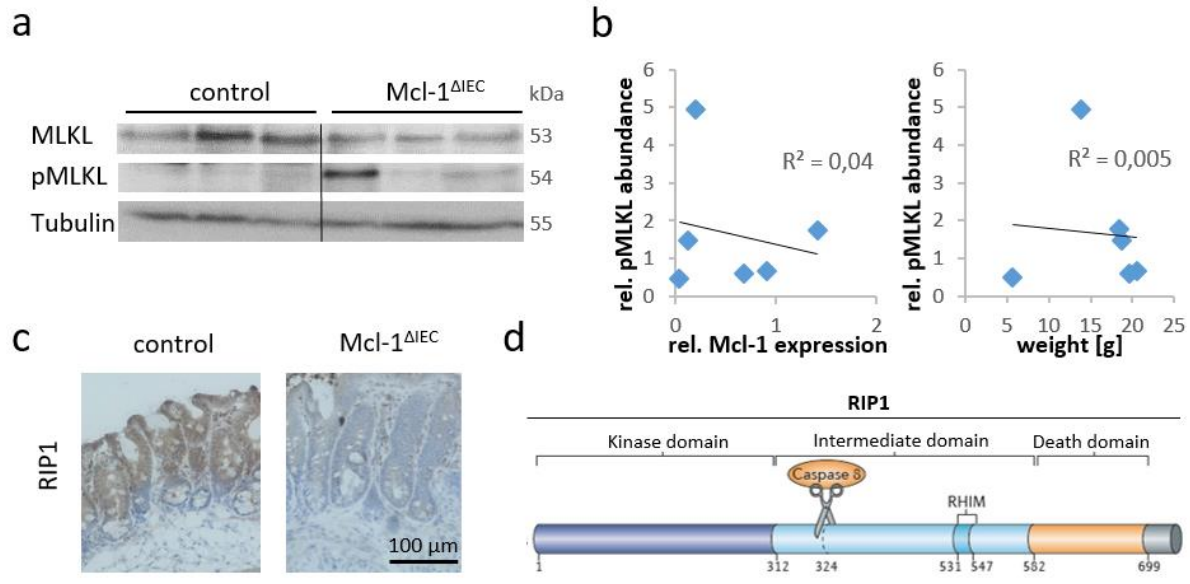

Figure 34: Analysis of necroptosis in Mcl-$1^{\Delta IEC}$ mice. **a)** Representative Western blots, detecting MLKL (upper panel) and phosphorylated MLKL (pMLKL; central panel) in the colon of Mcl-$1^{\Delta IEC}$ and control mice. Tubulin served as loading control. **b)** Correlation between the relative pMLKL abundance and the level of remaining Mcl-1 in the colon (left, R^2 = 0,04) and between the relative pMLKL abundance and the body weight (right, R^2 = 0,005), determined by Western blot analysis. n = 6 animals. **c)** IHC staining of colonic specimens with an antibody against RIP1, revealing a markedly decline of RIP1 in Mcl-1 negative areas. Scale bar indicates magnification for both pictures. **d)** Schematic illustration of RIP1 with its Caspase 8 cleavage site at Asp 324 (modified from Ofengeim et al., Nat Rev, 2013).

Therefore, phosphorylation of MLKL, as a necroptosis-specific event, and total MLKL levels were determined by Western blot analysis (Figure 34 a). Thereby, a markedly increase of pMLKL was found in one Mcl-$1^{\Delta IEC}$ animal. But if compared with the Mcl-1 expression levels (Figure 34 b; control group: animal 1,3,4; Mcl-$1^{\Delta IEC}$ group: animal 2,4,5), no correlation between pMLKL and the remaining Mcl-1 was detectable (Figure 34 b; R^2 = 0,04). As an alternative parameter, the amount of pMLKL was plotted against the body weight, leading to a coefficient of determination of R^2 = 0,005. In addition, expression levels of RIP1, as a central molecular switch between extrinsic

apoptosis and necroptosis, have been determined by immunohistochemical staining. The results clearly show that RIP1 is almost absent in Mcl-1 negative tissue sections (Figure 34 c). Since activated Caspase 8 negatively regulates necroptosis by cleaving RIP1 (Figure 34 d)[179], the observed phenotype points to apoptosis as responsible mechanism for cell death execution.

3.3.2.2 The Death of intestinal epithelial Cells in Mcl-1$^{\Delta IEC}$ mice is accompanied by increased Proliferation

In order to address the question, whether high cell death levels are accompanied by a counter-regulatory increase of proliferation, an immunohistochemical staining against Ki67 was done. While in control mice, Ki67 positive cells were exclusively located at the crypt base, higher amounts of proliferating intestinal epithelial cells were found in Mcl-1$^{\Delta IEC}$ mice (Figure 35 a). Here, Ki67 positive cells not only covered the crypt base but also 30-50% of the total crypt height. In Mcl-1$^{\Delta IEC}$ mice with a patchy expression patter, clear differences, regarding Ki67 positivity, occurred between Mcl-1 positive and negative areas (Figure 35 b).

To validate the observations made after immunohistochemical staining of Ki67, RNA was isolated from the colon of 10 animals. Subsequent to reverse transcription, relative expression levels of PCNA, as an alternative marker for proliferating cells, were determined by qRT-PCR. If plotted against Mcl-1, the negative correlation between Mcl-1 expression and the amount of proliferating cells was confirmed (R^2 = 0,58). The mRNA abundance of Cyclin D1, which is an important driver of the G1/S-phase transition, shows the same trend (R^2 = 0,34). As a further proof, mRNA abundance of the cell cycle inhibitor p21 was measured and plotted against Mcl-1. By contrast to the proliferation markers PCNA and Cyclin D1, p21 levels show a positive correlation with the Mcl-1 expression (R^2 = 0,71) (Figure 35 c).

At this point the question rose, whether the observed increase of proliferation is a mere counter-regulatory event, caused by high cell death rates, or if the loss of Mcl-1 independently influences cell cycle progression or cellular differentiation.

For investigating whether the stem cell compartment is expanded in the crypts of Mcl-1$^{\Delta IEC}$ mice, an immunohistochemical double-staining of Ki67 and Lgr5, as a marker for intestinal stem cells, could be done. Unfortunately, there is no Lgr5 antibody available which would be suitable for the IHC staining of murine tissue. Hence, Lgr5 protein levels were determined by Western blot analysis (Figure 35 d). Thereby, no differences were found between control and Mcl-1$^{\Delta IEC}$ mice, arguing for an unaltered amount of stem cells.

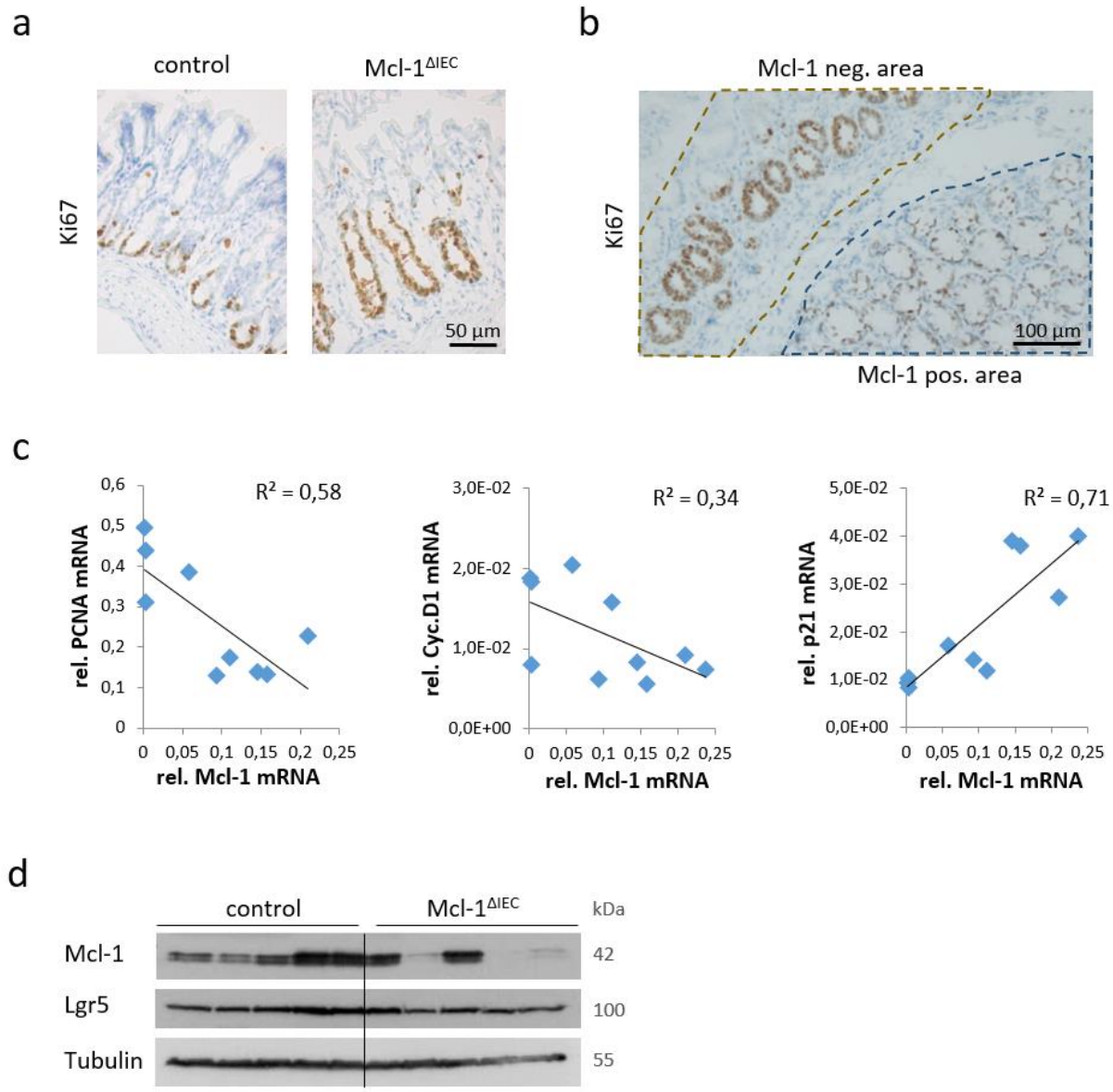

Figure 35: Analysis of proliferation in Mcl-1$^{\Delta IEC}$ mice. **a)** IHC staining of colonic specimens with an antibody against Ki67, revealing a markedly increase of proliferating IECs in Mcl-1$^{\Delta IEC}$ mice. Scale bar indicates magnification for both pictures. **b)** Ki67 staining on a colonic specimen which displays a patchy Mcl-1 expression. The Mcl-1 negative area is surrounded by the brown dashed line and the Mcl-1 positive area by the blue dashed line. **c)** Correlation between the level of remaining Mcl-1 and the relative amount of PCNA (left, R^2 = 0,58), Cyclin D1 (central, R^2 = 0,34) or p21 (right, R^2 = 0,71), determined by qRT-PCR. n = 10 animals.

3.3.2.3 Mcl-1$^{\Delta IEC}$ mice display severe Inflammation in the entire Intestine

If HE stained colon section are appraised, the number of infiltrating cells is clearly increased in tissue samples derived from Mcl-1ΔIEC mice (Figure 36 a). They accumulate in the inter-crypt space, leading to irregularly spaced crypts which lose their typical packed structure. Additionally, the absence of secretory Goblet cells gets visible in HE stained sections and was verified by a trained pathologist (Prof. Dr. Wilfried Roth, University Hospital Mainz). In a H&E staining, the mucins

containing Goblet cells appear normally as unstained spots within the crypt, as depicted in the control section (black arrow). Compared to this, no such spots were detectable in Mcl-1 negative areas. In order to investigate whether Paneth cells, as another important secretory cell line in the intestine, are also affected, an immunohistochemical staining with an antibody against Lysozyme was done. In control specimens, Paneth cells were localized in the small intestine in between the stem cells. By contrast, no Lysozyme positive cells were found in Mcl-1 negative areas, indicating a loss of this secretory cell type in the small intestine of Mcl-1ΔIEC mice (Figure 36 a). The loss of Goblet and Paneth cells, as important effectors of the intestinal innate immunity, facilitates the intrusion of pathobionts and undigested food particles, causing an inflammation. If the innate immune system gets overactivated, a previously local inflammation can get systemic. In line with this, splenomegaly, as an indicator for systemic inflammation, was observed in some Mcl-1ΔIEC mice (Figure 36 b).

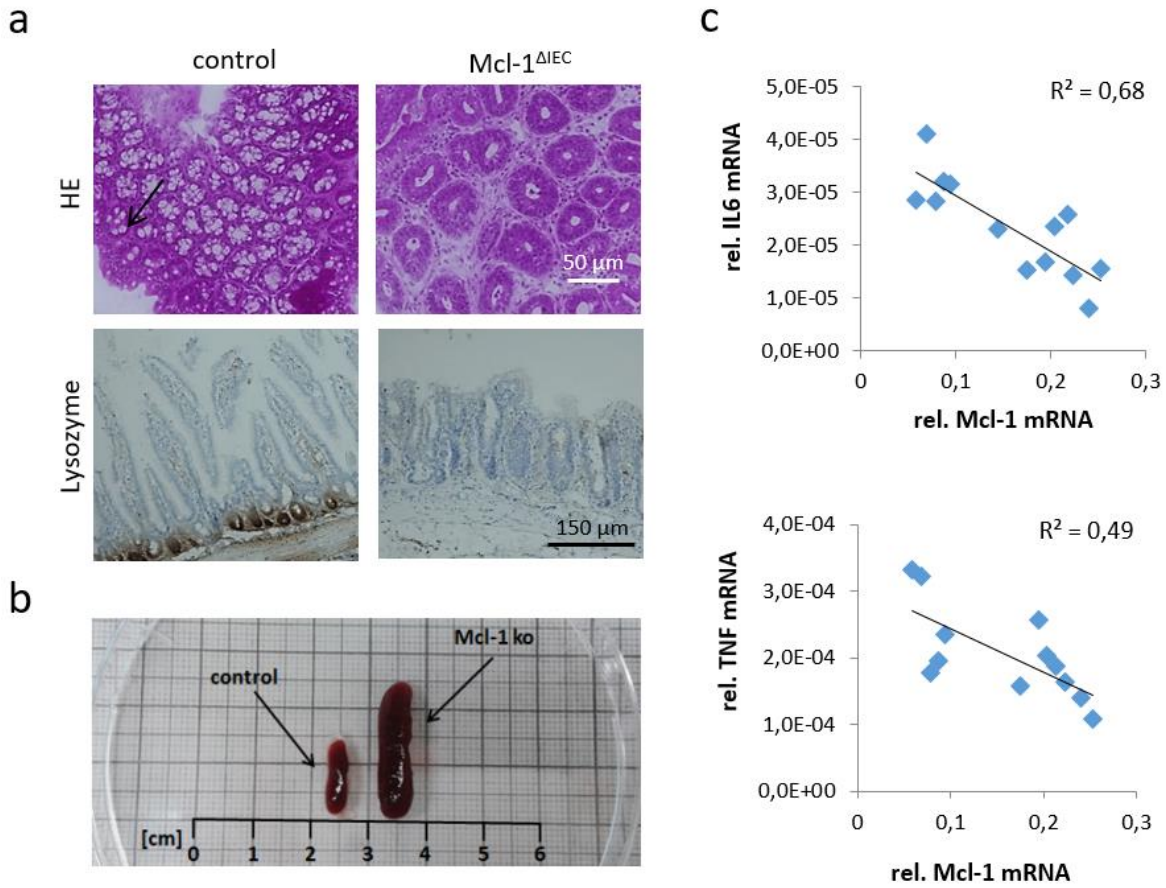

Figure 36: Analysis of inflammation in Mcl-1$^{\Delta IEC}$ mice. **a)** Hematoxylin and Eosin (H&E) staining of colonic specimens (upper panel), revealing a noteworthy number of infiltrating cells in Mcl-1 negative areas, as well as the loss of Goblet cells (black arrow) in the colon of Mcl-1$^{\Delta IEC}$ mice. Scale bar indicates magnification for both pictures. IHC staining of small intestinal specimens with an antibody against Lysozyme (lower panel), unveiling the absence of Paneth cells in Mcl-1 negative areas. Scale bar indicates magnification for both pictures. **b)** Exemplary picture of an enlarged spleen, how it was found in some Mcl-1$^{\Delta IEC}$ animals. **c)** Correlation between the level of remaining Mcl-1 and the relative amount of tumor necrosis factor (TNF; left, R^2 = 0,49) and interleukin 6 (IL6; right, R^2 = 0,68), determined by qRT-PCR. n = 12 animals.

That the level of the innate immune response and the level of remaining Mcl-1 correlate, was proven by qRT-PCR. Therefor, RNA was isolated from the colons of 12 animals and subsequent to reverse transcription, levels of TNF, IL6 (interleukin 6) and Mcl-1 were determined. TNF is mainly secreted by macrophages, whereas IL6 gets primarily produced by neutrophils. The respective plots show a negative correlation between the abundance of TNF (R2 = 0,49) and IL6 (R2 = 0,68) and the levels of remaining Mcl-1 (Figure 36 c).

In order to identify the infiltrating cells, immunohistochemical staining with antibodies against CD3, CD20 and CD68 were done. Quantification of CD3 positive cells showed a decrease of T-cells in the mucosa of Mcl-1$^{\Delta IEC}$ mice if compared to controls. However, the decline was not statistically significant. For CD20 positive B-cells, a slight but not significant increase was detected. But still, B-cells have been found to be rather rare in the intestinal mucosa. The by far highest number of infiltrating cells were identified as CD68 positive macrophages ($p < 0,05$), what explains high TNF levels in the intestine of Mcl-1$^{\Delta IEC}$ mice (Figure 37 a and b).

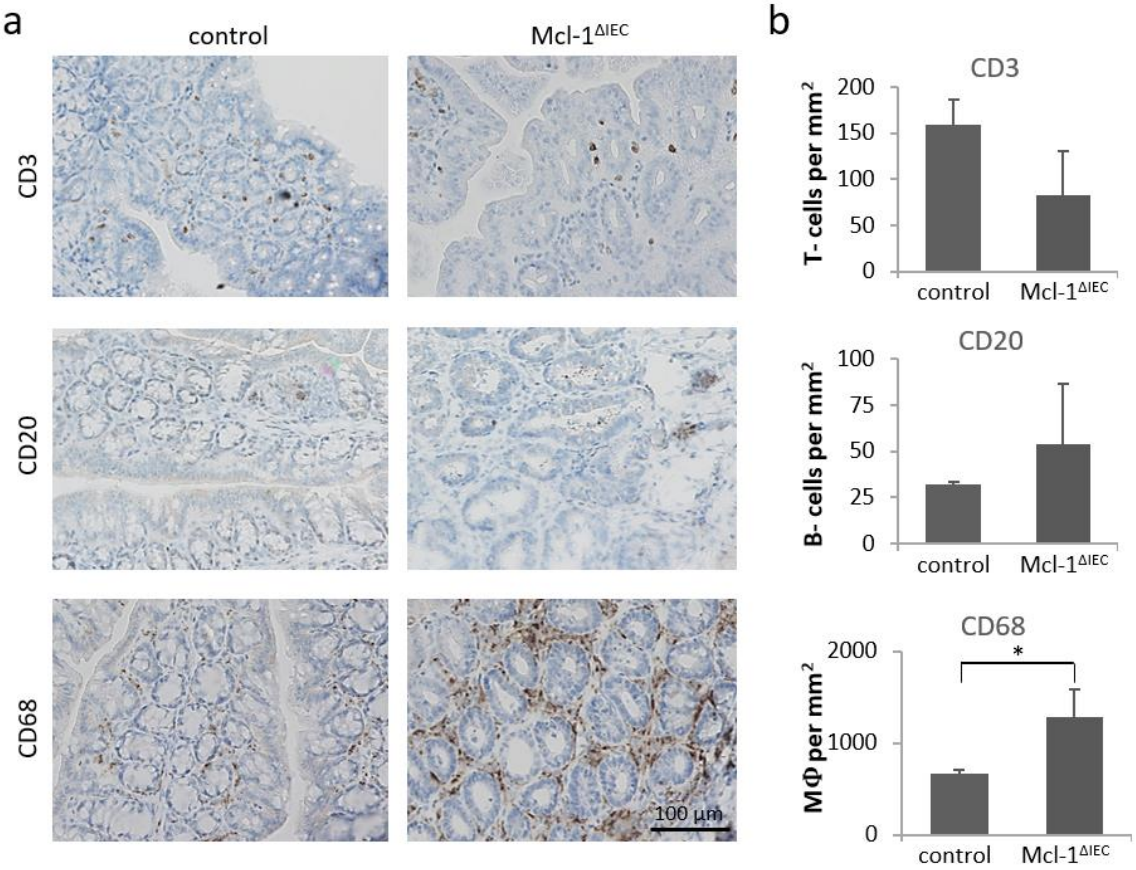

Figure 37: Analysis of immune cell infiltration in Mcl-1$^{\Delta IEC}$ mice. **a)** IHC staining of colonic specimens with antibodies against CD3 (T-cells), CD20 (B-cells) and CD68 (macrophages (MΦ)), identifying MΦ as the mainly invading cell type. Scale bar indicates magnification for all pictures. **b)** For quantification of positive cells per mm^2, 5 pictures per sample were captured and cell numbers were determined by counting. n = 3 animals per group. Values are expressed as means + SD. *$p < 0,05$.

3.3.2.4 Mcl-1$^{\Delta IEC}$ mice show spontaneous Tumor Development in the Intestine

Even though the overall survival of Mcl-1$^{\Delta IEC}$ mice with a complete loss of Mcl-1 in the intestine is limited, the one of mice expressing Mcl-1 in a patchy manor is comparable with control mice, if followed up to one year.

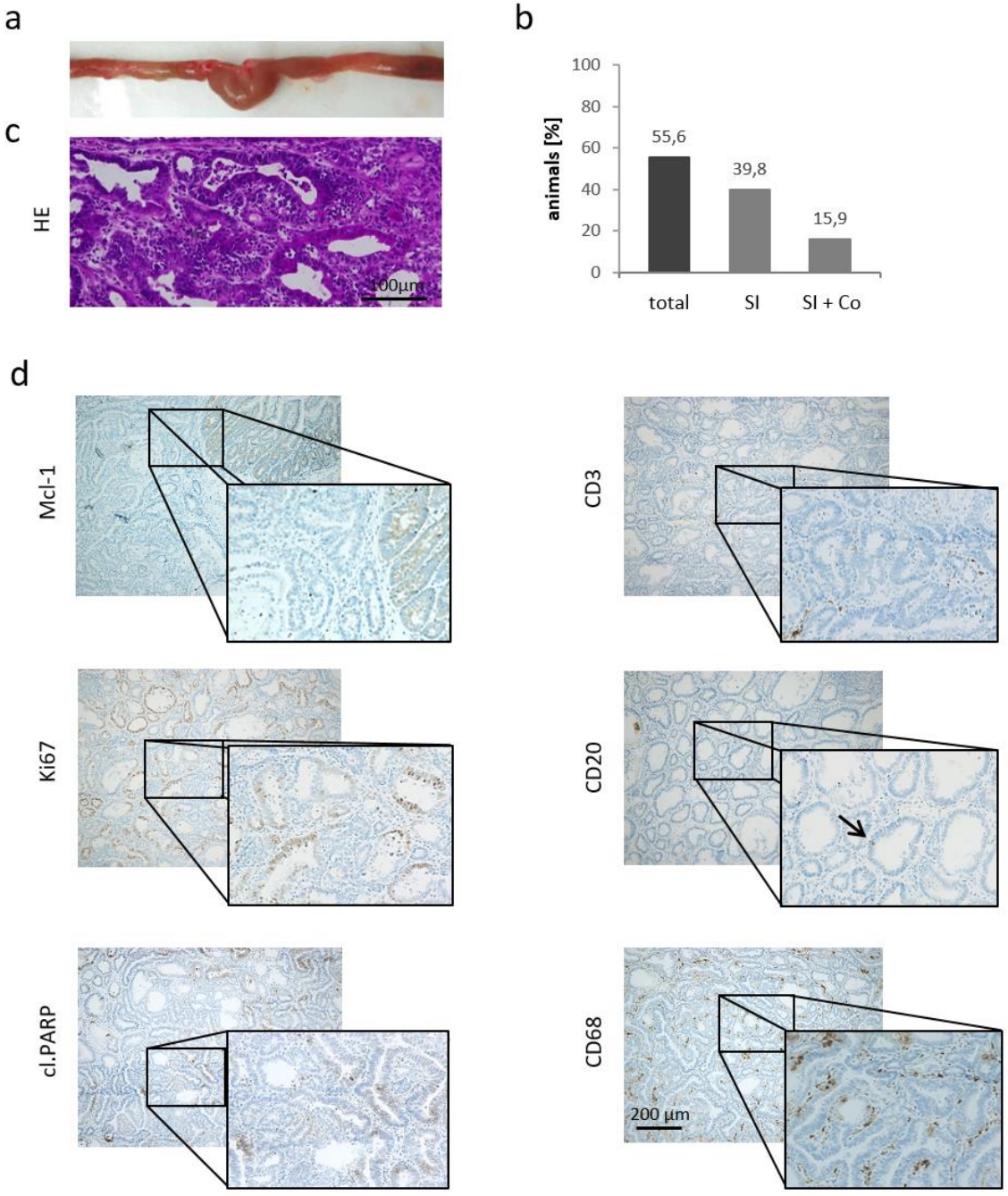

Figure 38: Analysis of proliferation, apoptosis and lymphocyte infiltration in tumors derived from Mcl-1$^{\Delta IEC}$ mice. **a)** Macroscopic picture of a tumor located in the small intestine of a Mcl-1$^{\Delta IEC}$ mouse. **b)** Percentage of tumor developing Mcl-1$^{\Delta IEC}$ animals with an age of > 6 month (black bar; n = 18) and tumor localization (grey bars). SI = small intestine; Co = colon. **c)** Hematoxylin and Eosin (HE) staining of a small intestinal tumor section, derived from a Mcl-1$^{\Delta IEC}$ mouse. **d)** IHC staining with antibodies against Mcl-1, Ki67 and cl.PARP, revealing relatively high cellular turnover rates in Mcl-1 negative tumors. Staining against CD3 (T-cells), CD20 (B-cells) and CD68 (macrophages (MΦ)), identifying MΦ as the mainly invading cell type. Scale bar indicates magnification for all panels except the enlarged sections. n = tumors derived from 6 Mcl-1$^{\Delta IEC}$ animals.

From an age of six months, about half of these mice (55,6%) spontaneously start to develop tumors, which are primarily located in the small intestine (Figure 38 a). Only a sixth of all animals develop colorectal tumors in addition (Figure 38 b). Hematoxylin and Eosin stained tumors were assessed by a trained pathologist (Prof. Dr. Wilfried Roth, University Hospital Mainz) and identified as well differentiated adenocarcinomas (Figure 38 c). Immunohistochemical staining of tumors derived from 12 animals revealed that the tumor tissue is always Mcl-1 negative, even though tumor carrying animals showed a patchy expression (Figure 38 d, upper left panel).

This argues for Mcl-1 having a decisive tumor suppressing function, that goes beyond its role in the prevention of inflammatory processes in the gut. This would be in line with the observed downregulation of Mcl-1 in human adenomas and adenocarcinomas.

Immunohistochemical staining with an antibody against Ki67 showed that the emerged neoplasias are highly proliferative. At the same time, there is a noteworthy level of apoptotic cells in the tumors, as determined by staining against cleaved PARP. Staining against CD3, CD20 and CD68 again identified macrophages as the mainly invading cell type, what is in line with the observations made in Mcl-1 negative mucosa. Similar thereto, only very few B-cells (CD20) and a moderate number of T-cells (CD3) were detectable in the tumor tissue (Figure 38 d, right column).

In order to further dissect whether tumor formation is a secondary, inflammation-based event or whether the loss of Mcl-1 directly promotes malignant transformation, Mcl-1$^{\Delta IEC}$ mice were housed in a germ-free surrounding. This was done by our cooperation partners, the group of Prof. Dr. med. Achim Weber in Zurich. The germ-free housing led to an impressive decrease of inflammation but had almost no effect on tumor incidences (manuscript in preparation). This further supports the hypothesis that Mcl-1 directly suppresses tumor formation in the intestine.

Based on this assumption, the microsatellite stability in Mcl-1 negative tumors was assessed by Sanger sequencing. Therefor, DNA from tumor tissue was isolated subsequent to manual microdissection. Due to the patchy expression pattern, control DNA could be isolated from Mcl-1 positive, small intestinal mucosa of the same animals. Subsequently, a set of non-coding long mononucleotide markers was analyzed to detect potential signs of mismatch repair deficiency. In addition, coding mononucleotide markers located in the genes Sdccag1, Elavl3, Glis2, and Tmem107 were evaluated for the presence of length alterations between Mcl-1-negative tumor regions and Mcl-1-positive mucosa[201].

Analyses showed, that all tested markers presented with identical profiles in all samples, suggesting that microsatellite instability, which is commonly observed in DNA mismatch repair-deficient tumor cells, is absent or at least a rare event in Mcl-1-negative tumors.

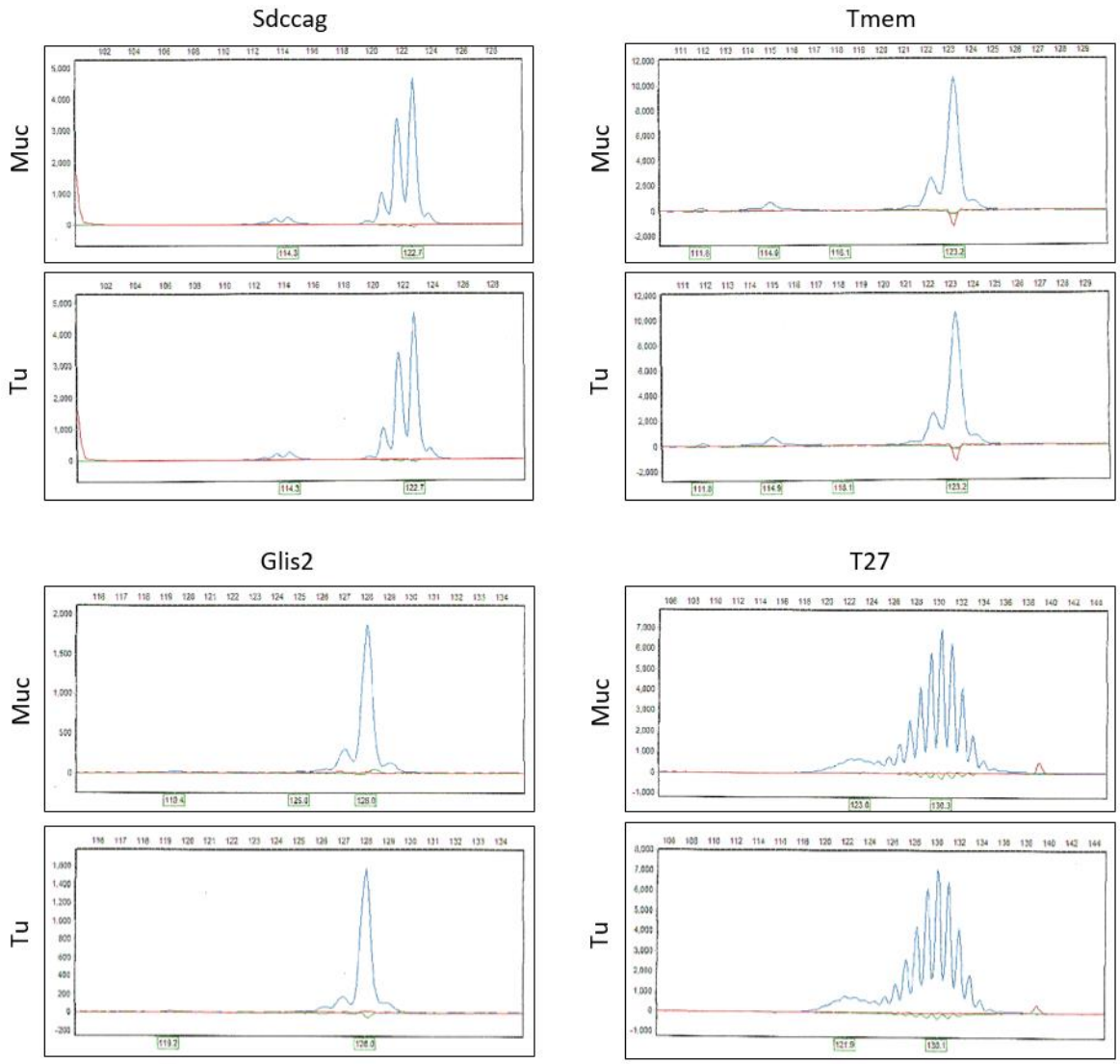

Figure 39: Test for microsatellite instability in tumors derived from Mcl-1$^{\Delta IEC}$ mice. Subsequently to the isolation of DNA from tumor tissue and Mcl-1 positive mucosa, a set of murine microsatellite instability markers were analyzed by Sanger sequencing to detect potential signs of mismatch repair deficiency. Some resulting profiles are exemplarily shown for one pair of tumor (Tu) and mucosa (Muc), indicating that tumors derived from Mcl-1$^{\Delta IEC}$ mice are not microsatellite instable.

In summary, the results obtained from Mcl-1$^{\Delta IEC}$ mice suggest that Mcl-1 is inalienable for the maintenance of the murine intestinal mucosa and that its loss cannot be compensated by kin anti-apoptotic proteins. The spontaneous tumorigenesis in Mcl-1$^{\Delta IEC}$ mice seems promoted but not caused by the inflammatory milieu, pointing to a cell death-independent tumor suppressor role of Mcl-1.

3.4 Inhibition of anti-apoptotic Bcl-2 Proteins in a 3D Cell Culture Approach

The following experiments aimed at evaluating whether the inhibition of anti-apoptotic Bcl-2 proteins might be beneficial for the treatment of colorectal cancer patients. The insights gathered by the performed *in vitro* and *in vivo* experiments, point to a unique role of Mcl-1 for the

maintenance of intestinal tissue homeostasis. If taken into account that it is downregulated in human adenomas and adenocarcinomas and that its loss causes a massive inflammatory phenotype in the intestine of Mcl-$1^{\Delta IEC}$ mice, Mcl-1 seems an uneligible target for chemical inhibition in the context of CRC treatment. Bcl-x_L, by contrast, gets significantly upregulated in human adenocarcinomas and its loss renders Bcl-$x_L^{\Delta IEC}$ mice less vulnerable towards chemically induced carcinogenesis. Hence, the Mcl-1 sparing inhibitor ABT-737 was chosen for evaluating the value of anti-apoptotic protein inhibition in a translational approach. The BH3 mimetic ABT-737 shows an affinity to the BH3 groove of Bcl-x_L and Bcl-2.

As a pre-experiment, a 3D cell culture system was used for long-term cell culture of human HT29 cells in a tissue mimicking environment. Cells were seeded onto the scaffolds and kept for 48 h in cell culture medium, what allowed the cells to migrate in.

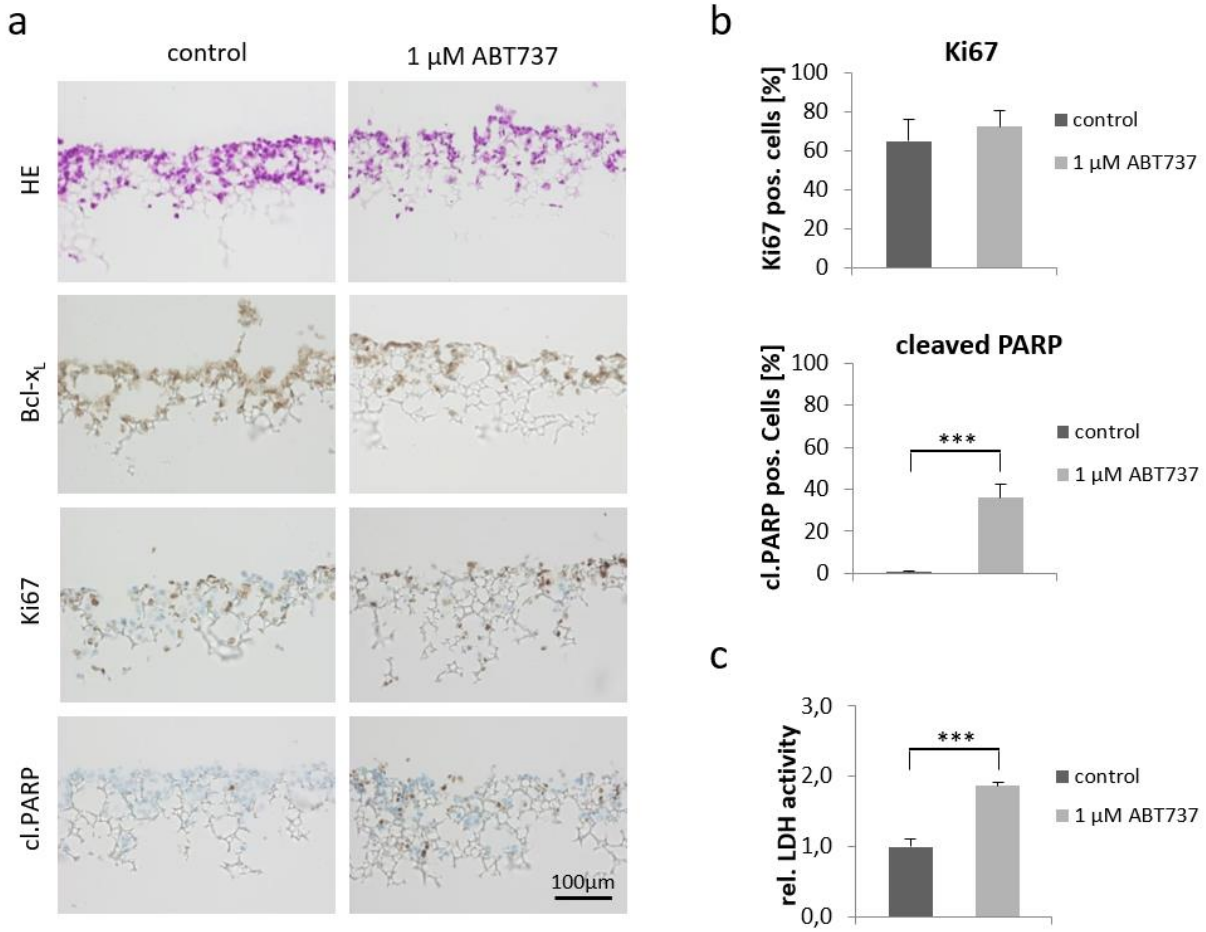

Figure 40: Evaluation of the Bcl-x_L/Bcl-2 inhibitor ABT-737 in a 3D cell culture approach. **a** Hematoxylin and Eosin (HE) staining (upper panel) and IHC against Bcl-x_L, Ki67 and cleaved PARP on scaffold sections, revealing a noteworthy increase of apoptotic HT29 cells in ABT-737 (1 µM for 4 days) treated samples (n=5 scaffolds per group). DMSO treated samples served as control. Scale bar indicates magnification for all panels. **b)** Correlating quantification of Ki67 and cleaved PARP positive cells, determined by counting, showing a significant increase ($p < 0,001$) of dead cells (cleaved PARP) but no significant changes in the proliferative capacity (Ki67) under ABT-737 treatment (n=5 scaffolds per group). **c)** Measurement of lactate dehydrogenase (LDH) in the supernatant of scaffolds after 4 days of treatment with the inhibitor (1 µM), showing a 1,9-fold higher concentration under treatment ($p < 0,001$). Values are expressed as means + SD. ***$p < 0,001$.

Subsequently, medium was supplemented with ABT-737 (1 µM) or DMSO as control for another 96 h, whereupon scaffolds were sectioned and stained for cleaved PARP. The immunohistochemical staining revealed a remarkable increase in the amount of apoptotic cells (36%) in ABT-737 treated samples. By contrast, almost no cell death was detectable in DMSO treated controls (0,5%, $p < 0,001$; Figure 40 a and b). An increased cell death in presence of the inhibitor was further validated by measuring the level of lactate dehydrogenase (LDH) in the supernatant. In line with the cleaved PARP staining, LDH activity was found to be almost doubled (1,9-fold; $p < 0,001$) in supernatants of ABT-737 treated scaffolds, further substantiating the potency of Bcl-x_L inhibition in long-term 3D cell culture (Figure 40 c). The expression of Bcl-x_L itself was not altered in presence of the inhibitor (Figure 40 a). In order to investigate whether the increased cell death induces alterations in the proliferation rate, scaffold sections were stained for Ki67. In line with the data obtained after siRNA mediated knockdown of Bcl-x_L in CRC cells and with the observations made in Bcl-$x_L^{\Delta IEC}$ mice, no changes in the proliferative capacity of HT29 cells were detected under ABT-737 treatment (Figure 40 a and b).

3.5 Inhibition of anti-apoptotic Bcl-2 Proteins in an ex vivo Tissue Culture System

To evaluate the potential of ABT-737 in a human *ex vivo* system, vital CRC specimens of 10 patients were treated with ABT-737 (5 µM) or DMSO for 72 h. Therefor, tumor tissues were sectioned, placed onto a filter membrane and kept at the air-liquid interface, directly upon surgical resection. For treatment, culture medium was supplemented with the inhibitor or DMSO in a respective concentration. Subsequently, tissue slices were paraffin-embedded, sectioned and H&E stained, to allow assessment of vital tumor cell content and tissue quality by a pathologist. Thereupon, specimens derived from 5 patients were further analyzed with regard to cell death and proliferation. Immunohistochemical staining for cleaved PARP revealed a significant increase in the number of dead cells from 8,9% to 31,5% under ABT-737 treatment ($p < 0,05$). Results from a Ki67 staining were in line with the findings obtained in our mouse model and the *in vitro* experiments, showing no significant changes in the proliferative capacity of CRC tissue in the presence of the inhibitor (Figure 41 a, b and c). In order to prove the cell death phenotype, an additional ATP assay was performed. In this assay, the measured luminescence directly correlates with the amount of ATP within the tissue and thus with its viability. ABT-737 treatment induced a significant ($p < 0,05$) decreased of luminescence to 44% of the basic value. This further argues for a subsidence of tissue viability in presence of the inhibitor (Figure 41 d).

Together, the findings from the 3D cell culture and the tissue culture assay suggest that inhibition of Bcl-x_L /Bcl-2 could be an interesting approach in the context of CRC treatment.

a

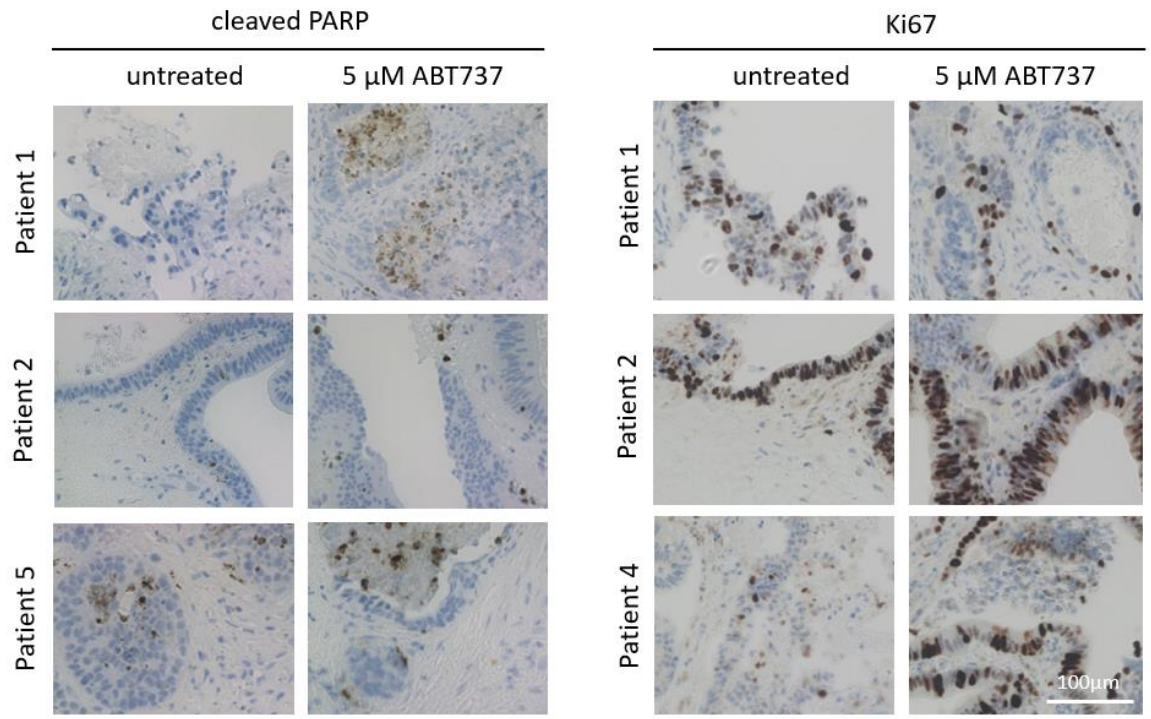

b

	Fold-change	
Sample	**cl.PARP**	**Ki67**
Pat. 1	20,09	1,08
Pat. 2	3,46	0,87
Pat. 3	3,97	1,00
Pat. 4	2,54	8,22
Pat. 5	2,16	0,91

c

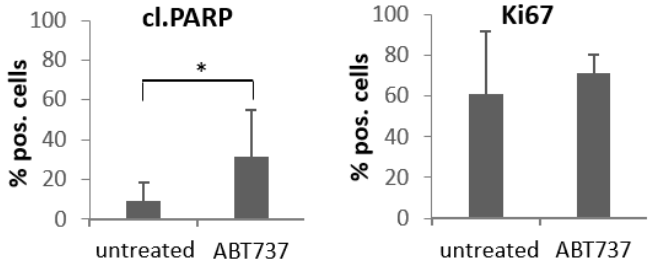

d

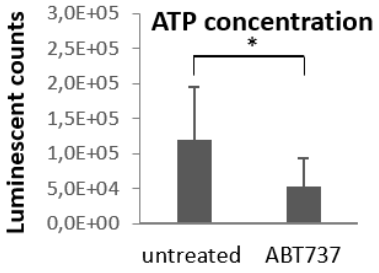

Figure 41: Evaluation of the Bxl-x$_L$/Bcl-2 inhibitor ABT737 in an ex vivo tissue culture approach. Human CRC specimens were sliced and kept in culture for 94 h. After 24 h, the medium was supplemented with 5 µM ABT737 or DMSO as control. **a)** IHC against cleaved PARP (left) and Ki67 (right) on tissue culture sections from three patients. Scale bar indicates magnification for all panels. **b and c)** Table and graphs summarizing changes of cleaved PARP and Ki67 positive cells which were determined by counting of control (DMSO) and ABT737 treated specimens. Quantification revealed a significant increase ($p < 0,05$) of dead cells (cleaved PARP) but an unaltered proliferative capacity (Ki67) of ABT737 treated tumor tissue. **d)** ATP assay, showing a decreased ATP content in ABT737 treated tissue specimens ($p < 0,05$; n=5 scaffolds per group). Values are expressed as means + SD. *$p < 0,0$.

Colorectal cancer (CRC) is the third most common tumor entity worldwide and additionally a main cause for cancer related death in humans. In developed countries, more than 4 % of the population will develop CRC during the course of lifetime[17]. Even though, there is good progress in the development of surgical techniques and targeted therapies, especially patients in a metastasized state still face a poor prognosis. Compared to patients diagnosed with CRC in a localized stage, the presence of distant metastasis declines five-year survival rates from over 90 % to 12 %[25]. In order to form metastasis, transformed cells need to avoid cell death via anoikis after detaching from neighboring cells. Furthermore, they need to acquire a more mesenchymal phenotype, what enables them to migrate and invade distant tissues[209].

In the past, the Bcl-2 protein family has been extensively studied with regard to their cell death regulating function. Structural and functional analyses lead to their division into three subgroups. Pro-apoptotic proteins like Bax and Bak are able to form pores in the outer mitochondrial membrane, thereby initiating mitochondrial activation as "point of no return" within the intrinsic apoptotic cascade. Proteins of the anti-apoptotic subgroup, comprising Bcl-2, Bcl-x_L and Mcl-1, maintain the integrity of the outer mitochondrial membrane by sequestering their pro-apoptotic relatives. BH3-only proteins, which share only the third out of four Bcl-2 homology domains (BH), represent the third subgroup. Since their expression gets induced by apoptotic stimuli, they work as a molecular switch, sensing and transmitting cytotoxic events by either neutralizing anti-apoptotic proteins[78] or directly activating the pro-apoptotic ones[79].

Since avoidance of apoptosis is a classical hallmark of cancer, the fact that anti-apoptotic Bcl-2 proteins are frequently overexpressed in diverse tumor entities is comprehensible[192,193]. Thus, members of this subgroup are predestined targets for clinical application, what lead to the development of small molecule inhibitors, called BH3-mimetics[210]. Similar to their endogen templates, BH-3 mimetics work by interfering with anti-apoptotic proteins, what thence facilitates mitochondrial activation and cell death[211]. Despite the fact, that BH3-mimetics already entered clinical trials[212,213], there is only limited knowledge regarding alternative functions of anti-apoptotic Bcl-2 proteins apart from their role in cell death regulation. Indeed, there is growing evidence, that these proteins are important for other cellular processes, such as autophagy[132], proliferation[196,214] and DNA damage response[198]. Since anti-apoptotic Bcl-2 proteins are a promising target in the context of CRC treatment, a better understanding of their influence on intestinal tissue homeostasis and colorectal carcinogenesis is crucial.

This thesis aimed at investigating the role of Bcl-2, Bcl-x_L and Mcl-1 for physiology and pathophysiology of the intestine by pursuing approaches *in vitro, in vivo* and *ex vivo.*

4.1 Expression Levels of anti-apoptotic Bcl-2 Proteins in human colorectal Cancer Cells and their Impact on Proliferation

In a first step, this study aimed at evaluating the expression of anti-apoptotic proteins in human intestinal mucosa, in primary colorectal tumors and in corresponding liver metastases. Therefore, immunohistochemical staining was done on a tissue microarray containing spots of normal mucosa, adenomas and adenocarcinomas. It revealed an upregulation of Bcl-x_L in adenomal tissue with a further increase in the malignant state. This is in line with previous reports by Zhang et al.[215] and Jin-Song et al.[194], which found Bcl-x_L expression to be positively correlated with the malignancy of CRC and poorer overall survival. Since the avoidance of apoptosis is a key feature of malignant cells, the upregulation of Bcl-x_L as an anti-apoptotic protein is comprehensible. Surprisingly, Mcl-1 has been found to be significantly downregulated in adenomas, with a slight rebound in adenocarcinomas. Even though, a similar pattern showing a decrease of Mcl-1 during malignant transformation has been described by Henderson-Jackson et al.[216], the downregulation of Mcl-1 in CRC is contradicting to its classical apoptosis-preventing function. In case of Bcl-2, no significant alterations in the expression levels have been observed. By contrast, Krajewska et al.[217] found Bcl-2 to be rather decreased in adenocarcinomas, what would support the finding, that high Bcl-2 expression seems correlated with a better clinical outcome[195,218]. The discrepancy between the presented results and the study by Krajewska et al. might be due to a, *per se*, inhomogeneous expression of Bcl-2, what impedes the detection of weak phenotypes in a relatively small collective. Since until today, very little is known about the expression profiles of anti-apoptotic Bcl-2 proteins in CRC derived metastases, immunohistochemical staining on primary colorectal tumors and corresponding liver metastases has been done. Even though, subsequent analysis revealed a trend which pursued the observed alterations in mucosa and primary tumors, neither Bcl-x_L nor Mcl-1 showed significantly different expression levels. This might be primarily caused by their extremely heterogeneous expression in metastases and again by a relatively small collective of only ten patients.

With regard to their classical, apoptosis-preventing function, anti-apoptotic Bcl-2 proteins have always been described as being redundant. But their different expression profiles in normal intestinal mucosa and in colorectal carcinomas indicate additional functions, going beyond cell death regulation. In order to get more insight how anti-apoptotic Bcl-2 proteins might influence other properties important for malignant cells, such as proliferation and invasiveness, Bcl-2, Bcl-x_L and Mcl-1 were downregulated in two different human CRC cell lines by RNA interference. If migration and invasiveness of cells are of interest, it is mandatory to analyze viability and proliferation first, because cells affected by an impaired metabolism are considered as *a priori* less prone to migrate and invade[219]. Results obtained in a MTT assay showed, that the knockdown of

none of the anti-apoptotic Bcl-2 proteins lead to a decrease in the viability of HT29 or SW480 cells. Since MTT assays always display combined information about cell death and proliferation, this finding was further validated by FACS analysis of cleaved PARP-positive cells, showing that the number of apoptotic cells does not increase after silencing of anti-apoptotic Bcl-2 proteins. In the context of cell cycle regulation, the exact function of Bcl-2 and Bcl-x_L remains controversial. On the one hand they have been shown to coordinately delay G0–G1 transition, arresting cells in the G-phase[214]. Furthermore, overexpression of Bcl-x_L seems to stabilize a G2-M-phase arrest in cells affected by DNA damage[220]. On the other hand, it has been shown that cell cycle delay, induced by the Bcl-2 targeting microRNA miR-206, can be overcome by overexpression of Bcl-2 in glioblastoma cells, what indicates a pro-proliferative function[221]. Mcl-1 has been shown to inhibit cell cycle progression through the S- and G2-phase via binding of proliferating cell nuclear antigen (PCNA)[196] and Cyclin depending kinase 1 (CDK1)[197]. However, no detailed information about the role of anti-apoptotic Bcl-2 proteins for cell cycle control in CRC cells was available. Therefore, the proliferative capacity of HT29 and SW480 has been evaluated subsequent to siRNA mediated knockdown of Bcl-2, Bcl-x_L or Mcl-1. Data obtained by the following BrdU FACS analysis clearly showed that Bcl-2 and Bcl-x_L have no significant effects on proliferation and cell cycle progression in CRC cells. By contrast, knockdown of Mcl-1 led to higher total cell counts, enhanced BrdU incorporation (Figure 10) and increased levels of Ki67 (Figure 12), indicating an anti-proliferative function of Mcl-1 in CRC cells. This finding could be a potential explanation for the decreased Mcl-1 expression in intestinal adenomas and adenocarcinomas, where an increased proliferation through lowered levels of Mcl-1 might be very beneficial for tumor cells (Figure 6). This would also implicate, that the increase in proliferation is at least partially purchased at the expense of cell death prevention, if not compensated by other anti-apoptotic Bcl-2 proteins. In the presented work, it has been shown for the first time that Mcl-1 exerts an anti-proliferative effect on intestinal epithelial cells[235].

4.2 The Role of anti-apoptotic Bcl-2 Proteins for colorectal Cancer Cell Migration and Invasiveness

Since the obtained results indicate that a single knockdown of either Bcl-2, Bcl-x_L or Mcl-1 is well compensated in CRC cells with regard to viability and proliferation, the set up could be used to further study the influence of anti-apoptotic Bcl-2 proteins on CRC cell migration. The capacity of a cancer cell to migrate and invade foreign tissue is a prerequisite for distant metastasis formation[222]. Interestingly, there is growing evidence that apoptosis propensity and metastatic potential of cancer cells are inversely correlated[223]. Del Bufalo et al. demonstrated that the overexpression of Bcl-2 in breast cancer cells not only enhances their tumorigenicity but also their metastatic

potential if transferred into nude mice[224]. In line with this, other studies showed that endogenous overexpression of Bcl-2 promotes the progression of prostate carcinoma cells towards an enhanced metastatic phenotype[225,226]. There are several steps in the complex course of metastasation which presumably rely on apoptosis resistance. In order to spread, cancer cells need to detach from the extracellular matrix (ECM) and remodel their cytoskeleton. Normally both processes are sufficient to induce cell death via anoikis or amorphosis respectively[227]. Martin et al. could show in several studies that overexpression of Bcl-2 or Bcl-x_L is capable of preventing cytoskeleton-based death, what promotes detachment and intravasation as initial steps of metastatic dissemination[228,229]. Solitary cancer cells which entered the vasculature get moreover affected by patrolling immune cells and mechanical stresses like haemodynamic sheering[230]. Subsequent to extravasation, spreading tumor cells need to survive and regain their proliferative capacity, even though they are exposed to a foreign ECM. In this context, Wong et al. could show that overexpression of Bcl-2 significantly decreased apoptosis of disseminated cancer cells in the lungs of nude mice[231]. In addition to their cytoprotective properties, Bcl-2 and Mcl-1 have been identified as direct modulators of migration and invasion in various cancer cell lines[232–234]. However, their influence on the migratory capacity and invasiveness of colorectal cancer cells had not been investigated so far. Therefore, gap closure was measured in a wound healing assay, subsequent to siRNA mediated downregulation of Bcl-2, Bcl-x_L or Mcl-1. Both cell lines are well characterized and it is known that SW480 cells are tumorigenic but non-invasive in an orthotopic tumor model, whereas HT29 cells are tumorigenic, invasive and metastatic in xenografts[207]. In both HT29 and SW480 cells, a significant inhibition of gap closure was observed subsequent to protein silencing, with the most striking phenotype after downregulation of Bcl-2[219]. As a proof of principle, anti-apoptotic Bcl-2 proteins were overexpressed thereafter, what indeed led to a completely reversed phenotype, with the strongest effect again observed for Bcl-2. To further validate the made observations, a three-dimensional cell culture system was used. Compared with two-dimensional cell culture approaches, the employed scaffolds better reflect the physiological situation by allowing cells to migrate, proliferate and interact more freely[235–237]. Even though morphology of both cell lines changed if grown in scaffolds, the results, regarding migration, closely resembled the ones obtained in 2D. Again, silencing of Bcl-2 caused the most remarkable inhibition of migration. The migratory capacity is only one property of disseminating cancer cells which is a prerequisite for distant metastasis formation. Another one is the ability to actively penetrate the ECM in order to leave the primary tumor[238,239]. To mimic the *in vivo*-situation, a Boyden chamber invasion assay was carried out, in which cells had to overcome a Matrigel layer, mimicking the ECM. Since pre-experiments revealed the very limited invasive potential of HT29 cells, invasion assays were performed by using the SW480 cell line. The obtained results show that the knockdown of all three anti-apoptotic Bcl-2

proteins causes a remarkable drop in the invasiveness of CRC cells, with especially strong phenotypes after silencing of Bcl-2 or Mcl-1. These findings are in line with studies published by Wick et al., showing that overexpression of Bcl-2 or Bcl-x_L enhances Matrigel invasion of glioma cells[234,240]. Furthermore, a study on CRC revealed a reduced invasiveness after adenovirus-mediated siRNA targeting of Bcl-x_L[241]. But since the employed LoVo cells in this study additionally showed decreased proliferation and spontaneous cell death induction after downregulation of Bcl-x_L, the observed reduction of cells which overcame the Matrigel barrier cannot be clearly assigned to a lowered invasiveness. By contrast, the here presented migratory and invasive phenotypes are clearly independent from cell cycle regulation and cell death induction in HT29 and SW480 cells[219]. Because the silencing experiments drew a clear picture about the importance of anti-apoptotic Bcl-2 proteins for the migratory capacity of CRC cells, it was evaluated whether similar effects can be achieved by chemical inhibition. This approach would provide the opportunity of a transfer into the clinic. Therefor, HT29 and SW480 cells were treated with the BH3-mimetic Obatoclax, which simultaneously inhibits Bcl-2, Bcl-x_L and Mcl-1. Upon titration, clinically relevant doses were determined which did not reach the compound IC_{50} reported for Obatoclax in phase I clinical trials[242,243]. Because it has been reported that Obatoclax treatment leads to a degradation of anti-apoptotic proteins in lymphoma cells[204], expression levels of Mcl-1, Bcl-2 and Bcl-x_L were determined under different inhibitor concentrations. Western blot analysis revealed no significant differences in the level of anti-apoptotic Bcl-2 proteins under Obatoclax treatment. Since the above mentioned study demonstrates apoptosis of lymphoma cells under Obatoclax treatment, the downregulation of anti-apoptotic Bcl-2 proteins might be a secondary event, occurring in the course of cell death. In order to analyze the effect of the inhibitor on migration, HT29 cells were kept in 3D cell culture, allowing a long-time treatment for seven days, what better resembles the patient situation. In a first step the non-lethality of applied doses was proved by immunohistochemical staining for cleaved PARP. In addition, cells were stained for Ki67 to evaluate the effect of Obatoclax on proliferation. Staining revealed an unaltered viability what is in line with the results obtained after siRNA mediated knockdown of anti-apoptotic Bcl-2 proteins. The proliferative capacity, by contrast, significantly decreased in presence of the inhibitor. An additionally performed FACS analysis discovered a G1-phase arrest in Obatoclax treated HT29 cells, which was interestingly not antagonized by overexpression of anti-apoptotic Bcl-2 proteins. This observation speaks for a Bcl-2 protein independent effect of Obatoclax on cell cycle control. The underlying mechanism might comprise the binding of Obatoclax to mTOR, which has recently been reported[244].

Even though the observed differences in proliferation potentially influence the migratory capacity, the invasion depth of HT29 cells in scaffolds was determined. Strikingly, sublethal doses of Obatoclax significantly inhibited covered distances of HT29 cells. To verify the observed migration

phenotype, an additional scratch assay with HT29 and SW480 cells was performed. The results clearly show that Obatoclax massively impairs the migratory capacity of CRC cells in a dose-dependent manner. As described for the siRNA mediated knockdown of anti-apoptotic Bcl-2 proteins, invasiveness was separately evaluated by utilization of a Boyden chamber invasion assay. Similar to the result obtained in the migration assay, invasion was remarkably inhibited by Obatoclax, again displaying dose-dependency. These findings are in line with a study published by Vogt et al.[245], delineating an inhibitory effect of Obatoclax on migration and adhesiveness of hepatoblastoma cells. In this context they show a lowered efficiency in the formation of lamellipodia, caused by a Caspase 3-mediated degradation of the Rho GTPase Cdc42 (cell division control protein 42 homolog), which is involved in the formation of focal adhesion complexes[246] and in actin polymerization[247]. Even though, they also use sub-lethal inhibitor doses, Caspase 3 seems slightly activated after Obatoclax-mediated inhibition of anti-apoptotic Bcl-2 proteins. Cdc42 has been reported to be overexpressed in a variety of human cancers, including CRC[248–250] and in the course of malignant transformation, high Cdc42 levels seem to correlate with a rather mesenchymal phenotype[251]. The process in which cells lose their apical-basal polarity and acquire a spindle-like morphology that increases motility, is termed epithelial-to-mesenchymal transition (EMT). This process plays not only a role for malignant tumor progression but also for physiological processes like organ formation during embryogenesis or tissue regeneration[252,253]. EMT can be induced by various stimuli, such as hypoxia, metabolic or mechanical stress and growth factor signal transduction, like TGF-ß (transforming growth factor beta) signaling[254]. Subsequently, transcriptional repressors like SNAIL and SLUG get upregulated, what leads to an inhibited expression of epithelial genes, including E-Cadherin. On the other hand, mesenchymal genes like N-Cadherin and the intermediate filament Vimentin get transcriptionally induced. Cadherins are key molecules in adherens junctions, mediating cellular adhesion via their extracellular domain[255]. The downregulation of E-Cadherin and the increased expression of N-Cadherin during EMT is termed as Cadherin-switch and is commonly seen as a central step in cancer cell dissemination. Besides an increased motility, EMT renders tumor cells less sensitive to senescence and cell death and increases chemoresistance, what further promotes metastasis formation[256]. Later on, circulating cancer cells seem to undergo a reverse process, called mesenchymal-to-epithelial transition (MET), what facilitates colonization and metastatic outgrowth in distant organs[257,258].

In order to investigate whether the impaired migration of HT29 and SW480 cells, observed after knockdown or inhibition of anti-apoptotic Bcl-2 proteins, is accompanied by MET, expression levels of E- and N-Cadherin have been determined. In a first approach, the basal expression levels of E- and N-Cadherin in SW480 and HT29 cells were evaluated by Western blot analysis. Even though HT29 cells do not overcome the Matrigel-coated Boyden chambers in the experimental set up, they

have been described as being tumorigenic, invasive and metastatic *in vivo*, whereas SW480 cells are tumorigenic but non-invasive[207]. In addition, CaCo2 and Colo205, two other human colorectal cancer cell lines, were used as a comparison. By contrast to SW480 and HT29 cells, these cell lines are non-tumorigenic[208]. Impressively, Western blot analysis revealed an inverse correlation between E-Cadherin expression and the tumorigenicity of the utilized cell lines. By contrast, N-Cadherin expression was only detectable in HT29 cells and lay below the detection threshold in Western blot as well as qRT-PCR analyses in all other cell lines used. To investigate, whether siRNA mediated knockdown of anti-apoptotic Bcl-2 proteins might recover E-Cadherin expression in SW480 and HT29 cells, transfection and subsequent Western blot analysis were performed. In HT29 cells, the knockdown of Mcl-1, Bcl-2 or Bcl-x_L did not lead to an increased expression above the detection threshold, whereas in SW480 cells, E-Cadherin expression was clearly increased after siRNA-mediated knockdown of Bcl-2. This is in line with the observations made in previous migration and invasion experiments, where strongest phenotypes were always observed after knockdown of Bcl-2. The findings get moreover supported by a study published by An et al.[259], showing that overexpression of Bcl-2 in human mammary epithelial cells induces decreased E-Cadherin expression. A very recent study by Choi et al.[260] showed that a certain fraction of Bcl-x_L, located in the nucleus, directly promotes EMT and cell migration of pancreatic neuroendocrine tumor cells by enhancing TGF-ß transcription. By using two Bcl-x_L mutants, displaying defective anti-apoptotic function, they elegantly show that the migratory phenotype is independent of cellular viability.

Since chemical inhibition of anti-apoptotic Bcl-2 proteins also reduced the migratory and invasive capacity of CRC cells, E-Cadherin expression levels were additionally measured under Obatoclax treatment. Except of SW480, all cell lines sowed a remarkable recovery of E-Cadherin in presence of the inhibitor. Expression levels of other markers, like the transcription factors SNAIL and SLUG or Vimentin, were inconsistent and seemed rather correlated with confluency and passage number. The high plasticity of cancer cells makes it anyway difficult to clearly assign them to a specific state. Recent studies support the existence of a hybrid phenotype, which is characterized by the concomitant expression of epithelial as well as mesenchymal markers[261,262]. Furthermore, for CRC the transient character of EMT has explicitly been shown by Brabletz et al.[263].

Since the decreased cancer cell motility and the recovery of E-Cadherin expression point to the induction of MET, chemosensitivity of CRC cells was investigated after siRNA mediated downregulation of Mcl-1, Bcl-2 or Bcl-x_L. The applied chemotherapeutic agents, Oxaliplatin, 5-Fluorouracil (5-FU) and Irinotecan, are clinically relevant and commonly used in the treatment course of colorectal cancer. Evaluation of cellular viability by a MTT assay revealed that a knockdown of Mcl-1, Bcl-2 or Bcl-x_L noticeably sensitized HT29 cells to Oxaliplatin-induced cell

death, whereas the effects of 5-FU and Irinotecan were not significantly enhanced. This discrepancy might be caused by the different mechanisms of action the applied agents show. By contrast to 5-FU and Irinotecan, Oxaliplatin causes DNA double strand breaks and since at least Mcl-1 has been shown to actively promote DNA damage repair[198], its knockdown might enhance the efficiency of Oxaliplatin.

4.3 The Role of anti-apoptotic Bcl-2 Proteins for intestinal Tissue Homeostasis and colorectal Cancer Onset and Progression in Mice

In order to get more insight into the function of anti-apoptotic Bcl-2 proteins for the maintenance of intestinal tissue homeostasis as well as for colorectal cancer development and progression, they were further studied *in vivo*.

Constitutive deletion of the anti-apoptotic proteins Bcl-2, A1 or Bcl-w leads to viable progeny. Bcl-$2^{-/-}$ mice display growth retardation and a short overall survival of only 1-2 month[163]. They show immune deficiencies because of an apoptotic involution of thymus and spleen and due to a defective melanin synthesis, they get gray fur. Finally, Bcl-$2^{-/-}$ mice succumb to polycystic kidney disease, caused by defective renal epithelial cells[164]. Previous studies on constitutive Bcl-2 knockout mouse models came to differing results regarding intestinal tissue homeostasis. Kamada et al. observed impaired proliferation, resulting in distorted villi in the small intestine[264]. Another study showed an increased amount of cell death events at the base of colonic crypts, whereas the small intestine was unaffected[165]. By contrast, two other studies did not detect any abnormalities in the intestine of Bcl-$2^{-/-}$ mice[163,164]. Very recently, van der Heijden and colleagues closely analyzed the effects of Bcl-2 deficiency on the gut and they could show that Bcl-2 is dispensable for the maintenance of intestinal tissue homeostasis and regeneration[265]. However, its loss impairs intestinal tumorigenesis, suggesting that Bcl-2 plays a role in CRC onset.

A1 and Bcl-w seem to play only subsidiary roles for development and tissue homeostasis in the intestine and in sharp contrast to Mcl-1 and Bcl-x_L, the constitutive deletion of Bcl-2, A1 and Bcl-w does not result in embryonic lethality. Mcl1$^{-/-}$ embryos die at a very early time point because they fail to implant *in utero*. Interestingly, this is not due to an increased apoptosis rate, but rather to a delayed maturation of the blastocyst, indicating additional roles of Mcl-1 beyond cell death regulation[161]. Studies on conditional Mcl-1 knockout mouse models revealed its importance for the survival of B-cells, T-cells, neutrophils and hematopoietic stem cells[266–268]. Furthermore, it has been shown to be a key regulator of apoptosis during cortical neurogenesis and that it protects neurons against DNA-damage induced cell death[269]. In the murine liver, loss of Mcl-1 renders hepatocytes more susceptible towards spontaneous as well as death-receptor triggered apoptosis[270].

Interestingly, this study showed that the decreased hepatocytic viability is accompanied by an increased proliferation rate, what nicely resembles the *in vitro* findings on human CRC cells, presented in this work. Even though no inflammatory response was detected, the increased proliferation of Mcl-1 negative hepatocytes finally culminated in hepatocarcinogenesis[271]. If the enhanced death of Mcl-1 deficient hepatocytes would trigger an immune response, tumor development as a secondary event of an inflammatory environment would be reasonable. But since this is not the case, occurring hepatocarcinogenesis suggests a cell death-independent tumor suppressor role of Mcl-1.

Constitutive deletion of Bcl-x_L also leads to fetal death *in utero*. Bcl-$x_L^{-/-}$ embryos survive until day 13.5 of embryogenesis and die from cell death-related defects in hematopoiesis and neuronal development[162]. In adult mice, transduction of a Bcl-x_L fusion protein into neurons significantly decreased cerebral infarction upon focal ischemia[272]. In contrast to Mcl-1, studies on conditional Bcl-x_L knockout mouse models revealed a rather classic function of this protein, preventing cell death induction in various tissues[273,274].

However, no intestine-specific knockout mouse models were available for Mcl-1 and Bcl-x_L until now. In order to shed light on their role in physiology and pathophysiology of the murine intestine, Mcl-1 and Bcl-x_L were deleted in a spatially controlled manner, by utilizing the Cre/loxP system. To reach intestine-specificity, the Cre recombinase was expressed under control of the Villin promotor in these mice. Because the expression of Cre in the gastrointestinal tract of mice has been shown to induce gastric epithelial atrophy and metaplasia in the absence of floxed alleles[202], Villin-Cre mice were chosen as control group for all experiments.

4.3.1 The intestine-specific Bcl-x_L knockout Mouse

As described for Bcl-2, Bcl-x_L seems dispensable for intestinal development and homeostasis. Furthermore, crossbreeding of heterozygously floxed mice led to offspring with an expected distribution of genotypes. The fact that Bcl-$x_L^{\Delta IEC}$ mice were born in the expected mendelian ratio suggests that the intestine-specific knockout had no impact on embryogenesis. With regard to body size, weight and overall survival, Bcl-$x_L^{\Delta IEC}$ mice are indistinguishable from their control littermates, indicating a normal functioning of the intestine in terms of food digestion and nutritional uptake. Morphometric analysis of small intestinal and colonic tissue showed no alterations in crypt architecture or composition. Since the loss of an anti-apoptotic protein might lead to spontaneous cell death induction, a TUNEL assay was performed. Compared to the DNAse treated positive control, neither Cre control nor Bcl-$x_L^{\Delta IEC}$ animals showed a noteworthy amount of TUNEL positive cells in their colon mucosa. Besides its anti-apoptotic function, Bcl-x_L has been shown to inhibit cell

cycle progression by delaying G0-G1 transition[214]. Furthermore, overexpression of Bcl-x_L seems to stabilize a G2-M-phase arrest in cells affected by DNA damage[220]. Therefore, proliferation levels in the intestinal mucosa of control and Bcl-$x_L^{\Delta IEC}$ mice were evaluated by immunohistochemical staining of Ki67. The staining revealed equal amounts of proliferating cells which are located at the crypt base. This nicely resembles the presented *in vitro* data, where the knockdown of Bcl-x_L in human CRC cell lines did not alter their proliferative capacity. The discrepancy between the presented data and the mentioned studies might be caused by differences in the experimental set up. While the cited studies evaluated the influence Bcl-x_L has on cell cycle control after either DNA damage or serum deprivation, the presented work focusses on its basal influence on the proliferative capacity of unchallenged cells.

Autophagy as another cellular mechanism in which Bcl-x_L is involved, gains more and more attention in the context of inflammatory bowel disease. For instance, a genome-wide association study, reported a correlation between Crohn´s Disease and a single nucleotide polymorphism in the Atg16L1 gene as a key player in the autophagic machinery[275]. Due to their secretory function, Paneth cells are especially dependent on autophagy as mechanism for vesicle formation. But Hematoxylin and Eosin staining and immunohistochemical staining against Lysozyme revealed normal abundance of Goblet as well as Paneth cells as the main secretory cells lines in the intestine. Since the analysis of the tissue microarray showed that Bcl-x_L is significantly upregulated in human colorectal adenocarcinomas, it was reasonable to conclude that Bcl-x_L could have a function for intestinal tumor development or progression and that Bcl-$x_L^{\Delta IEC}$ mice might be more resistant to experimentally induced tumorigenesis. In order to trigger intestinal tumor formation, the AOM/DSS model was applied[276]. The mutagenic agent azoxymethan (AOM) initiates cancer development by alkylation of DNA, what promotes base mispairing[277]. After intraperitoneal injection, AOM first needs to get activated in the liver. The complete activation mechanism remains elusive, but Cytochrome P450 2E1-mediated hydroxylation seems to be a crucial step[278]. Subsequently, the derivate methylazoxymethanol reaches the intestine via the bile, where it gets further transformed to methyldiazonium by the colonic flora. A study on germ-free rats suggests that this secondary metabolization step significantly enhances the colonotropic mutagenicity of AOM[279]. Since Bcl-$x_L^{\Delta IEC}$ mice have a C57BL/6 genetic background, they were expected to show only moderate susceptibility towards AOM induced carcinogenesis[280]. Hence, carcinogenesis was promoted by three cycles of the pro-inflammatory reagent dextran sodium sulfate (DSS) in the drinking water[281]. Thus, the AOM/DSS model resembles inflammation-driven tumorigenesis as seen in patients suffering from inflammatory bowel disease. Molecular analysis furthermore revealed that AOM-induced tumors display mutational patterns, such as alterations in the Wnt-signaling pathway or mutation of K-ras, which are also frequently observed in human CRC[282–284]. In the study of Suzuki and co-workers[280],

the combination of AOM and DSS resulted in an adenocarcinoma incidence of 50% in C57BL/6 mice. Therefore, it is a feasible model because it provides the opportunity to study the effect of a genetic knockout on tumor formation in both directions.

Results obtained in the AOM/DSS experiment clearly showed that the lack of Bcl-x_L in intestinal epithelial cells renders mice less susceptible towards chemically induced carcinogenesis. The fact that Bcl-$x_L^{\Delta IEC}$ mice carried less tumors which additionally exhibited smaller diameters suggests that Bcl-x_L plays a role in CRC onset and progression[276]. For the analysis, several possibilities how Bcl-x_L potentially influences tumorigenesis have been considered. First, cell death levels in tumors derived from control and Bcl-$x_L^{\Delta IEC}$ animals were evaluated. The discovery of significantly increased apoptosis levels in tumors derived from Bcl-$x_L^{\Delta IEC}$ mice, identified Bcl-x_L as a key player for cell death prevention in CRC cells, whose loss cannot be compensated by kin anti-apoptotic proteins. This is in line with a publication showing that in large B-cell lymphoma, low levels of Bcl-x_L are also associated with enhanced apoptosis[285]. Further immunoblotting was done in order to characterize the subtype of cell death in tumors of Bcl-$x_L^{\Delta IEC}$ mice. Since Bcl-x_L prevents permeabilization of the outer mitochondrial membrane, Caspase 9 cleavage is in line with the reported function of the protein[77]. Activation of Caspase 8, as initiator Caspase of the extrinsic apoptotic pathway, could be caused by an additional extracellular stimulus, such as lymphocytes, triggering cell death. But immunohistochemical staining of B- and T-cells showed no differences in lymphocyte infiltration. An additionally performed qRT-PCR analysis furthermore detected unaltered mRNA levels of the pan-leukocyte marker CD45. Since Bcl-x_L has been described to play a role in cell cycle control after DNA damage, an altered proliferative capacity of intestinal epithelial cells could also be responsible for differences in tumor progression[220]. Hence, proliferation was investigated by immunohistochemical staining against Ki67 and by qRT-PCR analysis of PCNA expression levels. Obtained results concordantly showed unaltered proliferation rates in tumors derived from control and Bcl-$x_L^{\Delta IEC}$ mice. Taken together, the data conclusively show that the lower tumor burden found in AOM/DSS treated Bcl-$x_L^{\Delta IEC}$ mice is not caused by differences in the immune response or in proliferation, but solely relays on an enhancement of canonical intrinsic apoptosis as responsible mechanism.

During the course of treatment, Bcl-$x_L^{\Delta IEC}$ mice showed a better health status mirrored by less severe diarrhea and less pronounced weight loss during DSS cycles. In order to evaluate the inflammatory events occurring during a DSS cycle, T-cell infiltration was additionally evaluated in mice treated with DSS only. Immunohistochemical staining against CD3 revealed higher amounts T-cells in colon tissue derived from Bcl-$x_L^{\Delta IEC}$ mice. This finding may point to an accelerated apoptosis initiation under unfavorable conditions in Bcl-$x_L^{\Delta IEC}$ mice. A fast but controlled immune response could thereby prevent chaotic cellular destruction. Following this hypothesis, the better health status of

Bcl-$x_L^{\Delta IEC}$ mice in terms of diarrhea severity, weight loss and recovery time during the treatment course, would be due to a swift and immediately executed apoptosis of Bcl-x_L negative IECs, caused by a lowered cell death threshold that prevents greater tissue damage and subsequent mucosal inflammation. Since lately, there is growing evidence that apoptotic cells can have a beneficial effect on tissue recovery[286,287].

4.3.2 The intestine-specific Mcl-1 knockout Mouse

By contrast to Bcl-2 and Bcl-x_L, Mcl-1 plays a crucial role for the maintenance of intestinal tissue homeostasis but not for development. If crossbred in a heterozygous manner, Mcl-$1^{\Delta IEC}$ mice are born in the expected mendelian ratio. The minor discrepancy between estimated (18,75%) and effectively born (15,8%) mice that show homozygosity with regard to their flox status in addition to Cre positivity (flox/flox Cre^+), suggests an unaltered prenatal lethality. Interestingly, male mice carrying two floxed Mcl-1 alleles are infertile already in absence of the Cre-recombinase. The reason therefor was found by Okamoto and colleagues who showed that Mcl-1^{FLOX} mice are essentially normal with regard to organ development, composition of the hematopoietic compartment and tissue homeostasis[288]. Spermatogenesis, by contrast, is abrogated due to a severe atrophy of testis. Closer analysis revealed that the integrated loxP sites in these mice slightly altered transcription, what leads to the expression of a Mcl-1 protein which displays 13 additional amino acids at the N-terminus. The emerging protein fully retains its anti-apoptotic function but it shows delayed turnover. After the first wave of spermatogenesis, apoptosis is required for the clearance of excess germ cells. Hence, Okamoto et al. hypothesize that the delayed degradation of Mcl-1 renders germ cells less susceptible towards cell death induction, what leads to a damage of the supporting Sertoli cells and finally abrogates adult spermatogenesis.

Another phenomenon became manifested after crossbreeding of the Mcl-1^{FLOX} and the Villin-Cre parental strains. First immunohistochemical analysis revealed that most Mcl-$1^{\Delta IEC}$ mice displayed a patchy Mcl-1 expression pattern in their intestines. Unexpectedly, only 15% of Mcl-$1^{\Delta IEC}$ animals showed a complete loss of the protein in the entire intestine. Since none of the parental strains led to an incomplete knockout if crossbred with other mouse lines, the underlying mechanism remains elusive. In Bcl-$x_L^{\Delta IEC}$ mice, which also express the Cre-recombinase under control of the Villin promotor, no Bcl-x_L positive IEC has ever been detected[289]. On the other hand, crossbreeding of Mcl-1^{FLOX} mice with a strain that expresses the Cre-recombinase under control of the Albumin promoter (Alb-Cre) leads to offspring with a complete loss of the protein in all hepatocytes[271]. One fairly reasonable explanation is offered by a study by Voojis et al., showing that differences in the chromatin state can influence the accessibility of loxP sites what in turn affects recombination

efficiency[290]. Since there is a high plasticity among cell types regarding the chromatin state[291], this could cause differences in the recombination efficiency of Mcl-1 in liver and intestine.

Further analysis showed that Mcl-$1^{\Delta IEC}$ mice with a complete loss of Mcl-1 in the intestine are exceptionally small and lightweight and normally die within the first six months. By contrast, if Mcl-$1^{\Delta IEC}$ mice display a patchy expression of Mcl-1, the overall survival is comparable to the one of their control littermates. This means that the incomplete knockout provides the opportunity to study protein function also in late adulthood. Morphometric analyses of Hematoxylin and Eosin stained colonic crypt sections revealed a markedly altered crypt architecture, with regard to crypt diameter and number, in Mcl-1 negative areas. Furthermore, the staining showed intestinal epithelial cells undergoing cell death, what was additionally verified by a TUNEL assay. Notably, an inverse correlation between the number of TUNEL-positive cells and the remaining level of Mcl-1 was found. Hence, Mcl-1 seems crucial for the survival of IECs, what is in sharp contrast to Bcl-2 and Bcl-x_L which are dispensable for intestinal tissue homeostasis. Since Mcl-1 has classically been described to maintain the integrity of the outer mitochondrial membrane, elevated levels of cleaved PARP, found in the intestinal mucosa of Mcl-$1^{\Delta IEC}$ mice, are plausible. Instead, the observation of a strong activation of Caspase 8, as initiator Caspase of the extrinsic pathway, and a relatively low amount of cleaved Caspase 9, as initiator Caspase of the intrinsic pathway, was rather unexpected. It is known that Caspase 9 can also get activated by a conformational change, but normally apoptosis is accompanied by autocatalytic cleavage of Caspase 9 and also by its effector Caspase-mediated proteolysis[90]. Levels of truncated Bid (tBid), as an interconnecting element between the extrinsic and the intrinsic pathway, were also notably increased in Mcl-$1^{\Delta IEC}$ mice. The fact that Bcl-2 and Bcl-x_L were found to be downregulated in Mcl-1 negative areas is most likely caused by the Caspase-dependent cleavage of anti-apoptotic proteins, which has been shown to enhance the apoptotic signaling in dying cells[292,293]. By contrast to Bcl-2 and Bcl-x_L, the pro-apoptotic family members Bax and Bak are not known as a substrate for activated Caspases. Accordingly, no correlation was found between their expression and the abundance of Mcl-1.

Since Mcl-1 does not only play a role for maintaining the integrity of the outer mitochondrial membrane, but also influences autophagy and mitochondrial respiration[294], other cell death forms besides apoptosis could additionally contribute to the phenotype observed in Mcl-$1^{\Delta IEC}$ mice. Mcl-1 deficient cardiomyocytes, for instance, exhibit mitochondrial dysfunction, culminating in a rather necrotic cell death[295,296]. Moreover, it has been shown, that the pan-Bcl-2 inhibitor Obatoclax induces autophagy, whereby the assembly of the necrosome gets promoted on autophagosomal membranes, leading to enhanced necroptosis rates[297]. Since the phosphorylation of MLKL is a necroptosis specific event, total MLKL and phospho-MLKL (pMLKL) levels were determined. Thereby, no correlation between the pMLKL level and the remaining Mcl-1 or the body weight was

detectable. These findings argue for necroptosis being a secondary event, which might be induced by concomitant inflammatory processes. The tight correlation between Mcl-1 levels and the abundance of indicators for apoptosis, such as cleaved PARP and cleaved Caspase levels, rather point to apoptosis as key mechanism being responsible for increased cell death rates in Mcl-1$^{\Delta IEC}$ mice. In addition, expression levels of RIP1, as a central molecular switch between extrinsic apoptosis and necroptosis, have been determined by immunohistochemical staining. The results clearly show that RIP1 is almost absent in Mcl-1 negative tissue sections. Since activated Caspase 8 negatively regulates necroptosis by cleaving RIP1[298], the observed phenotype also points to apoptosis as responsible mechanism for cell death execution.

Several studies accordingly show that mice with increased levels of apoptosis in the intestinal epithelium more likely develop an enteritis or colitis[299,300]. Due to a loosening of tight junctions, the epithelial barrier is not proficient anymore to prevent invasion of luminal microbes. In Mcl-1$^{\Delta IEC}$ mice, the intrusion of pathobionts gets even more facilitated by the loss of Goblet and Paneth cells. Goblet cells secret large glycoproteins, named mucins, which together build a mucus layer that protects the epithelium from mechanical or chemical harm caused by undigested food particles or microbes. Furthermore, it impedes the attachment of pathobionds to the enterocytes and their invasion through the epithelial layer[301]. Paneth cells secrete large amounts of antimicrobial peptides, such as α-defensins and Lysozyme in response to certain bacteria[302]. Since the bactericidal activity of α-defensins predominantly affects non-commensal bacteria, they have been shown to balance the composition of the intestinal microbiota[303,304]. As a result of the enhanced apoptosis of IECs and the loss of secretory cell lines, Mcl-1$^{\Delta IEC}$ mice develop a severe intestinal inflammation. Immunohistochemical staining identified the majority of infiltrating cells as being CD68 positive macrophages, what fits to the high levels of TNF, found in Mcl-1 negative areas. If the innate immune system gets overactivated, a previously local inflammation can get a systemic immune reaction. In line with this, splenomegaly, as an indicator for systemic inflammation, was observed in some Mcl-1$^{\Delta IEC}$ mice[305].

The fact that the fraction of Mcl-1$^{\Delta IEC}$ mice which shows a complete loss of the protein in the entire intestine survives at all under these circumstances, points to an increased renewal of the epithelial lining, what could at least partly compensate high cell death rates. Indeed, an inverse correlation between the abundance of Mcl-1 and the amount of proliferating cells was found. Both immunohistochemical staining of Ki67 as well as determination of PCNA expression levels by qRT-PCR analysis concordantly showed enhanced proliferation in Mcl-1 negative areas. Furthermore, the mRNA abundance of Cyclin D1, which is an important driver of the G1/S-phase transition, shows the same trend, whereas mRNA abundance of the cell cycle inhibitor p21 showed a positive correlation with the Mcl-1 expression. The increased proliferation is in line with the observations

made *in vitro* after siRNA mediated silencing of Mcl-1. Furthermore, it resembles the phenotype found by Vick and colleagues in the liver-specific Mcl-1 knockout mouse where increased levels of apoptotic hepatocytes were also accompanied by compensatory proliferation[270]. At this point the question rose, whether the observed increase of proliferation is a mere counter-regulatory event, caused by high cell death rates, or if the loss of Mcl-1 independently influences cell cycle progression. On the one hand, apoptotic cells have been shown to promote tissue regeneration by triggering proliferation of neighboring cells[286]. In this context, a study by Li et al. found that unstressed stem cells are stimulated to divide in presence of mouse embryonic fibroblast (MEFs) that have been exposed to high levels of irradiation[306]. On the other hand, the presented *in vitro* results show that human CRC cells displayed increased proliferation after silencing of Mcl-1 but no decline of viability, what argues for an, at least partially, cell death-independent role of Mcl-1 for proliferation. This hypothesis gets further supported by studies revealing an inhibitory effect of Mcl-1 on cell cycle progression via binding of PCNA[196] and CDK1[197]. Another option would be an influence of Mcl-1 on cellular differentiation as it has already been shown for keratinocytes[307]. If Mcl-1 negative intestinal epithelial stem cells would show delayed differentiation this could also cause an expanded stem cell compartment with an increased number of proliferating cells. In order to solve this question, an immunohistochemical double-staining of Ki67 and Lgr5, as a marker for intestinal stem cells, would be the best approach. Unfortunately, there is no Lgr5 antibody available which would be suitable for the IHC staining of murine tissue. Hence, Lgr5 protein levels were determined by Western blot analysis. Thereby, no differences were found between control and Mcl-1$^{\Delta IEC}$ mice, arguing for an unaltered amount of stem cells. As an alternative to an immunohistochemical staining, a fluorescent *in situ* hybridization (FISH) could be done to exactly identify and localize Lgr5 positive cells within the crypt. This is prospectively planned in order to validate the finding gained by Western blot analysis.

However, from an age of six months about half of the Mcl-1$^{\Delta IEC}$ animals spontaneously start do develop intestinal adenocarcinomas which are primarily located in the small intestine. This is most probably the result of the enhanced proliferation in addition to the inflammatory environment, what further promotes tumorigenesis. The reason why the tumors more frequently occur in the small intestine could not be finally clarified. Mcl-1 is expressed in the small intestine and the colon as well and both sections are demonstrably affected by enhanced proliferation and inflammation.

What differs is that Paneth cells, which are lost in Mcl-1 negative areas, are important for the homeostasis of the small intestine but not for the colon. This might not be the decisive mechanism but it could further promote tumor formation and it would fit to the observation that neoplastic lesions are more frequently but not exclusively found in the small intestine. Interestingly, immunohistochemical staining revealed that the tumor tissue is always Mcl-1 negative, even

though tumor carrying animals showed a patchy expression. This argues for Mcl-1 having a decisive tumor suppressing function, that goes beyond its role in the prevention of inflammatory processes in the gut. This hypothesis gets further supported by the observed downregulation of Mcl-1 in human adenomas and adenocarcinomas. A Ki67 staining showed that the emerged neoplasias are highly proliferative. At the same time, there is a noteworthy level of apoptotic cells in the tumors, as determined by staining against cleaved PARP. Furthermore, tumor tissue displayed high levels of infiltrating macrophages as it was already detected in Mcl-1 negative mucosa. In order to dissect, whether tumor formation is a secondary, inflammation-based event or whether the loss of Mcl-1 directly promotes malignant transformation, Mcl-1$^{\Delta IEC}$ mice were housed in a germ-free surrounding. This was done by our cooperation partners, the group of Prof. Dr. med. Achim Weber in Zurich. The germ-free housing led to an impressive decrease of inflammation but lowered tumor incidence only marginally (manuscript in preparation). This finding further supports the hypothesis that Mcl-1 directly suppresses tumor formation in the intestine. One possible mechanism how Mcl-1 could exert a tumor suppressing function is its role in DNA repair. In response to DNA damage, it translocates into the nucleus and associates with the chromatin in order to maintain cell cycle arrest in the G2-phase, giving the cell time to repair damaged DNA[198,308]. Thus, the loss of Mcl-1 causes a premature cell cycle reentry and accordingly genomic instability. Based on this assumption, the microsatellite stability in Mcl-1 negative tumors was assessed by Sanger sequencing. Analyses showed, that all tested markers presented with identical profiles in all samples, suggesting that microsatellite instability, which is commonly observed in DNA mismatch repair-deficient tumor cells, is absent or at least a rare event in Mcl-1-negative tumors. Nevertheless, an impaired DNA damage repair still seems plausible as responsible mechanism for the tumor formation in Mcl-1$^{\Delta IEC}$ mice. Since Mcl-1 has been found to associate with gamma-H2AX and NBS1 (Nijmegen breakage syndrome)[198], it plays most probably a role in homologous recombination[309].

4.4 Clinical Relevance of the chemical Inhibition of anti-apoptotic Bcl-2 Proteins

The overexpression of anti-apoptotic Bcl-2 proteins in a variety of tumor entities and the thereby increased chemo-resistance has manifoldly been described[310–313]. Hence, great effort has already been done to develop specific inhibitors targeting this protein family. A very promising approach is the utilization of BH3 mimetics, which bind to the hydrophobic groove of anti-apoptotic Bcl-2 proteins to inhibit their cell death-preventing function. A variety of BH3 mimetics, such as the pan-Bcl-2 inhibitor Obatoclax, already entered clinical trials[242]. Unfortunately, Obatoclax shows off-target effects like the induction of an endoplasmic reticulum stress response and dose escalation is limited by neurologic toxicity[314,315]. For the Bcl-2/Bcl-x$_L$/Bcl-w specific compound ABT-737 and its

orally available derivate ABT-263 (Navitoclax), promising data for different entities were reported in phase I/II clinical trials[316–318]. Because Bcl-2 has been shown to be exceptionally important for cancer cell survival in CLL (chronic lymphocytic leukemia), the Bcl-2 specific inhibitor ABT-199 (Venetoclax) has been developed and recently approved by the FDA (Food and Drug Administration) for treatment of a CLL subtype[319]. This shows, that development and testing of inhibitors against anti-apoptotic Bcl-2 proteins are clinically relevant. Whether and to which extend ABT-199 could be beneficial for the treatment of colorectal cancer is not known so far.

In order to evaluate the effect of anti-apoptotic Bcl-2 protein inhibition in human CRC, fresh tumor tissue was cultured in presence of a BH3 mimetic. The fact that the pan-Bcl-2 inhibitor Obatoclax was capable of sensitizing HT29 cells to platin-based chemotherapy already suggests a possibly beneficial effect for colorectal cancer patients. If considered that Mcl-1 is downregulated in human adenomas and adenocarcinomas and that its loss causes a massive inflammatory phenotype in the intestine of Mcl-$1^{\Delta IEC}$ mice, Mcl-1 seems an uneligible target for chemical inhibition in the context of CRC treatment. Bcl-x_L, by contrast, gets significantly upregulated in human adenocarcinomas and its loss renders Bcl-$x_L^{\Delta IEC}$ mice less vulnerable towards chemically induced carcinogenesis. Hence, the Mcl-1 sparing inhibitor ABT-737 was chosen for evaluating the value of anti-apoptotic protein inhibition in a translational approach. In a pre-experiment with HT29 cells the compound already induced a remarkable decrease of cell viability. In order to investigate whether the increased cell death induces alterations in the proliferation rate, scaffold sections were stained for Ki67. In line with the data obtained after siRNA mediated knockdown of Bcl-x_L in CRC cells and with the observations made in Bcl-$x_L^{\Delta IEC}$ mice, no changes in the proliferative capacity of HT29 cells were detected under ABT-737 treatment. Since these preliminary data seemed very promising, ABT-737 was subsequently tested in an *ex vivo* system, in which vital human CRC specimens were treated with the compound. Immunohistochemical staining for cleaved PARP as well as analysis of ATP levels concordantly revealed a significant decrease of viability in ABT-737 treated samples. Results from a Ki67 staining were in line with the findings obtained in Bcl-$x_L^{\Delta IEC}$ mice and the *in vitro* experiments, showing no significant changes in the proliferative capacity of CRC tissue in presence of the inhibitor.

Taken together, the presented data show that human CRC cells are highly dependent on the expression of Bcl-x_L for their survival and that the selective inhibition of Bcl-x_L/Bcl-2 seems already sufficient to decrease cellular viability even in absence of an additional chemotherapeutic agent.

4.5 Conclusion

Taken together, the performed *in vitro* experiments show that anti-apoptotic Bcl-2 proteins are dysregulated in human CRC and that they influence tumor-relevant processes beyond cell death regulation. Mcl-1, which gets downregulated in the course of malignant transformation, seems the only one among the group of anti-apoptotic Bcl-2 proteins that plays an anti-proliferative role in CRC cells. Its loss might be beneficial for transforming cells even if this happens on the expense of cell death prevention. Furthermore, all anti-apoptotic Bcl-2 proteins have been shown to promote the migratory ability and invasiveness of CRC cells with the strongest phenotypes observed for Bcl-2. Their siRNA mediated silencing or chemical inhibition not only reduced cancer cell motility but also enhanced the sensitivity towards chemotherapeutic treatment with Oxaliplatin.

The generated intestine-specific knockout mouse models revealed a strong discrepancy between Bcl-x_L and Mcl-1 with regard to their role for the maintenance of intestinal tissue homeostasis and for colorectal cancer development and progression. Bcl-x_L, which seems dispensable for normal tissue homeostasis, was found to be a crucial factor for colorectal cancer cell survival, what confers a tumor-promoting property and explains the overexpression of Bcl-x_L in human adenomas and adenocarcinomas. The loss of Mcl-1, by contrast, causes a severe intestinal phenotype, including high levels of apoptotic IECs and massive inflammation. The spontaneous tumorigenesis in Mcl-$1^{\Delta IEC}$ mice is promoted by the loss of the anti-proliferative effect Mcl-1 exerts on IECs and by the inflammatory environment, what confers Mcl-1 tumor-suppressing properties and explains its downregulation in human adenomas and adenocarcinomas. For clinical application, it is thus highly recommended to utilize Mcl-1 sparing inhibitors. In the presented work, a first step in this direction was done by treating human CRC tissue *ex vivo* with the Bcl-x_L/Bcl-2 specific BH3 mimetic ABT-737. The results are promising and show a markedly decreased viability of tumor cells even in absence of an additional chemotherapeutic agent.

4.6 Outlook

The results presented in this work clearly show, that Mcl-1, but not Bcl-x_L, plays a crucial role for intestinal tissue homeostasis. The high levels of apoptotic cells, found in Mcl-1 negative areas, and the absence of a cell death phenotype in Bcl-$x_L^{\Delta IEC}$ mice indicate that Mcl-1 is the central anti-apoptotic protein in intestinal epithelial cells. Surprisingly, a strong activation of Caspase 8, as initiator caspase of the extrinsic apoptotic pathway, was determined in the mucosa of Mcl-$1^{\Delta IEC}$ mice. Since Mcl-1 has classically been described to maintain the integrity of the outer mitochondrial membrane and thereby the initiation of the intrinsic pathway, this finding, together with the low

levels of cleaved Caspase 9, were counterintuitive. In order to validate the mentioned observations, an additional caspase activity assay should be performed. Furthermore, the biological relevance of Caspase 8 activation will be evaluated in an intestine-specific Mcl-1/Caspase 8 double-knockout mouse model. The respective Caspase 8^{FLOX} strain was already obtained and the breeding has been started.

Besides increased cell death levels, high proliferation rates have been observed in the intestinal mucosa of Mcl-$1^{\Delta IEC}$ mice. This was in line with the results obtained *in vitro* after siRNA mediated downregulation of Mcl-1 in human colorectal cancer cells. However, it remains elusive whether the loss of Mcl-1 exerts a pro-proliferative effect on differentiated IECs or if its knockout impairs proper stem cells differentiation, what would lead to an enlarged stem cell compartment. To answer this question, a co-staining of Ki67 and Lgr5, as marker for intestinal stem cells, would be a good approach. But since unfortunately no suitable antibody against Lgr5 is available for immunohistochemical staining of murine tissue, an *in situ* hybridization should be done. If the loss of Mcl-1 indeed impedes differentiation, as it has been shown for keratinocytes[307], this would also be a possible reason for the spontaneous and inflammation-independent tumor formation in Mcl-$1^{\Delta IEC}$ mice. Certainly, the exact mechanism of malignant transformation of Mcl-1 negative IECs needs further attention.

In the context of CRC treatment, it would be worth to follow the approach of chemical Bcl-x_L inhibition *in vivo*. Therefor, tumor formation in control and inhibitor treated wild type mice could be induced by using the AOM/DSS model. Subsequently, tumor number and sizes would be compared to identify the influence the inhibitor has on CRC onset and progression.

1 Heath JP. Epithelial cell migration in the intestine. *Cell Biol Int* 1996; **20**: 139–146.

2 Darwich AS, Aslam U, Ashcroft DM, Rostami-Hodjegan A. Meta-analysis of the turnover of intestinal epithelia in preclinical animal species and humans. *Drug Metab Dispos Biol Fate Chem* 2014; **42**: 2016–2022.

3 Leblond CP, Walker BE. Renewal of cell populations. *Physiol Rev* 1956; **36**: 255–276.

4 Hall PA, Coates PJ, Ansari B, Hopwood D. Regulation of cell number in the mammalian gastrointestinal tract: the importance of apoptosis. *J Cell Sci* 1994; **107 (Pt 12)**: 3569–3577.

5 Gerbe F, Legraverend C, Jay P. The intestinal epithelium tuft cells: specification and function. *Cell Mol Life Sci CMLS* 2012; **69**: 2907–2917.

6 Ireland H, Houghton C, Howard L, Winton DJ. Cellular inheritance of a Cre-activated reporter gene to determine Paneth cell longevity in the murine small intestine. *Dev Dyn Off Publ Am Assoc Anat* 2005; **233**: 1332–1336.

7 Sato T, van Es JH, Snippert HJ, Stange DE, Vries RG, van den Born M *et al.* Paneth cells constitute the niche for Lgr5 stem cells in intestinal crypts. *Nature* 2011; **469**: 415–418.

8 Schweizer L, Varmus H. Wnt/Wingless signaling through beta-catenin requires the function of both LRP/Arrow and frizzled classes of receptors. *BMC Cell Biol* 2003; **4**: 4.

9 de Lau W, Barker N, Low TY, Koo B-K, Li VSW, Teunissen H *et al.* Lgr5 homologues associate with Wnt receptors and mediate R-spondin signalling. *Nature* 2011; **476**: 293–297.

10 Carmon KS, Gong X, Lin Q, Thomas A, Liu Q. R-spondins function as ligands of the orphan receptors LGR4 and LGR5 to regulate Wnt/beta-catenin signaling. *Proc Natl Acad Sci U S A* 2011; **108**: 11452–11457.

11 Barker N, van Es JH, Kuipers J, Kujala P, van den Born M, Cozijnsen M *et al.* Identification of stem cells in small intestine and colon by marker gene Lgr5. *Nature* 2007; **449**: 1003–1007.

12 van Es JH, van Gijn ME, Riccio O, van den Born M, Vooijs M, Begthel H *et al.* Notch/gamma-secretase inhibition turns proliferative cells in intestinal crypts and adenomas into goblet cells. *Nature* 2005; **435**: 959–963.

13 van Es JH, Sato T, van de Wetering M, Lyubimova A, Nee ANY, Gregorieff A *et al.* Dll1+ secretory progenitor cells revert to stem cells upon crypt damage. *Nat Cell Biol* 2012; **14**: 1099–1104.

14 Wong VWY, Stange DE, Page ME, Buczacki S, Wabik A, Itami S *et al.* Lrig1 controls intestinal stem-cell homeostasis by negative regulation of ErbB signalling. *Nat Cell Biol* 2012; **14**: 401–408.

15 Haramis A-PG, Begthel H, van den Born M, van Es J, Jonkheer S, Offerhaus GJA *et al.* De novo crypt formation and juvenile polyposis on BMP inhibition in mouse intestine. *Science* 2004; **303**: 1684–1686.

16 Rothenberg ME, Nusse Y, Kalisky T, Lee JJ, Dalerba P, Scheeren F *et al.* Identification of a cKit(+) colonic crypt base secretory cell that supports Lgr5(+) stem cells in mice. *Gastroenterology* 2012; **142**: 1195–1205.e6.

17 Torre LA, Bray F, Siegel RL, Ferlay J, Lortet-Tieulent J, Jemal A. Global cancer statistics, 2012. *CA Cancer J Clin* 2015; **65**: 87–108.

18 Center MM, Jemal A, Ward E. International trends in colorectal cancer incidence rates. *Cancer Epidemiol Biomark Prev Publ Am Assoc Cancer Res Cosponsored Am Soc Prev Oncol* 2009; **18**: 1688–1694.

19 DeSantis CE, Lin CC, Mariotto AB, Siegel RL, Stein KD, Kramer JL *et al.* Cancer treatment and survivorship statistics, 2014. *CA Cancer J Clin* 2014; **64**: 252–271.

20 Jiang Y, Ben Q, Shen H, Lu W, Zhang Y, Zhu J. Diabetes mellitus and incidence and mortality of colorectal cancer: a systematic review and meta-analysis of cohort studies. *Eur J Epidemiol* 2011; **26**: 863–876.

21 Jess T, Rungoe C, Peyrin-Biroulet L. Risk of colorectal cancer in patients with ulcerative colitis: a meta-analysis of population-based cohort studies. *Clin Gastroenterol Hepatol Off Clin Pract J Am Gastroenterol Assoc* 2012; **10**: 639–645.

22 Theodoratou E, Montazeri Z, Hawken S, Allum GC, Gong J, Tait V *et al.* Systematic meta-analyses and field synopsis of genetic association studies in colorectal cancer. *J Natl Cancer Inst* 2012; **104**: 1433–1457.

23 Kohler BA, Ward E, McCarthy BJ, Schymura MJ, Ries LAG, Eheman C *et al.* Annual report to the nation on the status of cancer, 1975-2007, featuring tumors of the brain and other nervous system. *J Natl Cancer Inst* 2011; **103**: 714–736.

24 Bosetti C, Levi F, Rosato V, Bertuccio P, Lucchini F, Negri E *et al.* Recent trends in colorectal cancer mortality in Europe. *Int J Cancer* 2011; **129**: 180–191.

25 Siegel R, DeSantis C, Virgo K, Stein K, Mariotto A, Smith T *et al.* Cancer treatment and survivorship statistics, 2012. *CA Cancer J Clin* 2012; **62**: 220–241.

26 Brenner H, Kloor M, Pox CP. Colorectal cancer. *Lancet Lond Engl* 2014; **383**: 1490–1502.

27 Darmkrebs: Früherkennung, Diagnose, Therapie, Nachsorge. https://www.krebsinformationsdienst.de/tumorarten/darmkrebs/index.php (accessed 4 Oct2016).

28 Gill S, Loprinzi CL, Sargent DJ, Thomé SD, Alberts SR, Haller DG *et al.* Pooled analysis of fluorouracil-based adjuvant therapy for stage II and III colon cancer: who benefits and by how much? *J Clin Oncol Off J Am Soc Clin Oncol* 2004; **22**: 1797–1806.

29 André T, Boni C, Navarro M, Tabernero J, Hickish T, Topham C *et al.* Improved overall survival with oxaliplatin, fluorouracil, and leucovorin as adjuvant treatment in stage II or III colon cancer in the MOSAIC trial. *J Clin Oncol Off J Am Soc Clin Oncol* 2009; **27**: 3109–3116.

30 Douillard JY, Cunningham D, Roth AD, Navarro M, James RD, Karasek P *et al.* Irinotecan combined with fluorouracil compared with fluorouracil alone as first-line treatment for metastatic colorectal cancer: a multicentre randomised trial. *Lancet Lond Engl* 2000; **355**: 1041–1047.

31 Nyati MK, Morgan MA, Feng FY, Lawrence TS. Integration of EGFR inhibitors with radiochemotherapy. *Nat Rev Cancer* 2006; **6**: 876–885.

32 Kinzler KW, Vogelstein B. Lessons from hereditary colorectal cancer. *Cell* 1996; **87**: 159–170.

33 Rubinfeld B, Souza B, Albert I, Müller O, Chamberlain SH, Masiarz FR *et al.* Association of the APC gene product with beta-catenin. *Science* 1993; **262**: 1731–1734.

34 Andreyev HJ, Norman AR, Cunningham D, Oates JR, Clarke PA. Kirsten ras mutations in patients with colorectal cancer: the multicenter 'RASCAL' study. *J Natl Cancer Inst* 1998; **90**: 675–684.

35 Armaghany T, Wilson JD, Chu Q, Mills G. Genetic alterations in colorectal cancer. *Gastrointest Cancer Res GCR* 2012; **5**: 19–27.

36 Roelen BAJ, Cohen OS, Raychowdhury MK, Chadee DN, Zhang Y, Kyriakis JM *et al.* Phosphorylation of threonine 276 in Smad4 is involved in transforming growth factor-beta-induced nuclear accumulation. *Am J Physiol Cell Physiol* 2003; **285**: C823-830.

37 Lane DP, Benchimol S. p53: oncogene or anti-oncogene? *Genes Dev* 1990; **4**: 1–8.

38 Peltomäki P. DNA mismatch repair gene mutations in human cancer. *Environ Health Perspect* 1997; **105 Suppl 4**: 775–780.

39 Peltomäki P, de la Chapelle A. Mutations predisposing to hereditary nonpolyposis colorectal cancer. *Adv Cancer Res* 1997; **71**: 93–119.

40 Lynch HT, de la Chapelle A. Genetic susceptibility to non-polyposis colorectal cancer. *J Med Genet* 1999; **36**: 801–818.

41 Schwitalle Y, Kloor M, Eiermann S, Linnebacher M, Kienle P, Knaebel HP *et al.* Immune response against frameshift-induced neopeptides in HNPCC patients and healthy HNPCC mutation carriers. *Gastroenterology* 2008; **134**: 988–997.

42 Dolcetti R, Viel A, Doglioni C, Russo A, Guidoboni M, Capozzi E *et al.* High prevalence of activated intraepithelial cytotoxic T lymphocytes and increased neoplastic cell apoptosis in colorectal carcinomas with microsatellite instability. *Am J Pathol* 1999; **154**: 1805–1813.

43 Galon J, Pagès F, Marincola FM, Angell HK, Thurin M, Lugli A *et al.* Cancer classification using the Immunoscore: a worldwide task force. *J Transl Med* 2012; **10**: 205.

44 Le DT, Uram JN, Wang H, Bartlett BR, Kemberling H, Eyring AD *et al.* PD-1 Blockade in Tumors with Mismatch-Repair Deficiency. *N Engl J Med* 2015; **372**: 2509–2520.

45 Toyota M, Ahuja N, Ohe-Toyota M, Herman JG, Baylin SB, Issa JP. CpG island methylator phenotype in colorectal cancer. *Proc Natl Acad Sci U S A* 1999; **96**: 8681–8686.

46 Bettington M, Walker N, Clouston A, Brown I, Leggett B, Whitehall V. The serrated pathway to colorectal carcinoma: current concepts and challenges. *Histopathology* 2013; **62**: 367–386.

47 Herman JG, Umar A, Polyak K, Graff JR, Ahuja N, Issa JP *et al.* Incidence and functional consequences of hMLH1 promoter hypermethylation in colorectal carcinoma. *Proc Natl Acad Sci U S A* 1998; **95**: 6870–6875.

48 *Untersuchungen über die Entwicklungsgeschichte der Geburtshelferkröte (Alytes obstetricans).* Jent, 1842.

49 'Programmed Cell Death-II. Endocrine Potentiation of the Breakdown of the Intersegmental Muscles of Silkmoths' (1964), by Richard A. Lockshin and Carroll M. Williams | The Embryo Project Encyclopedia. https://embryo.asu.edu/pages/programmed-cell-death-ii-endocrine-potentiation-breakdown-intersegmental-muscles-silkmoths (accessed 4 Oct2016).

50 Kerr JF, Wyllie AH, Currie AR. Apoptosis: a basic biological phenomenon with wide-ranging implications in tissue kinetics. *Br J Cancer* 1972; **26**: 239–257.

51 Zaleske DJ. Development of the upper limb. *Hand Clin* 1985; **1**: 383–390.

52 Yuan J, Yankner BA. Apoptosis in the nervous system. *Nature* 2000; **407**: 802–809.

53 Thompson CB. Apoptosis in the pathogenesis and treatment of disease. *Science* 1995; **267**: 1456–1462.

54 Hengartner MO. The biochemistry of apoptosis. *Nature* 2000; **407**: 770–776.

55 Thornberry NA, Lazebnik Y. Caspases: enemies within. *Science* 1998; **281**: 1312–1316.

56 Lippens S, Kockx M, Knaapen M, Mortier L, Polakowska R, Verheyen A *et al.* Epidermal differentiation does not involve the pro-apoptotic executioner caspases, but is associated with caspase-14 induction and processing. *Cell Death Differ* 2000; **7**: 1218–1224.

57 Hofmann K, Bucher P, Tschopp J. The CARD domain: a new apoptotic signalling motif. *Trends Biochem Sci* 1997; **22**: 155–156.

58 Valmiki MG, Ramos JW. Death effector domain-containing proteins. *Cell Mol Life Sci CMLS* 2009; **66**: 814–830.

59 Coleman ML, Sahai EA, Yeo M, Bosch M, Dewar A, Olson MF. Membrane blebbing during apoptosis results from caspase-mediated activation of ROCK I. *Nat Cell Biol* 2001; **3**: 339–345.

60 Croft DR, Coleman ML, Li S, Robertson D, Sullivan T, Stewart CL *et al.* Actin-myosin-based contraction is responsible for apoptotic nuclear disintegration. *J Cell Biol* 2005; **168**: 245–255.

61 Rao L, Perez D, White E. Lamin proteolysis facilitates nuclear events during apoptosis. *J Cell Biol* 1996; **135**: 1441–1455.

62 Brancolini C, Lazarevic D, Rodriguez J, Schneider C. Dismantling cell-cell contacts during apoptosis is coupled to a caspase-dependent proteolytic cleavage of beta-catenin. *J Cell Biol* 1997; **139**: 759–771.

63 Steinhusen U, Weiske J, Badock V, Tauber R, Bommert K, Huber O. Cleavage and shedding of E-cadherin after induction of apoptosis. *J Biol Chem* 2001; **276**: 4972–4980.

64 Savill J, Fadok V. Corpse clearance defines the meaning of cell death. *Nature* 2000; **407**: 784–788.

65 Napirei M, Karsunky H, Zevnik B, Stephan H, Mannherz HG, Möröy T. Features of systemic lupus erythematosus in Dnase1-deficient mice. *Nat Genet* 2000; **25**: 177–181.

66 Cheung WL, Ajiro K, Samejima K, Kloc M, Cheung P, Mizzen CA *et al.* Apoptotic phosphorylation of histone H2B is mediated by mammalian sterile twenty kinase. *Cell* 2003; **113**: 507–517.

67 Ura S, Masuyama N, Graves JD, Gotoh Y. Caspase cleavage of MST1 promotes nuclear translocation and chromatin condensation. *Proc Natl Acad Sci U S A* 2001; **98**: 10148–10153.

68 Enari M, Sakahira H, Yokoyama H, Okawa K, Iwamatsu A, Nagata S. A caspase-activated DNase that degrades DNA during apoptosis, and its inhibitor ICAD. *Nature* 1998; **391**: 43–50.

69 Lüthi AU, Martin SJ. The CASBAH: a searchable database of caspase substrates. *Cell Death Differ* 2007; **14**: 641–650.

70 Lane JD, Lucocq J, Pryde J, Barr FA, Woodman PG, Allan VJ *et al.* Caspase-mediated cleavage of the stacking protein GRASP65 is required for Golgi fragmentation during apoptosis. *J Cell Biol* 2002; **156**: 495–509.

71 Lane JD, Allan VJ, Woodman PG. Active relocation of chromatin and endoplasmic reticulum into blebs in late apoptotic cells. *J Cell Sci* 2005; **118**: 4059–4071.

72 Karbowski M, Norris KL, Cleland MM, Jeong S-Y, Youle RJ. Role of Bax and Bak in mitochondrial morphogenesis. *Nature* 2006; **443**: 658–662.

73 Tsujimoto Y, Cossman J, Jaffe E, Croce CM. Involvement of the bcl-2 gene in human follicular lymphoma. *Science* 1985; **228**: 1440–1443.

74 Cleary ML, Smith SD, Sklar J. Cloning and structural analysis of cDNAs for bcl-2 and a hybrid bcl-2/immunoglobulin transcript resulting from the t(14;18) translocation. *Cell* 1986; **47**: 19–28.

75 Vaux DL, Cory S, Adams JM. Bcl-2 gene promotes haemopoietic cell survival and cooperates with c-myc to immortalize pre-B cells. *Nature* 1988; **335**: 440–442.

76 Kvansakul M, Yang H, Fairlie WD, Czabotar PE, Fischer SF, Perugini MA *et al.* Vaccinia virus anti-apoptotic F1L is a novel Bcl-2-like domain-swapped dimer that binds a highly selective subset of BH3-containing death ligands. *Cell Death Differ* 2008; **15**: 1564–1571.

77 Llambi F, Moldoveanu T, Tait SWG, Bouchier-Hayes L, Temirov J, McCormick LL *et al.* A unified model of mammalian BCL-2 protein family interactions at the mitochondria. *Mol Cell* 2011; **44**: 517–531.

78 Willis SN, Fletcher JI, Kaufmann T, van Delft MF, Chen L, Czabotar PE *et al.* Apoptosis initiated when BH3 ligands engage multiple Bcl-2 homologs, not Bax or Bak. *Science* 2007; **315**: 856–859.

79 Letai A, Bassik MC, Walensky LD, Sorcinelli MD, Weiler S, Korsmeyer SJ. Distinct BH3 domains either sensitize or activate mitochondrial apoptosis, serving as prototype cancer therapeutics. *Cancer Cell* 2002; **2**: 183–192.

80 Sattler M, Liang H, Nettesheim D, Meadows RP, Harlan JE, Eberstadt M *et al.* Structure of Bcl-xL-Bak peptide complex: recognition between regulators of apoptosis. *Science* 1997; **275**: 983–986.

81 Chen L, Willis SN, Wei A, Smith BJ, Fletcher JI, Hinds MG *et al.* Differential targeting of prosurvival Bcl-2 proteins by their BH3-only ligands allows complementary apoptotic function. *Mol Cell* 2005; **17**: 393–403.

82 Gavathiotis E, Suzuki M, Davis ML, Pitter K, Bird GH, Katz SG *et al.* BAX activation is initiated at a novel interaction site. *Nature* 2008; **455**: 1076–1081.

83 Griffiths GJ, Dubrez L, Morgan CP, Jones NA, Whitehouse J, Corfe BM *et al.* Cell damage-induced conformational changes of the pro-apoptotic protein Bak in vivo precede the onset of apoptosis. *J Cell Biol* 1999; **144**: 903–914.

84 Suzuki M, Youle RJ, Tjandra N. Structure of Bax: coregulation of dimer formation and intracellular localization. *Cell* 2000; **103**: 645–654.

85 Westphal D, Dewson G, Czabotar PE, Kluck RM. Molecular biology of Bax and Bak activation and action. *Biochim Biophys Acta* 2011; **1813**: 521–531.

86 Wei MC, Zong WX, Cheng EH, Lindsten T, Panoutsakopoulou V, Ross AJ *et al.* Proapoptotic BAX and BAK: a requisite gateway to mitochondrial dysfunction and death. *Science* 2001; **292**: 727–730.

87 Lindsten T, Ross AJ, King A, Zong WX, Rathmell JC, Shiels HA *et al.* The combined functions of proapoptotic Bcl-2 family members bak and bax are essential for normal development of multiple tissues. *Mol Cell* 2000; **6**: 1389–1399.

88 Du C, Fang M, Li Y, Li L, Wang X. Smac, a mitochondrial protein that promotes cytochrome c-dependent caspase activation by eliminating IAP inhibition. *Cell* 2000; **102**: 33–42.

89 Shi Y. Mechanical aspects of apoptosome assembly. *Curr Opin Cell Biol* 2006; **18**: 677–684.

90 Twiddy D, Cain K. Caspase-9 cleavage, do you need it? *Biochem J* 2007; **405**: e1-2.

91 Li P, Nijhawan D, Budihardjo I, Srinivasula SM, Ahmad M, Alnemri ES *et al.* Cytochrome c and dATP-dependent formation of Apaf-1/caspase-9 complex initiates an apoptotic protease cascade. *Cell* 1997; **91**: 479–489.

92 Joza N, Susin SA, Daugas E, Stanford WL, Cho SK, Li CY *et al.* Essential role of the mitochondrial apoptosis-inducing factor in programmed cell death. *Nature* 2001; **410**: 549–554.

93 Li LY, Luo X, Wang X. Endonuclease G is an apoptotic DNase when released from mitochondria. *Nature* 2001; **412**: 95–99.

94 Chai J, Du C, Wu JW, Kyin S, Wang X, Shi Y. Structural and biochemical basis of apoptotic activation by Smac/DIABLO. *Nature* 2000; **406**: 855–862.

95 Yang Q-H, Church-Hajduk R, Ren J, Newton ML, Du C. Omi/HtrA2 catalytic cleavage of inhibitor of apoptosis (IAP) irreversibly inactivates IAPs and facilitates caspase activity in apoptosis. *Genes Dev* 2003; **17**: 1487–1496.

96 Itoh N, Yonehara S, Ishii A, Yonehara M, Mizushima S, Sameshima M *et al.* The polypeptide encoded by the cDNA for human cell surface antigen Fas can mediate apoptosis. *Cell* 1991; **66**: 233–243.

97 Schall TJ, Lewis M, Koller KJ, Lee A, Rice GC, Wong GH *et al.* Molecular cloning and expression of a receptor for human tumor necrosis factor. *Cell* 1990; **61**: 361–370.

98 Pan G, O'Rourke K, Chinnaiyan AM, Gentz R, Ebner R, Ni J *et al.* The receptor for the cytotoxic ligand TRAIL. *Science* 1997; **276**: 111–113.

99 Pan G, Ni J, Wei YF, Yu G, Gentz R, Dixit VM. An antagonist decoy receptor and a death domain-containing receptor for TRAIL. *Science* 1997; **277**: 815–818.

100 Chinnaiyan AM, O'Rourke K, Yu GL, Lyons RH, Garg M, Duan DR *et al.* Signal transduction by DR3, a death domain-containing receptor related to TNFR-1 and CD95. *Science* 1996; **274**: 990–992.

101 Pan G, Bauer JH, Haridas V, Wang S, Liu D, Yu G *et al.* Identification and functional characterization of DR6, a novel death domain-containing TNF receptor. *FEBS Lett* 1998; **431**: 351–356.

102 Locksley RM, Killeen N, Lenardo MJ. The TNF and TNF receptor superfamilies: integrating mammalian biology. *Cell* 2001; **104**: 487–501.

103 Boldin MP, Mett IL, Varfolomeev EE, Chumakov I, Shemer-Avni Y, Camonis JH *et al.* Self-association of the 'death domains' of the p55 tumor necrosis factor (TNF) receptor and Fas/APO1 prompts signaling for TNF and Fas/APO1 effects. *J Biol Chem* 1995; **270**: 387–391.

104 Schulze-Osthoff K, Ferrari D, Los M, Wesselborg S, Peter ME. Apoptosis signaling by death receptors. *Eur J Biochem FEBS* 1998; **254**: 439–459.

105 Fearon ER, Cho KR, Nigro JM, Kern SE, Simons JW, Ruppert JM *et al.* Identification of a chromosome 18q gene that is altered in colorectal cancers. *Science* 1990; **247**: 49–56.

106 Keino-Masu K, Masu M, Hinck L, Leonardo ED, Chan SS, Culotti JG *et al.* Deleted in Colorectal Cancer (DCC) encodes a netrin receptor. *Cell* 1996; **87**: 175–185.

107 Yonehara S, Ishii A, Yonehara M. A cell-killing monoclonal antibody (anti-Fas) to a cell surface antigen co-downregulated with the receptor of tumor necrosis factor. *J Exp Med* 1989; **169**: 1747–1756.

108 Trauth BC, Klas C, Peters AM, Matzku S, Möller P, Falk W *et al.* Monoclonal antibody-mediated tumor regression by induction of apoptosis. *Science* 1989; **245**: 301–305.

109 Kayagaki N, Kawasaki A, Ebata T, Ohmoto H, Ikeda S, Inoue S *et al.* Metalloproteinase-mediated release of human Fas ligand. *J Exp Med* 1995; **182**: 1777–1783.

110 Kischkel FC, Hellbardt S, Behrmann I, Germer M, Pawlita M, Krammer PH *et al.* Cytotoxicity-dependent APO-1 (Fas/CD95)-associated proteins form a death-inducing signaling complex (DISC) with the receptor. *EMBO J* 1995; **14**: 5579–5588.

111 Wang J, Chun HJ, Wong W, Spencer DM, Lenardo MJ. Caspase-10 is an initiator caspase in death receptor signaling. *Proc Natl Acad Sci U S A* 2001; **98**: 13884–13888.

112 Sprick MR, Rieser E, Stahl H, Grosse-Wilde A, Weigand MA, Walczak H. Caspase-10 is recruited to and activated at the native TRAIL and CD95 death-inducing signalling complexes in a FADD-dependent manner but can not functionally substitute caspase-8. *EMBO J* 2002; **21**: 4520–4530.

113 Barnhart BC, Alappat EC, Peter ME. The CD95 type I/type II model. *Semin Immunol* 2003; **15**: 185–193.

114 Luo X, Budihardjo I, Zou H, Slaughter C, Wang X. Bid, a Bcl2 interacting protein, mediates cytochrome c release from mitochondria in response to activation of cell surface death receptors. *Cell* 1998; **94**: 481–490.

115 Safa AR. c-FLIP, a master anti-apoptotic regulator. *Exp Oncol* 2012; **34**: 176–184.

116 Fricker N, Beaudouin J, Richter P, Eils R, Krammer PH, Lavrik IN. Model-based dissection of CD95 signaling dynamics reveals both a pro- and antiapoptotic role of c-FLIPL. *J Cell Biol* 2010; **190**: 377–389.

117 Golks A, Brenner D, Krammer PH, Lavrik IN. The c-FLIP-NH2 terminus (p22-FLIP) induces NF-kappaB activation. *J Exp Med* 2006; **203**: 1295–1305.

118 Catz SD, Johnson JL. Transcriptional regulation of bcl-2 by nuclear factor kappa B and its significance in prostate cancer. *Oncogene* 2001; **20**: 7342–7351.

119 Kreuz S, Siegmund D, Scheurich P, Wajant H. NF-kappaB inducers upregulate cFLIP, a cycloheximide-sensitive inhibitor of death receptor signaling. *Mol Cell Biol* 2001; **21**: 3964–3973.

120 Stehlik C, de Martin R, Kumabashiri I, Schmid JA, Binder BR, Lipp J. Nuclear factor (NF)-kappaB-regulated X-chromosome-linked iap gene expression protects endothelial cells from tumor necrosis factor alpha-induced apoptosis. *J Exp Med* 1998; **188**: 211–216.

121 Baker SJ, Reddy EP. Modulation of life and death by the TNF receptor superfamily. *Oncogene* 1998; **17**: 3261–3270.

122 Micheau O, Tschopp J. Induction of TNF receptor I-mediated apoptosis via two sequential signaling complexes. *Cell* 2003; **114**: 181–190.

123 Van Herreweghe F, Festjens N, Declercq W, Vandenabeele P. Tumor necrosis factor-mediated cell death: to break or to burst, that's the question. *Cell Mol Life Sci CMLS* 2010; **67**: 1567–1579.

124 Levine B, Kroemer G. Autophagy in the pathogenesis of disease. *Cell* 2008; **132**: 27–42.

125 Suzuki K, Ohsumi Y. Molecular machinery of autophagosome formation in yeast, Saccharomyces cerevisiae. *FEBS Lett* 2007; **581**: 2156–2161.

126 Yang Z, Klionsky DJ. Mammalian autophagy: core molecular machinery and signaling regulation. *Curr Opin Cell Biol* 2010; **22**: 124–131.

127 Hosokawa N, Hara T, Kaizuka T, Kishi C, Takamura A, Miura Y *et al.* Nutrient-dependent mTORC1 association with the ULK1-Atg13-FIP200 complex required for autophagy. *Mol Biol Cell* 2009; **20**: 1981–1991.

128 Jung CH, Jun CB, Ro S-H, Kim Y-M, Otto NM, Cao J *et al.* ULK-Atg13-FIP200 complexes mediate mTOR signaling to the autophagy machinery. *Mol Biol Cell* 2009; **20**: 1992–2003.

129 Hamasaki M, Furuta N, Matsuda A, Nezu A, Yamamoto A, Fujita N *et al.* Autophagosomes form at ER-mitochondria contact sites. *Nature* 2013; **495**: 389–393.

130 Ravikumar B, Moreau K, Jahreiss L, Puri C, Rubinsztein DC. Plasma membrane contributes to the formation of pre-autophagosomal structures. *Nat Cell Biol* 2010; **12**: 747–757.

131 Vergne I, Deretic V. The role of PI3P phosphatases in the regulation of autophagy. *FEBS Lett* 2010; **584**: 1313–1318.

132 Vytiska-Binstorfer E, Brehm R, Huber JC, Reinold E. [Course of pregnancy of insulin-dependent diabetic patients 1978-1985 at the 1st Vienna University gynecologic clinic]. *Z Für Geburtshilfe Perinatol* 1987; **191**: 55–59.

133 Ropolo A, Grasso D, Pardo R, Sacchetti ML, Archange C, Lo Re A *et al.* The pancreatitis-induced vacuole membrane protein 1 triggers autophagy in mammalian cells. *J Biol Chem* 2007; **282**: 37124–37133.

134 Webber JL, Tooze SA. New insights into the function of Atg9. *FEBS Lett* 2010; **584**: 1319–1326.

135 Mizushima N, Noda T, Yoshimori T, Tanaka Y, Ishii T, George MD *et al.* A protein conjugation system essential for autophagy. *Nature* 1998; **395**: 395–398.

136 Ichimura Y, Kirisako T, Takao T, Satomi Y, Shimonishi Y, Ishihara N *et al.* A ubiquitin-like system mediates protein lipidation. *Nature* 2000; **408**: 488–492.

137 Klionsky DJ, Abdalla FC, Abeliovich H, Abraham RT, Acevedo-Arozena A, Adeli K *et al.* Guidelines for the use and interpretation of assays for monitoring autophagy. *Autophagy* 2012; **8**: 445–544.

138 Kabeya Y, Mizushima N, Yamamoto A, Oshitani-Okamoto S, Ohsumi Y, Yoshimori T. LC3, GABARAP and GATE16 localize to autophagosomal membrane depending on form-II formation. *J Cell Sci* 2004; **117**: 2805–2812.

139 Hanada T, Noda NN, Satomi Y, Ichimura Y, Fujioka Y, Takao T *et al.* The Atg12-Atg5 conjugate has a novel E3-like activity for protein lipidation in autophagy. *J Biol Chem* 2007; **282**: 37298–37302.

140 Mizushima N, Yamamoto A, Hatano M, Kobayashi Y, Kabeya Y, Suzuki K *et al.* Dissection of autophagosome formation using Apg5-deficient mouse embryonic stem cells. *J Cell Biol* 2001; **152**: 657–668.

141 Nakatogawa H, Ichimura Y, Ohsumi Y. Atg8, a ubiquitin-like protein required for autophagosome formation, mediates membrane tethering and hemifusion. *Cell* 2007; **130**: 165–178.

142 Yu L, McPhee CK, Zheng L, Mardones GA, Rong Y, Peng J *et al.* Termination of autophagy and reformation of lysosomes regulated by mTOR. *Nature* 2010; **465**: 942–946.

143 Galluzzi L, Vitale I, Abrams JM, Alnemri ES, Baehrecke EH, Blagosklonny MV *et al.* Molecular definitions of cell death subroutines: recommendations of the Nomenclature Committee on Cell Death 2012. *Cell Death Differ* 2012; **19**: 107–120.

144 Koike M, Shibata M, Tadakoshi M, Gotoh K, Komatsu M, Waguri S *et al.* Inhibition of autophagy prevents hippocampal pyramidal neuron death after hypoxic-ischemic injury. *Am J Pathol* 2008; **172**: 454–469.

145 Zhu H, Tannous P, Johnstone JL, Kong Y, Shelton JM, Richardson JA *et al.* Cardiac autophagy is a maladaptive response to hemodynamic stress. *J Clin Invest* 2007; **117**: 1782–1793.

146 Sentelle RD, Senkal CE, Jiang W, Ponnusamy S, Gencer S, Selvam SP *et al.* Ceramide targets autophagosomes to mitochondria and induces lethal mitophagy. *Nat Chem Biol* 2012; **8**: 831–838.

147 Holler N, Zaru R, Micheau O, Thome M, Attinger A, Valitutti S *et al.* Fas triggers an alternative, caspase-8-independent cell death pathway using the kinase RIP as effector molecule. *Nat Immunol* 2000; **1**: 489–495.

148 Feng S, Yang Y, Mei Y, Ma L, Zhu D, Hoti N *et al.* Cleavage of RIP3 inactivates its caspase-independent apoptosis pathway by removal of kinase domain. *Cell Signal* 2007; **19**: 2056–2067.

149 Zong W-X, Ditsworth D, Bauer DE, Wang Z-Q, Thompson CB. Alkylating DNA damage stimulates a regulated form of necrotic cell death. *Genes Dev* 2004; **18**: 1272–1282.

150 He S, Wang L, Miao L, Wang T, Du F, Zhao L *et al.* Receptor interacting protein kinase-3 determines cellular necrotic response to TNF-alpha. *Cell* 2009; **137**: 1100–1111.

151 Wright A, Reiley WW, Chang M, Jin W, Lee AJ, Zhang M *et al.* Regulation of early wave of germ cell apoptosis and spermatogenesis by deubiquitinating enzyme CYLD. *Dev Cell* 2007; **13**: 705–716.

152 Cho YS, Challa S, Moquin D, Genga R, Ray TD, Guildford M *et al.* Phosphorylation-driven assembly of the RIP1-RIP3 complex regulates programmed necrosis and virus-induced inflammation. *Cell* 2009; **137**: 1112–1123.

153 Degterev A, Huang Z, Boyce M, Li Y, Jagtap P, Mizushima N *et al.* Chemical inhibitor of nonapoptotic cell death with therapeutic potential for ischemic brain injury. *Nat Chem Biol* 2005; **1**: 112–119.

154 Dondelinger Y, Declercq W, Montessuit S, Roelandt R, Goncalves A, Bruggeman I *et al.* MLKL compromises plasma membrane integrity by binding to phosphatidylinositol phosphates. *Cell Rep* 2014; **7**: 971–981.

155 Wang H, Sun L, Su L, Rizo J, Liu L, Wang L-F *et al.* Mixed lineage kinase domain-like protein MLKL causes necrotic membrane disruption upon phosphorylation by RIP3. *Mol Cell* 2014; **54**: 133–146.

156 Sauer B. Inducible gene targeting in mice using the Cre/lox system. *Methods San Diego Calif* 1998; **14**: 381–392.

157 Abremski K, Hoess R. Bacteriophage P1 site-specific recombination. Purification and properties of the Cre recombinase protein. *J Biol Chem* 1984; **259**: 1509–1514.

158 Kos CH. Cre/loxP system for generating tissue-specific knockout mouse models. *Nutr Rev* 2004; **62**: 243–246.

159 Feil R, Brocard J, Mascrez B, LeMeur M, Metzger D, Chambon P. Ligand-activated site-specific recombination in mice. *Proc Natl Acad Sci U S A* 1996; **93**: 10887–10890.

160 el Marjou F, Janssen K-P, Chang BH-J, Li M, Hindie V, Chan L *et al.* Tissue-specific and inducible Cre-mediated recombination in the gut epithelium. *Genes N Y N 2000* 2004; **39**: 186–193.

161 Rinkenberger JL, Horning S, Klocke B, Roth K, Korsmeyer SJ. Mcl-1 deficiency results in peri-implantation embryonic lethality. *Genes Dev* 2000; **14**: 23–27.

162 Motoyama N, Wang F, Roth KA, Sawa H, Nakayama K, Nakayama K *et al.* Massive cell death of immature hematopoietic cells and neurons in Bcl-x-deficient mice. *Science* 1995; **267**: 1506–1510.

163 Veis DJ, Sorenson CM, Shutter JR, Korsmeyer SJ. Bcl-2-deficient mice demonstrate fulminant lymphoid apoptosis, polycystic kidneys, and hypopigmented hair. *Cell* 1993; **75**: 229–240.

164 Nakayama K, Nakayama K, Negishi I, Kuida K, Sawa H, Loh DY. Targeted disruption of Bcl-2 alpha beta in mice: occurrence of gray hair, polycystic kidney disease, and lymphocytopenia. *Proc Natl Acad Sci U S A* 1994; **91**: 3700–3704.

165 Merritt AJ, Potten CS, Watson AJ, Loh DY, Nakayama K, Nakayama K *et al.* Differential expression of bcl-2 in intestinal epithelia. Correlation with attenuation of apoptosis in colonic crypts and the incidence of colonic neoplasia. *J Cell Sci* 1995; **108 (Pt 6)**: 2261–2271.

166 Hamasaki A, Sendo F, Nakayama K, Ishida N, Negishi I, Nakayama K *et al.* Accelerated neutrophil apoptosis in mice lacking A1-a, a subtype of the bcl-2-related A1 gene. *J Exp Med* 1998; **188**: 1985–1992.

167 Xiang Z, Ahmed AA, Möller C, Nakayama K, Hatakeyama S, Nilsson G. Essential role of the prosurvival bcl-2 homologue A1 in mast cell survival after allergic activation. *J Exp Med* 2001; **194**: 1561–1569.

168 Knudson CM, Tung KS, Tourtellotte WG, Brown GA, Korsmeyer SJ. Bax-deficient mice with lymphoid hyperplasia and male germ cell death. *Science* 1995; **270**: 96–99.

169 Mason KD, Carpinelli MR, Fletcher JI, Collinge JE, Hilton AA, Ellis S *et al.* Programmed anuclear cell death delimits platelet life span. *Cell* 2007; **128**: 1173–1186.

170 Rathmell JC, Lindsten T, Zong W-X, Cinalli RM, Thompson CB. Deficiency in Bak and Bax perturbs thymic selection and lymphoid homeostasis. *Nat Immunol* 2002; **3**: 932–939.

171 Villunger A, Michalak EM, Coultas L, Müllauer F, Böck G, Ausserlechner MJ *et al.* p53- and drug-induced apoptotic responses mediated by BH3-only proteins puma and noxa. *Science* 2003; **302**: 1036–1038.

172 Jeffers JR, Parganas E, Lee Y, Yang C, Wang J, Brennan J *et al.* Puma is an essential mediator of p53-dependent and -independent apoptotic pathways. *Cancer Cell* 2003; **4**: 321–328.

173 Qiu W, Wu B, Wang X, Buchanan ME, Regueiro MD, Hartman DJ *et al.* PUMA-mediated intestinal epithelial apoptosis contributes to ulcerative colitis in humans and mice. *J Clin Invest* 2011; **121**: 1722–1732.

174 Bouillet P, Metcalf D, Huang DC, Tarlinton DM, Kay TW, Köntgen F *et al.* Proapoptotic Bcl-2 relative Bim required for certain apoptotic responses, leukocyte homeostasis, and to preclude autoimmunity. *Science* 1999; **286**: 1735–1738.

175 Yin XM, Wang K, Gross A, Zhao Y, Zinkel S, Klocke B *et al.* Bid-deficient mice are resistant to Fas-induced hepatocellular apoptosis. *Nature* 1999; **400**: 886–891.

176 Nunes T, Bernardazzi C, de Souza HS. Cell death and inflammatory bowel diseases: apoptosis, necrosis, and autophagy in the intestinal epithelium. *BioMed Res Int* 2014; **2014**: 218493.

177 Günther C, Martini E, Wittkopf N, Amann K, Weigmann B, Neumann H *et al.* Caspase-8 regulates TNF-α-induced epithelial necroptosis and terminal ileitis. *Nature* 2011; **477**: 335–339.

178 Welz P-S, Wullaert A, Vlantis K, Kondylis V, Fernández-Majada V, Ermolaeva M *et al.* FADD prevents RIP3-mediated epithelial cell necrosis and chronic intestinal inflammation. *Nature* 2011; **477**: 330–334.

179 Lin Y, Devin A, Rodriguez Y, Liu ZG. Cleavage of the death domain kinase RIP by caspase-8 prompts TNF-induced apoptosis. *Genes Dev* 1999; **13**: 2514–2526.

180 Oberst A, Dillon CP, Weinlich R, McCormick LL, Fitzgerald P, Pop C *et al.* Catalytic activity of the caspase-8-FLIP(L) complex inhibits RIPK3-dependent necrosis. *Nature* 2011; **471**: 363–367.

181 Wittkopf N, Günther C, Martini E, He G, Amann K, He Y-W *et al.* Cellular FLICE-like inhibitory protein secures intestinal epithelial cell survival and immune homeostasis by regulating caspase-8. *Gastroenterology* 2013; **145**: 1369–1379.

182 Nenci A, Becker C, Wullaert A, Gareus R, van Loo G, Danese S *et al.* Epithelial NEMO links innate immunity to chronic intestinal inflammation. *Nature* 2007; **446**: 557–561.

183 Greten FR, Eckmann L, Greten TF, Park JM, Li Z-W, Egan LJ *et al.* IKKbeta links inflammation and tumorigenesis in a mouse model of colitis-associated cancer. *Cell* 2004; **118**: 285–296.

184 Kajino-Sakamoto R, Inagaki M, Lippert E, Akira S, Robine S, Matsumoto K *et al.* Enterocyte-derived TAK1 signaling prevents epithelium apoptosis and the development of ileitis and colitis. *J Immunol Baltim Md 1950* 2008; **181**: 1143–1152.

185 Pickert G, Neufert C, Leppkes M, Zheng Y, Wittkopf N, Warntjen M *et al.* STAT3 links IL-22 signaling in intestinal epithelial cells to mucosal wound healing. *J Exp Med* 2009; **206**: 1465–1472.

186 Bollrath J, Phesse TJ, von Burstin VA, Putoczki T, Bennecke M, Bateman T *et al.* gp130-mediated Stat3 activation in enterocytes regulates cell survival and cell-cycle progression during colitis-associated tumorigenesis. *Cancer Cell* 2009; **15**: 91–102.

187 Pierdomenico M, Negroni A, Stronati L, Vitali R, Prete E, Bertin J *et al.* Necroptosis is active in children with inflammatory bowel disease and contributes to heighten intestinal inflammation. *Am J Gastroenterol* 2014; **109**: 279–287.

188 Wu J, Huang Z, Ren J, Zhang Z, He P, Li Y *et al.* Mlkl knockout mice demonstrate the indispensable role of Mlkl in necroptosis. *Cell Res* 2013; **23**: 994–1006.

189 Newton K, Sun X, Dixit VM. Kinase RIP3 is dispensable for normal NF-kappa Bs, signaling by the B-cell and T-cell receptors, tumor necrosis factor receptor 1, and Toll-like receptors 2 and 4. *Mol Cell Biol* 2004; **24**: 1464–1469.

190 Takahashi N, Vereecke L, Bertrand MJM, Duprez L, Berger SB, Divert T *et al.* RIPK1 ensures intestinal homeostasis by protecting the epithelium against apoptosis. *Nature* 2014; **513**: 95–99.

191 Lansdorp-Vogelaar I, van Ballegooijen M, Zauber AG, Habbema JDF, Kuipers EJ. Effect of rising chemotherapy costs on the cost savings of colorectal cancer screening. *J Natl Cancer Inst* 2009; **101**: 1412–1422.

192 Sieghart W, Losert D, Strommer S, Cejka D, Schmid K, Rasoul-Rockenschaub S *et al.* Mcl-1 overexpression in hepatocellular carcinoma: a potential target for antisense therapy. *J Hepatol* 2006; **44**: 151–157.

193 Krajewska M, Krajewski S, Epstein JI, Shabaik A, Sauvageot J, Song K *et al.* Immunohistochemical analysis of bcl-2, bax, bcl-X, and mcl-1 expression in prostate cancers. *Am J Pathol* 1996; **148**: 1567–1576.

194 Jin-Song Y, Zhao-Xia W, Cheng-Yu L, Xiao-Di L, Ming S, Yuan-Yuan G *et al.* Prognostic significance of Bcl-xL gene expression in human colorectal cancer. *Acta Histochem* 2011; **113**: 810–814.

195 Manne U, Myers RB, Moron C, Poczatek RB, Dillard S, Weiss H *et al.* Prognostic significance of Bcl-2 expression and p53 nuclear accumulation in colorectal adenocarcinoma. *Int J Cancer* 1997; **74**: 346–358.

196 Fujise K, Zhang D, Liu J, Yeh ET. Regulation of apoptosis and cell cycle progression by MCL1. Differential role of proliferating cell nuclear antigen. *J Biol Chem* 2000; **275**: 39458–39465.

197 Jamil S, Sobouti R, Hojabrpour P, Raj M, Kast J, Duronio V. A proteolytic fragment of Mcl-1 exhibits nuclear localization and regulates cell growth by interaction with Cdk1. *Biochem J* 2005; **387**: 659–667.

198 Jamil S, Stoica C, Hackett T-L, Duronio V. MCL-1 localizes to sites of DNA damage and regulates DNA damage response. *Cell Cycle Georget Tex* 2010; **9**: 2843–2855.

199 Chan FK-M, Moriwaki K, De Rosa MJ. Detection of necrosis by release of lactate dehydrogenase activity. *Methods Mol Biol Clifton NJ* 2013; **979**: 65–70.

200 Hughes CS, Postovit LM, Lajoie GA. Matrigel: a complex protein mixture required for optimal growth of cell culture. *Proteomics* 2010; **10**: 1886–1890.

201 Woerner SM, Tosti E, Yuan YP, Kloor M, Bork P, Edelmann W *et al.* Detection of coding microsatellite frameshift mutations in DNA mismatch repair-deficient mouse intestinal tumors. *Mol Carcinog* 2015; **54**: 1376–1386.

202 Huh WJ, Mysorekar IU, Mills JC. Inducible activation of Cre recombinase in adult mice causes gastric epithelial atrophy, metaplasia, and regenerative changes in the absence of 'floxed' alleles. *Am J Physiol Gastrointest Liver Physiol* 2010; **299**: G368-380.

203 Becker C, Fantini MC, Neurath MF. High resolution colonoscopy in live mice. *Nat Protoc* 2006; **1**: 2900–2904.

204 Martínez-Paniagua MA, Baritaki S, Huerta-Yepez S, Ortiz-Navarrete VF, González-Bonilla C, Bonavida B *et al.* Mcl-1 and YY1 inhibition and induction of DR5 by the BH3-mimetic

Obatoclax (GX15-070) contribute in the sensitization of B-NHL cells to TRAIL apoptosis. *Cell Cycle Georget Tex* 2011; **10**: 2792–2805.

205 Wheelock MJ, Shintani Y, Maeda M, Fukumoto Y, Johnson KR. Cadherin switching. *J Cell Sci* 2008; **121**: 727–735.

206 Gravdal K, Halvorsen OJ, Haukaas SA, Akslen LA. A switch from E-cadherin to N-cadherin expression indicates epithelial to mesenchymal transition and is of strong and independent importance for the progress of prostate cancer. *Clin Cancer Res Off J Am Assoc Cancer Res* 2007; **13**: 7003–7011.

207 de Vries JE, Dinjens WN, De Bruyne GK, Verspaget HW, van der Linden EP, de Bruïne AP *et al.* In vivo and in vitro invasion in relation to phenotypic characteristics of human colorectal carcinoma cells. *Br J Cancer* 1995; **71**: 271–277.

208 Li Y, Xiao B, Tu S, Wang Y, Zhang X. Cultivation and identification of colon cancer stem cell-derived spheres from the Colo205 cell line. *Braz J Med Biol Res Rev Bras Pesqui Médicas E Biológicas Soc Bras Biofísica Al* 2012; **45**: 197–204.

209 Tiwari N, Gheldof A, Tatari M, Christofori G. EMT as the ultimate survival mechanism of cancer cells. *Semin Cancer Biol* 2012; **22**: 194–207.

210 Cragg MS, Harris C, Strasser A, Scott CL. Unleashing the power of inhibitors of oncogenic kinases through BH3 mimetics. *Nat Rev Cancer* 2009; **9**: 321–326.

211 Labi V, Grespi F, Baumgartner F, Villunger A. Targeting the Bcl-2-regulated apoptosis pathway by BH3 mimetics: a breakthrough in anticancer therapy? *Cell Death Differ* 2008; **15**: 977–987.

212 Vela L, Marzo I. Bcl-2 family of proteins as drug targets for cancer chemotherapy: the long way of BH3 mimetics from bench to bedside. *Curr Opin Pharmacol* 2015; **23**: 74–81.

213 Koehler BC, Jäger D, Schulze-Bergkamen H. Targeting cell death signaling in colorectal cancer: current strategies and future perspectives. *World J Gastroenterol* 2014; **20**: 1923–1934.

214 Janumyan YM, Sansam CG, Chattopadhyay A, Cheng N, Soucie EL, Penn LZ *et al.* Bcl-xL/Bcl-2 coordinately regulates apoptosis, cell cycle arrest and cell cycle entry. *EMBO J* 2003; **22**: 5459–5470.

215 Zhang Y-L, Pang L-Q, Wu Y, Wang X-Y, Wang C-Q, Fan Y. Significance of Bcl-xL in human colon carcinoma. *World J Gastroenterol* 2008; **14**: 3069–3073.

216 Henderson-Jackson EB, Helm J, Ghayouri M, Hakam A, Nasir A, Leon M *et al.* Correlation between Mcl-1 and pAKT protein expression in colorectal cancer. *Int J Clin Exp Pathol* 2010; **3**: 768–774.

217 Krajewska M, Moss SF, Krajewski S, Song K, Holt PR, Reed JC. Elevated expression of Bcl-X and reduced Bak in primary colorectal adenocarcinomas. *Cancer Res* 1996; **56**: 2422–2427.

218 Buglioni S, D'Agnano I, Cosimelli M, Vasselli S, D'Angelo C, Tedesco M *et al.* Evaluation of multiple bio-pathological factors in colorectal adenocarcinomas: independent prognostic role of p53 and bcl-2. *Int J Cancer* 1999; **84**: 545–552.

219 Koehler BC, Scherr A-L, Lorenz S, Urbanik T, Kautz N, Elssner C *et al.* Beyond cell death - antiapoptotic Bcl-2 proteins regulate migration and invasion of colorectal cancer cells in vitro. *PloS One* 2013; **8**: e76446.

220 Schmitt E, Beauchemin M, Bertrand R. Nuclear colocalization and interaction between bcl-xL and cdk1(cdc2) during G2/M cell-cycle checkpoint. *Oncogene* 2007; **26**: 5851–5865.

221 Hao W, Luo W, Bai M, Li J, Bai X, Guo J *et al.* MicroRNA-206 Inhibited the Progression of Glioblastoma Through BCL-2. *J Mol Neurosci MN* 2016. doi:10.1007/s12031-016-0824-6.

222 Alderton GK. Metastasis: Epithelial to mesenchymal and back again. *Nat Rev Cancer* 2013; **13**: 3.

223 Glinsky GV, Glinsky VV, Ivanova AB, Hueser CJ. Apoptosis and metastasis: increased apoptosis resistance of metastatic cancer cells is associated with the profound deficiency of apoptosis execution mechanisms. *Cancer Lett* 1997; **115**: 185–193.

224 Del Bufalo D, Biroccio A, Leonetti C, Zupi G. Bcl-2 overexpression enhances the metastatic potential of a human breast cancer line. *FASEB J Off Publ Fed Am Soc Exp Biol* 1997; **11**: 947–953.

225 McConkey DJ, Greene G, Pettaway CA. Apoptosis resistance increases with metastatic potential in cells of the human LNCaP prostate carcinoma line. *Cancer Res* 1996; **56**: 5594–5599.

226 Furuya Y, Krajewski S, Epstein JI, Reed JC, Isaacs JT. Expression of bcl-2 and the progression of human and rodent prostatic cancers. *Clin Cancer Res Off J Am Assoc Cancer Res* 1996; **2**: 389–398.

227 Celià-Terrassa T, Kang Y. Distinctive properties of metastasis-initiating cells. *Genes Dev* 2016; **30**: 892–908.

228 Martin SS, Leder P. Human MCF10A mammary epithelial cells undergo apoptosis following actin depolymerization that is independent of attachment and rescued by Bcl-2. *Mol Cell Biol* 2001; **21**: 6529–6536.

229 Martin SS, Ridgeway AG, Pinkas J, Lu Y, Reginato MJ, Koh EY *et al.* A cytoskeleton-based functional genetic screen identifies Bcl-xL as an enhancer of metastasis, but not primary tumor growth. *Oncogene* 2004; **23**: 4641–4645.

230 Mehlen P, Puisieux A. Metastasis: a question of life or death. *Nat Rev Cancer* 2006; **6**: 449–458.

231 Wong CW, Lee A, Shientag L, Yu J, Dong Y, Kao G *et al.* Apoptosis: an early event in metastatic inefficiency. *Cancer Res* 2001; **61**: 333–338.

232 Grutzmacher C, Park S, Elmergreen TL, Tang Y, Scheef EA, Sheibani N *et al.* Opposing effects of bim and bcl-2 on lung endothelial cell migration. *Am J Physiol Lung Cell Mol Physiol* 2010; **299**: L607-620.

233 Gao J, Li L, Wu M, Liu M, Xie X, Guo J *et al.* MiR-26a inhibits proliferation and migration of breast cancer through repression of MCL-1. *PloS One* 2013; **8**: e65138.

234 Wick W, Wagner S, Kerkau S, Dichgans J, Tonn JC, Weller M. BCL-2 promotes migration and invasiveness of human glioma cells. *FEBS Lett* 1998; **440**: 419–424.

235 Schutte M, Fox B, Baradez M-O, Devonshire A, Minguez J, Bokhari M *et al.* Rat primary hepatocytes show enhanced performance and sensitivity to acetaminophen during three-dimensional culture on a polystyrene scaffold designed for routine use. *Assay Drug Dev Technol* 2011; **9**: 475–486.

236 Bokhari M, Carnachan RJ, Cameron NR, Przyborski SA. Culture of HepG2 liver cells on three dimensional polystyrene scaffolds enhances cell structure and function during toxicological challenge. *J Anat* 2007; **211**: 567–576.

237 Dubois F, Yourassowsky C, Monnom O, Legros J-C, Debeir O, Van Ham P *et al.* Digital holographic microscopy for the three-dimensional dynamic analysis of in vitro cancer cell migration. *J Biomed Opt* 2006; **11**: 54032.

238 Christofori G. New signals from the invasive front. *Nature* 2006; **441**: 444–450.

239 Hagedorn EJ, Sherwood DR. Cell invasion through basement membrane: the anchor cell breaches the barrier. *Curr Opin Cell Biol* 2011; **23**: 589–596.

240 Wick W, Platten M, Weller M. Glioma cell invasion: regulation of metalloproteinase activity by TGF-beta. *J Neurooncol* 2001; **53**: 177–185.

241 Yang J, Sun M, Zhang A, Lv C, De W, Wang Z. Adenovirus-mediated siRNA targeting Bcl-xL inhibits proliferation, reduces invasion and enhances radiosensitivity of human colorectal cancer cells. *World J Surg Oncol* 2011; **9**: 117.

242 Hwang JJ, Kuruvilla J, Mendelson D, Pishvaian MJ, Deeken JF, Siu LL *et al.* Phase I dose finding studies of obatoclax (GX15-070), a small molecule pan-BCL-2 family antagonist, in patients with advanced solid tumors or lymphoma. *Clin Cancer Res Off J Am Assoc Cancer Res* 2010; **16**: 4038–4045.

243 Zhai D, Jin C, Satterthwait AC, Reed JC. Comparison of chemical inhibitors of antiapoptotic Bcl-2-family proteins. *Cell Death Differ* 2006; **13**: 1419–1421.

244 Espona-Fiedler M, Soto-Cerrato V, Hosseini A, Lizcano JM, Guallar V, Quesada R *et al.* Identification of dual mTORC1 and mTORC2 inhibitors in melanoma cells: prodigiosin vs. obatoclax. *Biochem Pharmacol* 2012; **83**: 489–496.

245 Vogt F, Lieber J, Dewerth A, Hoh A, Fuchs J, Armeanu-Ebinger S. BH3 mimetics reduce adhesion and migration of hepatoblastoma and hepatocellular carcinoma cells. *Exp Cell Res* 2013; **319**: 1443–1450.

246 Nobes CD, Hall A. Rho, rac, and cdc42 GTPases regulate the assembly of multimolecular focal complexes associated with actin stress fibers, lamellipodia, and filopodia. *Cell* 1995; **81**: 53–62.

247 Stengel K, Zheng Y. Cdc42 in oncogenic transformation, invasion, and tumorigenesis. *Cell Signal* 2011; **23**: 1415–1423.

248 Gómez Del Pulgar T, Valdés-Mora F, Bandrés E, Pérez-Palacios R, Espina C, Cejas P *et al.* Cdc42 is highly expressed in colorectal adenocarcinoma and downregulates ID4 through an epigenetic mechanism. *Int J Oncol* 2008; **33**: 185–193.

249 Liu Y, Wang Y, Zhang Y, Miao Y, Zhao Y, Zhang P-X *et al.* Abnormal expression of p120-catenin, E-cadherin, and small GTPases is significantly associated with malignant phenotype of human lung cancer. *Lung Cancer Amst Neth* 2009; **63**: 375–382.

250 Tucci MG, Lucarini G, Brancorsini D, Zizzi A, Pugnaloni A, Giacchetti A *et al.* Involvement of E-cadherin, beta-catenin, Cdc42 and CXCR4 in the progression and prognosis of cutaneous melanoma. *Br J Dermatol* 2007; **157**: 1212–1216.

251 Gandalovičová A, Vomastek T, Rosel D, Brábek J. Cell polarity signaling in the plasticity of cancer cell invasiveness. *Oncotarget* 2016; **7**: 25022–25049.

252 Thiery JP, Acloque H, Huang RYJ, Nieto MA. Epithelial-mesenchymal transitions in development and disease. *Cell* 2009; **139**: 871–890.

253 Nieto MA. Epithelial plasticity: a common theme in embryonic and cancer cells. *Science* 2013; **342**: 1234850.

254 Zavadil J, Böttinger EP. TGF-beta and epithelial-to-mesenchymal transitions. *Oncogene* 2005; **24**: 5764–5774.

255 Nagafuchi A. Molecular architecture of adherens junctions. *Curr Opin Cell Biol* 2001; **13**: 600–603.

256 Vega S, Morales AV, Ocaña OH, Valdés F, Fabregat I, Nieto MA. Snail blocks the cell cycle and confers resistance to cell death. *Genes Dev* 2004; **18**: 1131–1143.

257 Ocaña OH, Córcoles R, Fabra A, Moreno-Bueno G, Acloque H, Vega S *et al.* Metastatic colonization requires the repression of the epithelial-mesenchymal transition inducer Prrx1. *Cancer Cell* 2012; **22**: 709–724.

258 Chaffer CL, Brennan JP, Slavin JL, Blick T, Thompson EW, Williams ED. Mesenchymal-to-epithelial transition facilitates bladder cancer metastasis: role of fibroblast growth factor receptor-2. *Cancer Res* 2006; **66**: 11271–11278.

259 An J, Lv J, Li A, Qiao J, Fang L, Li Z *et al.* Constitutive expression of Bcl-2 induces epithelial-Mesenchymal transition in mammary epithelial cells. *BMC Cancer* 2015; **15**: 476.

260 Choi S, Chen Z, Tang LH, Fang Y, Shin SJ, Panarelli NC *et al.* Bcl-xL promotes metastasis independent of its anti-apoptotic activity. *Nat Commun* 2016; **7**: 10384.

261 Yu M, Bardia A, Wittner BS, Stott SL, Smas ME, Ting DT *et al.* Circulating breast tumor cells exhibit dynamic changes in epithelial and mesenchymal composition. *Science* 2013; **339**: 580–584.

262 Jolly MK, Tripathi SC, Jia D, Mooney SM, Celiktas M, Hanash SM *et al.* Stability of the hybrid epithelial/mesenchymal phenotype. *Oncotarget* 2016; **7**: 27067–27084.

263 Brabletz T, Jung A, Reu S, Porzner M, Hlubek F, Kunz-Schughart LA *et al.* Variable beta-catenin expression in colorectal cancers indicates tumor progression driven by the tumor environment. *Proc Natl Acad Sci U S A* 2001; **98**: 10356–10361.

264 Kamada S, Shimono A, Shinto Y, Tsujimura T, Takahashi T, Noda T *et al.* bcl-2 deficiency in mice leads to pleiotropic abnormalities: accelerated lymphoid cell death in thymus and

spleen, polycystic kidney, hair hypopigmentation, and distorted small intestine. *Cancer Res* 1995; **55**: 354–359.

265 van der Heijden M, Zimberlin CD, Nicholson AM, Colak S, Kemp R, Meijer SL *et al.* Bcl-2 is a critical mediator of intestinal transformation. *Nat Commun* 2016; **7**: 10916.

266 Dzhagalov I, St John A, He Y-W. The antiapoptotic protein Mcl-1 is essential for the survival of neutrophils but not macrophages. *Blood* 2007; **109**: 1620–1626.

267 Opferman JT, Letai A, Beard C, Sorcinelli MD, Ong CC, Korsmeyer SJ. Development and maintenance of B and T lymphocytes requires antiapoptotic MCL-1. *Nature* 2003; **426**: 671–676.

268 Opferman JT, Iwasaki H, Ong CC, Suh H, Mizuno S, Akashi K *et al.* Obligate role of anti-apoptotic MCL-1 in the survival of hematopoietic stem cells. *Science* 2005; **307**: 1101–1104.

269 Arbour N, Vanderluit JL, Le Grand JN, Jahani-Asl A, Ruzhynsky VA, Cheung ECC *et al.* Mcl-1 is a key regulator of apoptosis during CNS development and after DNA damage. *J Neurosci Off J Soc Neurosci* 2008; **28**: 6068–6078.

270 Vick B, Weber A, Urbanik T, Maass T, Teufel A, Krammer PH *et al.* Knockout of myeloid cell leukemia-1 induces liver damage and increases apoptosis susceptibility of murine hepatocytes. *Hepatol Baltim Md* 2009; **49**: 627–636.

271 Weber A, Boger R, Vick B, Urbanik T, Haybaeck J, Zoller S *et al.* Hepatocyte-specific deletion of the antiapoptotic protein myeloid cell leukemia-1 triggers proliferation and hepatocarcinogenesis in mice. *Hepatol Baltim Md* 2010; **51**: 1226–1236.

272 Cao G, Pei W, Ge H, Liang Q, Luo Y, Sharp FR *et al.* In Vivo Delivery of a Bcl-xL Fusion Protein Containing the TAT Protein Transduction Domain Protects against Ischemic Brain Injury and Neuronal Apoptosis. *J Neurosci Off J Soc Neurosci* 2002; **22**: 5423–5431.

273 Hikita H, Takehara T, Shimizu S, Kodama T, Li W, Miyagi T *et al.* Mcl-1 and Bcl-xL cooperatively maintain integrity of hepatocytes in developing and adult murine liver. *Hepatol Baltim Md* 2009; **50**: 1217–1226.

274 Iwasawa M, Miyazaki T, Nagase Y, Akiyama T, Kadono Y, Nakamura M *et al.* The antiapoptotic protein Bcl-xL negatively regulates the bone-resorbing activity of osteoclasts in mice. *J Clin Invest* 2009; **119**: 3149–3159.

275 Hampe J, Franke A, Rosenstiel P, Till A, Teuber M, Huse K *et al.* A genome-wide association scan of nonsynonymous SNPs identifies a susceptibility variant for Crohn disease in ATG16L1. *Nat Genet* 2007; **39**: 207–211.

276 Neufert C, Becker C, Neurath MF. An inducible mouse model of colon carcinogenesis for the analysis of sporadic and inflammation-driven tumor progression. *Nat Protoc* 2007; **2**: 1998–2004.

277 Papanikolaou A, Shank RC, Delker DA, Povey A, Cooper DP, Rosenberg DW. Initial levels of azoxymethane-induced DNA methyl adducts are not predictive of tumor susceptibility in inbred mice. *Toxicol Appl Pharmacol* 1998; **150**: 196–203.

278 Sohn OS, Fiala ES, Requeijo SP, Weisburger JH, Gonzalez FJ. Differential effects of CYP2E1 status on the metabolic activation of the colon carcinogens azoxymethane and methylazoxymethanol. *Cancer Res* 2001; **61**: 8435–8440.

279 Reddy BS, Weisburger JH, Narisawa T, Wynder EL. Colon carcinogenesis in germ-free rats with 1,2-dimethylhydrazine and N-methyl-n'-nitro-N-nitrosoguanidine. *Cancer Res* 1974; **34**: 2368–2372.

280 Suzuki R, Kohno H, Sugie S, Nakagama H, Tanaka T. Strain differences in the susceptibility to azoxymethane and dextran sodium sulfate-induced colon carcinogenesis in mice. *Carcinogenesis* 2006; **27**: 162–169.

281 Okayasu I, Hatakeyama S, Yamada M, Ohkusa T, Inagaki Y, Nakaya R. A novel method in the induction of reliable experimental acute and chronic ulcerative colitis in mice. *Gastroenterology* 1990; **98**: 694–702.

282 Maltzman T, Whittington J, Driggers L, Stephens J, Ahnen D. AOM-induced mouse colon tumors do not express full-length APC protein. *Carcinogenesis* 1997; **18**: 2435–2439.

283 Takahashi M, Nakatsugi S, Sugimura T, Wakabayashi K. Frequent mutations of the beta-catenin gene in mouse colon tumors induced by azoxymethane. *Carcinogenesis* 2000; **21**: 1117–1120.

284 Vivona AA, Shpitz B, Medline A, Bruce WR, Hay K, Ward MA *et al.* K-ras mutations in aberrant crypt foci, adenomas and adenocarcinomas during azoxymethane-induced colon carcinogenesis. *Carcinogenesis* 1993; **14**: 1777–1781.

285 Bai M, Skyrlas A, Agnantis NJ, Kamina S, Tsanou E, Grepi C *et al.* Diffuse large B-cell lymphomas with germinal center B-cell-like differentiation immunophenotypic profile are associated with high apoptotic index, high expression of the proapoptotic proteins bax, bak and bid and low expression of the antiapoptotic protein bcl-xl. *Mod Pathol Off J U S Can Acad Pathol Inc* 2004; **17**: 847–856.

286 Ryoo HD, Bergmann A. The role of apoptosis-induced proliferation for regeneration and cancer. *Cold Spring Harb Perspect Biol* 2012; **4**: a008797.

287 Fan Y, Bergmann A. Apoptosis-induced compensatory proliferation. The Cell is dead. Long live the Cell! *Trends Cell Biol* 2008; **18**: 467–473.

288 Okamoto T, Coultas L, Metcalf D, van Delft MF, Glaser SP, Takiguchi M *et al.* Enhanced stability of Mcl1, a prosurvival Bcl2 relative, blunts stress-induced apoptosis, causes male sterility, and promotes tumorigenesis. *Proc Natl Acad Sci U S A* 2014; **111**: 261–266.

289 Scherr A-L, Gdynia G, Salou M, Radhakrishnan P, Duglova K, Heller A *et al.* Bcl-xL is an oncogenic driver in colorectal cancer. *Cell Death Dis* 2016; **7**: e2342.

290 Vooijs M, Jonkers J, Berns A. A highly efficient ligand-regulated Cre recombinase mouse line shows that LoxP recombination is position dependent. *EMBO Rep* 2001; **2**: 292–297.

291 Pinello L, Xu J, Orkin SH, Yuan G-C. Analysis of chromatin-state plasticity identifies cell-type-specific regulators of H3K27me3 patterns. *Proc Natl Acad Sci U S A* 2014; **111**: E344-353.

292 Kirsch DG, Doseff A, Chau BN, Lim DS, de Souza-Pinto NC, Hansford R *et al.* Caspase-3-dependent cleavage of Bcl-2 promotes release of cytochrome c. *J Biol Chem* 1999; **274**: 21155–21161.

293 Clem RJ, Cheng EH, Karp CL, Kirsch DG, Ueno K, Takahashi A *et al.* Modulation of cell death by Bcl-XL through caspase interaction. *Proc Natl Acad Sci U S A* 1998; **95**: 554–559.

294 Perciavalle RM, Stewart DP, Koss B, Lynch J, Milasta S, Bathina M *et al.* Anti-apoptotic MCL-1 localizes to the mitochondrial matrix and couples mitochondrial fusion to respiration. *Nat Cell Biol* 2012; **14**: 575–583.

295 Wang X, Bathina M, Lynch J, Koss B, Calabrese C, Frase S *et al.* Deletion of MCL-1 causes lethal cardiac failure and mitochondrial dysfunction. *Genes Dev* 2013; **27**: 1351–1364.

296 Thomas RL, Roberts DJ, Kubli DA, Lee Y, Quinsay MN, Owens JB *et al.* Loss of MCL-1 leads to impaired autophagy and rapid development of heart failure. *Genes Dev* 2013; **27**: 1365–1377.

297 Basit F, Cristofanon S, Fulda S. Obatoclax (GX15-070) triggers necroptosis by promoting the assembly of the necrosome on autophagosomal membranes. *Cell Death Differ* 2013; **20**: 1161–1173.

298 Ofengeim D, Yuan J. Regulation of RIP1 kinase signalling at the crossroads of inflammation and cell death. *Nat Rev Mol Cell Biol* 2013; **14**: 727–736.

299 Renehan AG, Bach SP, Potten CS. The relevance of apoptosis for cellular homeostasis and tumorigenesis in the intestine. *Can J Gastroenterol J Can Gastroenterol* 2001; **15**: 166–176.

300 Negroni A, Cucchiara S, Stronati L. Apoptosis, Necrosis, and Necroptosis in the Gut and Intestinal Homeostasis. *Mediators Inflamm* 2015; **2015**: 250762.

301 Kim YS, Ho SB. Intestinal goblet cells and mucins in health and disease: recent insights and progress. *Curr Gastroenterol Rep* 2010; **12**: 319–330.

302 Ayabe T, Satchell DP, Wilson CL, Parks WC, Selsted ME, Ouellette AJ. Secretion of microbicidal alpha-defensins by intestinal Paneth cells in response to bacteria. *Nat Immunol* 2000; **1**: 113–118.

303 Nakamura K, Sakuragi N, Takakuwa A, Ayabe T. Paneth cell α-defensins and enteric microbiota in health and disease. *Biosci Microbiota Food Health* 2016; **35**: 57–67.

304 Masuda K, Sakai N, Nakamura K, Yoshioka S, Ayabe T. Bactericidal activity of mouse α-defensin cryptdin-4 predominantly affects noncommensal bacteria. *J Innate Immun* 2011; **3**: 315–326.

305 Valdés-Ferrer SI, Rosas-Ballina M, Olofsson PS, Lu B, Dancho ME, Ochani M *et al.* HMGB1 mediates splenomegaly and expansion of splenic CD11b+ Ly-6C(high) inflammatory monocytes in murine sepsis survivors. *J Intern Med* 2013; **274**: 381–390.

306 Li F, Huang Q, Chen J, Peng Y, Roop DR, Bedford JS *et al.* Apoptotic cells activate the 'phoenix rising' pathway to promote wound healing and tissue regeneration. *Sci Signal* 2010; **3**: ra13.

307 Sitailo LA, Jerome-Morais A, Denning MF. Mcl-1 functions as major epidermal survival protein required for proper keratinocyte differentiation. *J Invest Dermatol* 2009; **129**: 1351–1360.

308 Pawlikowska P, Leray I, de Laval B, Guihard S, Kumar R, Rosselli F *et al.* ATM-dependent expression of IEX-1 controls nuclear accumulation of Mcl-1 and the DNA damage response. *Cell Death Differ* 2010; **17**: 1739–1750.

309 Kobayashi J, Antoccia A, Tauchi H, Matsuura S, Komatsu K. NBS1 and its functional role in the DNA damage response. *DNA Repair* 2004; **3**: 855–861.

310 Tóthová E, Fricova M, Stecová N, Kafková A, Elbertová A. High expression of Bcl-2 protein in acute myeloid leukemia cells is associated with poor response to chemotherapy. *Neoplasma* 2002; **49**: 141–144.

311 Real PJ, Sierra A, De Juan A, Segovia JC, Lopez-Vega JM, Fernandez-Luna JL. Resistance to chemotherapy via Stat3-dependent overexpression of Bcl-2 in metastatic breast cancer cells. *Oncogene* 2002; **21**: 7611–7618.

312 Minn AJ, Rudin CM, Boise LH, Thompson CB. Expression of bcl-xL can confer a multidrug resistance phenotype. *Blood* 1995; **86**: 1903–1910.

313 Akagi H, Higuchi H, Sumimoto H, Igarashi T, Kabashima A, Mizuguchi H *et al.* Suppression of myeloid cell leukemia-1 (Mcl-1) enhances chemotherapy-associated apoptosis in gastric cancer cells. *Gastric Cancer Off J Int Gastric Cancer Assoc Jpn Gastric Cancer Assoc* 2013; **16**: 100–110.

314 Albershardt TC, Salerni BL, Soderquist RS, Bates DJP, Pletnev AA, Kisselev AF *et al.* Multiple BH3 mimetics antagonize antiapoptotic MCL1 protein by inducing the endoplasmic reticulum stress response and up-regulating BH3-only protein NOXA. *J Biol Chem* 2011; **286**: 24882–24895.

315 Billard C. BH3 mimetics: status of the field and new developments. *Mol Cancer Ther* 2013; **12**: 1691–1700.

316 Wilson WH, O'Connor OA, Czuczman MS, LaCasce AS, Gerecitano JF, Leonard JP *et al.* Navitoclax, a targeted high-affinity inhibitor of BCL-2, in lymphoid malignancies: a phase 1 dose-escalation study of safety, pharmacokinetics, pharmacodynamics, and antitumour activity. *Lancet Oncol* 2010; **11**: 1149–1159.

317 Gandhi L, Camidge DR, Ribeiro de Oliveira M, Bonomi P, Gandara D, Khaira D *et al.* Phase I study of Navitoclax (ABT-263), a novel Bcl-2 family inhibitor, in patients with small-cell lung cancer and other solid tumors. *J Clin Oncol Off J Am Soc Clin Oncol* 2011; **29**: 909–916.

318 Roberts AW, Seymour JF, Brown JR, Wierda WG, Kipps TJ, Khaw SL *et al.* Substantial susceptibility of chronic lymphocytic leukemia to BCL2 inhibition: results of a phase I study of navitoclax in patients with relapsed or refractory disease. *J Clin Oncol Off J Am Soc Clin Oncol* 2012; **30**: 488–496.

319 Souers AJ, Leverson JD, Boghaert ER, Ackler SL, Catron ND, Chen J *et al.* ABT-199, a potent and selective BCL-2 inhibitor, achieves antitumor activity while sparing platelets. *Nat Med* 2013; **19**: 202–208.

Figure 1: Structure and cellular composition of the intestinal epithelium 12
Figure 2: The adenoma-carcinoma sequence.. 15
Figure 3: Caspase-mediated cellular decomposition. 19
Figure 4: Subgroups of the Bcl-2 protein family.. 20
Figure 5: Anti-apoptotic Bcl-2 proteins inhibit autophagy.. 25
Figure 6: Expression levels of anti-apoptotic Bcl-2 proteins in human CRC.. 61
Figure 7: Expression levels of Bcl-xL and Mcl-1 in primary tumors and liver metastases.. 62
Figure 8: siRNA mediated knockdown of anti-apoptotic Bcl-2 proteins in human CRC cells.. 63
Figure 9: Viability of CRC cells after knockdown of anti-apoptotic Bcl-2 proteins.. 64
Figure 10: Proliferation of CRC cells after knockdown of anti-apoptotic Bcl-2 proteins. 65
Figure 11: Migratory capacity of CRC cells after knockdown of anti-apoptotic Bcl-2 proteins. 66
Figure 12: Proliferation and migration of HT29 cells in 3D scaffolds after knockdown of Mcl-1, Bcl-2, Bcl-x_L 68
Figure 13: Overexpression of anti-apoptotic Bcl-2 proteins in human CRC cells. 69
Figure 14: Migratory capacity of human CRC cells after overexpression of anti-apoptotic Bcl-2 proteins. ... 71
Figure 15: Invasiveness of SW480 cells after knockdown of anti-apoptotic Bcl-2 proteins. 72
Figure 16: Cell death and proliferation of CRC cells under treatment with the inhibitor Obatoclax 73
Figure 17: Migratory capacity of human CRC cells under treatment with the inhibitor Obatoclax. 74
Figure 18: Invasiveness of SW480 cells under treatment with the inhibitor Obatoclax. 75
Figure 19: Expression of E- and N-Cadherin in CRC cells before and after downregulation or inhibition of anti-apoptotic Bcl-2 proteins. 76
Figure 20: Chemosensitivity of HT29 cells after knockdown or inhibition of anti-apoptotic Bcl-2 proteins... 78
Figure 21: Bcl-xL expression patterns in Bcl-xL$^{\Delta IEC}$ and control mice. 79
Figure 22: Genotyping of Bcl-xL$^{\Delta IEC}$ mice. 80
Figure 23: Basal characterization of Bcl-xL$^{\Delta IEC}$ mice.. 81
Figure 24: Bcl-xL$^{\Delta IEC}$ and control mice in an inflammation-driven model for intestinal carcinogenesis. 82
Figure 25: Analysis of immune cell infiltration in the colon of DSS treated Bcl-xL$^{\Delta IEC}$ and control mice. 83
Figure 26: Analysis of cell death events in AOM/DSS induced tumors. 84
Figure 27: Analysis of proliferation and lymphocyte infiltration in AOM/DSS induced tumors.. 85
Figure 28: Mcl-1 expression patterns in Mcl-1$^{\Delta IEC}$ and control mice. 87
Figure 29: Basal characterization of Mcl-1$^{\Delta IEC}$ mice. 88
Figure 30: Genotyping of Mcl-1$^{\Delta IEC}$ mice. 88
Figure 31: Morphometric analysis of colon specimens derived from Mcl-1$^{\Delta IEC}$ mice.. 89
Figure 32: Analysis of apoptosis subroutines in Mcl-1$^{\Delta IEC}$ mice. 90
Figure 33: Expression levels of other Bcl-2 proteins in the colon of Mcl-1$^{\Delta IEC}$ mice. 91
Figure 34: Analysis of necroptosis in Mcl-1$^{\Delta IEC}$ mice. 92
Figure 35: Analysis of proliferation in Mcl-1$^{\Delta IEC}$ mice. 94
Figure 36: Analysis of inflammation in Mcl-1$^{\Delta IEC}$ mice. 95
Figure 37: Analysis of immune cell infiltration in Mcl-1$^{\Delta IEC}$ mice.. 96
Figure 38: Analysis of proliferation, apoptosis and lymphocyte infiltration in tumors derived from Mcl-1$^{\Delta IEC}$ mice. 97
Figure 39: Test for microsatellite instability in tumors derived from Mcl-1$^{\Delta IEC}$ mice. 99
Figure 40: Evaluation of the Bcl-xL/Bcl-2 inhibitor ABT-737 in a 3D cell culture approach.. 100
Figure 41: Evaluation of the Bxl-xL/Bcl-2 inhibitor ABT737 in an ex vivo tissue culture approach.. 102

Table 1: siRNAs used for the transfection of eukaryotic cells. 35
Table 2: Components for the preparation of 2 x RIPA lysis buffer. 41
Table 3: Components for the preparation of supplemented 1 x RIPA lysis buffer. 41
Table 4: Components for the preparation of two acrylamid-gels. 44
Table 5: Components for the preparation of 5 x protein sample buffer. 44
Table 6: Components for the preparation of 10 x running buffer. 44
Table 7: Components for the preparation of 10 x transfer buffer. 45
Table 8: Antibodies used for Western blot analyses. 46
Table 9: Components for the preparation of the reverse transcription master mix. 49
Table 10: Components for the preparation of the quantitative real-time PCR master mix. 49
Table 11: Components for the preparation of the proteinase K buffer. 50
Table 12: Primers used for mouse genotyping. 51
Table 13: Components for the preparation of the indicated PCR master mixes and the corresponding PCR programs. 51
Table 14: Components for the preparation of 50 x TAE buffer. 52
Table 15: Mononucleotide markers and primers used for MSI analyses of murine intestinal tumors. 53
Table 16: Components for the preparation of the indicated PCR master mixes and the corresponding PCR programs. 54
Table 17: Antibodies used for immunohistochemical staining. 57

2D	two dimensional
2N	diploid
3D	three dimensional
4N	tetraploid
5-FU	5-fluorouracil
ACD	autophagic cell death
AIF	apoptosis-inducing factor
AMP	adenosine monophosphate
AMPK	AMP-activated protein kinase
AOM	azoxymethane
APAF1	apoptotic protease activating factor 1
APC	adenomatous polyposis coli
APS	ammonium persulfate
Atg	autophagy-related gene
ATP	adenosine triphosphate
BAD	Bcl-2 antagonist of cell death
Bak	Bcl-2 antagonist/ killer
Bax	Bcl-2 associated X protein
Bcl-2	B-cell lymphoma 2
Bcl-w	B-cell lymphoma w
Bcl-x_L	B-cell lymphoma extra-large
BH domain	B-cell lymphoma 2 homolgy domain
BID	Bcl-2-interacting domain death agonist
BIM	Bcl-2-interacting mediator of cell death
BL	body length
BMI	body mass index
BMP	bone morphogenetic protein
Bok	Bcl-2-related ovarian killer protein
BRAF	v-Raf murine sarcoma viral oncogene homolog B
BrdU	bromodeoxyuridine
BSA	bovine serum albumine
BW	body weight
CAD	caspase-activated DNase
CARD	caspase activation and recruitment domain
CD	cluster of differentiation
Cdc42	cell division control protein 42 homolog
CDK1	cyclin depending kinase 1
cDNA	complementary DNA
c-FLIP	cellular FLICE/caspase-8-inhibitory protein

cIAP	cellular inhibitor of apoptosis
CIMP	CpG island methylator phenotype
CIN	chromosomal instability
CK1α	serine/threonine kinases casein kinase 1 alpha
cl.PARP	cleaved PARP
CLL	chronic lymphocytic leukemia
CO_2	carbon dioxide
CpG	Cytosine-Guanosin dinucleotide
CRC	colorectal cancer
Cre	creates recombination
CreER	Cre-coupled estrogen receptor
CTLs	cytotoxic T-lymphocytes
CYLD	cylindromatosis
DAB	diaminobenzidine
DAPI	4',6-Diamidin-2-phenylindol
DCC	deleted in colorectal cancer
DD	death domain
ddH_2O	double distilled water
DED	death effector domain
DEDs	death effector domains
DISC	death inducing signaling complex
DMSO	dimethyl sulfoxide
DNA	Deoxyribonucleic acid
dNTPs	deoxynucleotides
DSS	dextran sodium sulfate
DTT	1,4 dithiothreitol
ECL	enhanced chemiluminescence
ECM	extracellular matrix
ECM	extracellular matrix
EDTA	ethylenediaminetetraacetic acid
EGF	epidermal growth factor
EGFR	epidermal growth factor receptor
EMT	epithelial-to-mesenchymal transition
ER	endoplasmatic reticulum
Erk	extracellular signal-regulated kinases
EtBr	ethidium bromide
EtOH	ethanol
FACS	fluorescence-activated cell sorting
FADD	FAS-associated protein with a DD
FAP	familial adenomatous polyposis
FASL	TNF receptor superfamily member 6 ligand
FCS	fetal calf serum

FDA	Food and Drug Administration
FIP200	focal adhesion kinase family interacting protein of 200 kD
FITC	fluorescein isothiocyanate
floxed	flanked by two loxP sites
for	forward
GABARAP	gamma-aminobutyric-acid-type-A-receptor-associated protein
GAPDH	glycerinaldehyde-3-phosphate-dehydrogenase
GATE-16	Golgi-associated ATPase enhancer of 16 kDa
GFP	green fluorescing protein
GRASP65	Golgi reassembling and stacking protein
GSK3	glycogen synthase kinase 3
GTP	Guanosine-5'-triphosphate
h	hour
H2AX	histone 2A, member X
H2B	histone 2B
H_2O	water
HCl	hydrochloric acid
HE	hematoxylin and eosin
HrK	activator of apoptosis harakiri
HRP	horseradish peroxidase
HtrA2	high temperature requirement protein A2
IAP	inhibitors of apoptosis
IBD	inflammatory bowel disease
IC_{50}	half maximal inhibitory concentration
ICAD	inhibitor of caspase activated DNase
IEC	intestinal epithelial cell
IHC	immunohistochemical staining
IKK	IκB kinase
IL	interleukin
IMS	intra-membrane space
IκB	inhibitor of NF-κB
KRAS	Kirsten rat sarcoma viral oncogene homolog
LC3	microtubule-associated protein light chain 3
LC3 I	cytosolic LC3
LC3 II	membrane bound LC3
LDH	lactate dehydrogenase
LEF	lymphoid enhancer-binding factor
Lgr5	leucine-rich repeat-containing G-protein coupled receptor 5
LIR	LC3-interacting region
loxP	locus of crossover in P1
LRP	low density lipoprotein receptor-related protein
Mcl-1	myeloid cell leukemia sequence 1

MEFs	mouse embryonic fibroblasts
Mek	mitogen-activated protein kinase kinase
MET	mesenchymal-to-epithelial transition
$MgCl_2$	magnesium chloride
MLH1	mutL homolog 1
MLKL	mixed linage kinase domain-like protein
MMP7	matrix metalloproteinase 7
MMR	mismatch repair
MOMP	mitochondrial outer membrane permeabilization
mRNA	massenger RNA
MSH2	mutS homolog 2
MSI	microsatellite instability
MSI-H	MSI high
MSS	microsatellite stability
MST1	mammalian sterile20
mTOR	mechanistic target of rapamycin
mTORC1	mammalien target of Rapamycin complex 1
MTT	3-(4,5-dimethylthiazol-2-yl)-2,5-diphenyltetrazolium bromide
Muc	mucosa
MΦ	macrophage
NaCl	sodium chloride
NAD	nicotinamide adenine dinucleotide
NaF	sodium fluoride
NBS1	Nijmegen breakage syndrome
NCT	National Center for Tumor Diseases
NF-κB	nuclear factor kappa-light-chain-enhancer of activated B cells
NK	natural killer
Oba	Obatoclax
OMM	outer mitochondrial membrane
Oxa	oxaliplatin
PAGE	polyacrylamide gel electrophoresis
PARP	Poly(ADP-ribose)-Polymerase
PAS	phagophore assembly side
PBS	phosphate buffered saline
PBS-T	PBS-Tween
PCD	programmed cell death
PCNA	proliferating cell nuclear antigen
PCR	polymerase chain reaction
PD-1	programmed death
PE	phosphatidylethanolamine
PFA	paraformaldehyde
PI	protease inhibitor

PI3KC1	class I phosphatidylinositol 3-kinase
PI3KC3	class III phosphatidylinositol 3-kinase
PIP	phosphatidylinositol phosphates
pMLKL	phospho-MLKL
PMSF	phenylmethyl sulphonyl fluoride
PS	phosphatidylserine
qRT-PCR	quantitative real-time polymerase chain reaction
rev	reverse
RIP1	receptor interacting serine/threonine kinase 1
RNA	ribonucleic acid
ROCK1	Rho associated coiled-coil containing protein kinase 1
ROS	reactive oxygen species
R-spondin	roof plate-specific spondin
RT	room temperature
SD	standard deviation
SDS	sodium dodecyl sulfate
siRNA	small interfering RNA
siSc	scrambled siRNA
SMAC	second mitochondria-derived activator of caspases
SMAD	mothers against decapentaplegic
SNPs	single nucleotide polymorphisms
SQSTM1/p62	sequestosome 1
ß-MeEtOH	β-mercaptoethanol
STS	staurosporine
TA	transit-amplifying
TAE	tris-acetate-EDTA
TAK 1	TGF-β-activated kinase 1
TAK1	TGF-beta activated kinase 1
Taq	Thermus aquaticus (bacterium)
tBID	truncated BID
TBS	tris-buffered saline
TCF	T-cell factor
TdT	terminal-deoxynucleotidyl-transferase
TEMED	tetra-methylethylenediamine
TGF-ß	transforming growth factor beta
TMA	tissue microarray
TNFAIP3	TNFα-induced protein 3
TNF-R1	TNF receptor 1
TNFα	tumor necrosis factor alpha
TNM	tumor node metastasis
TP53	tumor protein p53
TRADD	TNF-R associated death domain

TRAF2	TNF-R associated factor 2
TRAIL	TNF-related apoptosis inducing ligand
TTX	Triton X 100
Tu	tumor
TUNEL	terminal deoxynucleotidyl transferase dUTP nick end labeling
UICC	Union Internationale contre le Cancer
ULK	unc51-like kinase
UV	ultra-violet
v/v	volume per volume
VEGF	vascular endothelial growth factor
VilCre	Cre expressed under control of the Villin promotor
VMP1	vacuole membrane protein 1
Vps	vacuolar protein sorting
w/v	weight per volume
wt	wild type
XIAP	X-linked IAP

Scratch assays displayed in Figure 11, Figure 14 and Figure 17 were performed by our student apprentice Stephan Lorenz (Medical Faculty, University of Heidelberg). Western blot analyses shown in Figure 32 d and Figure 34 a were done by our Bachelor student (Molecular Biotechnology, University of Heidelberg) Umut Yildiz. Both students worked under my supervision. The germ-free housing of Mcl-$1^{\Delta IEC}$ mice, mentioned on page 98, was done by our cooperation partners, the group of Prof. Dr. med. Achim Weber (Institute of Surgical Pathology, University Hospital of Zurich, Switzerland). The manual microdissection of adenocarcinomal tissue derived from Mcl-$1^{\Delta IEC}$ mice and subsequent sequencing (Figure 39) was performed by our cooperation partner PD Dr. med. Matthias Kloor (Institute of Pathology, University Hospital Heidelberg, Germany) and culturing of human CRC tissue (Figure 41) was done in the lab of Dr. med. Georg Gdynia (Molecular Tumor Pathology, German Cancer Research Center (DKFZ), Heidelberg, Germany).

ACKNOWLEDGEMENTS

The process of writing a doctoral thesis is effortful and it certainly cannot be done single-handedly. I am exceptionally grateful for the tremendous support I received from various sides. First of all, I want to express my gratitude to Prof. Dr. med. Henning Schulze-Bergkamen for the opportunity to start my project in his group and for his guidance in research and writing. He always gave me the confidence to follow my ideas and approaches and helped me by realizing them. A special thank goes to Prof. Dr. Michael Boutros who kindly accepted to act as the first referee. Likewise, I thank Prof. Dr. med. Wilfried Roth, the third member of my thesis advisory committee. Together they gave insightful comments during my TAC meetings and always encouraged me to contemplate my research from different perspectives.

My sincere thanks also go to my supervisor Dr. med. Bruno Köhler, who invested so much time and effort, for his continuous motivation and patience. I could not have imagined a better advisor for supporting my PhD project. I´m very happy that we became not only colleagues but also friends.

Furthermore, I want to express my gratitude to Prof. Dr. med. Dirk Jäger, the head of our department, and to Dr. Inka Zörnig, our lab leader, for their consistent support and for providing a stimulating scientific surrounding. Additionally, I would like to thank the *Deutsche Forschungsgemeinschaft* (DFG) for the financial support of my PhD project.

I also thank my fellow lab mates Christin Elssner, Nicole Kautz, Adam Jassowicz, Dr. Toni Urbanik, Dr. med Stefan Welte, Umut Yildiz, Stephan Lorenz and Laura Wolpert, whit whom I had the pleasure to work together during the last four years. They gave me the chance to learn and to teach, to question and revise and I highly appreciate that scientific issues were always discussed in an equal and favorable manner. My thanks also go to my amazing office mates Mariam Salou, Julia Bitzer, Zeynep Kosaloglu, Silke Uhrig-Schmidt and Ruth Schübel for the warm atmosphere, the long discussions, the provided help and their friendship. A lot of help I also received by all the members of AG Jäger and AG Podar and especially by Dr. Patrick Schmidt who proofread this manuscript. Furthermore, I would like to name our cooperation partners Prof. Dr. med. Martin Schneider, Dr. Praveen Radhakrishnan, Dr. med. Georg Gdynia, Dr. Carmen Ruiz de Almodóvar, Dr. Franco Fortunato, Prof. Dr. med Achim Weber and Prof. Dr. Mathias Heikenwälder. I would like to express my sincere gratitude for their insights, help and advises and for their collegiality.

From the bottom of my heart, I want to thank my partner and my friends for listening to my nerdy monologs and for keeping a sense of humor when I had lost mine. Finally and foremost, I want to express my gratefulness to my parents for all the sacrifices they made on my behalf.